DOCTORAL DISSERTATION

Advances in the dynamic and seismic analysis of jacket structures for the support of offshore wind turbines

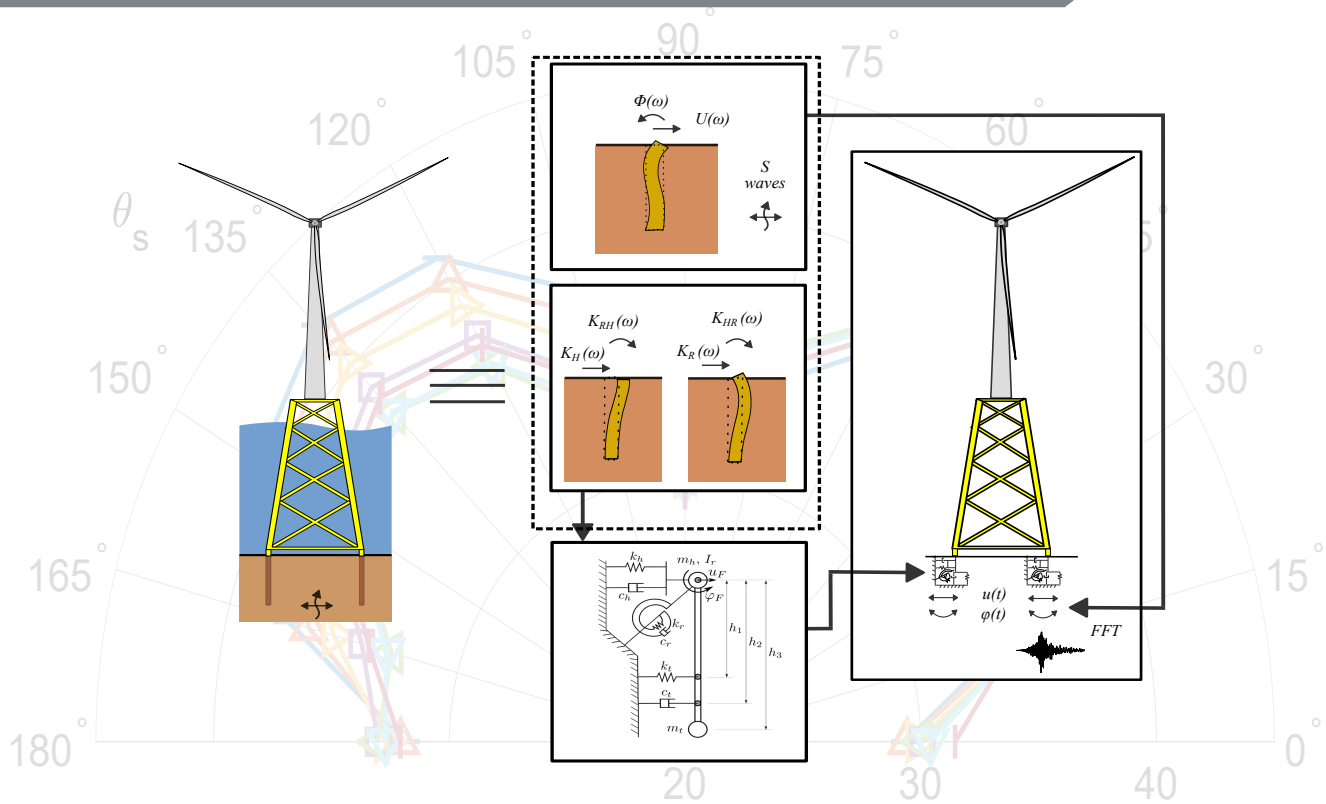

Carlos Romero Sánchez

Continuum Mechanics and Structures Division

Las Palmas de Gran Canaria • July 2025

INSTITUTO UNIVERSITARIO SIANI INGENIERIA COMPUTACIONAL

ULPGC Universidad de Las Palmas de Gran Canaria

Programa de Doctorado: Tecnologías de Telecomunicación e Ingeniería Computacional

Advances in the dynamic and seismic analysis of jacket structures for the support of offshore wind turbines

Carlos Romero Sánchez

Universidad de Las Palmas de Gran Canaria
Escuela de doctorado

Programa de doctorado
Tecnologías de Telecomunicación e Ingeniería Computacional

Director:
Luis Alberto Padrón Hernández

Las Palmas de Gran Canaria, July 2025

Acknowledgements

I would like to start by thanking my supervisor, Luis Alberto Padrón, for giving me the opportunity and the trust to carry out this project. Without his guidance and support, this work would not have been possible. He is not only a great researcher and professor, but also a true role model as a person.

I am very grateful to all the members of the Continuum Mechanics and Structures Division. The kindness and help I have received from the group have been a fundamental part of this thesis. In particular, I want to thank Jacob Rodríguez and Guillermo Álamo, whose help at the beginning of the project was essential to getting started in the right direction. I cannot forget to mention my colleagues from the office: Eduardo Rodríguez, Borja Benítez, Samuel González, Óscar Ramón and Antonio Romero. The many hours we spent discussing work and other topics made this process much more enjoyable.

I also wish to thank to Prof. Amir M. Kaynia and Dr. Ana M. Page for their guidance and friendship. It was a real honour to work with you at the Norwegian Geotechnical Institute. Thanks also to the whole Advanced Modelling Section for their warm welcome and the great experience during my research stay, and of course to my "Norwegian Fadder", Dr. Emily Anderson, for helping me with everything. Thank you very much!

Finally, I would like to thank all those who have been part of my life outside of academia during these years. Their support has played a fundamental role in helping me through this process. None of this would have been possible without the education, love and support of my family. Thank you, Dad. Thank you, Mom. Thank you, Pedro. This thesis is, in many ways, also your achievement.

The author was recipient of a predoctoral fellowship (TESIS2022010011) by the Agencia Canaria de Investigación, Innovación y Sociedad de la Información de la Consejería de Economía, Industria, Comercio y Conocimiento and by the European Social Fund (ESF), which also provided financial support for the short-therm research at Norwegian Geotechnical Institute (EST2024010003).

This work was supported by the Ministerio de Ciencia, Innovación y Universidades and the Agencia Estatal de Investigación of Spain (MCIN/AEI/10.13039/501100011033) and FEDER through research project PID2020-120102RB-I00 and by Consejería de Economía, Conocimiento Empleo (Agencia Canaria de la Investigación, Innovación Sociedad de la Información) of the Gobierno de Canarias and FEDER, Spain through research project ProID2020010025.

Las Palmas de Gran Canaria, July 2025
Carlos Romero Sánchez

CONTENTS

Contents i

1 Introduction and background 3
1.1 Introduction 3
1.2 Literature review 4
1.3 Aims and objectives 6
1.4 Research group 6
1.5 Published works derived from the PhD Thesis 7
1.5.1 Contributions in JCR journals 7
1.5.2 Conference contributions 8
1.6 Justification of the thematic unity and coherence of the PhD Thesis 8

2 Publications 13
2.1 First publication: Romero-Sánchez and Padrón, 2024, Influence of wind and seismic ground motion directionality on the dynamic response of four-legged jacket-supported Offshore Wind Turbines, Engineering Structures. 13
2.2 Second publication: Romero-Sánchez and Padrón, 2024, Seismic response of jacket-supported offshore wind turbines for different operational modes considering earthquake directionality, Ocean Engineering. 27
2.3 Third publication: Romero-Sánchez et al., 2024, Influence of Foundation–Soil–Foundation Interaction on the Dynamic Response of Offshore Wind Turbine Jackets Founded on Buckets, Journal of Marine Science and Engineering. 44
2.4 Autorship documents 68

3 Summary, conclusions and future research directions 75
3.1 Summary and conclusions 75
3.2 Future research directions 77

A Conference Papers 81
A.1 First conference paper: Romero-Sánchez and Padrón, CMN 2022, Implementation of Ground Input Motion and Dynamic Soil-Structure Interaction into Openfast for the Seismic Analysis of Offshore Wind Turbines. 81
A.2 Second conference paper: Romero-Sánchez and Padrón, COMPDYN 2023, An implementation of multi-support seismic input motion into OpenFast for the earthquake analysis of offshore wind turbines. 102
A.3 Third conference paper: Romero-Sánchez et al., EURODYN 2023, Comparative study of the influence of kinematic interaction on the seismic response of monopile and jacket supported offshore wind turbines. 117

CONTENTS

B Resumen en castellano **131**
B.1 Introducción 131
B.2 Objetivos 133
B.3 Publicaciones derivadas de la tesis doctoral 133
B.4 Justificación 134
B.5 Conclusiones 136

References **141**

1. Introduction and background

1.1 Introduction
1.2 Literature review
1.3 Aims and objectives
1.4 Research group
1.5 Published works derived from the PhD Thesis
1.6 Justification of the thematic unity and coherence of the PhD Thesis

1.1 Introduction

One of the immediate challenges facing our society is the development of an energy production system that is less reliant on fossil fuels. The reduction of CO_2 emissions is a central goal of The European Green Deal, spearheaded by the European Commission, which aims for climate neutrality by 2050. In the short term, member states have committed to align their legislation and production systems to achieve a 55% reduction in emissions by 2030. One of the key measures in the package is a proposal to raise the share of renewable energy sources to at least 40% of the European Union's total energy mix. Wind energy represents a significant opportunity for addressing this challenge, with offshore wind energy being one of the most promising options. In fact, offshore wind energy has experienced remarkable growth in recent years, with global installed capacity projected to reach 380 GW by 2030 [1].

Despite its potential, critical challenges in offshore wind development remain, including the technology required for installation, maintenance, and the reduction of environmental impact. Floating offshore wind technology is expected to gain market presence in the near furure. However, most currently installed wind turbines are fixed to the seabed, requiring suitable water depth conditions. As higher-capacity wind turbines are installed at increasing depths, the supporting structures are subjected to more demanding requirements. Thus, the expansion of this technology is oriented toward the development of increasingly complex designs capable of withstanding greater depths and larger distances from the coast. Regarding structural typologies, monopile foundations are the most widely used. Nonetheless, their market share is likely to decline in favour of jacket substructures, driven in part by the increasing average depth of future installations.

In this regard, both the distance from the coast, and the depth at which offshore wind farms are being installed, have been increasing due to several reasons among which one can cite the expansion of the technology and the opening of new markets, the need to avoid environmentally protected areas, or the visual pollution from offshore wind turbines (OWTs) installed near the coastline. For the same reasons, fixed-base offshore wind turbines are also increasingly being installed or planned in higher seismic risk areas. Fig. 1.1 illustrates the most commonly used fixed foundations for moderately deep and deep waters.

An OWT is subjected to time-varying loads, making it necessary to approach their design and analysis from the perspective of structural dynamics. The design of support structures for wind turbines must ensure that the system's natural frequencies are sufficiently separated from the frequency components of the primary dynamic loads it experiences. These loads include rotor unbalance, shadowing effects from the passing blades, wind spectra, and wave-induced forces. One subsystem that introduces significant uncertainties and simplifications in its analysis is the soil-foundation system, particularly for deep foundations such as piles and suction caissons. This issue is especially relevant for OWTs, where foundations based on monopiles, pile groups, or buckets are the standard technical solutions.

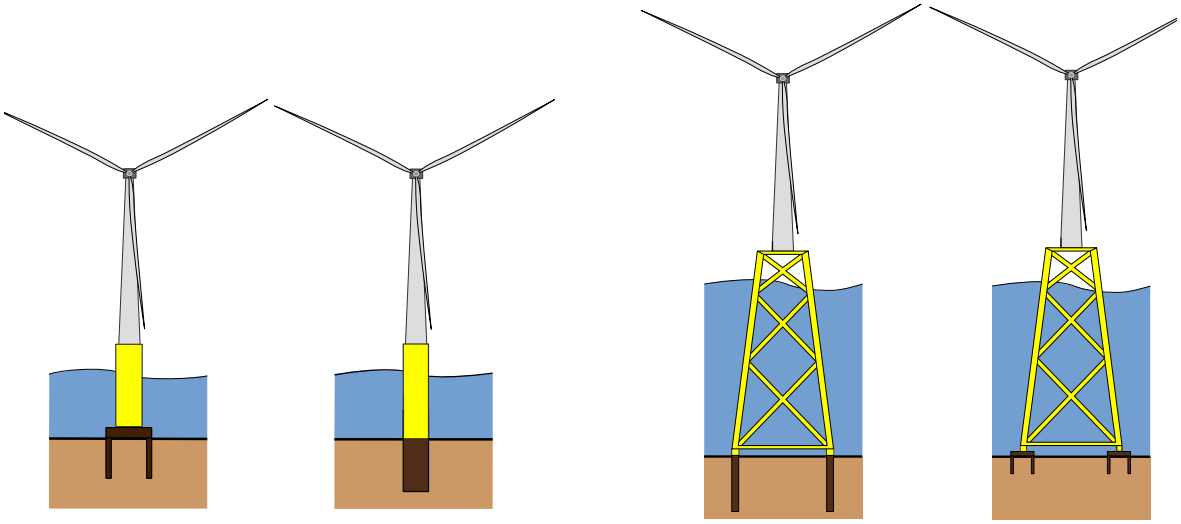

Figure 1.1. Fixed-bottom foundations for offshore wind turbines: monobucket, monopile and jacket substructures.

1.2 Literature review

The analysis of the dynamic structural response of onshore and offshore wind turbines is a relatively recent area of study that has been approached using a wide range of models and methodologies, depending on the specific objectives (see, e.g., [2–4]). Dynamic soil-structure interaction is a key aspect that integrated models must incorporate, as numerous studies have shown that this interaction not only alters the dynamic behavior of actual devices [5–8] but that soil-structure interaction effects can even be detrimental to the system. As a result, using fixed-base models may lead to unsafe designs [9–11].

Even when soil-structure interaction is included, many of the dynamic analysis models available in the literature rely on simple substructuring models that use discrete springs and dampers at the tower base (see, e.g., [12, 13]), with their values often estimated from simplified expressions or approximations. However, more accurate models can be obtained by employing advanced continuous medium formulations to calculate these parameters [14–19].

It is also important to note that most published studies on the dynamic and seismic response of offshore wind turbines focus on monopile turbines, while jacket substructures have received less attention. The works of Jalbi et al. [20–22], Couceiro et al. [23], and Abdullahi et al. [24] represent significant recent efforts to advance the understanding and design of this type of structure.

From the perspective of loads to be considered in designing these structures, the main guidelines and standards [25, 26] primarily focus on loads generated by wind, waves, currents, and ice under various conditions, such as power production, idling and stand-still as well as transient conditions (start-up, shutdown, faults...). Seismic loads, on the other hand, have received less attention, partly due to the perception that these structures are intrinsically safe during earthquakes [4], given their high fundamental

vibration periods relative to the characteristic frequencies of most earthquakes [27]. In contrast, a significant numbers of authors have emphasized the relevance of seismic actions on the structural systems of the OWTs (see, among others, [8, 28, 29]). In line with this motivation, it is worth highlighting the findings presented by Alati et al. [30]. In a specific case study, these authors concluded that the combination of wind, wave, and seismic loads is more unfavorable than the load combinations prescribed by the reference standard for the design of such structures. Cheng et al. [31] explored how the dynamic response of the jacket is influenced by varying wind and wave directions, highlighting the significant impact of emergency shutdown and parked conditions on the fragility assessments for severe damage states in the tower and the substructure. Ju and Huang [29] examined the NREL 5 MW jacket offshore wind turbine, emphasizing that the combination of seismic and environmental loads during power production typically governs the structural design of jacket substructures. Additionally, James and Haldar [32] focused on the performance of tubular jacket members under yield stress, incorporating multidirectional ground motion. Their findings underscored the importance of accounting for higher mode effects and multidirectional seismic forces when analysing the structural behaviour of OWTs, identifying the top and bottom segments of the jacket leg as particularly vulnerable.

Some of the previously discussed studies focus on the evaluation of the structural characteristics of OWTs using simplified structural models in frequency domain. The dynamic behaviour of these support structures is a critical factor in system design, and the different specific loading conditions, the variable geometry of the system resulting from blade rotation, and the impact of the control system, highlight the necessity for specialized tools capable of accurately modelling the different subsystems. To properly analyse both the structural and the dynamic responses, time-domain simulations that integrate nonlinear aero-hydro-servo-elastic effects are indispensable for capturing the dynamics of the system performance under different operational scenarios [29, 33–35]. One of the pieces of software built following this approach is OpenFAST [36], which is a widely-used open-source tool for simulating the coupled dynamic response of wind turbines in time domain. It is programmed in Fortran 95, and it might be considered not as a single program, but as a framework that couples computational modules for aerodynamics, hydrodynamics for offshore structures, control and electrical system dynamics, and structural dynamics. OpenFAST is a developing code with broad acceptance within the technical and scientific communities [37–40]; however, it currently lacks advanced models to represent dynamic interactions with soil and foundation. At the moment, two different methodologies are available for modelling soil-structure interaction within the SubDyn module [41]. The first approach utilizes the soil-structure interaction stiffness and mass matrices at the partially restrained bottom joints (constant springs). The second approach employs the apparent fixity (AF) method [42], which the foundation flexibility is represented by inclusion of a beam with fixed base below the mudline. Although the original version does not provide advanced models, various researchers and developers have been actively investigating and implementing alternative methodologies within OpenFAST [43–46].

1.3 Aims and objectives

This doctoral dissertation aims at advancing in the understanding of the dynamic and seismic structural response of offshore wind turbines supported by jacket structures with multiple supports on piles or suction caissons. In this way, the research aims to contribute to the advancement of this technology, particularly for applications in deep waters and locations with seismic risk.

The objectives of this project are fundamentally two:

1. To advance the development of methodologies, models, and tools for the dynamic and seismic analysis of jacket support structures for offshore wind turbines founded on the seabed, including advanced models of soil-foundation-structure dynamic interaction and taking into account the characteristics of the foundation soil.

2. To deepen the understanding of two relatively unexplored aspects in jacket substructures that may determine design outcomes in areas with significant seismic risk:

    - The study of foundation-soil-foundation dynamic interaction phenomena occurring in multi-supported structures.
    - The analysis of the influence of kinematic interaction on the overall seismic response of the system.

1.4 Research group

The research group of the Continuum Mechanics and Structures Division, where this PhD thesis is developed, specializes in the formulation and implementation of numerical models to solve problems related to structural dynamics and elastic wave propagation. The models created have provided numerical solutions to a variety of issues, including soil-water-structure interaction, seismic response of vault dams, soil-structure interaction problems, dynamic response of pile foundations or buried structures, dynamic behavior of poroelastic media, outdoor acoustic propagation, and the study and optimization of noise barrier effectiveness.

In this context, the research group has applied its experience in infinite media problems to address another important challenge: the design and analysis of support structures for offshore wind turbines. This is a critical issue, where the influence of soil-structure interaction on these devices must be considered. The present doctoral dissertation is based on previous work carried out by the research group in this field.

The development of models for analysing the dynamic and seismic response of the support structure of OWTs and their foundation are challenges that have been addressed by the group in two research projects: “Advances in the Development of Numerical Models for the Dynamic Characterization of Foundations for Wind Turbines” (BIA2014-57640-R, 2015-2017) and “Influence of Soil-Structure Interaction Phenomena

on the Seismic Response of Offshore Wind Turbines" (BIA2017-88770-R, 2018-2020). In the first project, two advanced numerical models of the soil-foundation system were formulated and implemented to analyse the dynamic response of OWT foundations using piles [17] or suction caissons [18]. In the second project, integrated models were developed to study the dynamic structural response while accounting for soil-structure interaction. These models incorporate all relevant elements (seabed, foundations, substructure, tower, and rotor-nacelle-blades) and their mutual interactions. Three different types of foundations were considered, with each specific case comprising one or several individual elements: a) gravity foundations, b) suction caissons (or buckets), and c) monopiles and piles.

During the course of this thesis, the research group has been actively involved in two projects within this field: (a)" Design of Offshore Wind Turbine Support Structures Using Neural Networks Including Advanced Soil-Structure Interaction Models and Seismic Excitation" (PID2020-120102RB-I00), aimed at deepening the understanding of certain aspects related to the seismic response of wind turbine support structures and the application of machine learning techniques for their design; and (b) "Computational Models for Structural Analysis of the Dynamic Response of Offshore Wind Turbines Founded on the Seabed. In addition, the influence of soil-structure interaction phenomena and application to the Canary Islands" (ProID2020010025), primarily focused on investigating the influence of soil-structure dynamic interaction phenomena on the dynamic characteristics of these structures, with particular application to the Canary Islands region.

The work presented in this thesis aligns with and extends the thematic focus of the research group, contributing to the advancement of knowledge in these lines of work, as the research presented here aims to develop dynamic and seismic analyses of jacket substructures through advanced numerical modelling. The study integrates the consideration of various subsystems and nonlinear phenomena, incorporating the influence of the dynamic soil-structure interaction in multi-supported substructures.

1.5 Published works derived from the PhD Thesis

The first three contributions in JCR journals listed below collectively constitute the compendium thesis. Additionally, two collaborations in JCR journal and various contributions to conferences derived from the doctoral thesis are also listed.

1.5.1 Contributions in JCR journals

- C. Romero-Sánchez and L. A. Padrón. Influence of wind and seismic ground motion directionality on the dynamic response of four-legged jacket-supported offshore wind turbines. Engineering Structures, 300:117191, 2024.
- C. Romero-Sánchez and L. A. Padrón. Seismic response of jacket-supported offshore wind turbines for different operational modes considering earthquake directionality. Ocean Engineering, 311:118798, 2024.

- C. Romero-Sánchez, J. D. R. Bordón and L. A. Padrón. Influence of foundation–soil–foundation interaction on the dynamic response of offshore wind turbine jackets founded on buckets. Journal of Marine Science and Engineering, 12(11):2089, 2024.

- A. J. Romero-Monzón, C. Romero-Sánchez, G. M. Álamo and L. A. Padrón. Can a simple static-equivalent model be used to predict major trends in the dynamic structural response of monopile offshore wind turbines?. Applied Sciences, 15(3):1633, 2025.

- A. M. Kaynia, D. M. Pedersen, H. Askheim and C. Romero-Sánchez. Implementation of seismic soil-structure interaction in OpenFAST and application to an offshore wind turbine on jacket structure. Marine Structures, 103:103832, 2025.

1.5.2 Conference contributions

- C. Romero-Sánchez and L. A. Padrón. Implementation of ground input motion and dynamic soil-structure interaction into OpenFAST for the seismic analysis of offshore wind turbines. Congress on Numerical Methods in Engineering, 2022.

- C. Romero-Sánchez and L. A. Padrón. An implementation of multi-support input motion into OpenFAST for the earthquake analysis of offshore wind turbines. COMPDYN Proceedings, 2023.

- C. Romero-Sánchez, L. A. Padrón, G. M. Álamo, C. Medina, J. J. Aznárez and O. Maeso. Comparative study of the influence of kinematic interaction on the seismic response of monopile and jacket supported offshore wind turbines. In Journal of Physics: Conference Series, volume 2647, 112002. IOP Publishing, 2024.

- C. Romero-Sánchez and L. A. Padrón. Dynamic structural response of four-legged jacket-supported offshore wind turbine considering the effect of wind and seismic ground motion directionality. 3rd Conference on Structural Dynamics (DinEst 2024), 2024.

1.6 Justification of the thematic unity and coherence of the PhD Thesis

The design of multi-supported structures, such as jacket substructures, is particularly complex, as it not only involves meeting structural strength requirements under specific conditions but also ensuring additional criteria related to the dynamic response of the wind turbine and maximizing the service life of the entire system, aspects that are closely interconnected. Moreover, dynamic interaction phenomena with the seabed can be significant, depending on the properties of both the seabed and the type of

foundation used. Consequently, the study of this problem generally requires analytical models that account for all involved components (structure, foundation, and seabed), their mutual interactions, and, in particular, the characterization of the seabed as a semi-infinite and, in general, heterogeneous medium.

Initially, the thesis focuses on coupling the advanced soil-foundation-structure dynamic interaction models developed by the research group with a hydro-aero-structural code for wind turbines capable of detailed dynamic response modelling. Specifically, the employed hydro-aero-structural code is OpenFAST [36], the open-source code supported by the National Renewable Energy Laboratory for this purpose. Given the nonlinear nature of certain subsystems within the wind turbine (which is also a time-variant system), the system state equations are solved in the time domain using a step-by-step scheme. In contrast, the advanced models developed by the group have been formulated in the frequency domain [17, 18, 56], allowing for the utilisation of its advantages in dynamic system analysis. Therefore, it is necessary to explore and implement the required numerical and methodological strategies to enable coupling of both schemes. Figure 1.2 summarises schematically the proposed implementation of the dynamic soil-structure interaction in OpenFAST [53].

On the other hand, verifications of the resulting models through comparison with results, available in the scientific literature are presented in different publications [52, 53]. Subsequent to the integration and verification of the methodology, different studies were conducted to investigate the dynamic and seismic behaviour of jacket substructures:

- The influence of wind and seismic ground motion directionality on the dynamic response of four-legged jacket-supported OWTs is studied in the first publication [47]. The study discusses the specific ranges of the angle of misalignment between wind and seismic shaking directions within which the maximum internal forces are expected to be found.

- The analysis of the seismic response for different operational modes for jackets on piles is presented in the second publication [48]. The study aims to analyse how jacket-supported OWTs functioning in three different operational modes (power production, emergency shutdown and parked mode) respond to seismic actions when subject to different incoming wind directions and ground motion shaking directions.

- Finally, the third research publication investigates the impact of soil–structure interaction and foundation–soil–foundation interaction on the dynamic behaviour of jacket substructures founded on buckets for offshore wind turbines [49].

Additionally, the influence of kinematic interaction phenomena on the dynamic and seismic response of offshore wind turbines supported by multi-supported jacket structures founded on piles or suction caissons has been evaluated. In particular, a comparative study was conducted in [54] to examine the influence of kinematic interaction on the seismic response of monopile and jacket supported OWTs.

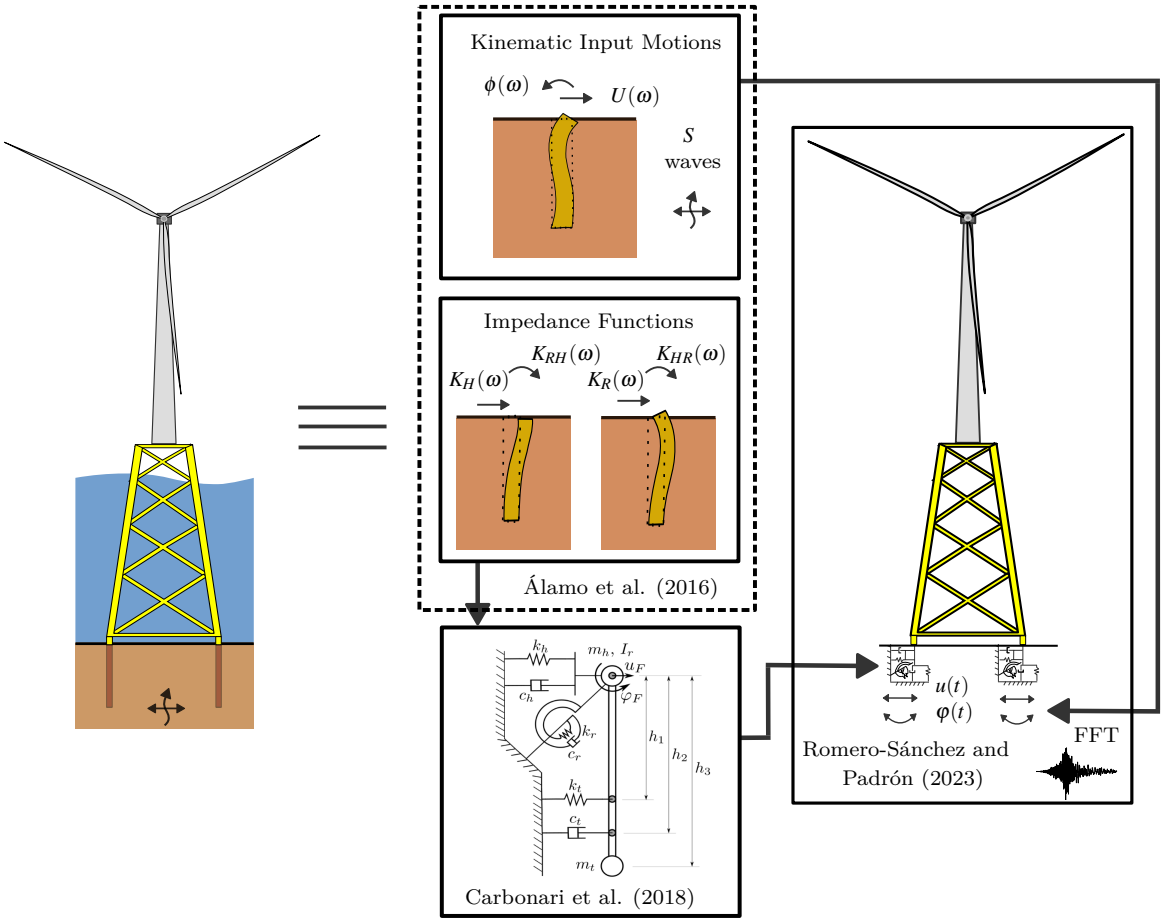

Figure 1.2. Schematic soil-structure interaction modelling in aero-servo-hydro-elastic code.

This document is structured into three chapters. The first comprises the current introduction, the second contains the published papers that constitutes the compendium thesis, and the third provides a summary of the main conclusions and future directions derived from this piece of research. Furthermore, Appendix A contains three additional conference papers and the final appendix provides a summary of the work in Spanish.

2. Publications

2.1 First publication: Romero-Sánchez and Padrón, 2024, Influence of wind and seismic ground motion directionality on the dynamic response of four-legged jacket-supported Offshore Wind Turbines, Engineering Structures.

2.2 Second publication: Romero-Sánchez and Padrón, 2024, Seismic response of jacket-supported offshore wind turbines for different operational modes considering earthquake directionality, Ocean Engineering.

2.3 Third publication: Romero-Sánchez et al., 2024, Influence of Foundation-Soil-Foundation Interaction on the Dynamic Response of Offshore Wind Turbine Jackets Founded on Buckets, Journal of Marine Science and Engineering.

2.4 Autorship documents

2.1 First publication: Romero-Sánchez and Padrón, 2024, Influence of wind and seismic ground motion directionality on the dynamic response of four-legged jacket-supported Offshore Wind Turbines, Engineering Structures.

Table 2.1. First publication data.

Title	Influence of wind and seismic ground motion directionality on the dynamic response of four-legged jacket-supported Offshore Wind Turbines
Authors	C. Romero-Sánchez and L.A. Padrón
Journal	Engineering Structures
DOI	10.1016/j.engstruct.2023.117191
ISSN	0141-0296
Impact factor	5.6
CiteScore	10.2
Category	ENGINEERING, CIVIL
Quartile	Q1
Publisher	ELSEVIER SCI LTD
Volume	300
Date	February 2024

Engineering Structures 300 (2024) 117191

Contents lists available at ScienceDirect

Engineering Structures

journal homepage: www.elsevier.com/locate/engstruct

Influence of wind and seismic ground motion directionality on the dynamic response of four-legged jacket-supported Offshore Wind Turbines

Carlos Romero-Sánchez *, Luis A. Padrón

Instituto Universitario de Sistemas Inteligentes y Aplicaciones Numéricas en Ingeniería (SIANI), Universidad de Las Palmas de Gran Canaria (ULPGC), Las Palmas de Gran Canaria, 35017, Spain

ARTICLE INFO

Keywords:
Offshore wind turbine
Jacket
Soil–structure interaction
Ground motion directionality
OpenFAST

ABSTRACT

This paper aims at investigating the influence of the direction of wind and seismic ground motion on the structural response of four-legged jacket support substructures for bottom-fixed Offshore Wind Turbines located in areas with non-negligible seismic risk. To do that, a parametric analysis that considers thirteen seismic shaking directions, seven wind directions and four earthquake records is carried out. The results are presented in terms of accelerations, axial forces, bending moments and shear forces in the jacket substructure. The NREL 5 MW wind turbine supported on the jacket designed for the phase I of the OC4 project is considered. The response of the system is simulated using an OpenFAST model that takes into account multi-support seismic input, soil–structure interaction and kinematic interaction. The results show that load combinations with aligned wind and ground motion directions are never the worst-case scenario. On the contrary, the largest accelerations are found when the shaking direction acts along the side-to-side direction, and the most significant internal forces are usually found when the ground motion is aligned with one of the diagonals of the base of the jacket and not aligned with the wind direction. The paper also discusses the specific ranges of the angle of misalignment between wind and seismic shaking directions within which the maximum internal forces are expected to be found.

1. Introduction

The distance from the coast and the depth at which offshore wind farms are being installed has been increasing due to several reasons, among which one can cite the expansion of the technology and the opening of new markets, the need to avoid environmentally protected areas, or the visual pollution from Offshore Wind Turbines (OWT) installed near the coastline. Although floating wind energy is being rapidly developed, fixed-base wind turbines are still the dominant technology and a feasible possibility in many cases. In the case of significant depths, jacket support structures tend to be an option. In fact, although the monopile is clearly the preferred technology, jackets are the second preferred choice of developers (11.6% in 2021) and are expected to account for 13.4% of the near future [1].

Thus, fixed-base offshore wind turbines are moving to larger depths and, due to the expansion of the technology over the world, they are also increasingly being installed or planned in higher seismic risk areas. These two factors (depth and seismic risk) increase the relevance of Soil–Structure Interaction (SSI) on the design and on the response of the support structures of these turbines. Current standards and design guidelines state that earthquake resistance should be demonstrated for locations where seismic loads might be critical [2,3], but the experience in this field is limited because the technology is relatively recent for such sites.

The extensive research on the influence of dynamic SSI in the field of monopile-supported OWTs has repeatedly demonstrated that it significantly modifies the dynamic response of the system (see, for instance, [4–7]). Some of the strategies employed to take SSI into account in the analysis of the seismic response of monopiled offshore wind turbines are the use of: linear or non-linear springs and dashpots as part of the structural models [8–11], frequency-dependent stiffness and damping functions to represent the monopile–soil subsystem [7], Lumped Parameter Models (LPM) to fit impedance functions of monopile–soil subsystems into time-domain simulations [12,13], nonlinear Winkler p-y and Q-z springs [14–16], or finite element models of the system as a whole, including support structure, foundation and surrounding soil [17,18]. In all these studies, the foundation dynamic characteristics play a fundamental role in the overall dynamic and seismic response of the support structure and in the reduction of the damage.

The amount of research devoted to the study of the dynamic response of OWTs on jacket substructures taking SSI into account is

* Corresponding author.
E-mail addresses: carlos.romero@ulpgc.es (C. Romero-Sánchez), luis.padron@ulpgc.es (L.A. Padrón).

https://doi.org/10.1016/j.engstruct.2023.117191

Available online 22 November 2023
0141-0296/© 2023 The Author(s). Published by Elsevier Ltd. This is an open access article under the CC BY-NC-ND license (http://creativecommons.org/licenses/by-nc-nd/4.0/).

much more limited. The strategies used in case of jacket-supported OWTs founded on piles are, similarly to the case of monopiled OWTs: linear or non-linear springs and dashpots [19], nonlinear Winkler p-y and Q-z springs [20–22] or finite element models [23]. Thus, Alati et al. [20] analysed the response of the NREL 5 MW [24] turbine using a full model implemented in BLADED [25] and considering a jacket substructure founded on piles. The study showed that seismic loading may cause a significant increase of stress resultant demands, demonstrating the need for a seismic assessment in sites at risk from earthquakes. Later, Abhinav and Saha [26] studied the nonlinear dynamic behaviour of jacket-supported OWTs noting that ignoring SSI tends to over-estimate the ultimate strength characteristics of the OWT by 3%–60%. In addition, Abhinav and Saha [27] demonstrated the importance of SSI influence in loose sand and that the response of the jacket under dynamic loading is largely governed by the stiffness of the soil. On the other hand, Jalbi and Bhattacharya [19] developed closed-form solutions for the fundamental frequency of these jacket-supported OWTs taking SSI into account. Later, the same authors proposed a methodology for the design of the jacket substructures in the concept stage [28]. Jalbi et al. [29] also discussed the design of these structures, focused on the importance of the natural frequencies, and suggested that designer needs to optimize the configuration of the jacket and must choose the vertical stiffness of the foundation such that rocking modes of vibrations are prevented as they may interfere with the 1P frequencies of the rotor. At the same time, Gelagoti et al. [23] explored the SSI effects in OWT support structures under seismic loading. This comparative study discussed the structural behaviour of an OWT supported on a monopile and on a four-legged jacket, and the authors concluded that for the same loading combination, jackets may be more efficient in mitigating seismically induced lateral rotations than monopiles.

The effect of ground motion directionality on the seismic dynamic response of monopile supported OWTs was analysed by Mo et al. [30, 31]. These studies were carried out in the time domain using OpenFAST [32] and taking into account different possible modes of operation, parked condition and normal operation. The results showed that the structural responses of the system are significantly affected by the shaking direction. They also found that bi-directional horizontal ground motion cases considering the excitation of the wind turbine in the fore–aft and side-to-side directions result in a significant underestimation of the structural responses while the environmental wind and wave loads can contribute to either mitigate or increase the effect of ground motion directionality. Jackets for OWTs subjected to different shaking directions were studied in some recent papers [33,34]. Ju and Huang [33] established an analysis framework for jacket-supported offshore wind turbines, considering some different ground motion directions (fore–aft, side-to-side and diagonal direction) and environmental loads. The results indicated that the combination of seismic and environmental loads, during power production around the rated wind speed, normally controls the design. A three-dimensional finite element model of the soil–pile–jacket–tower was developed in Abaqus by James et al. [34]. They showed the importance of considering higher modes and multi-directional ground motion, including the vertical component, on the dynamic response of offshore wind turbines. In this regard, it is also worth mentioning the study of Mroczek et al. [35] on the optimal orientation of the jacket structure. Even though seismic loads are not considered in this study, the authors analyse in detail which orientation, relative to the site specific metocean conditions, of a three-legged jacket support structure, can provide the best structural response.

Thus, the influence of wind and ground motion directionality on the dynamic and seismic response of jacket-supported OWTs, and the identification of the most demanding combination, is still an open question. For this reason, this paper aims at studying the influence of wind and seismic ground motion directionality on the structural response of the jacket support structure of offshore wind turbines and at finding out whether there exist a set of combinations of wind and shaking directions that should be paid special attention to. More specifically, the study analyses the structural response of a four-legged jacket substructure for the NREL 5 MW OWT for a set of different wind and ground motion orientations using an OpenFAST model that includes dynamic SSI and multi-support seismic input motions. Kinematic interaction is also taken into account, as the seismic input signals are filtered in order to take into account the effects of the presence of the pile foundations in the stratified soil.

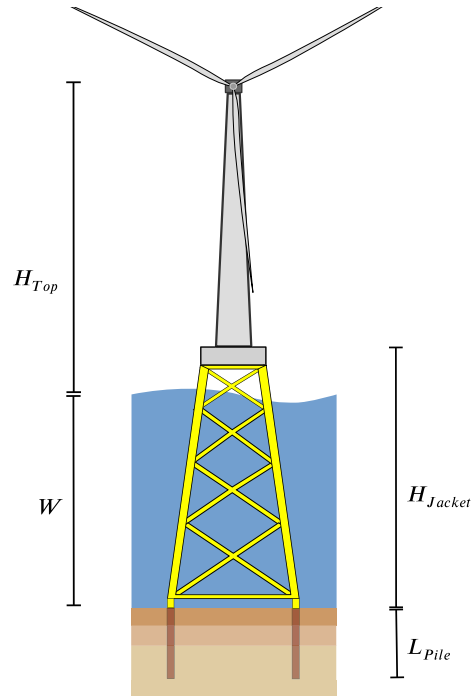

Fig. 1. General description of the jacket-supported OWT.

The present paper is structured in five sections. After the introduction, the parametric study to be performed is presented in Section 2, defining the wind turbine, the jacket substructure, the soil deposit, the seismic signals and the complete set of cases for the analysis. Once the problem has been described, the methodology for the study is presented in Section 3. Section 4 presents the most relevant results and provides a final discussion on the dynamic response of the four-legged jacket-supported OWT. Finally, a summary of the main conclusions from the manuscript is presented in Section 5.

2. Problem case description

2.1. Wind turbine and support structure

The present study on the influence of wind and seismic shaking directionality on the response of jacket-supported OWTs will be performed on the well known NREL 5 MW three-bladed turbine described in [24]. The support structure considered is the jacket support substructure designed for the phase I of the OC4 project, and described by Vorpahl et al. [36]. This four-legged jacket structure is designed using tubular members and consists of four bays. Table 1 and Fig. 1 summarize the main characteristics of the system. The material properties of the steel in the substructure are: Young's modulus $E = 210$ GPa, shear modulus $G = 80.8$ GPa, mass density $\rho = 7850\,\mathrm{kg/m^3}$ and damping ratio $\zeta = 2\%$.

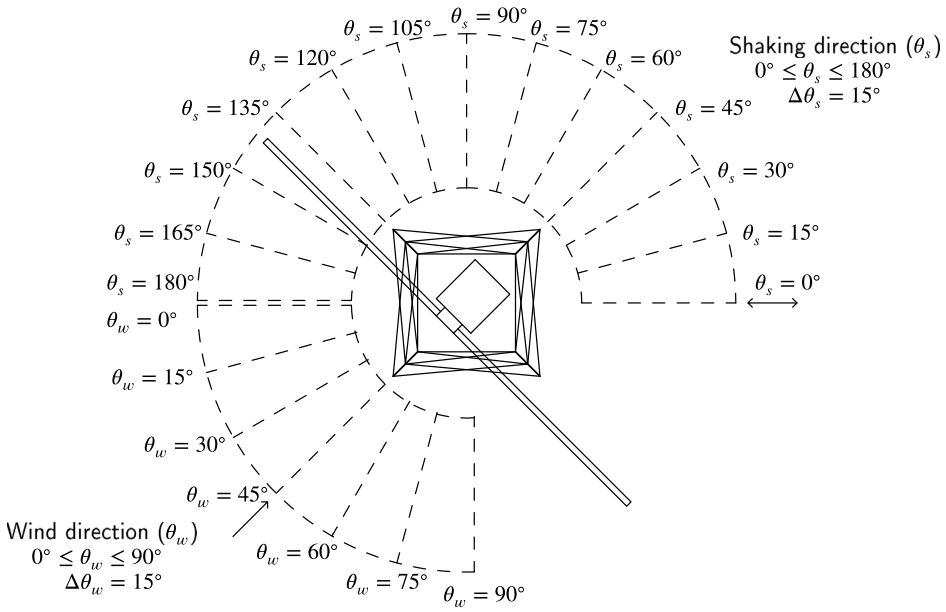

Fig. 2. Definitions of the wind and ground motion directions considered in the parametric analysis. Plan View.

Table 1
Key parameters of the OWT.

Rating [MW]	5
Rated wind speed [m/s]	11.4
Rotor diameter [m]	126
RNA mass [ton]	350
Tower top thickness [mm]	30
Tower base thickness [mm]	32
Tower top diameter [m]	4.00
Tower base diameter [m]	5.60
Tower top height from mean sea level (H_{Top}) [m]	88.15
Tower base height from mean sea level [m]	20.15
Water depth (W) [m]	50.00
Jacket height (H_{Jacket}) [m]	70.15
Number of legs	4
Top leg spacing [m]	8.00
Base leg spacing [m]	12.00
Number of bracing levels	4
Pile diameter [m]	2.082
Pile thickness [mm]	60.00
Pile depth (L_{Pile}) [m]	34.00

Table 2
Properties of the soil deposit.

Soil profile	layered
Type of soil	sand
Poisson's ratio, ν_s [-]	0.35
Density, ρ_s [kg/m^3]	2000
Shear modulus, G_s [MPa]	42.6 ($0 < z < 5$ m)
	61.9 ($5 < z < 14$ m)
	87.4 ($14 < z < \infty$)
Shear wave velocity, v_s [m/s]	145.9 ($0 < z < 5$ m)
	175.9 ($5 < z < 14$ m)
	209.0 ($14 < z < \infty$)
Damping, ζ_s [-]	0.05

The jacket is assumed to be founded on the three-layer sandy soil deposit defined by Jonkman et al. [37] for the OC3 project. Table 2 specifies the properties of the soil profile, while the properties of the piles (summarized in Table 1) are those given by Alati et al. [20].

2.2. Set of cases for analysis

Fig. 2 presents a sketch that illustrates the parametric analysis performed in this study. Assuming a fixed orientation of the four-legged jacket support structure, the study considers a wide range of independent wind and seismic shaking directions, in such a way that a significantly high number of combinations is studied. Taking into account the quarter symmetry of the structure, the wind is assumed to blow in a 90° range, with $0° \leq \theta_w \leq 90°$ and $\Delta\theta_w = 15°$, thus obtaining 7 different cases for the wind direction. Simultaneously, 13 different horizontal ground motion directions are considered within a 180° range, with $0° \leq \theta_s \leq 180°$ and $\Delta\theta_s = 15°$. The load combinations are summarized in Table 3. The dynamic response of the substructure is analysed considering the combination of environmental loads, frequently occurring operational loads and seismic loads, following the requirements established by the design guidelines for locations where seismic actions might be critical (see for instance IEC-61400-1 [2]). Taking into account the four seismic signals described below, all different combinations result in a total of 380 simulations, including two additional cases in parked mode and without SSI. Each simulated case has a total duration of 300 s, with the earthquake ground motion starting at $t = 200$ s, after the stationary operational response of the system has already been reached. The turbine is simulated in a power production operating mode. The wind turbine remains in power production mode when the earthquake occurs, i.e., the generator continues to run normally (emergency stop is not considered). In all cases, peak responses for any given variable are computed as $R_p = \max[(R_x(t)^2 + R_y(t)^2)^{1/2}]$, where $R_x(t)$ and $R_y(t)$ are the time histories of the responses along x and y directions respectively.

Wind and wave loads are defined according to IEC 61400-3 [38]. The wind loads are computed using Turbsim for a wind speed at hub $V_{hub} = 11.4$ m/s, the rated wind speed of the turbine, and considering Normal Turbulent Model (NTM [2]), Category B turbulent wind fields and a Kaimal spectral model. The hub is always positioned according to the wind direction. Aerodyn is used to computed the aerodynamic loads on blades and tower. In all cases, it is assumed that wind and waves both act in alignment based on IEC 61400-1 [2] and DNV-OS-J101 [3]. The load combinations are defined according to Section 11.6 [2] and to DLC 11.1 [39] of the design guidelines. HydroDyn is used to calculated

Table 3
Description of the set of cases studied.

Operating mode	Wind loads	Wave loads	Earthquakes	Cases
Parked mode			No earthquake	
	Wind speed = 11.4 m/s Category B, NTM	Significant wave height = 8 m Peak-spectral period = 10 s		7
Power production	Kaimal spectrum model $0^o \leq \theta_w \leq 90°$ ($\Delta\theta_w = 15°$)	JONSWAP spectrum Aligned – Wind direction	4 earthquakes $0^o \leq \theta_s \leq 180°$ ($\Delta\theta_s = 15°$) or no earthquake	371

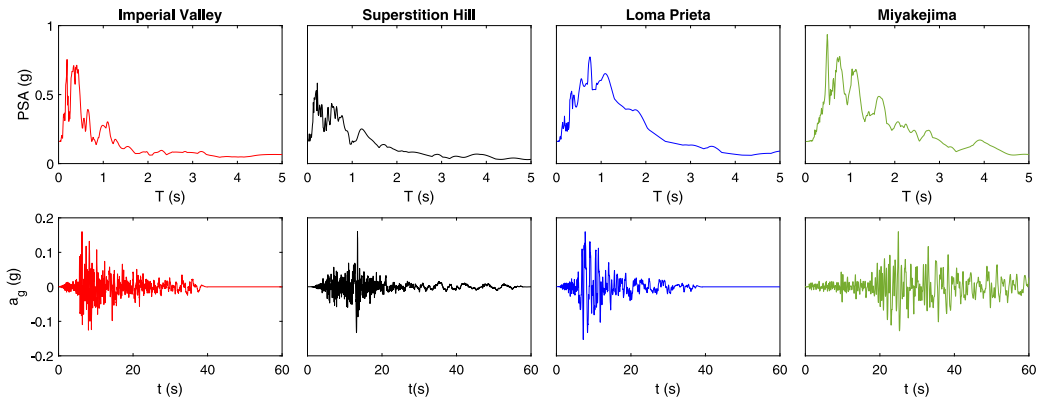

Fig. 3. Normalized pseudo-spectral accelerations (PSA) and accelerograms (a_g) of the selected seismic records.

Table 4
Information about the accelerograms.

Event name	Station name	$a_{g,max}$(g)	Observations	Database
Imperial Valley-06, 1979	Niland Fire Station	0.11	Onshore (RSN:186, Dir: 90°)	PEER
Superstition Hills-02,1987	El Centro Imp. Co. Cent.	0.36	Onshore (RSN:721, Dir: 0°)	PEER
Loma Prieta, 1984	Hollister City Hall	0.22	Onshore (RSN:777, Dir: 180°)	PEER
Miyakejima, 07/30/2000	Hiratsuka-ST1	0.19	Offshore (33.97N,139.40E, Dir: N-S)	K-NET

the wave loads. The significant height of the incident waves is 8 m. Regular and irregular waves are included.

2.3. Definition of the seismic input ground motions

In order to study the seismic response in this paper, four different accelerograms have been considered. A possible relevant factor in this type of problems is the difference between using accelerograms recorded at onshore or offshore stations (see Zhang and Zheng [40]). For this reason, and in order to evaluate the possible influence of this parameter, the four suitable accelerograms listed in Table 4 are used. Firstly, three acceleration signals from the PEER Ground Motion Database [41] where selected on the basis of the shear wave velocities at the location of the station, so that they are close to the average shear wave velocity of the soil deposit employed in this study. The selected earthquake signals were recorded by stations located over soils whose mean shear waves velocity $V_{s,30}$ is within the range from 190 to 220 m/s. Additionally, a seismic signal recorded at an offshore station was also selected from the K-NET Database [42]. All signals present relatively similar maximum ground accelerations ($a_{g,max}$). Table 4 presents the most relevant information of each recording.

Regarding the evaluation of the magnitudes of the Peak Ground Acceleration (PGA), the International Standard IEC 61400-1 [2] recommends the consideration of a 475-year recurrence period. In this study, a site within the seismic zone 2, structure's exposure level L2 and Seismic Risk Category SRC2 as defined by the ISO 19901-2 [43] is assumed. Spectral response accelerations $S_{a,map}(0.2) = 0.5$ g and $S_{a,map}(1.0) = 0.2$ g at 0.2 s and 1.0 s, respectively, are considered. These values are representative of a moderate seismic hazard, consistently with the hypothesis of linear structural behaviour and, taking into account the recurrence period mentioned above, lead to a PGA of 0.16 g. The selected recorded accelerograms are therefore normalized to this common PGA of 0.16 g, and Fig. 3 presents the normalized pseudo-spectral accelerations (PSA) and the accelerograms. These seismic signals are prescribed at free-field ground surface, and are assumed to be generated by vertically-incident far-field S-waves that produce the seismic ground motion in a particular direction for each configuration.

3. Methodology

The non-linear aero-hydro-servo-elastic code OpenFAST [32] is used herein to simulate the cases described above. In order to take into account Soil–Structure Interaction, ground input motion and Kinematic Interaction, the SubDyn module has been modified with the introduction of an LPM to represent the pile foundations embedded in the stratified soils and with the ability to consider the seismic input motion filtered by translational and rotational Kinematic Input Factors (KIFs). The impedance functions and the KIFs needed to define the systems are previously computed using a BEM–FEM model of the soil–foundation subsystem, as detailed below.

3.1. OpenFAST numerical model

The numerical tool used in this paper is based on OpenFAST [32], which is an open-source multi-physics and multi-fidelity tool for simulating the coupled dynamic response of wind turbines. This code might be considered not as a single program, but as a set of coupled computational modules, each one of them designed to simulate a specific subsystem. The different modules interact in a loosely coupled time-integration scheme, where a glue-code transfers data among modules

at each time step. This glue code is the FAST driver, that gathers all the information and drives the time-domain solution forward step-by-step using a predictor–corrector scheme.

The SubDyn module [44] was modified in order to be able to take into account dynamic soil–structure interaction and multi-support ground input motion. The input subroutine was modified to read the seismic records and the parameters of the soil–structure interaction model. The FEM subroutine and state-space formulation have been also modified. These modifications allow considering seismic loads using OpenFAST only (coupling with other software is not necessary). The code allows not only horizontal, but also vertical and rotational foundation input motion to be considered on multi-support substructures.

The equation of motion of the substructure is written as:

$$\mathbf{M}\,\ddot{\mathbf{u}}(t) + \mathbf{C}\,\dot{\mathbf{u}}(t) + \mathbf{K}\,\mathbf{u}(t) = \mathbf{F}(t) - \mathbf{M_g}\,\ddot{\mathbf{u}}_\mathbf{g}(t) - \mathbf{C_g}\,\dot{\mathbf{u}}_g(t) - \mathbf{K_g}\,\mathbf{u_g}(t) \tag{1}$$

where the expression for the effective seismic loading is obtained by separating the support motion effects from the response quantities and transferring these input terms to right hand side [45]. Thus, the motion vectors are partitioned to separate the response quantities from the input: $\mathbf{u}(t)$ includes the degrees of freedom of the structure and $\mathbf{u_g}(t)$ contains the components of the foundation input motions at each support. The dots represent differentiation with respect to time. The global mass, damping and stiffness matrices have been partitioned accordingly. $\mathbf{F}(t)$ represents the external forces acting at each degree of freedom of the structure. In contrast to the original SubDyn module which assumes a fixed base, the new approach considers that the vector of displacements at the boundary nodes, $\mathbf{u_R}(t)$, contains the displacements at the interface node with the tower, $\mathbf{u_I}(t)$, and the displacements at base nodes, which would move following the ground motion vector.

$$\mathbf{u}_R(t) = \begin{pmatrix} \mathbf{u}_g(t) \\ \mathbf{u}_I(t) \end{pmatrix} \tag{2}$$

The beam elements in the jacket substructure are modelled as Timoshenko three-dimensional beams, and discretized using two-nodes 12 degrees of freedom finite elements defined by the corresponding stiffness and mass matrices, considering linear response and rigid joints. On the other hand, the Craig–Bampton method is used to reduce the number of the internal generalized degrees of freedom of the substructure. Taking all this into account, the general equation of motion is transformed and the derived matrices are partitioned, so that one can write:

$$\begin{bmatrix} \tilde{\mathbf{M}}_{BB} & \tilde{\mathbf{M}}_{Bm} \\ \tilde{\mathbf{M}}_{mB} & I \end{bmatrix} \begin{pmatrix} \ddot{\mathbf{u}}_I(t) \\ \ddot{\mathbf{q}}_m(t) \end{pmatrix} + \begin{bmatrix} \tilde{\mathbf{C}}_{BB} & \tilde{\mathbf{C}}_{Bm} \\ \tilde{\mathbf{C}}_{mB} & \mathbf{C}_{mm} \end{bmatrix} \begin{pmatrix} \dot{\mathbf{u}}_I(t) \\ \dot{\mathbf{q}}_m(t) \end{pmatrix} + \begin{bmatrix} \tilde{\mathbf{K}}_{BB} & 0 \\ 0 & \mathbf{K}_{mm} \end{bmatrix} \begin{pmatrix} \mathbf{u}_I(t) \\ \mathbf{q}_m(t) \end{pmatrix} = \begin{pmatrix} \tilde{\mathbf{F}}_{tp}(t) \\ \tilde{\mathbf{F}}_m(t) \end{pmatrix} - \begin{bmatrix} \mathbf{M}_{Ib} \\ \mathbf{M}_{mb} \end{bmatrix} \ddot{\mathbf{u}}_g(t) - \begin{bmatrix} \mathbf{C}_{Ib} \\ \mathbf{C}_{mb} \end{bmatrix} \dot{\mathbf{u}}_g(t) - \begin{bmatrix} \mathbf{K}_{Ib} \\ \mathbf{K}_{mb} \end{bmatrix} \mathbf{u}_g(t) \tag{3}$$

where $\mathbf{M}_{[..]}$, $\tilde{\mathbf{M}}_{[..]}$, $\mathbf{C}_{[..]}$, $\tilde{\mathbf{C}}_{[..]}$, $\mathbf{K}_{[..]}$ and $\tilde{\mathbf{K}}_{[..]}$ are the resulting mass, damping and stiffness submatrices, which are computed during initialization; $\mathbf{q}_m(t)$ and $\tilde{\mathbf{F}}_m(t)$ represent the displacements and the external forces at the interior nodes approximated by a subset of the interior generalized DOFs; and $\tilde{\mathbf{F}}_{tp}(t)$ are the forces at the transition piece. The right-hand side of the equation shows the external forces on the substructure and the effective seismic loading. State-space formulation of the substructure structural dynamic is used to integrate SubDyn into the FAST driver. The equation of motion is cast into standard linear system state equation of the form:

$$\dot{\mathbf{x}}(t) = \mathbf{A}\mathbf{x}(t) + \mathbf{B}\mathbf{u}(t) + \mathbf{F}_x(t) \tag{4}$$

where $\mathbf{A}$ and $\mathbf{B}$ are matrices of constants coefficients.

The implementation of the multi-support input motion and of the dynamic soil–structure interaction model have been verified by comparison against results obtained from a finite-elements beam model of the offshore wind turbine without wind or waves. More details about the modifications and the verification cases are described in Romero-Sánchez and Padrón [46]. The code is available in OpenFAST version 3.0.0 and can be downloaded at: https://github.com/mmc-siani-es/openfast_3.0.0_multisupport.

Table 5
OWT Natural frequencies.

	Fixed-base model	Flexible-base mode
1st side-to-side mode	0.314 Hz (3.18 s)	0.302 Hz (3.31 s)
1st fore–aft mode	0.316 Hz (3.16 s)	0.300 Hz (3.33 s)
2nd side-to-side mode	1.165 Hz (0.86 s)	0.987 Hz (1.01 s)
2nd fore–aft mode	1.213 Hz (0.82 s)	0.949 Hz (1.05 s)

3.2. Soil–structure interaction and seismic action modelling

The impedance of the soil–foundation subsystem is introduced in the model through individual simplified Lumped Parameter Models for each pile foundation at the base of each leg. The mathematical details of this LPM are described in Carbonari et al. [47], while the details about its implementation into SubDyn can be found in Romero-Sánchez and Padrón [48]. This LPM configuration allows to model and fit the translational $K_{xx}(\omega)$, rotational $K_{\theta\theta}(\omega)$ and coupled horizontal-rocking $K_{x\theta}(\omega)$ complex-valued impedance functions simultaneously, while the spring–damper model is adopted for vertical $K_{zz}(\omega)$ and torsional $K_t(\omega)$ impedances. It also allows to introduce the most relevant aspects of these frequency-domain impedance functions into the time-domain simulation of the whole system in OpenFAST.

The lateral and rotational KIFs quantify the filtering effect that the presence of the foundation produce over the incoming seismic waves. Thus, these complex-valued frequency-domain factors $I_u(\omega)$ and $I_\theta(\omega)$ are defined as the ratio between the pile head displacement or rotation and the free-field motion. To obtain these functions, the embedded portion of a single pile, in the soil profile under consideration, is assumed to be subjected to vertically-incident S-waves. The standard Frequency Domain Method of response [49] is employed to filter the earthquake signals according to these KIFs.

Impedance functions and KIFs are all computed using the numerical model described by Álamo et al. [50] for the dynamic analysis of pile foundations in complex soil profiles. This model is based on the use of the integral expression of the reciprocity theorem together with specific Green's functions for a viscoelastic layered half-space for representing the soil behaviour, including its radiation and material damping.

Table 5 presents the first and second side-to-side (SS) and fore–aft (FA) natural frequencies of the system, obtained from the SS and FA accelerations at the tower top, when the wind turbine is in parked conditions and subjected to environmental loads. These computed values are very close to those obtained by Alati et al. [20] for this case. In order to show the relevance of soil–structure interaction, these natural frequencies are listed considering both fixed-base and flexible-base models. As expected, soil–structure interaction plays a significant role in the reduction of the natural frequency, causing, for instance, a 5% reduction in the fore–aft fundamental frequency.

In Fig. 4, these natural frequencies are presented on top the acceleration response spectra of the considered earthquakes. This figure highlights the fact that, even though all four seismic signals have been normalized to a common peak ground acceleration, the spectral values for the different earthquakes differ significantly around both natural frequencies. In most cases, the largest spectral values are found for the Loma Prieta signal, while the lowest are found for the Superposition Hill record. These observations will have an impact on the different functions that will be analysed later.

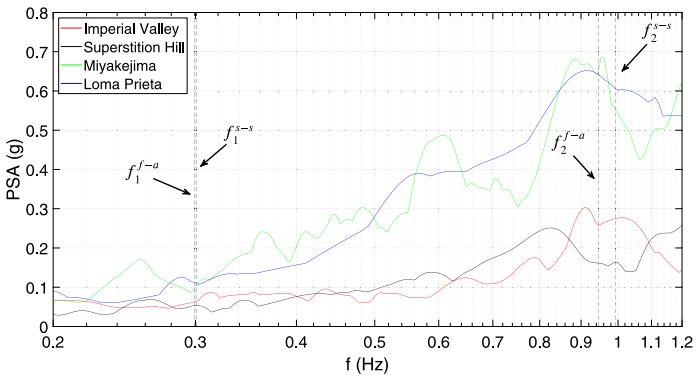

Fig. 4. Acceleration response spectra of the seismic signals considered and first and second natural frequencies of the structural system.

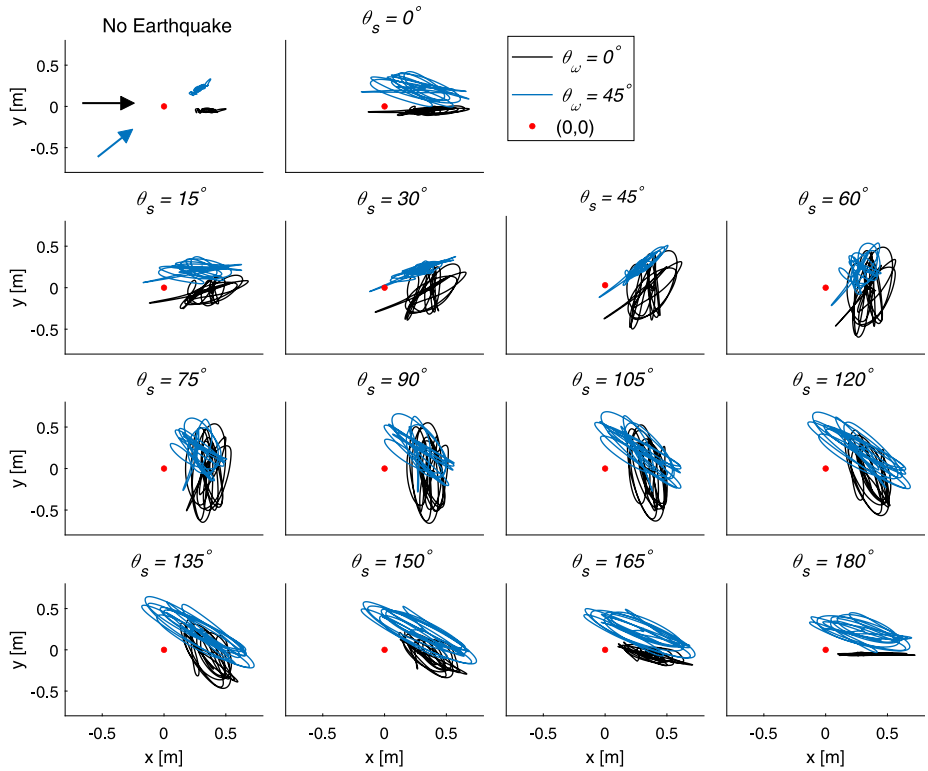

Fig. 5. Trajectories at the tower top during the seismic shaking, for the Loma Prieta seismic input and for $\theta_w = 0°$ and 45°.

4. Results

4.1. General response and tower top trajectories in different scenarios

The influence of the different load scenarios described in Section 2 can be qualitatively understood from Fig. 5, where the trajectories of tower top under the thirteen different ground motion directions for the Loma Prieta earthquake signal, and two wind directions, are depicted. The motions corresponding to the $\theta_w = 0°$ and 45° incoming wind directions are plotted in black and blue curves, respectively, and two arrows of the same colours are included in the first plot (in absence of earthquake) to represent such wind directions. The red dot represents the initial position of the tower top in unloaded conditions. In all cases, the motions are plotted between $t = 200$ and $t = 240$ s, coinciding with the duration of the seismic shaking.

These plots provide a sense on how the structural system is responding at the different configurations. When wind and seismic shaking directions are aligned (cases $\theta_w = 0°$ and $\theta_s = 0°$ or 180°, or $\theta_w = \theta_s = 45°$) the trajectories are located along an elongated area. As expected, motions describe a wider area when wind and seismic ground motion directions are misaligned. The major axis of the ellipse drawn during the motions tend to be oriented with the shaking direction, for this particular seismic input. When wind and ground motion direction are perpendicular (for instance, for $\theta_w = 0°$ and $\theta_s = 90°$) trajectories describe the largest area. In this regard, it is also observed that the amplitude of the excursion due to the seismic shaking (the length of the major axis of the ellipse) when wind and ground motion direction

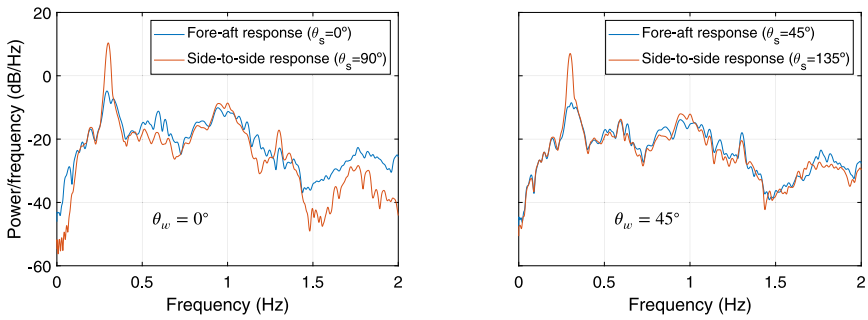

Fig. 6. Power Spectral Densities obtained from the tower top accelerations in power production conditions, under the Loma Prieta seismic input and for $\theta_w = 0°$ and 45°.

are perpendicular is significantly larger that the excursion due to the seismic shaking when wind and ground motion are aligned. This is because, in the first case, the shaking takes place in the side-to-side direction, for which the aeroelastic damping is much smaller than in the fore–aft direction. Another way to analyse the influence of the aeroelastic damping is to perform a frequency domain comparison. Fig. 6 presents the Power Spectral Densities obtained from the tower top accelerations under power production conditions. The wind direction is considered in two different cases (θ_w = 0° and 45°) and the Loma Prieta earthquake acts in fore–aft and side-to-side directions. As expected, the accelerations signals in fore–aft direction (blue line) are more damped than in the side-to-side direction. This phenomenon is due to the aeroelastic damping induced by the sweeping rotor in the fore–aft direction when the wind turbine is in operational conditions. This observation will be relevant later to provide some insight on how internal forces evolve for the different configurations. It is also worth noting that, in absence of seismic input and for both wind directions, the trajectories of the tower top are not exactly aligned with the undeformed (0,0) position due to the fact that the rotor is rotating and its effects are not symmetrical in the side-to-side direction.

4.2. Influence of ground motion directionality and seismic input signal

To study the influence of ground motion directionality and seismic input signal, Fig. 7 shows the peak responses of accelerations and several internal forces for all earthquake considered in this study. Specifically, the peak accelerations obtained at the transition piece, and the peak bending moments, axial and shear forces at specific nodes of the jacket substructure, are presented for all shaking directions in polar plot format. Results for θ_w = 0° and 90° are considered. A different colour has been used for each earthquake, considering the same colours as in Fig. 3. The internal forces are presented, for each case, at the jacket node where the highest peak value is registered for each one of the variables. In this regard, Fig. 8 illustrates the locations at which the peak internal forces are found. The nodes where the peak axial forces are developed are located near the bottom of the jacket legs, at the joint with the bottom bracing, while the greatest shear forces arise at the nodes of the upper part of the jacket legs, at the joint with the upper bracing. Finally the highest bending moments can be found at the nodes where the jacket is connected to each pile head, at mudline level. The descriptions of these locations hold true for all configurations even though the specific leg, among the four legs of the jacket, at which the peak value is located in every case, will obviously depend on the directions of wind and seismic shaking.

Fig. 7 shows that the evolutions observed for the different variables as a function of the ground motion direction θ_s are qualitatively equivalent among the different earthquakes considered, but the magnitude of the effects of each one of the seismic signals is clearly different. The Loma Prieta is the input signal that produces the largest accelerations and internal forces, while the Superstition Hill record generates significantly smaller effects. This is due to the differences found in the response spectra of the different earthquakes, especially around the natural frequencies of the system, as described in Section 3.2 (see Fig. 4). Thus, the shape of the polar plot for a particular variable and wind direction is common to the four earthquakes, although the scales change.

The evolution of the peak accelerations at the transition piece with the seismic shaking direction is quasi-symmetrical about the 90° axis. The maximum accelerations occur when the directions of wind and ground motion are perpendicular to each other (i.e., when the shaking acts along the side-to-side direction) and the minimum accelerations occur when both directions are aligned (i.e., when the shaking acts along the fore–aft direction). This is the expected behaviour, as aerodynamic damping is always much smaller in the side-to-side direction. Differences in these peak accelerations due to the ground motion directionality can reach percentages of 20%.

The evolution of the internal forces with the shaking direction is less symmetrical. Different from the previous case, where maximum peak accelerations at the transition piece arose for θ_s = 0° and 90° along the side-to-side directions, maximum peak internal forces develop, in most cases, for θ_s = 45° or 135° for any of the two considered wind directions. Minimum peak values are often found for θ_s = 0°, 90° or 180°, especially in the case of axial forces. Regarding the bending moments, an intersection between the curves corresponding to $\theta_w = 0°$ and 90° is produced when the shaking acts at 45° for all earthquakes. The highest peak response is produced at θ_s = 135°. The shapes of the polar curves, specially those of axial forces and shear forces, are evidently due to the relative orientation between the layout of the base of the structure and the direction defined as 0°, with a 45° angle between $\theta_w = 0°$ and the diagonal between legs (see Fig. 2). It is also clear from the results that, as expected, ground motion directions of 0° or 180° are not equivalent. Also, the polar plots obtained for the shear force for $\theta_w = 0°$ and 90° are almost identical, while the rest of response functions show a significant dependence on wind direction.

4.3. Influence of wind direction

Fig. 9 presents the evolution of the peak axial forces and bending moments at the nodes mentioned above (see Fig. 8) for all wind directions. Again, shaking direction is represented in the polar axis while, in this case, the different curves represent the different wind directions. In order to focus on the influence of wind direction on the system response, results are presented for only one seismic signal (Loma Prieta).

In this case, both peak axial forces and peak bending moments tend to reach the maximum values for θ_s = 135° and θ_w = 0°, with these internal force decreasing for increasing θ_w for this shaking direction. However, this trend, as a function of θ_w, is not common to all ground motion directions and is almost the opposite, for instance, for $\theta_s = 0°$. At $\theta_s \simeq 45°$, a crossing between the wind lines is observed for the peak

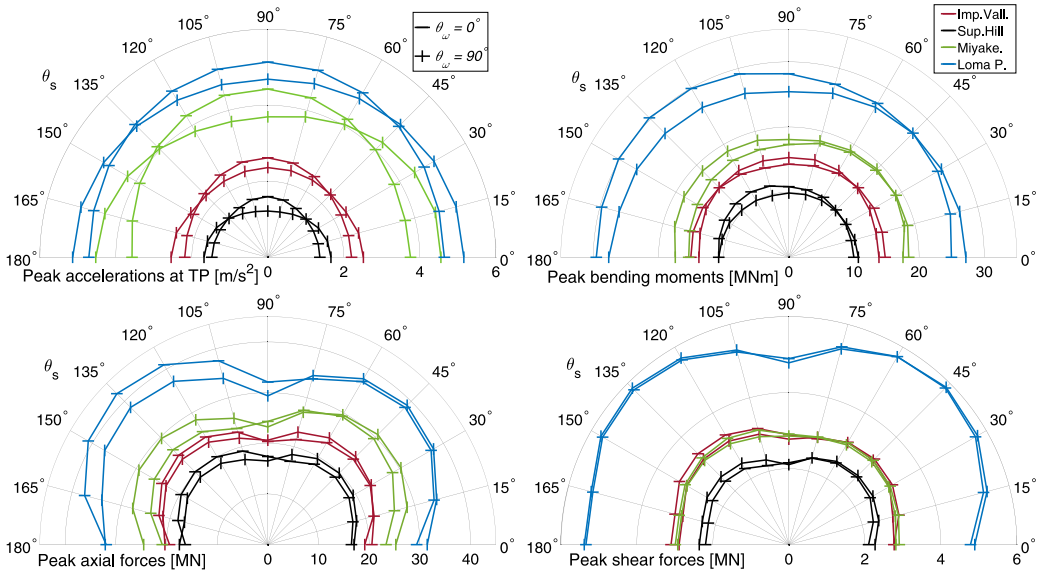

Fig. 7. Influence of seismic shaking direction on the peak response values in terms of accelerations at the transition piece, and of bending moments, axial and shear forces for $\theta_w = 0°$ and 90°.

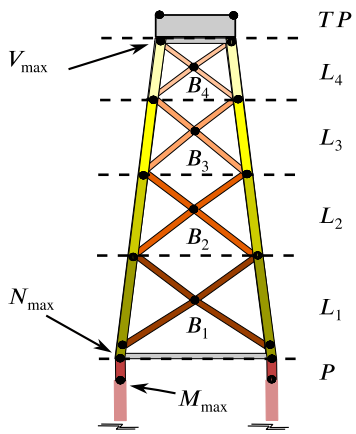

Fig. 8. Locations at which the different peak internal forces in the jacket substructure arise.

bending moments, while this point of crossing moves to $\theta_s \simeq 75°$ in the case of the axial forces. As mentioned above, the location of the maximum axial forces is affected by the geometry and orientation of the jacket, since the highest peak responses are found in this case when the earthquake acts in the direction of one of the supports.

The analysis of the results in terms of not only peak values, but also root mean square (rms) values, is useful to understand whether the observed trends are consistent along the responses, and are not only representative of isolated peaks. For this reason, Fig. 10 presents the rms values in terms of axial forces and bending moments, under the Loma Prieta earthquake, in such a way that the format of the figure is equivalent to that of Fig. 9. Here, rms values are computed along the significant duration of each seismic signal is presented. The common D_{a595} significant duration [51] is considered, which is defined as the time interval between 5%–95% of the Arias intensity [52]. The comparison between Figs. 9 and 10 shows that the conclusions that can be drawn in terms of both measures are equivalent to each other. The shape and relative magnitudes of the curves is comparable though, of course, magnitudes are different.

In order to examine more closely the influence of wind direction, Fig. 11 shows the variation of internal forces according to some particular ground motion direction for all seismic signals considered in this paper. The x-axis presents the 7 wind directions used, and each line of different colour represents one representative direction of the shaking. In this case, five relevant directions have been considered, specifically, $\theta_s = 0°$, 45°, 90°, 135° and 180°.

No clear common trends are observed between the different earthquakes or directions. However, some interesting conclusions can be drawn from these results. Firstly, the extend of the variation in the computed internal forces is generally larger for different ground motion directions than for different wind directions. In other words, the direction of the seismic shaking tends to have a larger influence on the span of these variables than wind direction. This is particularly so when studying shear forces. However, this is not always true, especially when looking at the axial forces, as the variations produced by shaking or wind directions are similar when the Superstition Hill earthquake is considered. Secondly, maximum peak axial forces and peak shear forces are always found for $\theta_s = 45°$ or 135° (orange and purple lines, respectively). This occurs for all wind directions. In the case of bending moments, this observation does not always hold true, as $\theta_s = 180°$ yields higher bending moments in Superstition Hill and Loma Prieta earthquakes when $\theta_w \geq 30°$. Finally, different behaviours are observed for different earthquakes, with only some exceptions where similar trends can be observed, and with the trends in the results for the Miyakejima earthquake (the only offshore recording) being different from any of the other cases. Thus, the need for considering always different seismic signals of different origins is clear.

4.4. Influence of the misalignment between ground motion and wind directions

After having studied the influence of wind and seismic shaking directions (in absolute terms) on the evolution of peak internal structural forces in the jacket substructure, it is interesting to analyse now the influence of the misalignments $\Delta = \theta_w - \theta_s$ between ground motion and wind directions. To do so, Fig. 12 illustrates the way in which the mean

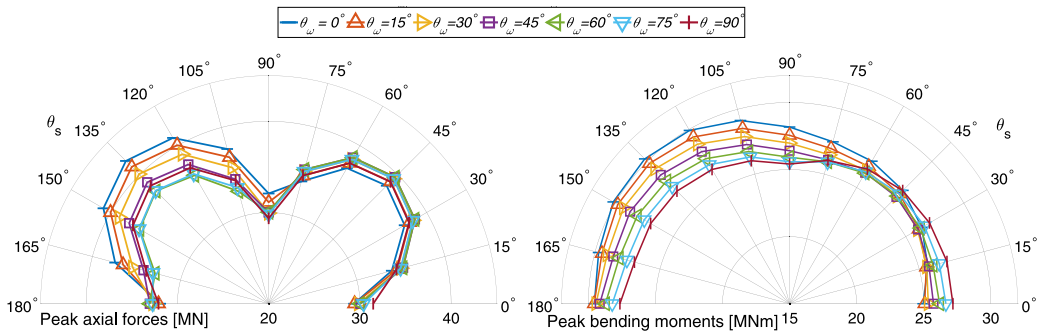

Fig. 9. Peak response values in terms of axial forces and bending moments in the jacket substructure under the Loma Prieta earthquake for all seismic shaking and wind directions.

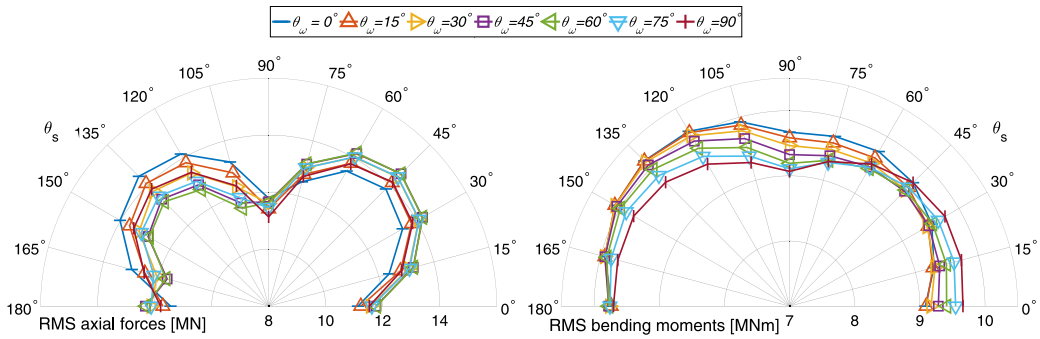

Fig. 10. Root-means-square values in terms of axial forces and bending moments in the jacket substructure under the Loma Prieta earthquake for all seismic shaking and wind directions.

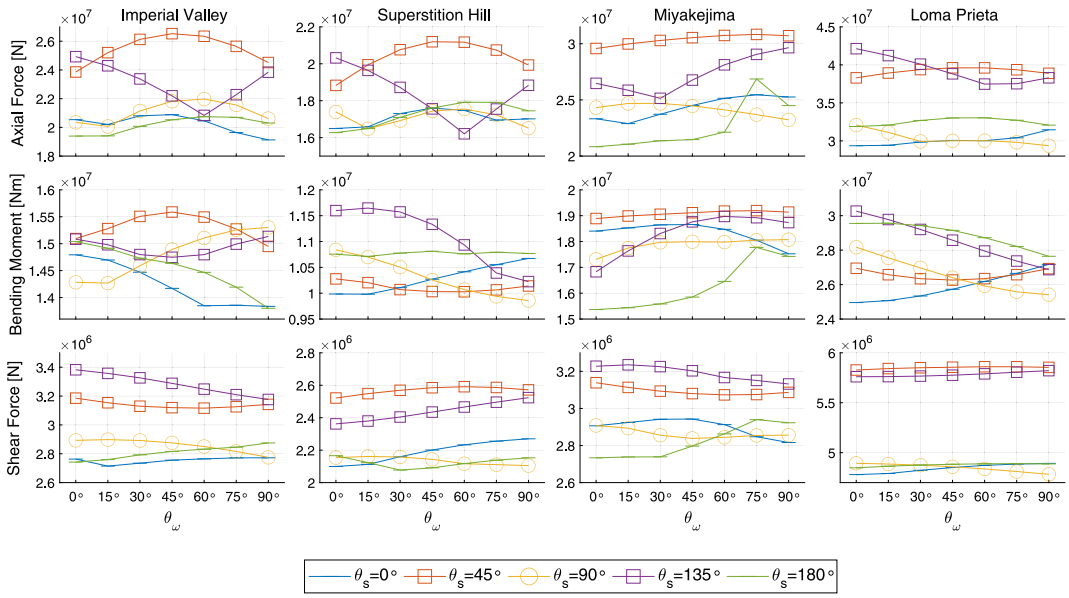

Fig. 11. Influence of wind direction on the peak response values in terms of axial forces, bending moments and shear forces in the jacket substructure for all earthquakes.

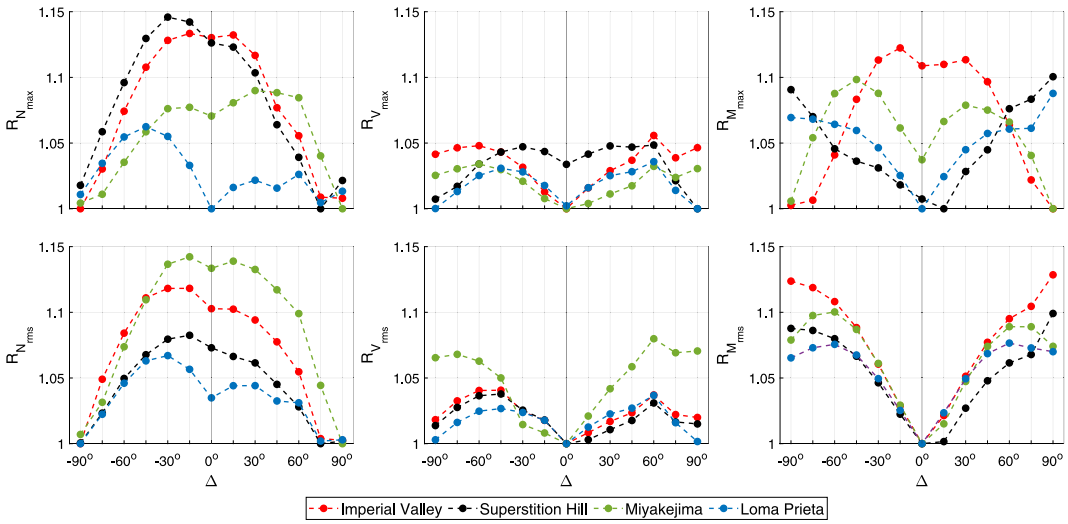

Fig. 12. Amplification ratios for axial forces, shear forces and bending moments for different misalignment angles between wind and ground motion direction.

peak or rms values of the three considered internal forces vary for the different misalignment values. For this purpose, results are presented in terms of the following amplification ratios:

$$R_{X_{max}}(\Delta) = \frac{\sum_{i=1}^{n}\left[X_{max}\left(\theta_{w_i}, \Delta + \theta_{w_i}\right)\right]/n}{\min_{\Delta}\left[\sum_{i=1}^{n}\left[X_{max}\left(\theta_{w_i}, \Delta + \theta_{w_i}\right)\right]/n\right]} \quad (5)$$

$$R_{X_{rms}}(\Delta) = \frac{\sum_{i=1}^{n}\left[X_{rms}\left(\theta_{w_i}, \Delta + \theta_{w_i}\right)\right]/n}{\min_{\Delta}\left[\sum_{i=1}^{n}\left[X_{rms}\left(\theta_{w_i}, \Delta + \theta_{w_i}\right)\right]/n\right]} \quad (6)$$

where X_{max} can be peak axial forces $N_{max}(\theta_w, \theta_s)$, shear forces $V_{max}(\theta_w, \theta_s)$ or bending moments $M_{max}(\theta_w, \theta_s)$ for a given combination of ground motion and wind directions; X_{rms} can be root-mean-square values of axial forces $N_{rms}(\theta_w, \theta_s)$, shear forces $V_{rms}(\theta_w, \theta_s)$ or bending moments $M_{rms}(\theta_w, \theta_s)$ for a given combination of ground motion and wind directions, and at the same member at which the peak values are found for each combination; and $n = 7$ is the number of combinations for any given Δ. This amplification factors provide information on how the peak or rms values found for a given combination of seismic shaking and wind directions with a certain misalignment between them relate to the case in which such misalignment angle yields the smallest forces among all of them.

The results show that the load combination that considers aligned wind and ground motion actions ($\Delta = 0°$) is never the worst-case scenario. This observation is in line with what was found by Mo et al. [30,31] for monopiled OWTs. On the contrary, the misalignment values for which the highest forces are found tend to be $15° \leq |\Delta| \leq 45°$ for the axial forces, $45° \leq |\Delta| \leq 75°$ for the shear forces, and $|\Delta| = 90°$ or $15° \leq |\Delta| \leq 45°$ for the bending moments, depending on the specific earthquake.

4.5. General trends considering wind and ground motion direction simultaneously

Another relevant factor to analyse within this study is how much the internal forces increase with the arrival of an earthquake. In order to quantify the significance of the seismic shaking, Fig. 13 shows the amplification ratios between the results computed taking into account, or disregarding (NS: Non-Seismic), the earthquake input, maintaining always the mode of operation in normal production. The horizontal axis denotes each one of the different wind direction considered, hence the direction of the hub. The different symbols represent the ground motion direction and the colours represent the four seismic signal considered. Left and right plots present the results in terms of axial forces or bending moments, respectively.

A first observation is that all amplification ratios are significantly higher than the unit ratio, which illustrates the relevance of the seismic actions in terms of the peak forces developed along the jacket support structure. The specific value depends on the earthquake signal and on the wind and ground motion directions, with ratios over 4 for axial forces and 7 for bending moments, for the Loma Prieta earthquake. Bending moments are more affected by the seismic loads. In the case of the axial forces, the highest ratios occur when wind directions are $\theta_w = 0°$ or 90°, and the ground motion direction is $\theta_s = 45°$. In the case of bending moments, the trends are not so clear with respect to wind direction, but the highest ratios are found, as mentioned above, when the shaking occurs in the side-to-side direction in each case.

Finally, and after having analysed in the detail the evolutions of the internal forces, Fig. 14 presents the rms values for the acceleration at the tower top considering all ground motion directions in the polar plot, and one curve for every wind direction, for the Loma Prieta earthquake.

As expected, maximum accelerations are found, again, when the shaking occurs along the side-to-side direction in each case. The evolution of the amplitudes is clear, with the smaller amplitudes arising when both actions are aligned, and increasing amplitudes of response when the shaking acts with larger angles of misalignment with respect to the wind direction. This tendency is due to the variability in the aeroelastic damping, and was already observed in Fig. 5.

5. Conclusions

The present research has looked into the influence of wind and seismic shaking directionality on the dynamic structural response of jacket-type support substructures for Offshore Wind Turbines located in areas with non-negligible seismic risk. To do that, a parametric study that included 13 seismic ground motion directions and 7 wind directions was carried out. Four different earthquake records were employed, and results were presented in terms of accelerations, bending moments, axial forces and shear forces in the jacket substructure. The response of the NREL 5 MW Offshore Wind Turbine on the jacket substructure defined for the phase I of the OC4 project was simulated using an OpenFAST model that included soil–structure interaction and multi-support input motion. Kinematic interaction was also taken into account, as the seismic input signals were filtered in order to take

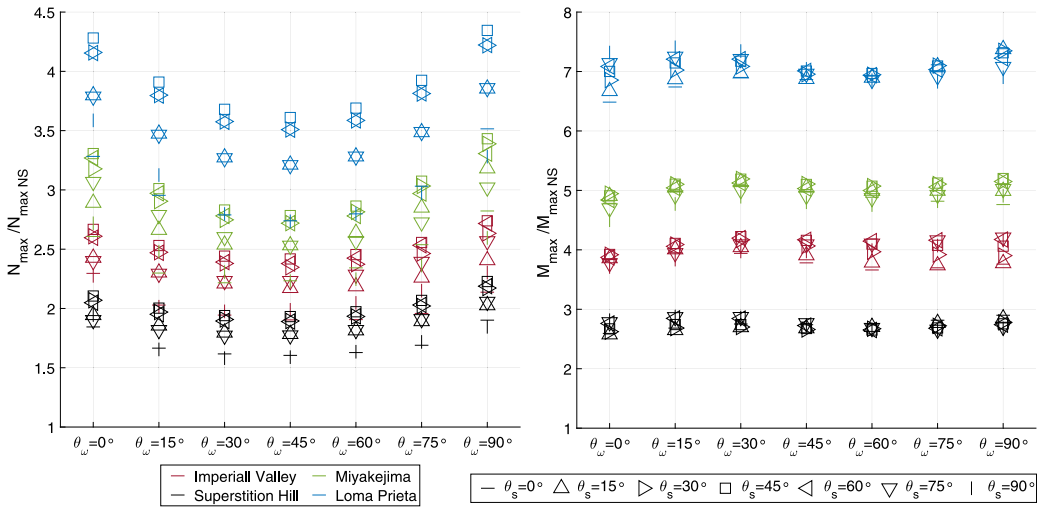

Fig. 13. Ratios between peak seismic response and peak non-seismic response of axial forces and bending moments in the jacket substructure.

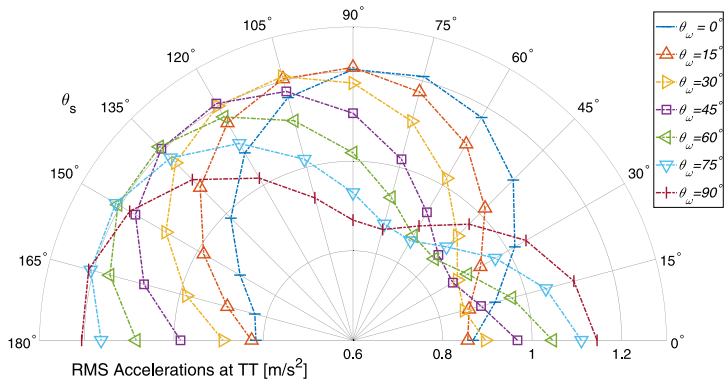

Fig. 14. Root-means-square values of accelerations at tower top for all ground motion and wind directions for the Loma Prieta seismic record.

into account the effects of the presence of the pile foundations in the stratified soil. The turbine was assumed to be in power production mode.

It was found that, due to aeroelastic damping (which is much higher in the fore–aft direction than in the side-to-side direction) the amplitude of the vibrations is much more relevant when the seismic shaking acts along the side-to-side direction, in comparison to the situation in which it acts along the fore–aft direction. However, due to the geometry of the jacket, the conclusion is not the same when looking at the internal forces. In this case, the maximum internal forces are usually found when the ground motion is aligned with the direction of the diagonal of the base of the jacket structure and not aligned with the wind direction. It is also worth noting that the seismic shaking direction tends to have a larger influence on the peak internal forces than wind direction. This is particularly so when studying shear forces.

In any case, it is clear that the load combinations that assume aligned wind and ground motion directions are never the worst-case scenario. On the contrary, the misalignment values for which the highest forces are found tend to be $15° \leq |\Delta| \leq 45°$ for the axial forces, $45° \leq |\Delta| \leq 75°$ for the shear forces, and $|\Delta| = 90°$ or $15° \leq |\Delta| \leq 45°$ for the bending moments. These ranges provide a relatively narrow margin within which the worst-case scenario combination can be found, although a specific combination cannot be specified for all cases. This is partly so because the combinations for which the maximum peak values are found vary, within these ranges, with different earthquakes. Consequently, a sufficiently large set of seismic signals (ideally including also offshore stations) and of combinations of ground motion and wind directions must be taken into account during the phases of detailed design of jacket substructures for Offshore Wind Turbines located in areas with sufficiently high level of seismic risk.

CRediT authorship contribution statement

Carlos Romero-Sánchez: Conceptualization, Methodology, Software, Validation, Formal analysis, Investigation, Writing – original draft, Writing – review & editing, Visualization, Supervision, Funding acquisition. **Luis A. Padrón:** Conceptualization, Methodology, Software, Validation, Formal analysis, Investigation, Writing – original draft, Writing – review & editing, Visualization, Supervision, Funding acquisition.

Declaration of competing interest

The authors declare that they have no known competing financial interests or personal relationships that could have appeared to influence the work reported in this paper.

Data availability

Data will be made available on request.

Acknowledgements

This research was funded by the Ministerio de Ciencia, Innovación y Universidades and the Agencia Estatal de Investigación of Spain (MCIN/AEI/10.13039/501100011033) and FEDER through research project PID2020-120102RB-I00 and by Consejería de Economía, Conocimiento y Empleo (Agencia Canaria de la Investigación, Innovación y Sociedad de la Información) of the Gobierno de Canarias and FEDER, Spain through research project ProID2020010025. In addition, C. Romero-Sánchez is a recipient of the research fellowship (TESIS2022 010011), from the Program of predoctoral fellowships from the Consejería de Economía, Conocimiento y Empleo (Agencia Canaria de la Investigación, Innovación y Sociedad de la Información), Spain of the Gobierno de Canarias and Fondo Social Europeo. The authors are grateful for this support.

References

[1] Musial W, Spitsen P, Duffy P, Beiter P, Marquis M, Hammond R, et al. Offshore wind market Report: 2022 edition. Technical report, National Renewable Energy Lab.(NREL), Golden, CO (United States); 2022.
[2] IEC. 61400-1:2020 Wind energy generation systems - Part 1: Design requirements. International Electrotechnical Commission; 2020.
[3] DNV. Design of offshore wind turbine structures. Offshore standard DNV-OS-J101. DetNorske Veritas AS; 2014.
[4] Lombardi D, Bhattacharya S, Wood DM. Dynamic soil–structure interaction of monopile supported wind turbines in cohesive soil. Soil Dyn Earthq Eng 2013;49:165–80.
[5] Zania V. Natural vibration frequency and damping of slender structures founded on monopiles. Soil Dyn Earthq Eng 2014;59:8–20.
[6] Álamo GM, Aznárez JJ, Padrón LA, Martínez-Castro AE, Gallego R, Maeso O. Dynamic soil-structure interaction in offshore wind turbines on monopiles in layered seabed based on real data. Ocean Eng 2018;156:14–24.
[7] Medina C, Álamo GM, Quevedo-Reina R. Evolution of the seismic response of monopile-supported offshore wind turbines of increasing size from 5 to 15 MW including dynamic soil-structure interaction. J Mar Sci Eng 2021;9(11):1285.
[8] Bazeos N, Hatzigeorgiou GD, Hondros ID, Karamaneas H, Karabalis DL, Beskos DE. Static, seismic and stability analyses of a prototype wind turbine steel tower. Eng Struct 2002;24:1015–25.
[9] Stamatopoulos GN. Response of a wind turbine subjected to near-fault excitation and comparison with the Greek aseismic code provisions. Soil Dyn Earthq Eng 2013;46:77–84.
[10] Krathe VL, Kaynia AM. Implementation of a non-linear foundation model for soil-structure interaction analysis of offshore wind turbines in FAST. Wind Energy 2016;20(4):695–712.
[11] Løken Ingrid B, Kaynia Amir M. Effect of foundation type and modelling on dynamic response and fatigue of offshore wind turbines. Wind Energy 2019;22(12):1667–83, arXiv:https://onlinelibrary.wiley.com/doi/pdf/10.1002/we.2394.
[12] Padrón LA, Carbonari S, Dezi F, Morici M, Bordón JDR, Leoni G. Seismic response of large offshore wind turbines on monopile foundations including dynamic soil–structure interaction. Ocean Eng 2022;257:111653.
[13] Damgaard M, Zania V, Andersen Lars V, Ibsen LB. Effects of soil–structure interaction on real time dynamic response of offshore wind turbines on monopiles. Eng Struct 2014;75:388–401.
[14] Shi S, Zhai E, Xu C, Iqbal K, Sun Y, Wang S. Influence of pile-soil interaction on dynamic properties and response of offshore wind turbine with monopile foundation in sand site. Appl Ocean Res 2022;126:103279.
[15] Liang F, Yuan Z, Liang X, Zhang H. Seismic response of monopile-supported offshore wind turbines under combined wind, wave and hydrodynamic loads at scoured sites. Comput Geotech 2022;144:104640.
[16] Zuo H, Bi K, Hao H. Dynamic analyses of operating offshore wind turbines including soil-structure interaction. Eng Struct 2018;157:42–62.
[17] Kjørlaug RA, Kaynia AM. Vertical earthquake response of megawatt-sized wind turbine with soil-structure interaction effects. Earthq Eng Struct Dyn 2015;44(13):2341–58.
[18] Kementzetzidis E, Corciulo S, Versteijlen WG, Pisanò F. Geotechnical aspects of offshore wind turbine dynamics from 3D non-linear soil-structure simulations. Soil Dyn Earthq Eng 2019;120:181–99.
[19] Jalbi S, Bhattacharya S. Closed form solution for the first natural frequency of offshore wind turbine jackets supported on multiple foundations incorporating soil-structure interaction. Soil Dyn Earthq Eng 2018;113:593–613.
[20] Alati N, Failla G, Arena F. Seismic analysis of offshore wind turbines on bottom-fixed support structures. Phil Trans R Soc A 2015;373(2035):20140086.
[21] Plodpradit P, Dinh VN, Kim K-D. Coupled analysis of offshore wind turbine jacket structures with pile-soil-structure interaction using FAST v8 and X-SEA. Appl Sci 2019;9(8):1633.
[22] Ju S-H, Hsieh C-H. Optimal wind turbine jacket structural design under ultimate loads using Powell's method. Ocean Eng 2022;262:112271.
[23] Gelagoti FM, Kourkoulis RS, Georgiou IA, Karamanos SA. Soil–structure interaction effects in offshore wind support structures under seismic loading. J Offshore Mech Arct Eng 2019;141(6).
[24] Jonkman J, Butterfield S, Musial W, Scott G. Definition of a 5-MW reference wind turbine for offshore system development. Technical report, National Renewable Energy Lab.(NREL), Golden, CO (United States); 2009.
[25] Bossanyi EA. Bladed for windows user manual. Bristol, UK.; 2000.
[26] Abhinav KA, Saha N. Coupled hydrodynamic and geotechnical analysis of jacket offshore wind turbine. Soil Dyn Earthq Eng 2015;73:66–79.
[27] Abhinav KA, Saha N. Nonlinear dynamical behaviour of jacket supported offshore wind turbines in loose sand. Mar Struct 2018;57:133–51.
[28] Jalbi S, Bhattacharya S. Concept design of jacket foundations for offshore wind turbines in 10 steps. Soil Dyn Earthq Eng 2020;139:106357.
[29] Jalbi S, Nikitas G, Bhattacharya S, Alexander N. Dynamic design considerations for offshore wind turbine jackets supported on multiple foundations. Mar Struct 2019;67:102631.
[30] Mo R, Cao R, Liu M, Li M. Effect of ground motion directionality on seismic dynamic responses of monopile offshore wind turbines. Renew Energy 2021;175:179–99.
[31] Mo R, Cao R, Liu M, Li M, Huang Y. Seismic fragility analysis of monopile offshore wind turbines considering ground motion directionality. Ocean Eng 2021;235:109414.
[32] National Renewable Energy Laboratory. OpenFAST documentation. Release v3.4.1. 2023, https://openfast.readthedocs.io/en/main/. Code published at https://github.com/OpenFAST/openfast.
[33] Ju S-H, Huang Y-C. Analyses of offshore wind turbine structures with soil-structure interaction under earthquakes. Ocean Eng 2019;187:106190.
[34] James M, Haldar S. Seismic vulnerability of jacket supported large offshore wind turbine considering multidirectional ground motions. Structures 2022;43:407–23.
[35] Mroczek MM, Arwade SR, Lackner MA. Design optimization of offshore wind jacket piles by assessing support structure orientation relative to metocean conditions. Wind Energy Sci 2023;8(5):807–17, URL https://wes.copernicus.org/articles/8/807/2023/.
[36] Vorpahl F, Popko W, Kaufer D. Description of a basic model of the "UpWind reference jacket" for code comparison in the OC4 project under IEA Wind Annex XXX. Fraunhofer Institute for Wind Energy and Energy System Technology (IWES), Germany 450; 2011.
[37] Jonkman J, Musial W. Offshore code comparison collaboration (OC3) for IEA Wind Task 23 offshore wind technology and deployment. 2010.
[38] IEC. 61400-3-1:2021 wind energy generation systems - Part 3-1: Design requirements for fixed offshore wind turbines. International Electrotechnical Commission; 2021.
[39] DNV. Loads and site conditions for wind turbines. Offshore standard DNV-ST-0437. DetNorske Veritas AS; 2016.
[40] Zhang Q, Zheng XY. Offshore earthquake ground motions: Distinct features and influence on the seismic design of marine structures. Mar Struct 2019;65:291–307.
[41] Pacific Earthquake Engineering Research Center (PEER)2022. NGA-West2 Ground Motion Database. 2022, Available online: ngawest2.berkeley.edu/. [Accessed on 20 November 2022].
[42] National Research Institute for Earth Science and Disaster Resilience (K-NET)2022. Strong-motion seismograph networks. 2022, Available online: https://www.kyoshin.bosai.go.jp/. [Accessed on 20 November 2022].
[43] ISO 19901-2. International Organization for Standardization. ISO 19901-2:2022 Petroleum and natural gas industries — Specific requirements for offshore structures — Part 2: Seismic design procedures and criteria. 2022.
[44] Damiani R, Jonkman J, Hayman G. SubDyn user's guide and theory manual. Technical report, National Renewable Energy Lab.(NREL), Golden, CO (United States); 2015.
[45] Clough RW, Penzien J. Dynamics of structures. 3rd ed.. Computers & Structures; 1995.
[46] Romero-Sánchez C, Padrón LA. An implementation of multi-support input motion into openfast for the earthquake analysis of offshore wind turbines. Eccomas Proceedia COMPDYN 2023;172–85, URL https://www.eccomasproceedia.org/conferences/thematic-conferences/compdyn-2023/10396.
[47] Carbonari S, Morici M, Dezi F, Leoni G. A lumped parameter model for time-domain inertial soil-structure interaction analysis of structures on pile foundations. Earthq Eng Struct Dyn 2018;47(11):2147–71.
[48] Romero-Sánchez C, Padrón LA. Implementation of ground input motion and dynamic soil-structure interaction into openfast for the seismic analysis of offshore wind turbines. In: Congress on numerical methods in engineering. International Center for Numerical Methods in Engineering (CIMNE); 2022.

[49] Chopra AK. Dynamics of structures. Theory and applications to earthquake engineering. 7th ed.. Pearson; 2017.
[50] Álamo GM, Bordón JDR, Aznárez JJ. On the application of the beam model for linear dynamic analysis of pile and suction caisson foundations for offshore wind turbines. Comput Geotech 2021;134:104107.
[51] Dobry R, Idriss IM, Ng E. Duration characteristics of horizontal components of strong-motion earthquake records. Bull Seismol Soc Am 1978;68(5):1487–520.
[52] Arias A, Hansen R. Seismic design for nuclear power plants. Measure Earthq Intensity 1970;438–83.

2.2 Second publication: Romero-Sánchez and Padrón, 2024, Seismic response of jacket-supported offshore wind turbines for different operational modes considering earthquake directionality, Ocean Engineering.

Table 2.2. Second publication data.

Title	Seismic response of jacket-supported offshore wind turbines for different operational modes considering earthquake directionality
Authors	C. Romero-Sánchez and L.A. Padrón
Journal	Ocean Engineering
DOI	10.1016/j.oceaneng.2024.118798
ISSN	0029-8018
Impact factor	4.6
CiteScore	7.3
Category	ENGINEERING, MARINE
Quartile	Q1
Publisher	ELSEVIER SCI LTD
Volume	311, Part 1
Date	November 2024

Ocean Engineering 311 (2024) 118798

Contents lists available at ScienceDirect

Ocean Engineering

journal homepage: www.elsevier.com/locate/oceaneng

Research paper

Seismic response of jacket-supported offshore wind turbines for different operational modes considering earthquake directionality

Carlos Romero-Sánchez *, Luis A. Padrón

Instituto Universitario de Sistemas Inteligentes y Aplicaciones Numéricas en Ingeniería (SIANI), Universidad de Las Palmas de Gran Canaria (ULPGC), Las Palmas de Gran Canaria, 35017, Spain

ARTICLE INFO

Keywords:
Offshore wind turbines
Jacket
Operational modes
OpenFAST
Ground motion directionality
Soil–structure interaction

ABSTRACT

This study aims to analyse how jacket-supported OWTs functioning in three different operational modes (power production, emergency shutdown and parked mode) respond to seismic actions when subject to different incoming wind directions and ground motion shaking directions. To do so, the seismic response of the NREL 5 MW OWT founded on the OC4 jacket substructure is simulated using an OpenFAST model that includes multi-support seismic input, soil–structure interaction and kinematic interaction. The impact of the working conditions and of the directionality of the loads on the jacket substructure is analysed and discussed. The tower top accelerations and displacements are examined for different sets of cases, and the seismic response of the jacket is studied in terms of internal forces and von Mises stresses along the different levels of the substructure. The results show, and quantify, the relevance of considering the different operational modes for a correct design of the substructure and of the foundation. The maximum structural stresses within the jacket substructure appear almost always in power production, with the exception of the top part of the legs, where higher stresses arise during emergency shutdown in several cases.

1. Introduction

Offshore wind technology is an increasingly cost-competitive and reliable source of renewable energies in constant expansion (Global Wind Energy Council, 2023). This expansion is boosting the interest for planning new offshore wind farms at greater sea depths, which encourages the use of jackets as support structures for fixed-bottom Offshore Wind Turbines (OWTs). In fact, for future proposed projects, there is a growing trend towards using jackets due to the increase in maximum water depths for fixed-bottom offshore wind energy (Musial et al., 2023). In recent years, projects with fixed-bottom offshore wind turbines at water depths of more than 60 and 70 metres have been announced (Musial et al., 2023).

Seismic-prone regions are also being increasingly considered for new offshore wind farms, which adds earthquake loads as a potentially critical design aspect. Thus, in such locations, structural design shall take into account the influence of damages caused by a combination of seismic and environmental loads. To do so, the standards (IEC, 2020; DNV, 2014) contemplate different operational modes for the wind turbine. More precisely, three typical operational modes are considered in the seismic response analysis (power production, parked mode and emergency shutdown). In the case of power production, the wind turbine continues to be in operation when an earthquake is detected. In the second operating state, the turbine is in a standstill or an idling condition. In the third scenario, emergency shutdown, the system rapidly disconnects the generator upon detecting a seismic load.

Two different approaches are generally considered when evaluating the seismic response of OWTs: nonlinear simulations in time domain or the response spectrum method (IEC, 2020). The combined effect of aerodynamic and seismic loadings considering the different operational modes should be computed in time domain analyses. Recent studies assume this approach for analysing the dynamic response of monopile-supported offshore wind turbines subjected to an earthquake event (Katsanos et al., 2017; Zuo et al., 2018; Asareh et al., 2016; Padrón et al., 2022; Zuo et al., 2019; Yang et al., 2019; Xi et al., 2023). On the basis of the results of the three typical operating scenarios, a fragility analysis was performed in monopiles substructures by Katsanos et al. (2017), highlighting the relevance of the earthquake excitations for the design of offshore wind turbines. Using a 3D FEM Abaqus model, and considering a specific case, Zuo et al. (2018) concluded that the maximum displacements at the top of the tower when the wind turbine rotates are larger than those when the wind turbine is in parked condition, although opposite conclusions were found, for instance, by Alati et al. (2015) and Yang et al. (2019) for similar problems. Padrón et al. (2022) analysed the seismic behaviour of

* Corresponding author.
E-mail addresses: carlos.romero@ulpgc.es (C. Romero-Sánchez), luis.padron@ulpgc.es (L.A. Padrón).

https://doi.org/10.1016/j.oceaneng.2024.118798
Received 26 April 2024; Received in revised form 16 July 2024; Accepted 21 July 2024
Available online 31 July 2024
0029-8018/© 2024 The Author(s). Published by Elsevier Ltd. This is an open access article under the CC BY-NC-ND license (http://creativecommons.org/licenses/by-nc-nd/4.0/).

monopile-supported OWTs of different rated powers and found that the way in which operational mode and dynamic soil–structure interaction influence the seismic response of the OWT depends on the size and rated power of the turbine, among other aspects. Zuo et al. (2019) investigated the dynamic behaviours of OWTs subjected to combined environmental and earthquake excitations in the power production and parked modes, considering offshore and onshore seismic motions. They concluded that, compared to the offshore earthquake ground motions, using onshore seismic motions as inputs in the analysis may underestimate the response of the OWTs in both modes of operation.

Another relevant factor in the study of the seismic response of OWTs under different operational modes is the environmental and ground motion directions. Yang et al. (2019) stated that the relative orientation of the ground motion with respect to the wind direction causes significant differences in the structural behaviour, highlighting the impact of the misalignment between the direction of the ground motion and of the environmental loads. In this regard, the effect of the different misalignments between wind and shaking on the combined seismic and aerodynamic loads for different operational scenarios has not been investigated in detail. Mo et al. (2021) performed a seismic fragility analysis of a monopile-supported OWT under different operational scenarios considering the ground motion directionality. They noted that the aerodynamic damping amplified the effect of shaking directionality in normal operation and suggested that the directionality of the ground motion, the wind and waves loads, and the aerodynamic damping should be taken into account in seismic analysis for OWTs. Additionally, Ishihara et al. (2024) studied the effects of combined seismic and aerodynamic loads for different operational modes. Here, the effect of the misalignment between loads is studied for a gravity foundation supporting the OWT, case for which it is found that the maximum tower base moments are obtained in power production.

The influence of the different operational modes of the turbine on the seismic response of the system in the case of jacket support structures has been explored in significantly less studies than for the monopile configuration. The dynamic behaviour of the jacket considering the wind and wave directions was studied by Cheng et al. (2023), who found that the emergency shutdown and parked modes played a significant role in the computed fragilities of severe damage states of the tower and the jacket substructure. Similarly, Alati et al. (2015) presented a study on the seismic response of jacket substructures under combined wind-wave-earthquake loadings for different load cases and found that structural stress demands are highly influenced by the operational mode. Ju and Huang (2019) studied the NREL 5 MW jacket-type OWT and concluded that the combination of seismic and environmental loads during power production often control the structural design in a jacket substructure. In addition, James and Haldar (2022) analysed the utilization of tubular members of the jackets in terms of yield stress considering multidirectional ground motion. They showed the need of considering higher modes and multidirectional ground motion on the seismic analysis of OWTs. The top and bottom sections of the jacket leg were found to be the most critical elements.

The analysis of the body of research outlined above reveals that there exists a clear influence of the different operational modes and of the misalignment between wind and ground motion direction on the dynamic response of the substructures. It is also clear that the response of jacked support structures is not as well studied as that of its monopile counterpart. For these reasons, this study aims to analyse the effects of the different operational scenarios on the structural response of jacket-supported offshore wind turbines considering wind and seismic ground motion directionality. For monopiles, the substructure is cylindrically symmetrical. However, this is not the case for jackets, so the loads directionality may be more relevant. The seismic response of the OWT under power production was studied in a previous paper (Romero-Sánchez and Padrón, 2024) that showed that load combinations with aligned wind and ground motion directions are never the worst-case scenario in terms of internal forces in the substructure. In this case, the influence of the different operational modes on a four-legged jacket-supported OWT is analysed.

Table 1
Main characteristics of the OWT.

Rating [MW]	5
Rotor diameter [m]	126
RNA mass [ton]	350
Hub height [m]	90.55
Rated wind speed [m/s] (V_r)	11.4
Cut-out wind speed [m/s] (V_{out})	25.0
Tower top height from mean sea level (H_{Top}) [m]	88.15
Tower base height from mean sea level [m]	20.15
Tower top thickness [mm]	30
Tower base thickness [mm]	32
Tower top diameter [m]	4.00
Tower base diameter [m]	5.60
Water depth (W) [m]	50.00
Jacket height (H_{Jacket}) [m]	70.15
Top leg spacing [m]	8.00
Base leg spacing [m]	12.00
Number of bracing levels	4
Number of legs	4
Pile diameter [m]	2.082
Pile thickness [mm]	60.00
Pile depth (L_{Pile}) [m]	34.00

Table 2
Soil profile properties.

Soil profile	Layered
Type of soil	sand
Poisson's ratio, ν_s [–]	0.35
Density, ρ_s [kg/m^3]	2000
Shear modulus, G_s [MPa]	42.6 ($0 < z < 5$ m)
	61.9 ($5 < z < 14$ m)
	87.4 ($14 < z < \infty$)
Shear wave velocity, υ_s [m/s]	145.9 ($0 < z < 5$ m)
	175.9 ($5 < z < 14$ m)
	209.0 ($14 < z < \infty$)
Damping, ζ_s [–]	0.05

The paper is organized in five sections. The problem definition is described in Section 2, where the jacket substructure for the NREL 5 MW OWT, the pile foundations, the characteristics of the stratified soil, the seismic signals and the set of cases for the analysis, are specified. Section 3 summarizes the numerical model employed for the parametric analysis, a modified OpenFAST model that includes soil–structure interaction, kinematic interaction and multi-support seismic input motion. The dynamic structural behaviour of the jacket substructure and the comparative analysis of the different operational modes are presented and discussed in Section 4, while the conclusions from the study are presented in Section 5.

2. Problem definition

2.1. Offshore wind turbine properties

The reference NREL 5 MW three-bladed turbine, as described in Jonkman et al. (2009), is assumed to be installed on the four-legged jacket substructure detailed in the OC4 project (Vorpahl et al., 2011). Vertical piles with a diameter of 2.082 m and a length of 34 m are assumed as foundation under each leg. Steel material properties are: Young's modulus 210 GPa, shear modulus 80.8 GPa, mass density 7850 kg/m^3 and damping ratio 2%. Table 1 summarizes the main characteristics of the system. The jacket consists of numerous tubular elements joined together, and organized in 4 bracing levels. Fig. 1 illustrates the levels of the jacket substructure and the different loads considered in the study. The soil profile properties, defined according to the parameters of the three layer sandy soil used in Jonkman and Musial (2010), Løken and Kaynia (2019), are shown in Table 2.

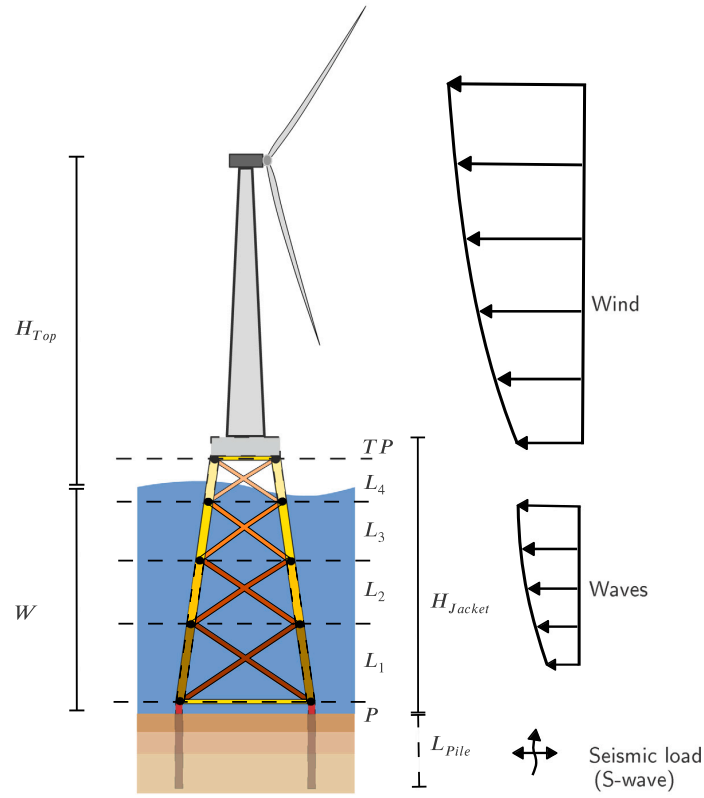

Fig. 1. Representation of the jacket-supported OWT subjected to wind, wave and earthquake loads.

2.2. Operational conditions

In this paper, the dynamic response of the OWT considering dynamic soil–structure interaction is studied for the different operational modes: power production (PP), emergency shutdown (ES) and parked mode (PM). According to IEC61400-1 (IEC, 2020), the earthquake loading shall be superposed with operational loading equal to the higher of: (a) earthquake with power production during normal operation (V_r); (b) loads during emergency stop at rated wind speed (V_r); and (c) loads during idling or parked condition at the cut-out wind speed (V_{out}).

For the power production scenario, when the earthquake arrives, the wind turbine is assumed to continue in operation. Environmental loads are defined according to IEC 61400-3 (IEC, 2021). The turbulent wind fields (Kaimal spectrum) are computed using Turbsim (Jonkman, 2009) for a mean wind speed at hub V_r = 11.4 m/s, assuming Normal Turbulent Model (NTM (IEC, 2020)) and Category B turbulent wind fields. The aerodynamic forces on blades and tower are computed using the Blade Element Mode (BEM) theory in the AeroDyn module (Moriarty and Hansen, 2005). The hub is positioned according to the wind direction. The Hydrodyn module is employed to compute the hydrodynamic loads considering regular and irregular waves (JONSWAP spectrum). The significant height and peak spectra period are defined in Table 4. The wind and waves loads act in alignment based on design guidelines (IEC, 2020; DNV, 2014).

For the power production and the emergency shutdown scenarios, the wind loads are generated based on the same rated wind speed (V_r). In the case of emergency shutdown, the generator is disconnected and the blades are pitched to feather with a pitching rate of 8 deg/s when the first significant peak of the earthquake strikes the OWT. The wave peak-spectral period and significant wave height are 10 s and 8 m, respectively.

In the case of the parked mode, the mean wind velocity at hub is assumed to coincide with the cut-out wind speed (V_{out}), i.e., 25 m/s. The significant height of the incident waves is 10 m. Regular and irregular waves are included. In this mode, blade pitch angle is set to 90°, so the aerodynamic load is insignificant compared with the other loads.

2.3. Ground motion selection

The system is assumed to be excited by vertically propagating shear waves (S-waves). Four different accelerograms are used to obtain the seismic response in the OWT. The acceleration signals are extracted from two different databases, PEER Ground Motion Database (Pacific Earthquake Engineering Research Center (PEER), 2022), and K-NET (National Research Institute for Earth Science and Disaster Resilience (K-NET), 2022). A recording from an offshore station is extracted from this last database. The earthquakes have been selected according to the average shear waves velocity $V_{s,30}$ measured at the recording location so that its value is similar to the range of $V_{s,30}$ of the soil profile considered in this study. Table 3 shows the main information of the selected accelerograms: name and year of the earthquake event, name of the station and maximum ground acceleration ($a_{g,max}$).

For the purpose of comparing the response to different accelerograms, the ground motion signals were linearly scaled to a Peak Ground Acceleration (PGA) of 0.16 g. This value is representative of a moderate seismic hazard, consistent with the hypothesis of linear structural behaviour and with the recommended recurrence period of 475 years (IEC, 2020) for a site within the seismic zone 2 (structure's exposure level L2 and Seismic Risk Category SRC2) defined by the

Table 3
Details of the accelerograms used in the study (before scaling).

No.	Event name	Station name	$a_{g,max}$(g)	Database	Observations
1	Imperial Valley-06, 1979	Niland Fire Station	0.11	PEER	Onshore (RSN:186, Dir: 90°)
2	Superstition Hills-02, 1987	El Centro Imp. Co. Cent.	0.36	PEER	Onshore (RSN:721, Dir: 0°)
3	Loma Prieta, 1984	Hollister City Hall	0.22	PEER	Onshore (RSN:777, Dir: 180°)
4	Miyakejima, 07/30/2000	Hiratsuka-ST1	0.19	K-NET	Offshore (33.97N,139.40E, Dir: N-S)

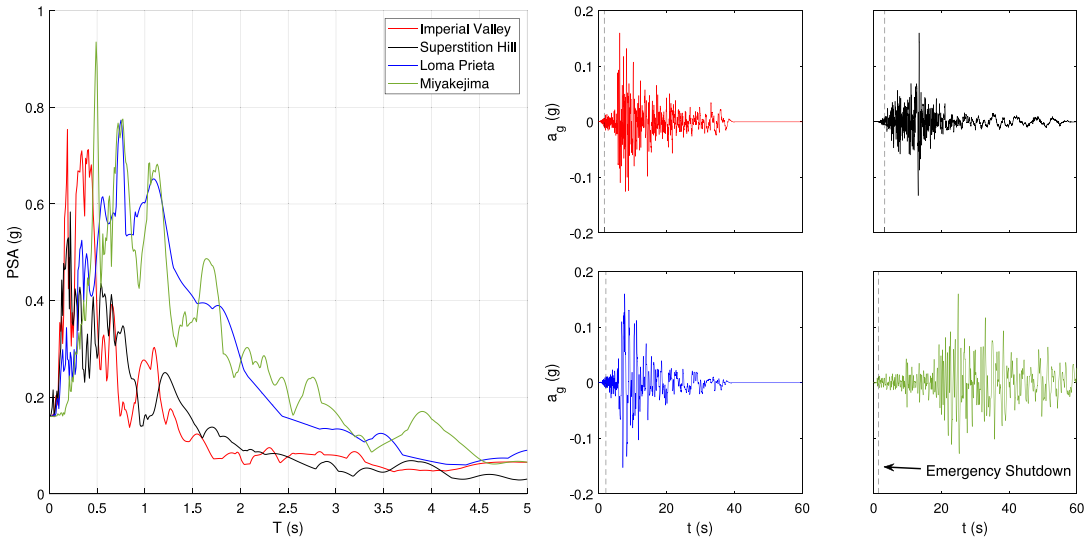

Fig. 2. Normalized pseudo-spectral accelerations (PSA) and ground acceleration (a_g) of the selected seismic signals. The vertical dashed lines mark the time at which ES is triggered in each case.

ISO 19901-2 (ISO 19901-2, 2022). The recurrence period corresponds to a probability of occurrence of 10% in 50 years, which is the one established by Eurcode 8 - Part 5 (2018) for performing seismic verifications. Fig. 2 represents the normalized acceleration spectra and the ground acceleration of the seismic records considered.

2.4. Environmental and earthquake loads combinations

In order to analyse the effects of the operational modes and of the misalignment between environmental and earthquake loads on the seismic response of the jacket substructure, different combinations of these parameters are studied. Different wind directions are established from $\theta_w = 0°$ to $\theta_w = 90°$ ($\Delta\theta_w = 15°$), while the ground motions are rotated from $\theta_s = 0°$ to $\theta_s = 180°$ with intervals of $\Delta\theta_s = 15°$. Fig. 3 shows a graphical overview of the different load combinations used in the analysis, and Table 4 presents a summary of the combinations analysed, resulting in a total of 1113 different simulations. Note that the hub is always oriented in the direction of the wind. The turbine is simulated in the three operational modes (power production, emergency shutdown and parked mode) mentioned above, as described in IEC-61400-1 (IEC, 2020) and DNV-ST-0437 (DNV, 2016) for seismic analysis. The simulation duration is 300 s in each case. In all cases, the ground motion was applied at the start of the 200 s in order to avoid the primary transient behaviour of the system.

3. Methodology

3.1. Numerical model

The seismic response of the system is computed through the code OpenFAST (National Renewable Energy Laboratory, 2024). OpenFAST is a multi-physics tool for simulating the coupled dynamic response of wind turbines. It consists of different computational modules (AeroDyn, HydroDyn, ServoDyn, ElastoDyn and SubDyn) that enable coupled nonlinear aero-hydro-servo-elastic simulation in time domain. The OpenFAST framework employs a modular approach, wherein the models that simulate different aspects of the system are programmed into modules that interact in a loosely coupled time-integration scheme through a glue code that controls and coordinates the simulation, transferring data among modules at each time step. Each module integrates its equations through its own solver. In order to be able to address the seismic analysis of the jacket-supported OWTs, the SubDyn module (Damiani et al., 2015) (that models the dynamic response of the substructure) was modified to include dynamic soil–structure interaction and multi-support ground input motion. This modification allows to consider horizontal, vertical and rotational foundation input motion on multi-support substructures. The elements in the jacket substructure are modelled as Euler–Bernoulli three-dimensional beams. The Craig–Bampton method is used to reduce the number of the internal generalized degrees of freedom of the substructure. The results obtained in OpenFAST are post-processed to obtain the internal forces along the entire length of the elements.

The equation of motion is described in Eq. (1), where the motion vectors have been partitioned to separate the response quantities from the input (Clough and Penzien, 1995). Thus, the motion vectors include the degrees of freedom of the structure, $\mathbf{u}(t)$, and the components of the foundation input motions at each support, $\mathbf{u}_g(t)$. The global mass, damping and stiffness matrices have been partitioned accordingly. The matrices related to the forces arising from the motions of the supports are denoted with the subindex g. $\mathbf{F}(t)$ represents the external forces acting at each degree of freedom of the substructure.

$$\mathbf{M}\,\ddot{\mathbf{u}}(t) + \mathbf{C}\,\dot{\mathbf{u}}(t) + \mathbf{K}\,\mathbf{u}(t) = \mathbf{F}(t) - \mathbf{M_g}\,\ddot{\mathbf{u}}_\mathbf{g}(t) - \mathbf{C_g}\,\dot{\mathbf{u}}_g(t) - \mathbf{K_g}\,\mathbf{u_g}(t) \tag{1}$$

The equations are rearranged into a state–space type formulation for time-domain resolution and for coupling with the rest of modules. During each subsequent time step, SubDyn is coupled to ElastoDyn

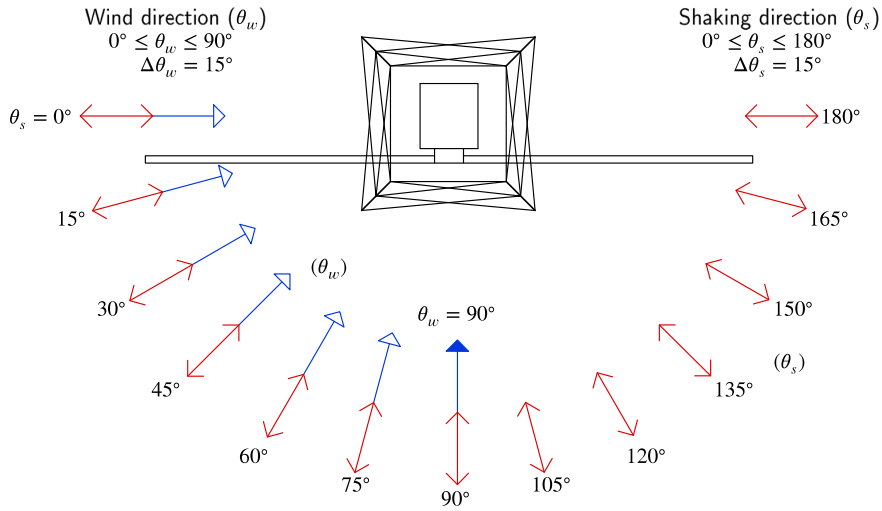

Fig. 3. Definitions of the wind and ground motion directions considered in the study.

Table 4
Summary of the set of cases considered.

Operational mode	Wind loads	Wave loads	Earthquakes	Cases
Power production	Wind speed = 11.4 m/s $0^o \leq \theta_w \leq 90°$ ($\Delta\theta_w = 15°$)	Significant wave height = 8 m Peak-spectral period = 10 s	4 earthquakes $0^o \leq \theta_s \leq 180°$ ($\Delta\theta_s = 15°$) or no earthquake	371
Emergency shutdown	Wind speed = 11.4 m/s $0^o \leq \theta_w \leq 90°$ ($\Delta\theta_w = 15°$)	Significant wave height = 8 m Peak-spectral period = 10 s	4 earthquakes $0^o \leq \theta_w \leq 90°$ ($\Delta\theta_w = 15°$) or no earthquake	371
Parked mode	Wind speed = 25.0 m/s $0^o \leq \theta_w \leq 90°$ ($\Delta\theta_w = 15°$)	Significant wave height = 10 m Peak-spectral period = 10 s	4 earthquakes $0^o \leq \theta_w \leq 90°$ ($\Delta\theta_w = 15°$) or no earthquake	371

(through the interaction forces between tower and substructure) and HydroDyn (through the hydrodynamics forces) modules. More details about the implementation into the Subdyn module and about the verification of the proposed approach are presented in Romero-Sánchez and Padrón (2023), where the modified version was validated by comparison with the results obtained from a finite-element beam model of a four-legged jacket-supported OWT.

3.2. Soil–structure interaction modelling

The foundation response, including its interaction with the surrounding soil, is represented by impedance functions and kinematic interaction factors (KIFs) which are computed through a previously developed continuum model for the dynamic analysis of pile foundations in layered soils (Álamo et al., 2016). Such continuum model is based on the integral expression of the reciprocity theorem and on specific Green's functions to represent the dynamic response of the layered half space used to model the soil. This model avoids the need to discretize any boundary, which reduces significantly the computational requirements and the numerical errors derived from the surface meshing. The model can be applied to study soils whose properties vary continuously with depth by modelling the continuous non-homogeneity through multiple zone-homogeneous horizontal layers. The lateral $I_u(\omega)$ and rotational $I_\theta(\omega)$ KIFs, complex-valued frequency-domain factors, are defined as the ratio between the pile head displacement or rotation and the free-field motion. The earthquake record is filtered using the standard Frequency Domain Method of response (Chopra, 2017) according to the KIFs. The substructuring procedure is schematically described in Fig. 4.

The soil-foundation subsystem is modelled in SubDyn through a Lumped Parameter Model (LPM) developed and validated by Carbonari et al. (2018) that is introduced in the finite elements model of the substructure as an additional element at mudline level (see Fig. 4). The LPM is fitted to the results of the advanced coupled model of boundary elements and finite elements (BEM-FEM model) described above (Álamo et al., 2016, 2021). This model allows to introduce the most relevant aspects of the dynamic response of the foundation into the OpenFAST time-domain simulation. The details about its implementation into SubDyn can be found in Romero-Sánchez and Padrón (2022).

3.3. Post-processing of results in terms of peak and root mean square functions

The structural seismic response for displacements, accelerations, shear forces and bending moments is computed as:

$$\mathrm{X}(t) = \sqrt{\mathrm{X}_x(t)^2 + \mathrm{X}_y(t)^2} \tag{2}$$

where $\mathrm{X}_x(t)$ and $\mathrm{X}_y(t)$ are the time histories of the responses along fore–aft and side-to-side directions, respectively.

The average peak and root mean square internal forces and stresses at a particular point are computed as:

$$\bar{\mathrm{X}}_{\mathrm{peak}} = \frac{1}{N_s}\sum_{i=1}^{N_s}\left(\max\left(|X_i(t)|\right)\right); \quad \bar{\mathrm{X}}_{\mathrm{rms}} = \frac{1}{N_s}\sum_{i=1}^{N_s}\left(\sqrt{\frac{1}{\mathrm{D}}\sum_{j=1}^{\mathrm{D}}\left(X_{j,i}^2(t)\right)}\right) \tag{3}$$

where $i = 1, 2, ., \mathrm{N_s}$; $\mathrm{N_s} = 4$ is the total number of accelerograms considered; $j = 1, 2, ., \mathrm{D}$; D represents the total number of values during the common significant duration (D_{a5-95}); and $\bar{\mathrm{X}}_{\mathrm{peak}}$ and $\bar{\mathrm{X}}_{\mathrm{rms}}$ represent the average of the peak and root mean square values, respectively.

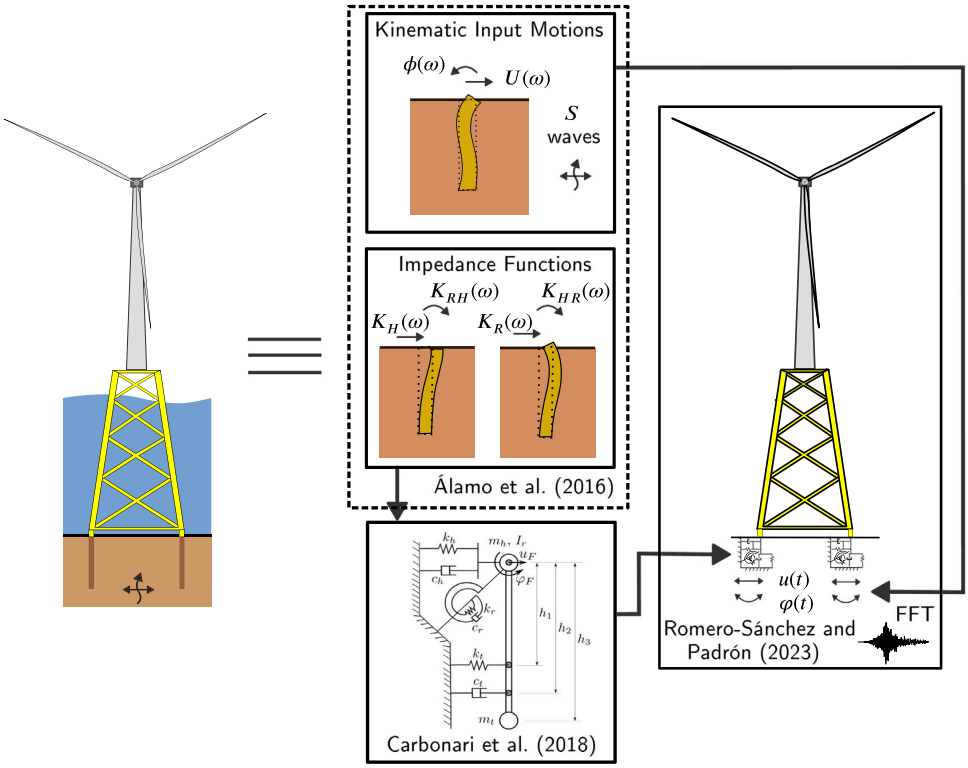

Fig. 4. Schematic soil–structure interaction modelling.

Analysing the results in terms of both peak and root mean square values is crucial to understand whether the trends obtained are consistent across all time responses, rather than just representative of isolated peaks. In this study, root mean square values were computed along the significant duration of each seismic signal. The common D_{a5-95} significant duration (Dobry et al., 1978) is considered, which is defined as the time interval between 5%–95% of the Arias intensity (Arias and Hansen, 1970).

4. Results and discussion

4.1. Displacements, accelerations and internal forces at the tower experienced for the different operational modes

In this section, displacements and accelerations at the tower are analysed for the different operational modes. The displacements are useful for investigating the dynamic behaviour and the magnitude of the response. The tower top accelerations affect the rotor nacelle assembly (RNA), leading to serviceability limitations and influencing the operational lifetime of the wind turbine. In addition, the internal forces obtained at the tower base are analysed.

Fig. 5 presents the tower top displacements of the wind turbine computed for the three different operational modes considered in this study and for a specific illustrative case in which the wind direction considered is $\theta_w = 0°$ and the earthquake (Imperial Valley in this case, chosen for illustration purposes) acts in two different directions, the fore–aft (FA), $\theta_s = 0°$, and side-to-side (SS), $\theta_s = 90°$. The displacements along the fore–aft and side-to-side directions are shown. In the second 200 (earthquake starting), there is a significant increase in the response when the seismic load is applied, highlighting its importance in absolute terms compared to the environmental loads. As expected, the effect of the emergency stop protocol is evident from the history of the tower top displacements along the FA direction. On the other hand, the much smaller relevance of the aeroelastic damping along the SS direction can be clearly seen in Fig. 5(b), as the responses for the three operational modes are very similar to each other and show much less damping that along the FA direction.

Fig. 6 shows the tower top accelerations computed for the same cases considered for Fig. 5. The peak values obtained for each operational mode are highlighted with circles. When the seismic load is considered, the peak acceleration in power production is 5 times higher than that of the reference case without seismic loads. The emergency shutdown scenario presents the highest acceleration in both directions. In contrast, the smallest maximum acceleration is obtained, as expected, for the power production mode when the earthquake acts along the FA direction. This is due to the higher aerodynamic damping, which has a beneficial effect by reducing the magnitude of the vibrations induced by the earthquake (Alati et al., 2015; Meng et al., 2020).

Fig. 7 shows the envelopes of the maximum accelerations along the tower for the FA and SS directions, considering the same cases described above. The maximum accelerations are observed at approximately 70% of the tower height. The accelerations envelopes obtained for the different operational modes differ by up to 90% along the FA direction due to the influence of the aerodynamic damping. Conversely, similar envelopes are observed for the SS direction. Emergency shutdown is the mode that produces the maximum accelerations along the tower in both directions.

The influence of the different load scenarios described in Section 2 can be seen in terms of accelerations in Fig. 8, where the average peak ($\bar{a}^{TT}_{peak}$) and root mean square ($\bar{a}^{TT}_{rms}$) accelerations at tower top are shown for the thirteen different ground motion directions and seven wind directions considered in the study. Instead of presenting the results for each individual earthquake, the average values obtained for all seismic

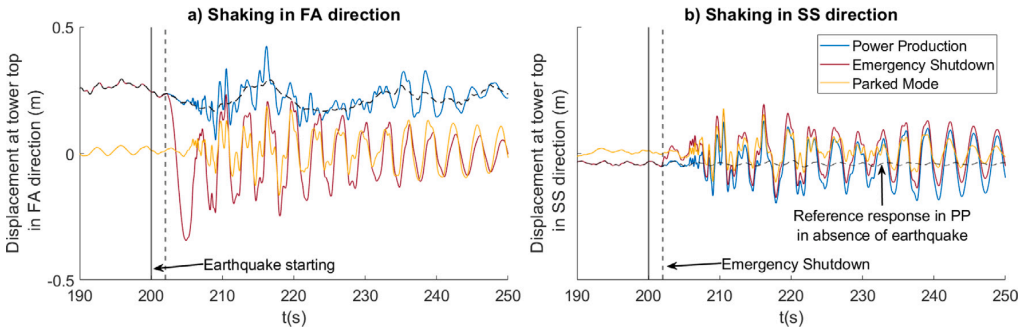

Fig. 5. Time histories of the tower top displacement along FA (a) and SS (b) directions for different operational modes for $\theta_w = 0°$. Imperial Valley. $\theta_s = 0°$ and $\theta_s = 90°$.

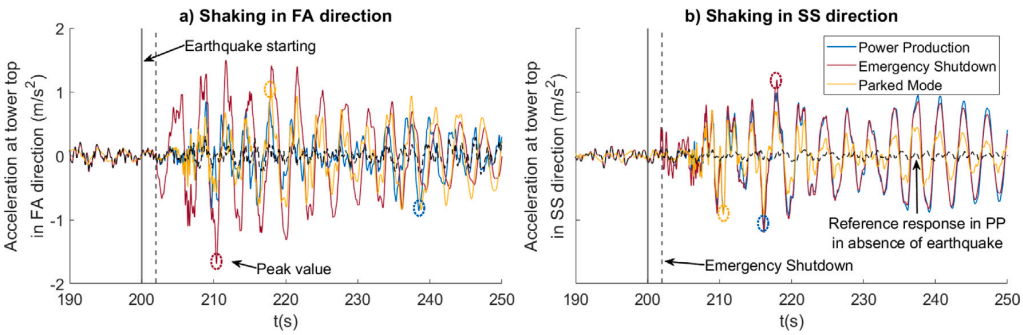

Fig. 6. Time histories of the tower top acceleration along FA (a) and SS (b) directions for different operational modes for $\theta_w = 0°$. Imperial Valley. $\theta_s = 0°$ and $\theta_s = 90°$.

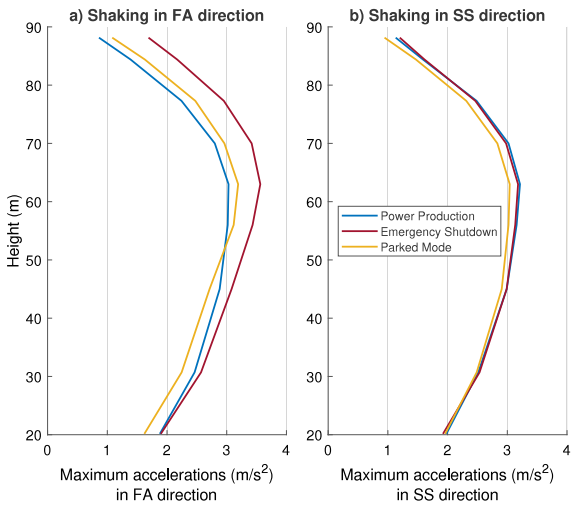

Fig. 7. Acceleration envelopes along the tower for the FA (a) and SS (b) directions for the different operational modes. $\theta_w = 0°$. Imperial Valley. $\theta_s = 0°$ and $\theta_s = 90°$.

loads are presented, as defined in Section 3.3. The results are depicted in polar plot. The accelerations corresponding to the different wind directions (from 0 to 90°) are represented by different colour lines. Two different operational modes, power production (in solid lines) and emergency shutdown (in dashed lines) are shown.

As already observed in Fig. 6, the maximum accelerations at the tower top are obtained for the emergency shutdown scenario. The average peak accelerations obtained for the parked mode (not shown) are lower than those obtained for the power production. At the same time, the highest maximum root mean square accelerations observed during power production are found when shaking occurs along the side-to-side direction. This can be clearly seen when the acceleration is presented in terms of root mean square values. For instance, when $\theta_w = 0°$, the maximum response when the turbine is functioning in power production is found at $\theta_s = 90°$, while for $\theta_w = 90°$, the maximum responses are found for $\theta_s = 0°$ and 180°. At the same time, the curves of these two cases ($\theta_w = 0°$ and $\theta_w = 90°$) cross each other at around $\theta_s = 45°$ and 135° when the turbine is working in such mode. Additionally, for any particular θ_s, the magnitude of the resulting response is clearly ordered from maximum to minimum response when the angle between ground shaking and incoming wind directions change from 0° to ±90°. These trends are due to the variations in the aeroelastic damping (Mo et al., 2021; Romero-Sánchez and Padrón, 2024). However, such tendencies, that are very clear in power production, are not so identifiable under emergency shutdown or parked modes, for which the relevance of the aeroelastic damping is much lower than in power production.

The time histories of the tower base shear force and bending moment for the different operational modes for the case when wind and shaking (Imperial Valley) act along FA direction are shown in Fig. 9. The wind loads exert a significant effect on the structural response in terms of internal forces at the tower base. The maximum internal forces in this particular case are obtained during power production.

4.2. *Effect of wind and ground motion relative directions on the substructure under different operational modes*

The influence of the three different operational modes and of the ground motion directionality on the seismic response of the four-legged jacket-supported OWT is analysed in this section. The response during power production (PP) is studied in Section 4.2.1, during emergency shutdown (ES) in Section 4.2.2 and in parked mode (PM) in Section 4.2.3. In addition, a comparison of the effect of the wind and

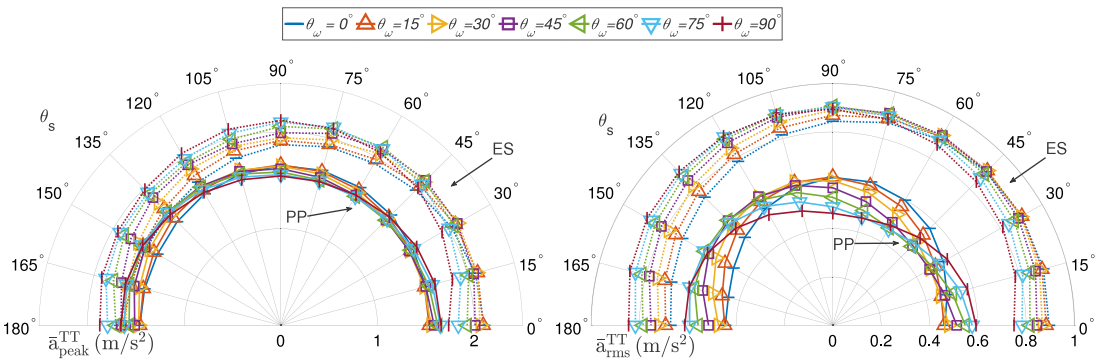

Fig. 8. Average peak and root mean square (rms) tower top (TT) accelerations for the different wind and shaking directions considered in this study in power production and emergency shutdown.

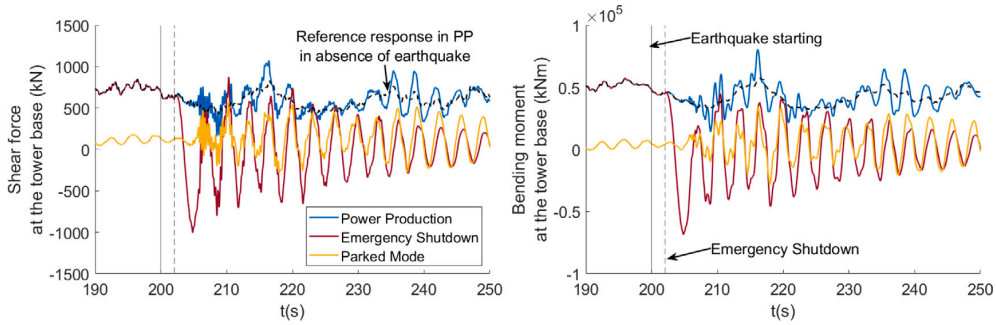

Fig. 9. Time histories of the tower base shear force and bending moment for different operational modes for $\theta_w = 0°$. Imperial Valley. $\theta_s = 0°$.

ground motion relative directions on von Mises stresses and internal forces at the substructure in each operational mode is shown in Section 4.2.4.

4.2.1. Power production

In this section, the peak internal forces and von Mises stresses at the members of the substructure are computed under power production mode. In addition, the effect of the misalignment between wind and ground shaking is analysed for each leg and bracing level of the jacket. To do so, Fig. 10 presents the average peak shear and axial forces obtained at any point of the jacket structure for each combination of wind and ground shaking direction. The points represented in Fig. 10 are located at the connection between leg and transition piece ($\bar{V}^{L4}_{peak}$), and at the joint between leg and pile ($\bar{N}^{L1}_{peak}$), respectively.

The highest average peak shear and axial forces are obtained when the ground shaking acts along one of the diagonals of the jacket (see for instance James and Haldar, 2022), and always arise along sections L4 and L1 (see Fig. 1) of the legs, respectively. The maximum values obtained for both forces are much more dependent on ground shaking direction than on incoming wind direction. In fact, the maximum average peak shear and axil forces vary up to 16% and 25%, respectively, as a function of θ_s, but only up to 4% and 13% as a function of θ_w. Maximum average axial forces are obtained when the earthquake acts within the ranges $30° \leq \theta_s \leq 60°$ and $120° \leq \theta_s \leq 150°$. The results are similar to those obtained for the shear forces, although the influence of wind direction is more relevant than in shear forces.

After having studied the impact of wind and seismic shaking directions (in absolute terms) on the evolution of average peak internal forces in the jacket substructure, it is relevant to analyse their influence in terms of misalignment between ground motion and wind directions ($\Delta = \theta_s - \theta_w$). To do so, Fig. 11 presents the average peak shear and axial forces in bar plot format as a function of the misalignment between loads.

Computed maximum shear forces (see Fig. 11a) are essentially identical for all misalignment angles although, for a given Δ, the values vary for each particular θ_w and the absolute maximum in each case is always obtained when the earthquake acts diagonally. This phenomenon can be clearly observed, for instance, when $\Delta = 0°$ and $\theta_w = 45°$, when $\Delta = 45°$ and $\theta_w = 0°$ ($\theta_s = 45°$) or when $\theta_w = 90°$ ($\theta_s = 135°$). On the other hand, the absolute maximum of the computed average axial peak forces (see Fig. 11b) decreases as the angle of misalignment increases. At the same time, the dispersion decreases and the average value for the different θ_w decreases slightly. Thus, the maximum and minimum mean peak axial force values are both obtained for $\Delta = 0°$. In summary, the internal forces in the four-legged jacket are more influenced by the shaking direction than by the misalignment between wind and shaking direction, although the results show that aligned shaking and wind directions ($\Delta = 0°$) can produce slightly higher maximum axial forces in the substructure.

The behaviour of the jacket for different misalignment angles can also be analysed in terms of amplification ratios defined as:

$$R_{X_{rms}}(\Delta) = \frac{\sum_{i=1}^{n}\left[X_{rms}\left(\theta_{w_i}, \Delta + \theta_{w_i}\right)\right]/n}{\min_{\Delta}\left[\sum_{i=1}^{n}\left[X_{rms}\left(\theta_{w_i}, \Delta + \theta_{w_i}\right)\right]/n\right]} \tag{4}$$

where X_{rms} represents root mean square values of the different internal forces (axial forces $N_{rms}(\theta_w, \theta_s)$, shear forces $V_{rms}(\theta_w, \theta_s)$ or bending moments $M_{rms}(\theta_w, \theta_s)$) for the different combinations of ground motion and wind directions within the range $-90° \leq \Delta \leq 90°$. Each ratio for any given Δ is computed with a combination of seven cases (n = 7).

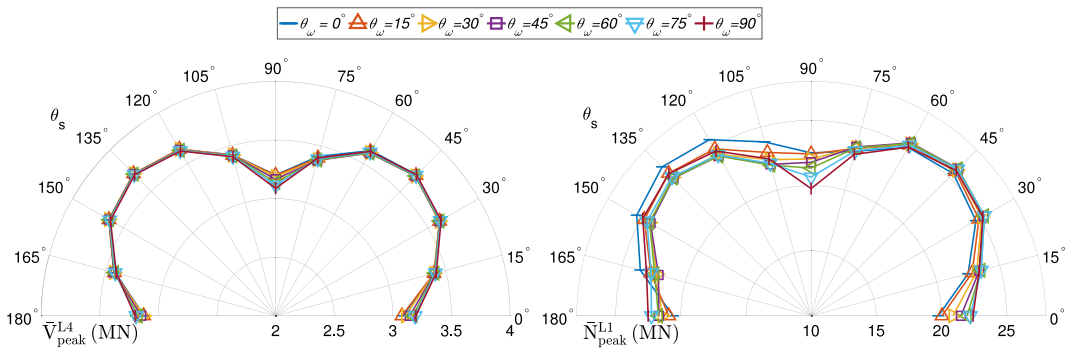

Fig. 10. Average peak response values in terms of shear and axial forces at leg levels 4 and 1, respectively, for the different wind and shaking directions during power production.

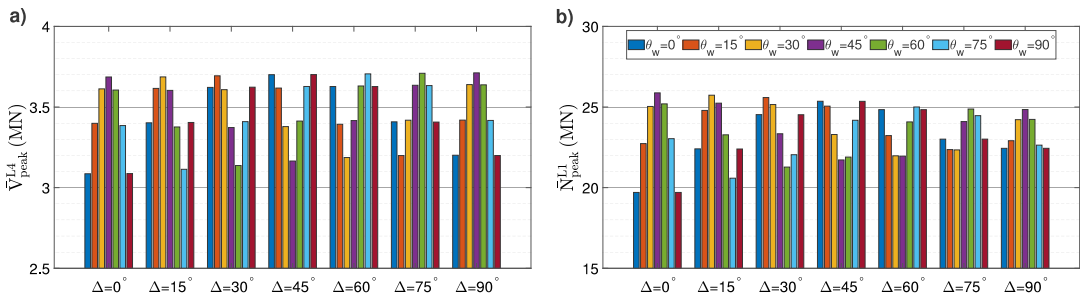

Fig. 11. Average peak response in terms of shear and axial forces at leg levels 4 and 1, respectively, as a function of the misalignment (Δ) between wind and shaking directions during power production.

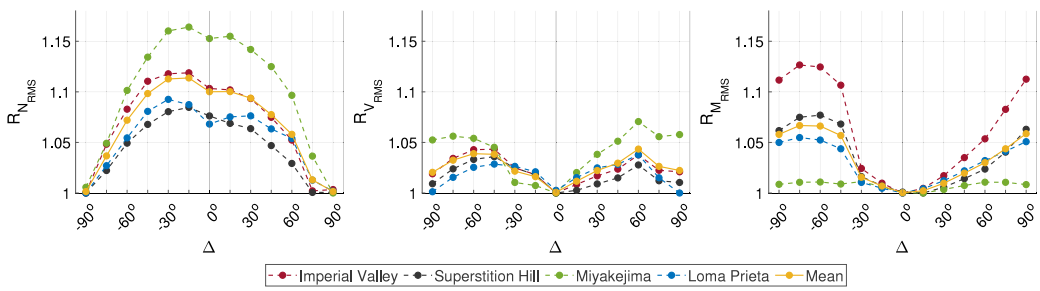

Fig. 12. Amplification ratios for axial forces, shear forces and bending moments at leg levels 1, 4 and pile head, respectively, for the different misalignment angles between wind and ground motion directions during power production.

This amplification factors provide information on how the root mean square values found for a given combination of seismic shaking and wind directions with a certain misalignment between them relate to the case in which such misalignment angle yields the smallest forces. Note that these values are computed for the common significant duration.

Fig. 12 shows the amplification ratios for the three internal forces considered, computed at the points where the peak values are observed, and for each of the earthquakes considered in the analysis. These amplification ratios correspond to the connection between legs and pile in the case of axial forces and bending moments, and to the connection between legs and transition piece in the case of shear forces. The mean response value (orange line) is also shown.

The highest amplification ratios are found for $-15° \leq \Delta \leq -30°$ in the case of axial forces, and for $45° \leq |\Delta| \leq 75°$ in the case of shear forces. The variability of the ratios between different earthquakes in axial forces is higher than in shear forces. The amplification ratio in axial forces reaches a maximum of 16%. For the bending moments, the highest amplification ratios are obtained within the $-75° \leq \Delta \leq -60°$ range. It is important to note the variability between the peak ratios between each of the earthquakes used in the study, despite the use of a common PGA. The maximum mean amplification ratio (11%) is obtained in axial forces.

After analysing the seismic response in terms of internal forces, the behaviour of the jacket is analysed in terms of von Mises stresses, computed as $\sigma_{VM} = (\sigma^2 + \tau^2)^{1/2}$, where σ is the meridional stress and τ is the planar shear stress (Eurocode 3 - Part 1-6, 2007). Fig. 13 presents, for each of the levels of the jacket, the average peak von Mises stresses for all wind and seismic directions. The results corresponding to each one of the levels is shown in a different subplot that presents the average of the maximum values obtained at the point along the element of that level where the maximum stresses appear. The von Mises stresses at the legs and at the bracings elements are represented

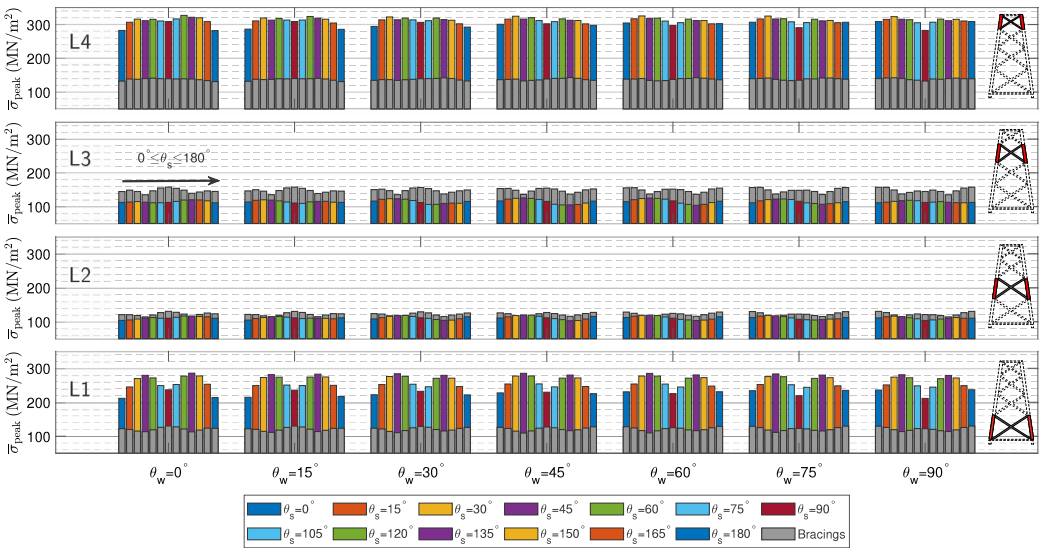

Fig. 13. Average peak response in terms of von Mises stress in the substructure for the different wind and shaking directions during power production. Colour bars are used for stresses in leg members, and grey bars for stresses in the bracing elements (θ_s according to the position).

separately by colour and grey bars, respectively. The sets of bars are ordered for increasing wind directions (θ_w) and, within each set, the bars are ordered for increasing shaking directions (θ_s) from 0° to 180°.

The maximum average stresses arise at level 4 of the leg, at the point where the highest shear forces are obtained, the connection of the leg to the transition piece. In all cases, the jacket zones with the highest stresses are located at the levels 1 and 4 of the main leg, as also found in James and Haldar (2022). Depending on the loads direction, the maximum stresses are found at different legs, but in the same section of the element. Maximum stresses appear when the earthquake direction acts diagonally to the jacket position ($30° \leq |\theta_s| \leq 60°$ and $120° \leq |\theta_s| \leq 150°$), for all wind directions. These ranges coincide with those in which the maximum internal forces are obtained, as shown in Fig. 10. The importance of the aeroelastic damping in the state of power production is observed, for instance, in $\theta_w = 0°$. Similar peak stresses are obtained when the earthquake acts at $\theta_s = 0°$ and $\theta_s = 180°$, but the stress increases when it acts in the side-to-side direction ($\theta_w = 0°$ and $\theta_s = 90°$). Note that the von Mises stresses at levels 2 and 3 are higher in the bracing elements (grey bars) than in the legs. The bracing elements presents similar stresses at all the different levels, in contrast to the legs.

4.2.2. Emergency shutdown

Fig. 14 shows the average peak shear and axial forces obtained at any point of the jacket substructure for all different wind and shaking directions considered in this study. Each colour line represents a different wind direction and the axis of the polar figure represents the shaking direction.

Similarly to what was observed for power production mode, the maximum average shear forces occur when the shaking direction acts along the diagonal of the jacket substructure, specifically within the ranges $30° \leq \theta_s \leq 60°$ and $120° \leq \theta_s \leq 150°$. The maximum axial forces are found for $120° \leq \theta_s \leq 150°$. It can be noted that the lowest forces arise when the shaking direction is midway between two legs, $\theta_s = 0°, 90°$ or 180° (see Fig. 3). Wind load directionality (θ_w) presents a greater influence on the axial forces than on the shear forces, in fact, the shear forces are almost independent of the wind direction, depending almost exclusively of the shaking direction (θ_s).

Fig. 15 represents the amplification ratios for the three internal forces considering emergency shutdown, computed at the points where the peak values of each of the internal forces is observed, and for each of the earthquakes considered in the analysis. Similar trends to those observed in the power production case are obtained, but with lower axial and shear forces amplification ratios. The importance of the misalignment is much lower than that observed in power production mode. This is due to the smaller wind loads arising after the emergency stop, as they decrease as the blades pitch to feather. In the cases of axial and shear forces, the range of the worst-case scenario is $30° \leq |\Delta| \leq 60°$ and the maximum value is around 5%. In the bending moments, the highest ratios are obtained for $-75° \leq \Delta \leq -60°$ and the mean amplification is higher (8%) than during power production. The maximum amplification ratios vary significantly between different earthquakes for bending moments (10%), but not for shear forces.

Fig. 16 presents the average peak von Mises stresses corresponding to the emergency stop situation for all wind and seismic directions. Considering that the emergency shutdown is beneficial in terms of stresses is not clear (see Fig. 13). Despite the lower aerodynamic load on the system, the legs present similar stresses to those obtained in power production mode. The highest values are obtained when the shaking acts along the diagonal direction of the jacket, $30° \leq \theta_s \leq 60°$ and $120° \leq \theta_s \leq 150°$. These ranges coincide with those obtained during power production. Von Mises stresses are similar or higher than during power production at the level 4 of the main leg, the level with the highest peak stress. In the emergency shutdown mode, the bracing level with the highest von Mises stresses is the level 3.

4.2.3. Parked mode

Fig. 17 presents the average peak shear and axial forces obtained at any point at the jacket substructure, considering the seven different wind directions and thirteen shaking directions. The angle of the wind direction is represented by different colour lines and the shaking direction is shown in the axis of the polar plot.

The maximum shear and axial forces are found at the legs, specifically at the level 4 and 1, respectively. The influence of the aerodynamic damping is not relevant in parked mode, The variation of the wind direction has practically no influence. The results obtained are very similar in fore–aft ($\theta_s = 0$) or side-to-side ($\theta_s = 90$) directions. The parked mode presents peak internal forces lower than those obtained during power production and emergency shutdown. The highest axial

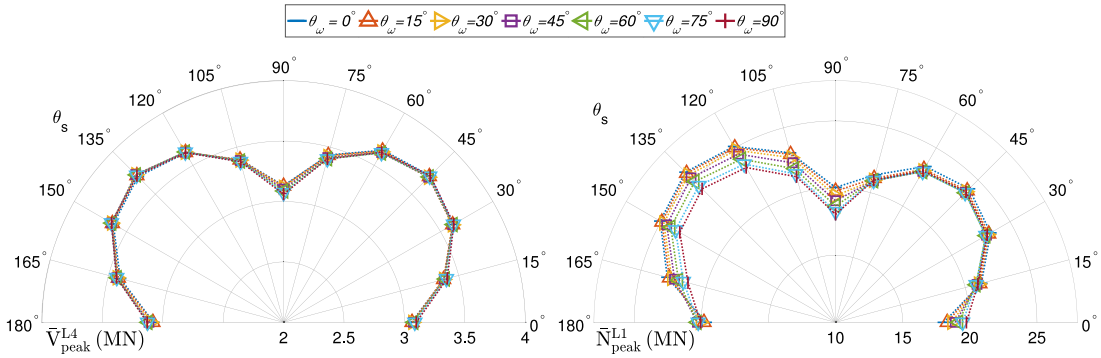

Fig. 14. Average peak response values in terms of bending moments and axial forces at leg levels 4 and 1, respectively, for the different wind and shaking directions considering emergency shutdown.

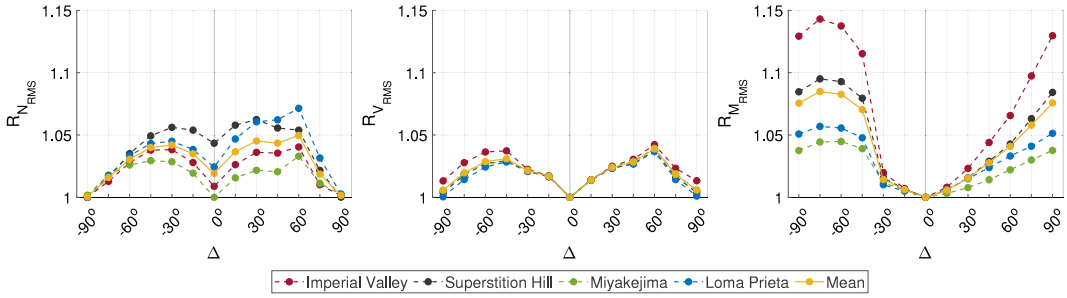

Fig. 15. Amplification ratios for axial forces, shear forces and bending moments at leg levels 1, 4 and pile head, respectively, for the different misalignment angles between wind and ground motion directions considering emergency shutdown.

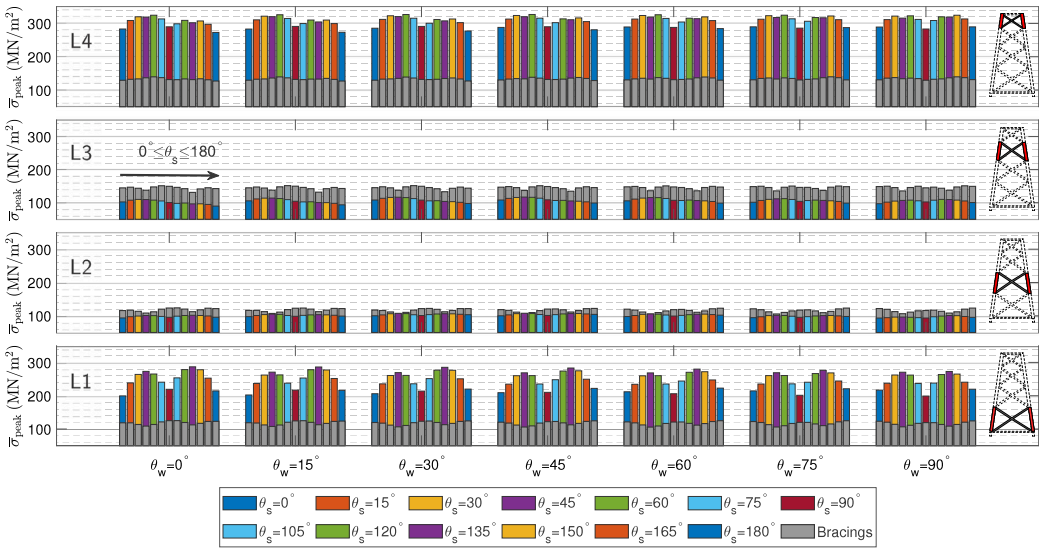

Fig. 16. Average peak response in terms of von Mises stress in the substructure for the different wind and shaking directions considering emergency shutdown. Colour bars are used for stresses in leg members, and grey bars for stresses in the bracing elements (θ_s according to the position).

and shear forces are obtained when earthquake loads act along the diagonal direction. In short, significant differences in the peak forces are only observed with the change of the shaking direction.

Fig. 18 presents the amplification ratios for the three internal forces considered, computed at the points where the peak values are observed in the jacket substructure, and for the four seismic loads considered. The orange line represents the mean response value of the different accelerograms.

In this working condition, the amplification ratios are lower than during power production in terms of axial and shear forces, but the values are similar to those obtained in emergency shutdown mode. The lowest ratios are obtained when the misalignment between wind and

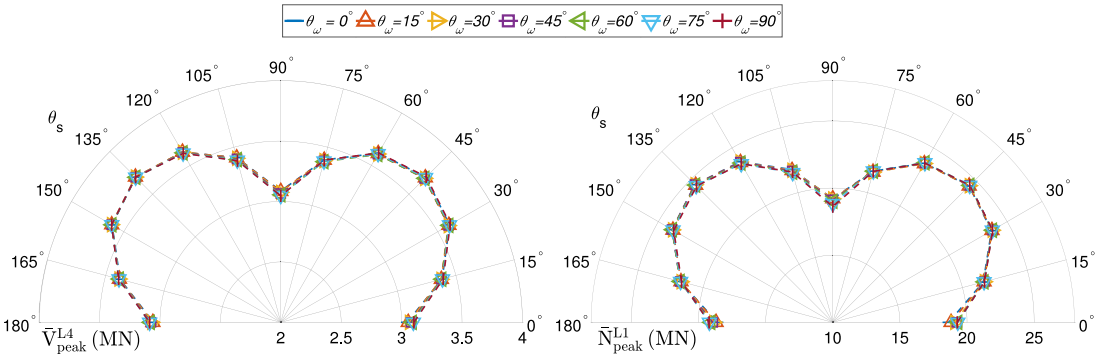

Fig. 17. Average peak response values in terms of shear and axial forces at leg levels 4 and 1, respectively, for the different wind and shaking directions in parked mode.

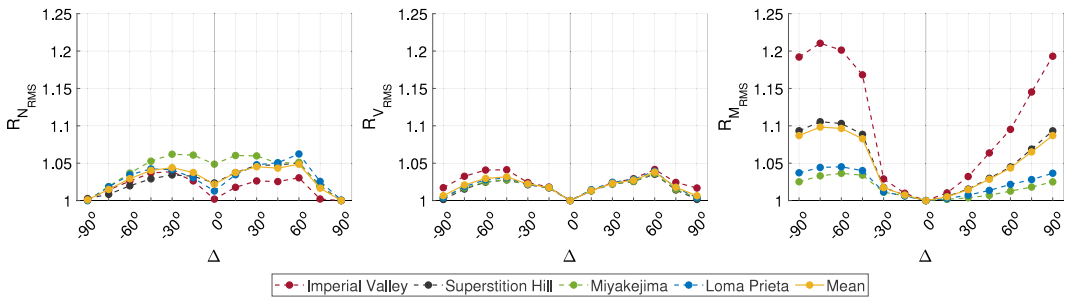

Fig. 18. Amplification ratios for axial forces, shear forces and bending moments at leg levels 1, 4 and pile head, respectively, for the different misalignment angles between wind and ground motion directions in parked mode.

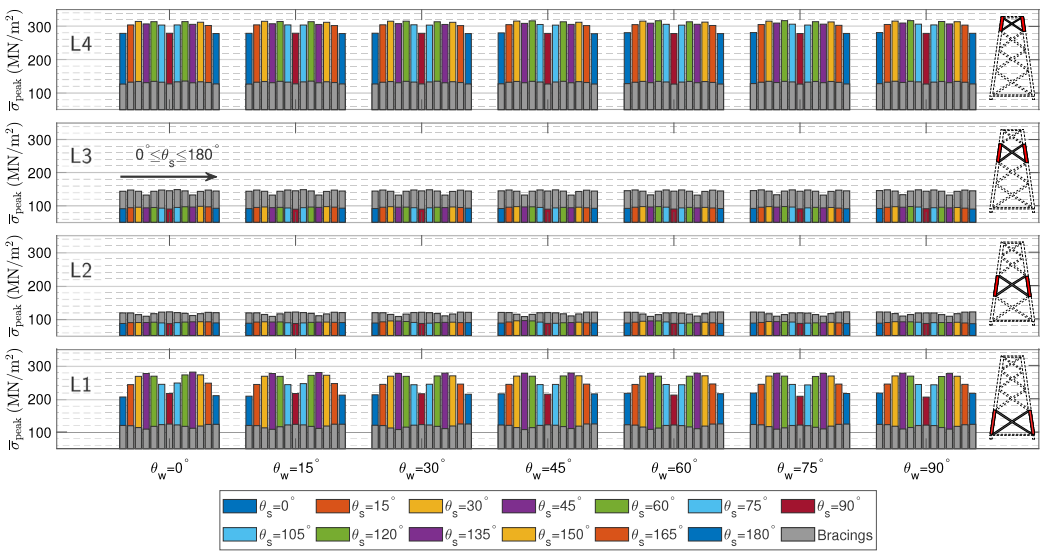

Fig. 19. Average peak response in terms of von Mises stress in the substructure for the different wind and shaking directions in parked mode. Colour bars are used for stresses in leg members, and grey bars for stresses in the bracing elements (θ_s according to the position).

shaking directions is 0°. The worst-case scenarios in terms of axial and shear amplification ratios are found for $30° \leq |\Delta| \leq 60°$. It is important to note that the highest bending moments ratios are obtained in parked mode. The highest bending moments ratios are found when the range is $60° \leq |\Delta| \leq 90°$.

Fig. 19 shows the average peak von Mises stresses in the different levels of the jacket (considering legs and bracings). In contrast to power production, the maximum values in each wind direction are quite similar. Unlike in the emergency shutdown and the power production modes, the increase in peak response when the earthquake acts along

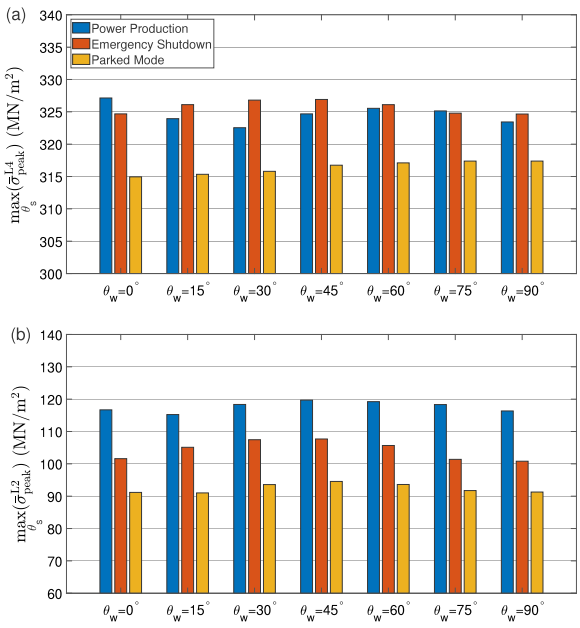

Fig. 20. Maximum average peak von Mises stresses at levels 4 (a) and 2 (b) of the legs for different operational modes among all the wind and shaking directions in the study.

the side-to-side direction is not observed. For instance, when $\theta_w = 0°$, similar stresses are observed when the shaking direction (θ_s) is 0°, 90° or 180°. The von Mises stresses are lower than those obtained during power production. The parked mode is beneficial in terms of stresses at the bracing and leg elements of the jacket.

4.2.4. Comparison between operational modes

A comparison among the maximum average peak von Mises stresses obtained at levels 4 ($\bar{\sigma}^{L4}_{\text{peak}}$) and 2 ($\bar{\sigma}^{L2}_{\text{peak}}$) of the legs for the different operational scenarios is shown in Fig. 20 for all the wind directions considered in the study. More precisely, the maximum value of those obtained among all ground shaking directions ($\max\{\bar{\sigma}_{\text{peak}}(\theta_s) : \theta_s = 0, 15..90°\}$) is presented in the figure for levels 2 and 4 and for each operational mode and wind direction.

The power production and the emergency stop modes are the operational modes that produce the highest average stress at the upper part of the legs. The reason why the emergency stop situation is sometimes the worst-case scenario can be understood by the fact that, although emergency stop is executed from the instant the first peak of the earthquake is noticed (with the largest shocks arriving later) and the influence of the wind load is vanishes gradually, the disconnection of the rotor causes a transitory increase in the peak internal forces within the jacket substructure. On the other hand, the greatest stress relative variations between the different operational modes arise along the central part of the legs, where the stress are the lowest. In this case, the power production mode is the one that produces always the highest average peak stresses. The lowest stresses along the whole length of the legs, are obtained, as expected, for the parked mode, situation at which the effect of the aerodynamic loads is minimal. In fact, the assumption of the parked mode for the structural design would lead to an underestimation of 6% at the top and 28% at the central levels of the legs, in terms of von Mises stress.

Figs. 21 shows the average von Mises stresses of the leg and bracing elements separately, at the points where the maximum stresses are obtained for the different levels of the substructure (points *a* to *e*, whose locations are depicted in the figure using red dots). The results presented in the figure correspond to $\theta_w = 0°$, and to different shaking directions ($\theta_s = 0°, 45°, 90°$). The three different modes of operation in this study are represented with three different colours and symbols. In parallel, Table 5 presents the percentage variations between the average peak von Mises stresses obtained during emergency stop compared to those obtained in power production ($\delta_{\text{ES-PP}}$), and obtained in parked mode compared to those obtained in power production ($\delta_{\text{PM-PP}}$), at the five key points *a* to *e* along the legs mentioned above.

Table 5
Variations of average peak von Mises stress at legs for the different operational modes.

Point	$\theta_s = 0°$		$\theta_s = 45°$		$\theta_s = 90°$	
	$\delta_{\text{ES-PP}}$	$\delta_{\text{PM-PP}}$	$\delta_{\text{ES-PP}}$	$\delta_{\text{PM-PP}}$	$\delta_{\text{ES-PP}}$	$\delta_{\text{PM-PP}}$
a	−0.2%	1.2%	−2.4%	1.3%	6.6%	10.5%
b	9.9%	23.8%	5.0%	21.2%	11.6%	24.6%
c	9.6%	22.7%	9.8%	24.9%	20.1%	37.7%
d	10.3%	9.0%	26.9%	9.5%	3.8%	9.7%
e	6.1%	3.1%	2.2%	1.3%	7.9%	9.6%

As already mentioned, the most stressed parts of the support structure are the sections of the legs connected to the transition piece and to the pile, as evidenced by the significantly higher stress levels at the top and bottom compared to the central levels of the jacket. The smallest average stresses in the legs are obtained when the shaking acts along the fore–aft direction ($\theta_s = 0°$, left plots of the figure), while the largest stresses are obtained when the earthquake acts along the diagonal direction of the jacket ($\theta_s = 45°$). At the points of highest stresses (top and bottom of the legs) the variations in stresses for the different modes tend to be small (< 10% in most cases), but in the intermediate parts of the legs, where the stresses are lower, the average peak von Mises stresses can vary up to 38% when comparing power production with parked mode, and up to 27% when comparing power production with emergency shutdown. A quite similar trend is observed in the bracing levels between each of them, but with the highest von Mises stresses arising at the level 3 in this case. As expected, the parked mode provides the lowest stresses in all cases. An interesting fact is that the highest average peak stresses are not always obtained for the same operational mode, as discussed above, depending of the wind and shaking directionality.

Finally, in order to make a comparison between the internal forces obtained at the pile head for different operational modes, Fig. 22 presents the average peak of bending moments and axial forces at the pile head as function as the misalignment between wind and shaking direction (Δ). The bending moments of the jacket substructure, for all cases considered in this work, reach their maximum value at the pile head.

The results show that in terms of bending moments, the worst-case scenario corresponds to the parked mode, specifically to the case when the shaking acts along the side-to-side direction, i.e., $\Delta = 90°$, although the difference with respect to the power production mode is only of 1.5%. Focusing on the misalignment between wind and shaking directions, the highest values are obtained for $75° \leq \Delta \leq 90°$. Nevertheless, these ranges do not correspond to those observed for maximum axial forces. The highest axial forces at the pile head are found for $0° \leq \Delta \leq 30°$ during power production. In particular, the peak axial force is obtained for $\Delta = 0°$. The difference with respect to the parked mode in this case is 6.3%. The results show that the average peak internal forces change by up to 4% in magnitude depending on the alignment between environmental and seismic loads, while the variability between operational modes reaches 8%.

5. Conclusions

This study outlined the main conclusions drawn from an analysis of the influence of the different operational modes (power production,

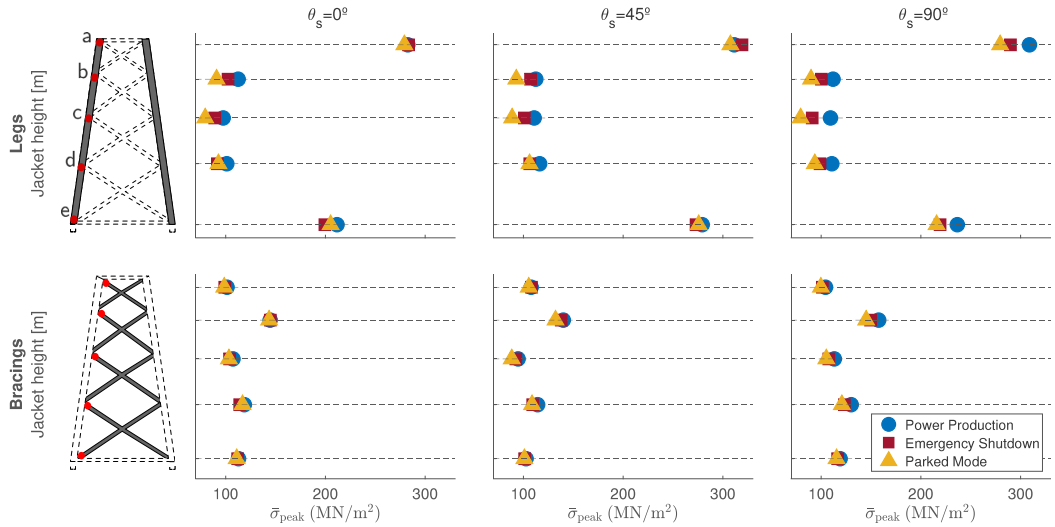

Fig. 21. Average peak von Mises stress at legs and bracings at the different levels of the substructure, for the different operational modes, for $\theta_w = 0°$ and for different shaking directions ($\theta_s = 0°, 45°, 90°$).

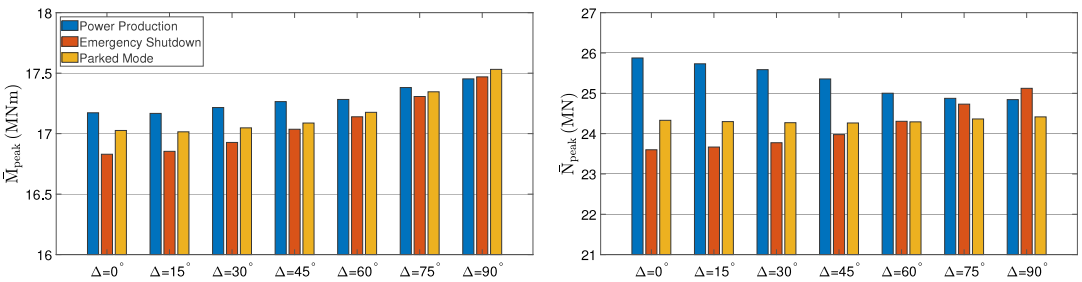

Fig. 22. Average peak bending moments and axial forces at the pile head for different operational modes considering the misalignment (Δ) between wind and shaking directions in this study.

emergency shutdown and parked mode) and of the effect of the wind and seismic shaking directionality on the seismic structural response of the NREL 5 MW offshore wind turbine founded on the OC4-project jacket support structure. The set of cases included thirteen different seismic ground motion directions, seven wind directions, and four different earthquake records, resulting in a total of 1113 time-domain simulations performed using a modified OpenFAST model that includes soil–structure interaction, kinematic interaction and multi-support input motion. Based on the results, the following conclusions can be drawn:

- Emergency shutdown is not necessarily beneficial in terms of reducing peak accelerations at the nacelle. The maximum accelerations in this case are 30% higher than during power production. On the other hand, the smallest peak accelerations are obtained for the power production mode when the earthquake acts along the fore–aft direction. This is due to the higher aerodynamic damping, which has a beneficial effect by reducing the magnitude of the vibrations induced by the earthquake. Emergency shutdown is also the mode that tends to produce the largest oscillations in displacements at the tower top.
- Due to the geometry of the four-legged jacket-supported OWT, the maximum internal forces and von Mises stresses are usually found when the ground shaking acts along one of the diagonals of the jacket structure and not aligned with the wind direction in the three operational modes. The shaking direction tends to have a larger influence on the peak internal forces than wind directionality. A greater influence of the misalignment between wind and shaking directions on the stresses at the jacket is observed in power production mode than in emergency shutdown and parked modes.
- The relative differences in the structural response in terms of maximum internal forces and stresses in the jacket structural members, when the turbine is working in the different operational modes, tend to be smaller than the differences in terms of accelerations at tower top.
- At the points of highest stresses (top and bottom of the legs) the percentage variations of the average peak von Mises stress for the different modes tend to be relatively small (<10% in most cases). On the contrary, along the intermediate parts of the legs, where the stresses are the lowest, the average peak von Mises stresses can vary up to 38% when comparing power production with

parked mode, and up to 27% when comparing power production with emergency shutdown.

- The maximum stresses appear almost always in the case of power production, with the exception of the top part of the legs, where higher stresses arise during emergency shutdown in several cases.
- The highest bending moments at the pile head are obtained when the shaking acts in side-to-side direction for the three modes. In this case, the maximum is obtained in parked mode. However, the maximum axial forces are observed when the misaligment between wind and shaking directions is 0° during power production. For emergency shutdown and parked modes, the maximum axial forces arise when the misaligment is 90°. In any case, the differences between the peak internal forces obtained for the different modes of operation, at the pile head, are below 8%.

In short, the results show that the structural response of the jacket is, under the occurrence of an earthquake, significantly influenced by the operational mode of the turbine at the time of arrival of the seismic waves, and by the misalignment between environmental and seismic loads. The magnitude of these influences has been quantified for the particular cases studied in this paper.

CRediT authorship contribution statement

Carlos Romero-Sánchez: Writing – review & editing, Writing – original draft, Visualization, Validation, Supervision, Software, Methodology, Investigation, Funding acquisition, Formal analysis, Conceptualization. **Luis A. Padrón:** Writing – review & editing, Validation, Supervision, Software, Methodology, Funding acquisition, Formal analysis, Conceptualization.

Declaration of competing interest

The authors declare that they have no known competing financial interests or personal relationships that could have appeared to influence the work reported in this paper.

Acknowledgements

This research was funded by the Ministerio de Ciencia, Innovación y Universidades, Spain and the Agencia Estatal de Investigación of Spain (MCIN/AEI/ 10.13039/501100011033) and FEDER, Spain through research project PID2020-120102RB-I00. In addition, C. Romero-Sánchez is a recipient of the research fellowship (TESIS2022010011), from the Program of predoctoral fellowships from the Consejería de Economía, Conocimiento y Empleo (Agencia Canaria de la Investigación, Innovación y Sociedad de la Información) of the Gobierno de Canarias and Fondo Social Europeo. The authors are grateful for this support.

References

Álamo, G., Bordón, J., Aznárez, J., 2021. On the application of the beam model for linear dynamic analysis of pile and suction caisson foundations for offshore wind turbines. Comput. Geotech. 134, 104107.

Álamo, G., Martínez-Castro, A., Padrón, L., Aznárez, J., Gallego, R., Maeso, O., 2016. Efficient numerical model for the computation of impedance functions of inclined pile groups in layered soils. Eng. Struct. 126, 379–390.

Alati, N., Failla, G., Arena, F., 2015. Seismic analysis of offshore wind turbines on bottom-fixed support structures. Phil. Trans. R. Soc. A 373 (2035), 20140086.

Arias, A., Hansen, R., 1970. Seismic design for nuclear power plants. In: A Measure of Earthquake Intensity. MIT Press Cambridge, pp. 438–483.

Asareh, M., Schonberg, W., Volz, J., 2016. Effects of seismic and aerodynamic load interaction on structural dynamic response of multi-megawatt utility scale horizontal axis wind turbines. Renew. Energy 86, 49–58.

Carbonari, S., Morici, M., Dezi, F., Leoni, G., 2018. A lumped parameter model for time-domain inertial soil-structure interaction analysis of structures on pile foundations. Earthq. Eng. Struct. Dyn. 47 (11), 2147–2171.

Cheng, Y., Luo, Y., Wang, J., Dai, K., Wang, W., El Damatty, A., 2023. Fragility and vulnerability development of offshore wind turbines under aero-hydro loadings. Eng. Struct. 293, 116625.

Chopra, A., 2017. Dynamics of Structures. Theory and Applications to Earthquake Engineering, Seventh ed. Pearson.

Clough, R., Penzien, J., 1995. Dynamics of Structures, third ed. Computers & Structures.

Damiani, R., Jonkman, J., Hayman, G., 2015. SubDyn User's Guide and Theory Manual. Technical Report, National Renewable Energy Lab.(NREL), Golden, CO (United States).

DNV, 2014. Design of Offshore Wind Turbine Structures. Offshore Standard DNV-OS-J101. DetNorske Veritas AS.

DNV, 2016. Loads and Site Conditions for Wind Turbines. Offshore Standard DNV-ST-0437. DetNorske Veritas AS.

Dobry, R., Idriss, I., Ng, E., 1978. Duration characteristics of horizontal components of strong-motion earthquake records. Bull. Seismol. Soc. Am. 68 (5), 1487–1520.

Eurcode 8 - Part 5, 2018. Eurocode 8: Design of Structures for Earthquake Resistance – Part 5: Foundations, Retaining Structures and Geotechnical Aspects. European Committee for Standardization.

Eurocode 3 - Part 1-6, 2007. Eurocode 3: Design of Steel Structures – Part 1-6: Strength and Stability of Shell Structures. European Committee for Standardization.

Global Wind Energy Council, 2023. Global Offshore Wind Report 2023. Technical Report, GWEC, Brussels, Belgium.

IEC, 2020. 61400-1:2020 Wind Energy Generation Systems - Part 1: Design Requirements. International Electrotechnical Commission.

IEC, 2021. 61400-3-1:2021 Wind Energy Generation Systems - Part 3-1: Design Requirements for Fixed Offshore Wind Turbines. International Electrotechnical Commission.

Ishihara, T., Iida, Y., Wang, L., 2024. Numerical study of combined seismic and aerodynamic loads on wind turbine support structures using coupled and uncoupled approaches. Structures 60, 105886.

ISO 19901-2, 2022. International Organization for Standardization. ISO 19901-2:2022 Petroleum and Natural Gas Industries — Specific Requirements for Offshore Structures — Part 2: Seismic Design Procedures and Criteria. International Organization for Standardization.

James, M., Haldar, S., 2022. Seismic vulnerability of jacket supported large offshore wind turbine considering multidirectional ground motions. Structures 43, 407–423.

Jonkman, B., 2009. TurbSim User's Guide: Version 1.50. Technical Report, National Renewable Energy Lab.(NREL), Golden, CO (United States).

Jonkman, J., Butterfield, S., Musial, W., Scott, G., 2009. Definition of a 5-MW Reference Wind Turbine for Offshore System Development. Technical Report, National Renewable Energy Lab.(NREL), Golden, CO (United States).

Jonkman, J., Musial, W., 2010. Offshore Code Comparison Collaboration (OC3) for IEA Wind Task 23 Offshore Wind Technology and Deployment. National Renewable Energy Lab.(NREL), Golden, CO (United States).

Ju, S.-H., Huang, Y.-C., 2019. Analyses of offshore wind turbine structures with soil-structure interaction under earthquakes. Ocean Eng. 187, 106190.

Katsanos, E., Sanz, A., Georgakis, C., Thöns, S., 2017. Multi-hazard response analysis of a 5MW offshore wind turbine. Procedia Eng. 199, 3206–3211.

Løken, I., Kaynia, A., 2019. Effect of foundation type and modelling on dynamic response and fatigue of offshore wind turbines. Wind Energy 22 (12), 1667–1683. http://dx.doi.org/10.1002/we.2394.

Meng, J., Dai, K., Zhao, Z., Mao, Z., Camara, A., Zhang, S., Mei, Z., 2020. Study on the aerodynamic damping for the seismic analysis of wind turbines in operation. Renew. Energy 159, 1224–1242.

Mo, R., Cao, R., Liu, M., Li, M., Huang, Y., 2021. Seismic fragility analysis of monopile offshore wind turbines considering ground motion directionality. Ocean Eng. 235, 109414.

Moriarty, P., Hansen, A., 2005. AeroDyn Theory Manual. Technical Report, National Renewable Energy Lab., Golden, CO (US).

Musial, W., Spitsen, P., Beiter, P., Duffy, P., D.M., H., Hammond, R., Shields, M., Marquis, M., 2023. Offshore Wind Market Report: 2023 Edition. Technical Report, National Renewable Energy Laboratory(NREL), Golden, CO (United States).

National Renewable Energy Laboratory, 2024. OpenFAST Documentation. Release v3.5.2. National Renewable Energy Laboratory, https://openfast.readthedocs.io/en/main/. Code published at https://github.com/OpenFAST/openfast.

National Research Institute for Earth Science and Disaster Resilience (K-NET), 2022. Strong-motion seismograph networks. Available online: https://www.kyoshin.bosai.go.jp/. (Accessed on 20 November 2022).

Pacific Earthquake Engineering Research Center (PEER), 2022. NGA-West2 ground motion database. Available online: ngawest2.berkeley.edu/. (Accessed 20 November 2022).

Padrón, L., Carbonari, S., Dezi, F., Morici, M., Bordón, J., Leoni, G., 2022. Seismic response of large offshore wind turbines on monopile foundations including dynamic soil–structure interaction. Ocean Eng. 257, 111653.

Romero-Sánchez, C., Padrón, L., 2022. Implementation of ground input motion and dynamic soil-structure interaction into openfast for the seismic analysis of offshore wind turbines. In: Congress on Numerical Methods in Engineering. CMN 2022, International Center for Numerical Methods in Engineering (CIMNE).

Romero-Sánchez, C., Padrón, L., 2023. An implementation of multi-support input motion into openfast for the earthquake analysis of offshore wind turbines. COMPDYN Proc..

Romero-Sánchez, C., Padrón, L., 2024. Influence of wind and seismic ground motion directionality on the dynamic response of four-legged jacket-supported Offshore Wind Turbines. Eng. Struct. 300, 117191.

Vorpahl, F., Popko, W., Kaufer, D., 2011. Description of a Basic Model of the "UpWind Reference Jacket" for Code Comparison in the OC4 Project under IEA Wind Annex XXX, vol. 450, Fraunhofer Institute for Wind Energy and Energy System Technology (IWES), Germany.

Xi, Y., Lin, K., Pan, J., Sun, L., Li, H., Wang, Z., 2023. Bending moment characteristic analysis of utility-scale onshore wind turbine blades based on monitoring data. Eng. Struct. 294, 116714.

Yang, Y., Bashir, M., Li, C., Wang, J., 2019. Analysis of seismic behaviour of an offshore wind turbine with a flexible foundation. Ocean Eng. 178, 215–228.

Zuo, H., Bi, K., Hao, H., 2018. Dynamic analyses of operating offshore wind turbines including soil-structure interaction. Eng. Struct. 157, 42–62.

Zuo, H., Bi, K., Hao, H., Li, C., 2019. Influence of earthquake ground motion modelling on the dynamic responses of offshore wind turbines. Soil Dyn. Earthq. Eng. 121, 151–167.

2.3 Third publication: Romero-Sánchez et al., 2024, Influence of Foundation–Soil–Foundation Interaction on the Dynamic Response of Offshore Wind Turbine Jackets Founded on Buckets, Journal of Marine Science and Engineering.

Table 2.3. Third publication data.

Title	Influence of Foundation–Soil–Foundation Interaction on the Dynamic Response of Offshore Wind Turbine Jackets Founded on Buckets
Authors	C. Romero-Sánchez, J.D.R. Bordón and L.A. Padrón
Journal	Journal of Marine Science and Engineering
DOI	10.3390/jmse12112089
ISSN	2077-1312
Impact factor	2.7
CiteScore	4.4
Category	ENGINEERING, MARINE
Quartile	Q1
Publisher	MDPI
Volume	12(11)
Date	November 2024

Journal of Marine Science and Engineering

MDPI

Article

Influence of Foundation–Soil–Foundation Interaction on the Dynamic Response of Offshore Wind Turbine Jackets Founded on Buckets

Carlos Romero-Sánchez *, Jacob D. R. Bordón and Luis A. Padrón

University Institute of Intelligent Systems and Numerical Applications in Engineering, Universidad de Las Palmas de Gran Canaria, 35017 Las Palmas de Gran Canaria, Spain; jacobdavid.rodriguezbordon@ulpgc.es (J.D.R.B.); luis.padron@ulpgc.es (L.A.P.)
* Correspondence: carlos.romero@ulpgc.es

Abstract: This study investigates the impact of soil–structure interaction (SSI) and foundation–soil–foundation interaction (FSFI) on the dynamic behaviour of jacket substructures founded on buckets for offshore wind turbines. A parametric analysis was conducted, focusing on critical load cases for conservative foundation design. Different load configurations were examined: collinear wind and wave (fluid–structure interaction) loads, along with misaligned configurations at 45° and 90°, to assess the impact of different loading directions. The dynamic response was evaluated through key structural parameters, including axial forces, shear forces, bending moments, and stresses on the jacket. Simulations employed the National Renewable Energy Laboratory (NREL) 5MW offshore wind turbine mounted on the OC4 project jacket founded on suction buckets. An additional optimised jacket design was also studied for comparison. An OpenFAST model incorporating SSI and FSFI considering a homogeneous soil profile was employed for the dynamic analysis. The results highlight the significant role of the FSFI on the dynamic behaviour of multi-supported jacket substructure, affecting the natural frequency, acceleration responses, and internal forces.

Keywords: offshore wind turbines; jacket; bucket foundations; suction caisson; soil–structure interaction; foundation–soil–foundation interaction; OpenFAST; structural response

check for updates

Citation: Romero-Sánchez, C.; Bordón, J.D.R.; Padrón, L.A. Influence of Foundation–Soil–Foundation Interaction on the Dynamic Response of Offshore Wind Turbine Jackets Founded on Buckets. *J. Mar. Sci. Eng.* **2024**, *12*, 2089. https://doi.org/10.3390/jmse12112089

Received: 29 October 2024
Revised: 13 November 2024
Accepted: 17 November 2024
Published: 19 November 2024

Copyright: © 2024 by the authors. Licensee MDPI, Basel, Switzerland. This article is an open access article distributed under the terms and conditions of the Creative Commons Attribution (CC BY) license (https://creativecommons.org/licenses/by/4.0/).

1. Introduction

In recent years, offshore wind energy has emerged as a crucial element in the expansion of renewable energy around the globe. Nowadays, most offshore wind turbines (OWTs) are installed in regions where sea depths allow for fixed-base units. Among these installations, monopiles constitute the most widely used substructure [1]. Nevertheless, the increasing deployment of wind farms in deeper waters has driven a significant rise in the adoption of multi-support substructures, such as jackets and tripods supported on piles or suctions caissons [2].

Determining the natural frequency of an offshore wind turbine is a critical aspect of the design process, as it helps to avoid resonance phenomena that could lead to structural failure or long-term deterioration due to fatigue. Consequently, it is essential to ensure that the system's fundamental frequency does not coincide with the rotor's operational speed range (1P) or the rotor blades' transition frequency (3P). Various studies have examined the influence of soil–structure interaction (SSI) on the natural frequencies of offshore wind turbines supported by monopiles [3–7] and jacket substructures [8–10], with significant effects observed.

The influence of SSI on the natural frequencies can be determined by using a complete soil–foundation–structure model, or by including the dynamic stiffnesses of the soil–foundation subsystem in the superstructure model. In order to determine the static

and dynamic stiffnesses, researchers have traditionally employed analytical methods applied to fundamental problems, such as the widely studied circular footing, which often yield closed-form solutions or methodologies that are both simple and of considerable practical utility, offering valuable physical insight [11,12]. While numerical methods like the Finite Element Method (FEM) and the Boundary Element Method (BEM) enable the analysis of more complex, general problems [13–15], the development of such models requires significant expertise and can be time-intensive. A relevant case is the application of this methodology to the calculation of stiffnesses and impedances of bucket foundations (see e.g., [16–19]). Consequently, considerable effort has been directed towards deriving closed-form expressions and stiffness charts based on numerical results. Some of these results [20,21] have been incorporated into various design codes, including the offshore standard DNV-OS-J101 [22].

Conversely, in comparison to the study of isolated foundations, the topic of the interaction between foundations has garnered less attention [23–27]. Some authors explore the dynamic interaction between rigid foundations on viscoelastic soils, using a 3D Boundary Element Method (BEM) and focusing on foundation–soil–foundation interaction (FSFI) [28–31], i.e., the effects of interaction through the soil between two or more foundations. This interaction results in a change in the stiffness of each element within the group when compared to the corresponding stiffness of the single foundation.

Thus, the volume of research focused on analysing the dynamic behaviour of OWT jackets founded on buckets including FSFI (or group effect) is small when compared with the number of studies conducted on monopod suction caissons. Furthermore, there is a significantly greater body of literature addressing jackets on piles compared to jackets on bucket foundations. For jackets on piles, SSI is typically modelled using approaches such as linear or nonlinear springs and dashpots [12,32–36]. In all of these studies, the dynamic characteristics of the foundation are critical to the overall dynamic response of the support structure. However, research focusing on jackets supported by suction caissons remains limited [16,37–43], despite their widespread use in current projects. Bhattacharya et al. [37] demonstrated that the fundamental eigenfrequency of vibration for offshore wind turbines (OWTs) supported by multiple shallow foundations (e.g., jackets mounted on three or four suction caissons) is primarily associated with low-frequency rocking modes of vibration about the principal axes. Jalbi et al. [38] demonstrated that a low vertical foundation stiffness, coupled with a low aspect ratio, facilitates the onset of a rocking mode of vibration in jacket-supported offshore wind turbines. Additionally, Cheng et al. [41] investigated the dynamic behaviour of the jacket structure under varying wind and wave directions, revealing that the parked mode significantly influenced the calculated fragilities associated with critical damage conditions in both the tower and the jacket structure. A contribution to the field of buckets is the work of Bordón et al. [44]. The authors propose a methodology for incorporating the foundation–soil–foundation interaction effects into the stiffness matrices of foundations of shallow and bucket foundations, and demonstrate its influence on the natural frequencies and stiffness of a jacket structure.

Several of the aforementioned studies primarily focus on the structural properties of OWTs using simplified models. However, the dynamic properties of these support structures play a crucial role in the system's design, and the distinctive characteristics of the OWTs including the specific nature of loads, the system's variable geometry due to blade rotation, and the continuous influence of the control system, suggest that specific tools, able to adequately model the various subsystems, should be used in structural and dynamic response analyses. For this reason, many authors analyse the dynamic response of OWTs by considering the combined effects of aerodynamic and wave loadings [45–48]. Time-domain analyses, incorporating nonlinear aero-hydro-servo-elastic simulations [32,34,35,49], are essential for accurately capturing the turbine's dynamic behaviour across different operational modes.

Thus, the review of the existing literature highlights the significant influence of SSI on the dynamic response of OWT jackets founded on buckets. Additionally, it highlights

the importance of considering various operating modes and the misalignment between wind and wave directions in assessing the dynamic behaviour of substructures. As a continuation in this line of research, this study evaluates the influence of the foundation–soil–foundation interaction on the dynamic response of jacket substructures for OWTs, founded on suction buckets. To do so, time-domain coupled analysis in OpenFAST will be used. Specifically, the paper analyses the structural response of the OC4 project four-legged jacket substructure for the NREL 5MW OWT subjected to different design load cases. The results obtained for an optimised jacket substructure are also presented.

2. Problem Definition

2.1. Offshore Wind Turbine Properties

The NREL 5 MW three-bladed turbine [50] is employed in this study. The main parameters of the OWT are given in Table 1. The support structure considered is the jacket support substructure designed for the phase I of the OC4 project, described by Vorpahl et al. [51]. Figure 1 provides an illustration of the main characteristics of the jacket structure for the OWT and Figure 2 details the geometry of the jacket. The properties of the steel material are as follows: shear modulus 80.8 GPa, Young's modulus 210 GPa, mass density 7850 kg/m^3, and damping ratio 2%. Bucket foundations are considered, with the characteristics provided by Salem et al. [52] for this structure. Thus, a diameter of 4.0 m and length of 4.0 m are considered. A homogeneous linear elastic half-space with a Poisson's ratio $\nu = 0.28$ and shear modulus $\mu = 15.625$ MPa is assumed.

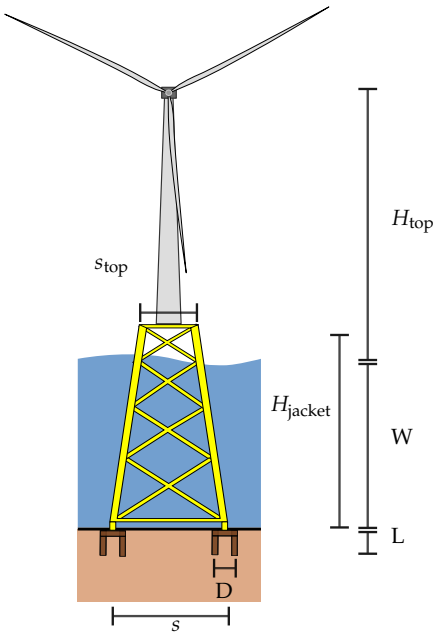

Figure 1. Representation of the NREL 5MW OWT mounted on a jacket founded on buckets.

Table 1. Key parameters of the offshore wind turbine.

Parameter	Value
Rotor diameter [m]	126
RNA mass [ton]	350
Rated wind speed [m/s] (V_r)	11.4
Hub height [m]	90.55
Tower top height from mean sea level [m] (H_{top})	88.15
Tower base height from mean sea level [m]	20.15

Table 1. *Cont.*

Parameter	Value
Thickness at the top of the tower [m]	30
Thickness at the tower base [m]	32
Tower top diameter [m]	4.00
Tower base diameter [m]	5.60
Water depth [m] (W)	50.00
Jacket height [m] (H_{jacket})	70.15
Top leg spacing [m] (s_{top})	8.00
Base leg spacing [m] (s)	12.00
Number of bracing levels	4
Number of legs	4

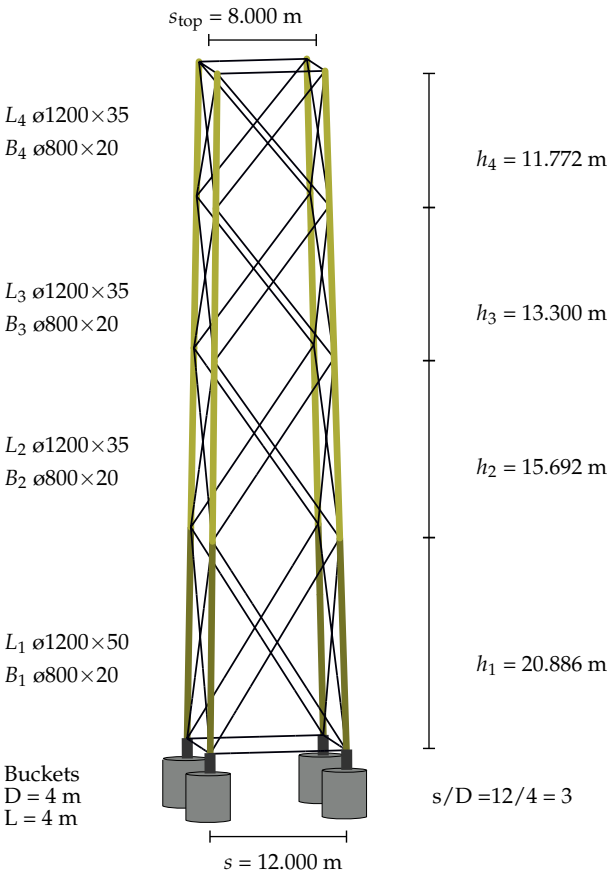

Figure 2. Geometry of the OC4 jacket with buckets. The diameter and thickness of each leg level L_i and bracings B_i are provided at the left of the figure in millimetres.

2.2. Load Cases

Wind turbines are exposed structures that must withstand a range of external influences, with the ability to operate under medium to high wind speeds being a fundamental requirement. Factors such as steady winds and turbulence serve as significant contributors to the overall loading experienced by wind turbines. The load analysis entails assessing the structural integrity of the system by evaluating a set of design load cases (DLCs). These DLCs are established in accordance with guidelines set by DNV [53].

Typically, design codes [53,54] describe hundreds of load cases for the design of offshore wind turbines, aimed at ensuring a service life of 25–30 years. However, not all these cases are pertinent to foundation design. For this study, the load cases outlined in Table 2 have been identified as the most relevant for performing a conservative analysis of the foundations, as described in Jalbi et al. [55] for jacket structures.

Table 2. Load scenarios.

SSI	**Fixed Base**	**SSI without FSFI**	**SSI with FSFI**
Operational Modes	**Power Production**	**Parked Mode**	
ID	**Case**	**Wind Model**	**Wave Model**
E-1	Normal Operational Conditions	Normal Turbulence Model (NTM) at the rated wind speed (V_r)	1-Year Extreme Sea States (ESS)
E-2	Extreme Wave Load Scenario	Extreme Turbulence Model (ETM) at the rated wind speed (V_r)	50-Year Extreme Wave Height (EWH)
E-3	Extreme Wind Load Scenario	Extreme Operating Gust (EOG) at the rated wind speed (V_r)	1-Year Extreme Wave Height (EWH)
Collinear 0° (C0)	Misalignment 90° (M90)	Misalignment 45° (M45)	Collinear 45° (C45)

The wind farm is situated at a location on the boundary waters between Dutch and British, with an average water depth of 50 m. Metocean conditions for this site are publicly accessible through the Dutch National Institute for Coastal and Marine Management. Extreme sea conditions, including Extreme Sea States (ESS) and Extreme Wave Height (EWH), are calculated as defined by DNVGL-ST-0437 [53], which classifies them into different categories based on wave height and frequency over specific periods. One-Year ESS and One-Year EWH correspond to extreme waves within a 1 year return period, with ESS determined by the average significant wave height ($H_{S,1}$) and EWH by the maximum recorded wave height ($H_{m,1}$). Similarly, 50-Year models pertain to a 50 year return period, where 50-year EWH is based on the Extreme Wave Height ($H_{m,50}$).

A summary of the metocean data is provided in Table 3. The wave loads in OpenFAST are computed through the module HydroDyn, where the wave kinematics model is chosen and defined. For the irregular waves, the JONSWAP spectrum was used since the sea state is considered developing when there are high wind speeds blowing on the wind turbine. The significant wave height and spectral wave period were detailed in accordance with the specified load case.

Table 3. Metocean data.

Parameter	**Value**
1-Year Significant Wave Height ($H_{S,1}$) [m]	6.6
1-Year Significant Wave Period ($T_{S,1}$) [s]	9.1
1-Year Maximum Wave Height ($H_{m,1}$) [m]	8.27
1-Year Maximum Wave Period ($T_{m,1}$) [s]	10.97
50-Year Maximum Wave Height ($H_{m,50}$) [m]	15.33
50-Year Maximum Wave Period ($T_{m,50}$) [s]	13.86

The turbulent wind fields, following the Kaimal spectrum, are generated in TurbSim for a hub-height mean wind speed of V_r = 11.4 m/s. This includes simulations under the Normal Turbulence Model (NTM), Extreme Turbulence Model (ETM), and Extreme Operating Gust (EOG), as well as Category B turbulent wind conditions [54]. The aerodynamic

forces acting on the blades and tower are calculated using the Blade Element Mode theory through the AeroDyn module.

The impacts of the operational modes and of the directionality of the loads on the jacket substructure have been previously analysed and discussed in [56]. The authors concluded that load combinations involving aligned wind and ground motion directions do not necessarily represent the worst-case scenario. The dynamic behaviour of the jacket, considering both wind and wave directions, was investigated by Cheng et al. [41], and they highlight the significant role of considering the parked mode in the computed fragilities of severe damage states for the tower and jacket structure. This effect is attributed to the increased aerodynamic damping, which helps mitigate the magnitude of vibrations induced by wind loads [32,57]. The analysis of the previous studies highlighted above reveals a clear influence of different operating modes and the misalignment between wave and wind directions on the dynamic response of the jacket.

In this paper, the dynamic response of the OWT is studied for two different operational modes: power production and parked modes, to compare the influence of the working conditions on the internal forces at the jacket substructure, considering bucket foundations. In addition, four potential loading scenarios can be considered: (C0) wind and wave loads are collinear, (M90) wind and wave loads are misaligned by 90°, (M45) wind and wave loads are misaligned by 45°, and (C45) wind and wave loads act at 45° relative to the structure. The hub is consistently oriented in the wind direction. Each of these scenarios must be evaluated against the load cases presented in Table 2. Figure 3 shows a graphical overview of the different load combinations used in the analysis.

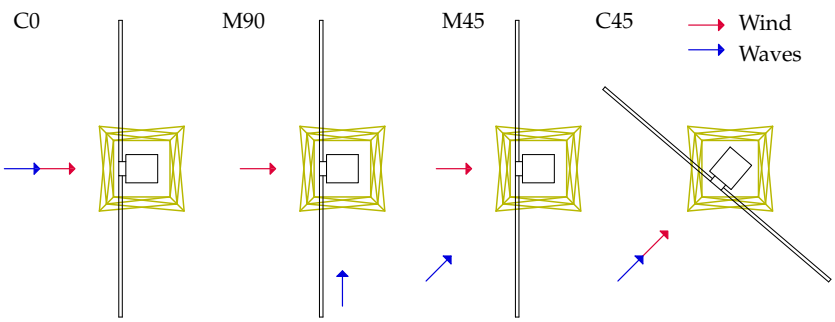

Figure 3. Plan view illustrating the loading direction on the OWT.

The analysis comprised a total of 144 distinct simulations. Each simulation lasted for 400 s, and the analysis was initiated at 150 s to mitigate the influence of the primary transient behaviour of the system. All load case combinations were simulated under three different conditions: fixed-based (No SSI), taking into account the foundation–soil–foundation interaction (SSI with FSFI), and considering the SSI using the corresponding stiffnesses to the single foundations without considering FSFI (SSI without FSFI).

3. Methodology

The incorporation of bucket–soil–bucket interaction effects into an OpenFAST model of a jacket-supported OWT requires the use of a model of this phenomenon formulated in such a way that it is compatible with the OpenFAST framework, without adding excessive complexity. With this idea in mind, bucket–soil–bucket interaction effects are herein incorporated through the alteration of the stiffness functions that define the response of each individual foundation. Such expressions are provided in closed-form format by Bordón et al. [44]. At the same time, and in order to be able to incorporate this information into OpenFAST, the SubDyn module was modified with the introduction of a stiffness matrix to represent the bucket foundations embedded in the homogeneous soils and with the ability to consider the foundation–soil–foundation interaction in multi-supported

structures. The OpenFAST model is employed to simulate the dynamic response of the OWTs considering different load cases. The primary practical contribution lies in its application to the time-domain analysis of polygonal configurations of multi-bucket jacket foundations for OWTs.

3.1. Soil–Structure Interaction

The formulation of a closed-form static stiffness matrix for bucket foundations and a set of formulas for correcting the stiffnesses obtained from single-foundation formulation are proposed by Bordón et al. [44,58]. A rigorous numerical model based on the Boundary Element Method (BEM) [17] is used to compute the stiffnesses of single foundations, and foundations as part of a group acting in a particular mode (vertical, horizontal, rocking, and torsion). The primary components consist of the stiffness parameters for the single foundation and the Green's function, which relates to the applied loads (including point forces and moments) and the observed responses (such as displacements and rotations) at the free surface.

These stiffness matrices can be readily incorporated into a superstructure finite element model to account for soil–structure interaction, including foundation–soil–foundation effects.

3.1.1. Simplified Stiffness Matrix

The stiffness matrix is derived in closed form from existing results pertaining to single foundations. The stiffness matrix attached to each jacket leg contains the six degrees of freedom and can be written as follows:

$$\mathbf{K}_0^{\text{no-int}} = \begin{bmatrix} K_H & 0 & 0 & 0 & -K_{SR} & 0 \\ 0 & K_H & 0 & K_{SR} & 0 & 0 \\ 0 & 0 & K_V & 0 & 0 & 0 \\ 0 & K_{SR} & 0 & K_{SR} & 0 & 0 \\ -K_{SR} & 0 & 0 & 0 & K_R & 0 \\ 0 & 0 & 0 & 0 & 0 & K_{KT} \end{bmatrix} \tag{1}$$

where K_H, K_V, K_R, K_{SR}, and K_T are the horizontal, vertical, rocking, coupled sway-rocking, and torsional stiffnesses. Specifically, the closed-form formulas for stiffness of rigid cylindrical foundations in homogeneous linear elastic half-space with depth L ($0 \leq$ L/D ≤ 6) and diameter D, perfectly bonded to the surrounding homogeneous soil with Poisson's ratio (ν) ($0 \leq \nu \leq 0.5$) and shear modulus μ, are employed in the present study. These formulas were derived for single foundations, which were used to fit enriched equations similar to those presented by Gazetas [20] and Wolf [59], leading to the following expressions:

$$K_V = \frac{2\mu D \ln(3-4\nu)}{1-2v}\left[1 + 1.08(1-0.76\nu)\left(\frac{L}{D}\right)^{0.82}\right] \tag{2}$$

$$K_H = \frac{4\mu D}{2-\nu}\left[1 + 1.85\left(\frac{L}{D}\right)^{0.75}\right] \tag{3}$$

$$K_R = \frac{\mu D^3}{3(1-v)}\left[1 + 7.7(1-1.2\nu)\left(\frac{L}{D}\right) + 10(1-0.7\nu)\left(\frac{L}{D}\right)^{2.5}\right] \tag{4}$$

$$K_{SR} = \frac{11\mu D^2}{4(15-17v)}\left[1 - 2\nu + 9.7(1-1.13\nu)\left(\frac{L}{D}\right) + 11.2(1-0.82\nu)\left(\frac{L}{D}\right)^{1.75}\right] \tag{5}$$

$$K_T = \frac{2\mu D^3}{3}\left[1 + 5.26\left(\frac{L}{D}\right)^{0.93}\right] \tag{6}$$

3.1.2. Foundation–Soil–Foundation Interaction

A practical way of incorporating the foundation–soil–foundation interaction into the computation of the stiffness of multi-bucket foundations is presented in [44], introducing a

set of closed-form correction factors to the common simplified stiffness matrix built from the already known stiffnesses of individual single buckets. The closed-form formulae were obtained for tripod and tetrapod arrangements of buckets in homogeneous and non-homogeneous soils.

Group effects are sensitive mainly to spacing ($\tilde{s} = s/D$), Poisson's ratio (ν), foundation shape ratio (L/D), diameter (D), and the number of foundations (N = 4). To quantify the magnitude of the foundation–soil–foundation interaction within the entire foundation system, the following group effect stiffness correction factors can be defined:

$$\gamma_{[\,]} = \frac{K^{\mathrm{FSFI}}_{[\,]}}{K_{[\,]}} \tag{7}$$

where the subindex [ ] = H,V,R,SR,T denotes any of the stiffness components. They relate stiffnesses including interaction and stiffnesses not including it. These group effect stiffness correction factors for multi-bucket foundations in homogeneous soil for tetrapod arrangements are approximated as follows:

$$\gamma_V = \frac{1}{1 + ((1-\nu)(1+\sqrt{2}/4)k_V)/\tilde{s}} \tag{8}$$

$$\gamma_H = \frac{1 + (p_1 k_H)/\tilde{s}}{1 + (q_1 k_H)/\tilde{s} + (q_2 k_H^2)/\tilde{s}} \tag{9}$$

$$\gamma_R = \frac{1 + (p_2 k_R/k_V)/\tilde{s}^2 + (p_3 k_R)/\tilde{s}^3 + (p_5 k_R^2/k_V)/\tilde{s}^5 + (p_6 k_R^2)/\tilde{s}^6}{(1 + (p_2 k_R/k_V)/\tilde{s}^2)(1 + (q_1 k_V)/\tilde{s} + (q_3 k_R)/\tilde{s}^3 + (q_4 k_R K_V)/\tilde{s}^4 (q_6 k_R^2)/\tilde{s}^6 + (q_7 K_R^2 k_V)/\tilde{s}^7)} \tag{10}$$

$$\gamma_{SR} = \left[1 + \frac{3(1-2\nu)}{16\pi}\frac{K_H K_V}{\mu K_{SR}}\right]\gamma_H \tag{11}$$

$$\gamma_T = \frac{1 + (p_2 k_T/k_H)/\tilde{s}^2 + (p_3 k_T)/\tilde{s}^3}{(1 + (p_2 k_T/k_H)/\tilde{s}^2)(1 + (q_1 k_H)/\tilde{s} + (q_3 k_T)/\tilde{s}^3 + (q_4 k_H k_T)/\tilde{s}^4)} \tag{12}$$

where $k_V = K_V/(\pi\mu D)$ is the dimensionless vertical stiffness; $k_H = K_H/(\pi\mu D)$ = is the dimensionless horizontal stiffness; $k_R = K_R/(\pi\mu D^3)$ is the dimensionless rocking stiffness; and $k_T = K_T/(\pi\mu D^3)$ is the dimensionless torsional stiffness. Each p and q coefficient is defined in Bordón et al. [44].

The previously defined correction factors allow a partial introduction of foundation–soil–foundation interaction effects, which is only valid when the global response of the rigidly connected foundation system is required. This applies specifically to the jacket structures examined in this study, which include a tie beam.

Finally, the aforementioned is incorporated into a stiffness matrix $\mathrm{K}^{\mathrm{FSFI}}$, which considers the foundation–soil–foundation interaction effects and, similarly to (1), is expressed as follows:

$$\mathbf{K}_0^{\mathrm{FSFI}} = \begin{bmatrix} K_H^{\mathrm{FSFI}} & 0 & 0 & 0 & -K_{SR}^{\mathrm{FSFI}} & 0 \\ 0 & K_H^{\mathrm{FSFI}} & 0 & K_{SR}^{\mathrm{FSFI}} & 0 & 0 \\ 0 & 0.0 & K_V^{\mathrm{FSFI}} & 0 & 0 & 0 \\ 0 & K_{SR}^{\mathrm{FSFI}} & 0 & K_R^{\mathrm{FSFI}} & 0 & 0 \\ -K_{SR}^{\mathrm{FSFI}} & 0 & 0 & 0 & K_R^{\mathrm{FSFI}} & 0 \\ 0 & 0.0 & 0 & 0 & 0 & K_{KT}^{\mathrm{FSFI}} \end{bmatrix} \tag{13}$$

Table 4 shows the values of the single stiffnesses (no-int) and considering the foundation–soil–foundation interaction (FSFI) employed in the study.

Table 4. Stiffness values computed for the single bucket foundations ($K^{\text{no-int}}$) and for the bucket foundations as part of a group, including FSFI (K^{FSFI}).

	$\boldsymbol{K}^{\text{no-int}}_{[\,]}$	$\gamma_{[\,]}$	$\boldsymbol{K}^{\text{FSFI}}_{[\,]}$
Vertical	3.3181×10^8 [N/m]	0.6525	2.1651×10^8 [N/m]
Horizontal	4.1424×10^8 [N/m]	0.5567	2.3061×10^8 [N/m]
Rocking	6.5522×10^9 [Nm]	1.0062	6.5928×10^9 [Nm]
Sway-rocking	1.0540×10^9 [N]	0.6176	6.5100×10^8 [N]
Torsional	4.1733×10^9 [Nm]	0.9819	4.0978×10^9 [Nm]

3.2. Numerical Model

The numerical tool employed in this study is built upon OpenFAST [60], an advanced open-source multi-physics and multi-fidelity platform developed in Fortran 95, designed for simulating the coupled dynamic behaviour of wind turbines in the time domain. Managed by the National Renewable Energy Laboratory, OpenFAST is not merely a standalone program but rather a comprehensive framework that integrates various computational modules. These modules interact through a loosely coupled time-integration scheme, where a glue code facilitates data exchange between them at each time step.

All time-domain simulations analysed in this study were carried out considering the following features: aerodynamic loads on the blades and tower were computed using the AeroDyn module [61], which incorporates rotor wake and induction effects, blade airfoil aerodynamics, tower influence on fluid behaviour near the blade nodes, and tower drag. Wind input files were generated by TurbSim [62]. The structural dynamic responses of the rotor, drivetrain, nacelle, and tower were modelled with the ElastoDyn module. ServoDyn module is employed for the modelling of the wind turbine's control and electrical subsystems. Wave loads and fluid–structure interaction effects were captured using the HydroDyn module [63], which utilises the potential flow theory, strip theory, or a combination of both to calculate hydrodynamic loads on the submerged portions of the substructure. The structural dynamic response of the substructure, from the transition piece to the foundation, was modelled using the SubDyn module [64], based on a linear frame finite element beam discretisation. Further details on each module can be found in the OpenFAST documentation [60].

In this study, the soil–structure interaction within OpenFAST is modelled using a substructuring approach. The SSI is represented by linear springs connected to the base of the jacket legs. The considered linear spring stiffnesses (see Table 4) represent the main mechanical behaviour of a foundation system of four buckets founded on a homogeneous linear elastic half-space. Such a simple model is reasonable for a first approach to the problem given the small displacements and low frequencies associated with the dynamic response of the system at hand. Other phenomena such as material and radiation damping, soil nonlinearities, soil degradation, and added mass from the foundation system are neglected from the dynamic analysis. If the considered model based on first principles reveals that the FSFI effects are relevant enough, refinements such as these mentioned should be included in future studies.

4. Results

4.1. Frequency Response

Figure 4 presents the fore-aft Power Spectral Densities (PSDs) of the OWT, obtained from fore-aft accelerations measured at the tower top under parked mode conditions and subjected to environmental loads. Results are presented for the three different approaches considered in this study: (a) fixed-base model (labelled No SSI), (b) compliant-base model, without considering FSFI (SSI without FSFI), and (c) compliant-base model, considering FSFI (SSI with FSFI).

The fundamental frequency is 0.31 Hz for the fixed-base scenario, 0.23 Hz when considering SSI without FSFI, and 0.21 Hz when FSFI is taken into account. FSFI plays a

significant role in the reduction of the fundamental frequency, causing approximately a 35% reduction in the fore–aft direction compared to the fixed-base case. These values are in close alignment with those reported by Salem et al. [52] for same the reference jacket structure. It can therefore be assumed that the OpenFAST model accurately represents the dynamic response of the system considering SSI and FSFI. The reduction of the fundamental frequency when considering FSFI may require a refinement of the design to accommodate an additional safety margin, in accordance with DNVGL [65] guidelines.

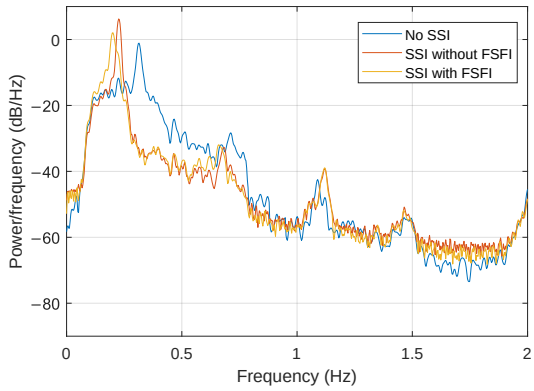

Figure 4. Power Spectral Densities in the fore–aft direction obtained from the response of the 5 MW OWT on the OC4 jacket in parked conditions, under fixed, SSI without FSFI, and SSI with FSFI hypotheses.

4.2. Time History Accelerations

To illustrate the influence of the SSI on the dynamic behaviour of the systems, Figure 5 presents a representative example of the time histories for fore-aft accelerations (0°) at the tower top of the OWT during power production mode. This scenario is subjected to environmental loads aligned with the fore-aft (FA) direction, specifically defined for load cases E-1 and E-2. This variable is relevant because the maximum accelerations in the rotor nacelle assembly (RNA) are limited due to serviceability constraints, and the average amplitude is related to the operational lifespan of the wind turbine.

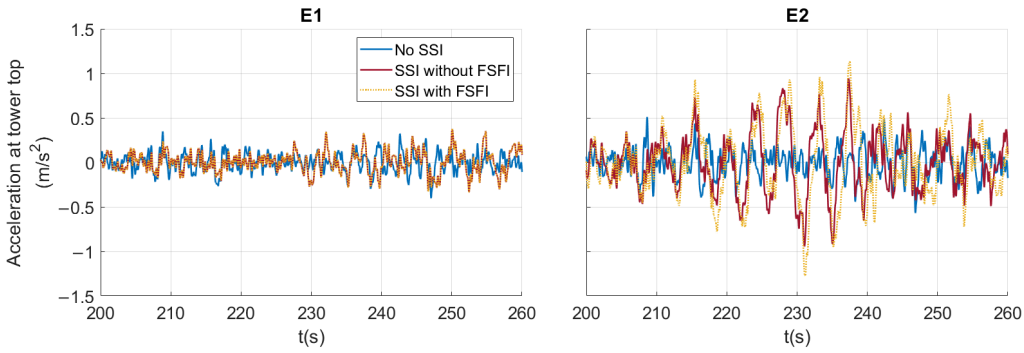

Figure 5. Time history responses corresponding to accelerations at the tower top subjected to environmental loads in the fore-aft direction during power production.

The added flexibility introduced by the foundation leads to amplified peak responses. SSI is critical for the dynamic behaviour of the tower top due to the increased accelerations and displacements observed in this region, particularly when FSFI is taken into account. This highlights the essential role of integrating FSFI to ensure a precise and robust evaluation of wind turbine design. These trends will be explored in more detail in the following subsections.

4.3. Structural Response

The influence of the three different SSI hypotheses in the different load cases is analysed in this section in terms of internal forces in the jacket. In all cases, responses for any given variable are computed as follows:

$$X(t) = \sqrt{X_x(t)^2 + X_y(t)^2} \tag{14}$$

where $X_x(t)$ and $X_y(t)$ are the time histories of the responses along the fore-aft and side-to-side directions, respectively. The results are analysed in terms of peak values and also of root mean squared (RMS) values, which is crucial for determining whether the observed trends are consistent throughout the entire time response, rather than just representative of isolated peaks. A detailed comparison of the results is conducted in terms of bending moments and shear forces at the base of the legs, which connects the foundation to the jacket, specifically at the leg where the maximum force value is obtained, and the tower top accelerations.

Figure 6 illustrates the peak values obtained for each load case and load alignment during power production. Each row shows the accelerations at the top of the tower, the shear forces and the bending moments at the base of the leg, while each column shows the three load cases with their respective load direction configurations. In addition, each coloured bar represents a different SSI hypothesis. As anticipated from Figure 5, accounting for SSI in the system leads to higher peak accelerations at the top of the tower due to the increased flexibility of the system. Increases in peak acceleration of up to 60% are observed between the fixed and SSI with FSFI hypotheses. FSFI reduces peak shear forces while, at the same time, increases peak bending moments. In terms of internal forces, the highest peak values are observed in load case E-2, particularly in scenarios where wave and wind loads are misaligned. The extreme wave loading scenario generates the most significant peak responses in the jacket substructure. However, the maximum acceleration values at the tower top are recorded in load case E-3, corresponding to the extreme wind load scenario. To determine whether the observed trends are consistent throughout the entire time response, Figure 7 presents the shear forces and bending moments at the base of the legs in terms of RMS values, following the same labelling as Figure 6.

The trends in terms of RMS shear forces are similar to those observed for peak shear forces. In terms of bending moments, the RMS values clearly show higher magnitudes when foundation–soil–foundation interaction is considered. This trend is not as evident when bending moments peak values are analysed, where, in some cases, higher values are observed in the fixed-base scenario.

The results indicate that, in terms of RMS values, the internal forces are greater when FSFI is considered, which may have a more significant impact in terms of fatigue. However, when individually analysing each internal force peak value, it can be concluded that the consideration of the FSFI can be either beneficial in terms of shear forces or detrimental in terms of bending moments at the base of the leg. For bending moments, the analysed values correspond to the maximums obtained in the substructure.

After analysing the accelerations and stresses in both peak and RMS values, Figure 8 presents the spectral analysis of the accelerations at the top of the tower, as well as of the shear forces and bending moments obtained at the base of the leg in the load case E-2, specifically when the load directions are aligned at 45 degrees (C45). Each line colour represents the different SSI hypotheses considered in the study. Focusing on the accelerations, it

is clearly observed that the peak value of the first mode decreases when SSI with FSFI is considered, highlighting the significant effect of considering FSFI on the system. Regarding the bending moment, its amplitude is notably affected. Furthermore, while the third mode is observed under fixed-base conditions, it vanishes when SSI and FSFI are taken into account. It is also worth noting that FSFI influences the response of the system along a narrow frequency band that expands, approximately, only between 0.1 and 0.8 Hz. In this range, the response of the model that includes FSFI tends to be slightly higher. However, above this frequency, SSI modifies the response of the compliant system if compared with the fixed-base counterpart, but the additional effect of FSFI is negligible.

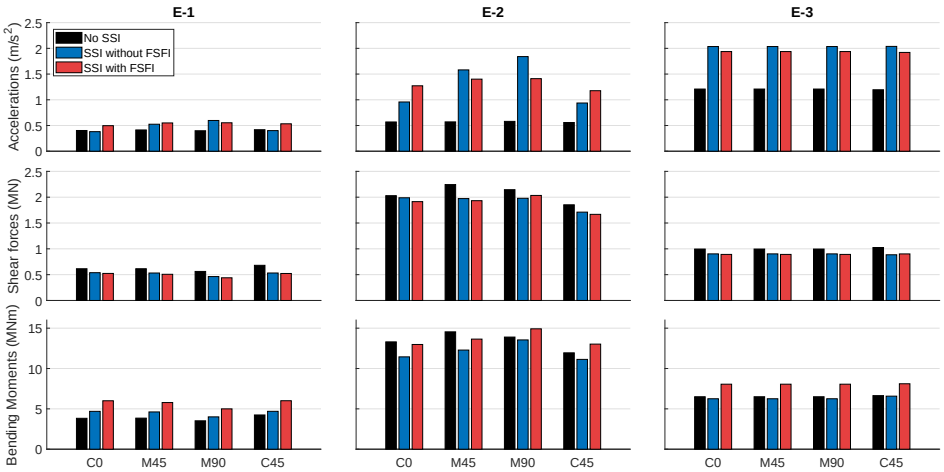

Figure 6. Peak response in terms of accelerations at the tower top, shear forces, and bending moments at the base of the legs for all load cases and SSI hypotheses, during power production. OC4 jacket.

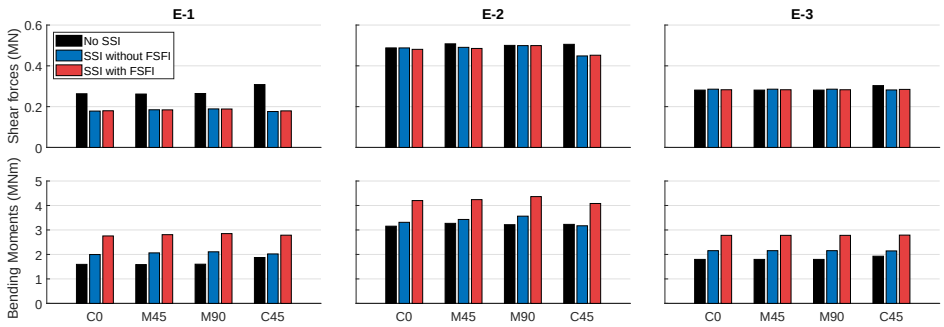

Figure 7. RMS response in terms of shear forces and bending moments at the base of the legs for all load cases and SSI hypotheses, during power production. OC4 jacket.

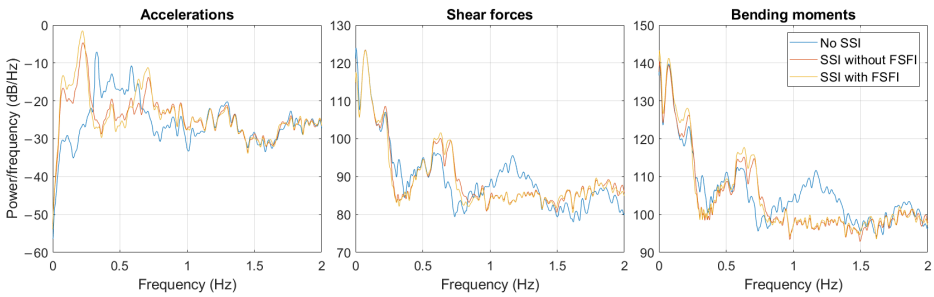

Figure 8. Frequency response for accelerations at the tower top, shear forces, and bending moments at the base of the leg obtained from the OWT on the OC4 jacket in power production, under fixed, SSI without FSFI, and SSI with FSFI hypotheses. Load case E-2. Load direction C45.

4.3.1. Influence of Operational Mode

To evaluate the impact of operational modes on the dynamic behaviour of the jacket supported by buckets, Figure 9 presents the RMS responses of shear forces and bending moments at the base of the legs for the different load cases considered in the study during power production and parked mode conditions. Each row corresponds to a distinct load state, while the vertical axes indicate the load alignments. Square markers denote power production, whereas triangular markers represent the parked mode.

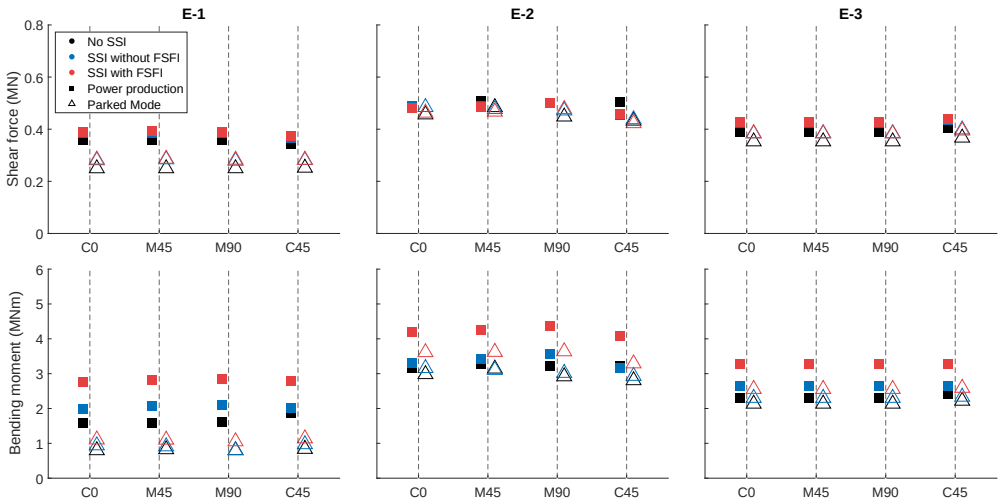

Figure 9. RMS response in terms of shear force and bending moment at the OC4 jacket during both power production and parked modes.

The response computed when FSFI (red markers) is considered tends to generate the highest internal forces, particularly under power production mode in terms of bending moments. However, for shear forces, this trend is less clear, as it varies depending on the specific case and the alignment of the loads. In certain instances, the highest shear forces are recorded when the fixed-base scenario is assumed. In the E-2 load state, smaller differences are observed between the values obtained in the different operational modes, as this scenario is designed to represent an extreme wave load in which aerodynamic influences are less significant. The power production mode is consistently the most unfavourable condition for the internal forces.

4.3.2. Stress Response

This section presents a comparative analysis of the von Mises stresses obtained at the substructure by considering the different SSI hypotheses. Stresses have been evaluated in the critical elements of the jacket, covering the different levels of the structure, including leg and bracing elements.

Figure 10 shows the peak and RMS values (different rows) at the four levels of the jacket (different columns) obtained for case E-2, in which the highest stresses were recorded compared to the other scenarios analysed. The von Mises stresses at the bracing and leg elements are displayed independently, with coloured and grey bars, respectively. Stress values were extracted at different levels of the jacket, allowing for an accurate assessment of the most structurally critical areas and elements. The most unfavourable case, in terms of von Mises stresses, is identified in load case E-2, specifically when the loads are aligned at 45 degrees relative to the position of the jacket.

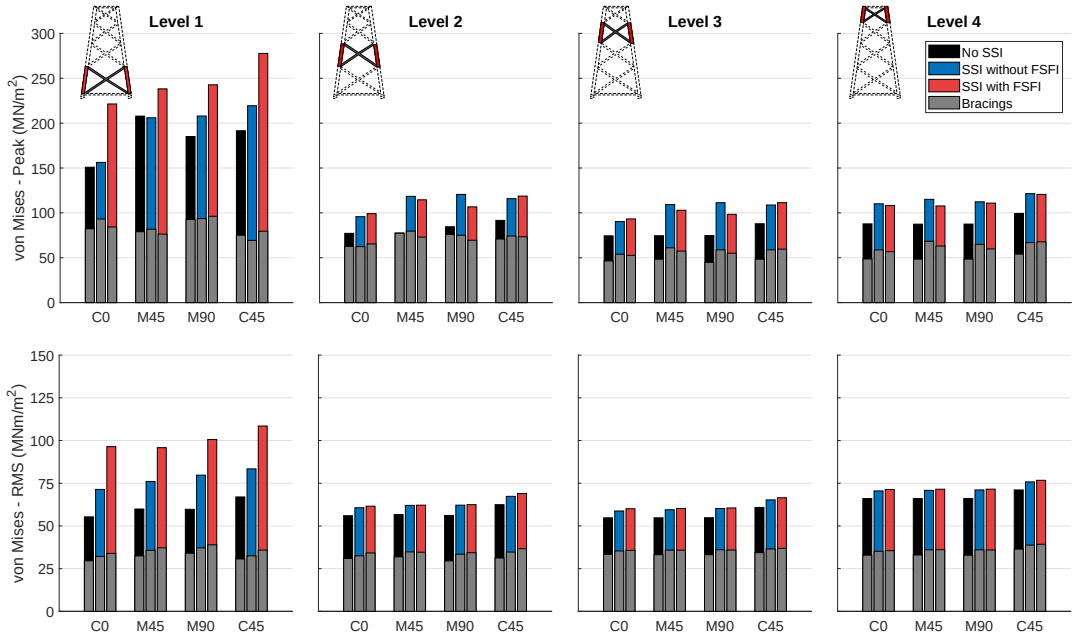

Figure 10. Peak and RMS von Mises stress responses in the OC4 jacket for the different load cases and SSI hypotheses under power production. Coloured bars are used to represent stresses in leg members, and grey bars for stresses in bracing elements.

The areas of the jacket with the highest stresses are located at level 1 of the leg. It is noteworthy that the von Mises stresses at level 2 are similar between the bracing elements and the legs, especially in the fixed-base configuration. Additionally, the bracing elements exhibit relatively uniform stresses across all levels, in contrast to the legs, where significant variations are observed.

The foundation–soil–foundation interaction is clearly significant in terms of von Mises stresses. Unlike what happens in terms of internal forces, in most cases, the maximum stresses occur when the group effect is considered, underscoring its relevance in the dynamic response analysis of jackets. This phenomenon is observed not only in peak responses but also in RMS values. In particular, in terms of peak values, a difference of up to 31% has been recorded when comparing cases that consider SSI with FSFI against those that do not, and a 13% difference between the fixed-base model and the model considering SSI without FSFI at the leg (level 1).

4.4. Impact of Jacket Design on Group Effect Influence in the Dynamic Response

The results presented above demonstrated that the structural responses of a specific jacket, including accelerations, internal forces, and stresses, vary significantly with the characteristics of soil–structure interaction. However, an important question arises: how do structural responses change if the jacket design is modified while external conditions remain constant?

To address this question, the response of a slightly different jacket structure is now analysed. To do so, the optimised structure computed by Couceiro et al. [66] is considered. Figure 11 shows the geometry of the optimised jacket. This choice enables a detailed comparison with the reference jacket, evaluating how variations in the SSI modelling affect structural responses under the same loading conditions. Furthermore, an analysis of the variations between both jackets will be included, highlighting the differences and similarities in structural behaviour, thus providing a comprehensive understanding of the effects of changing the jacket design.

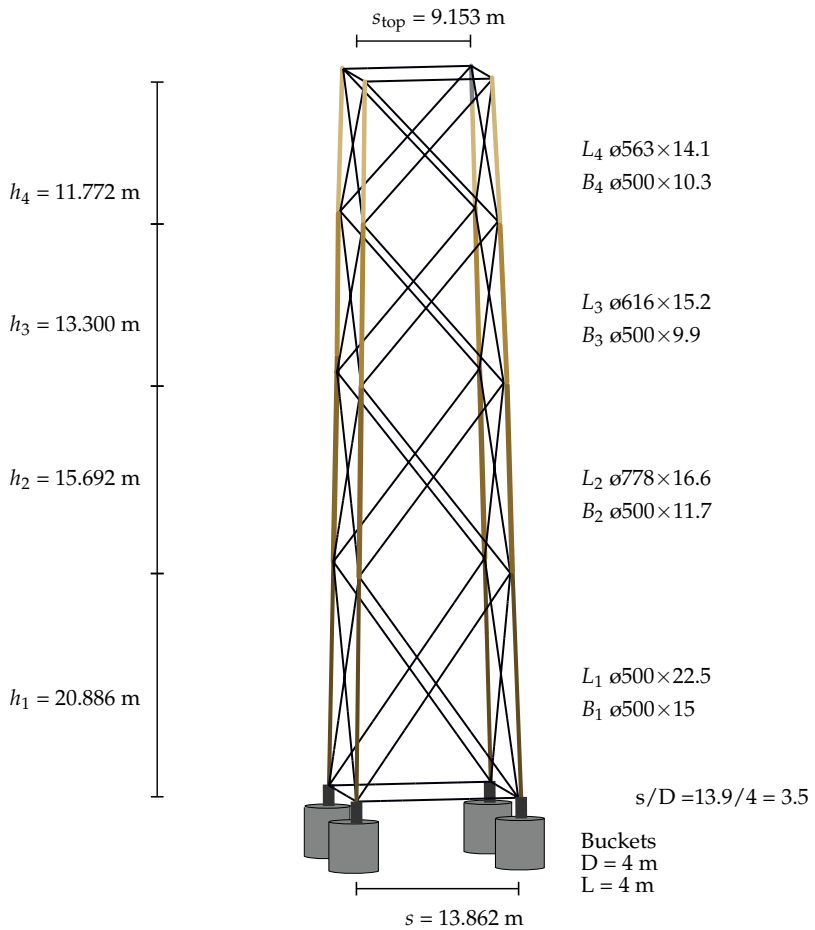

Figure 11. Geometry of the optimised jacket with buckets. The diameter and thickness of each leg level L_i and bracings B_i are provided at the right of the figure in millimetres.

Figure 12 shows the fore-aft PSDs of the offshore wind turbine mounted on the two different jackets, obtained from fore-aft accelerations measured at the tower top under parked conditions and environmental loads in the three different SSI scenarios.

The fundamental frequencies obtained for the optimised jacket are consistent with those presented by Couceiro et al. [66]. Table 5 summarises the fundamental frequency of the system under the three different modelling approaches. The consideration of FSFI significantly reduces the values of the first three natural frequencies, with reductions of approximately 35% and 20% in the fore-aft fundamental frequency for the original and optimised jackets, respectively.

It is important to highlight that the optimised structure was designed neglecting SSI, with a natural frequency closely aligned with the 1P frequency. As such, this design may be unsuitable for the proposed bucket foundation and soil parameters.

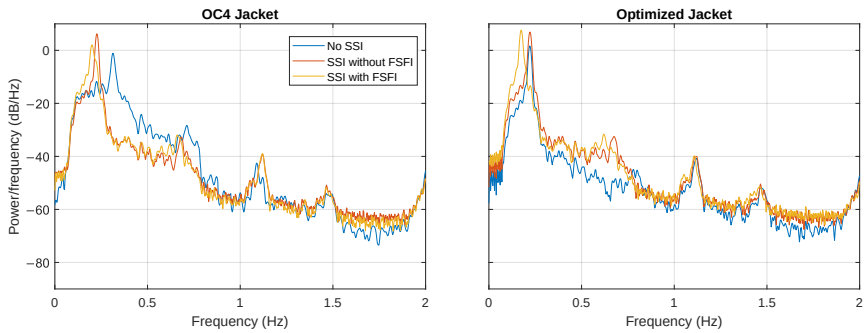

Figure 12. Power Spectral Densities in the fore–aft direction obtained from the response of the 5MW OWT on the OC4 jacket and of the optimised jacket in parked conditions, under fixed, SSI without FSFI, and SSI with FSFI hypotheses.

Table 5. OWT fundamental frequencies.

	Reference Jacket	Optimised Jacket
No SSI, fore-aft	0.314 Hz (3.18 s)	0.222 Hz (4.50 s)
SSI without FSFI, fore-aft	0.228 Hz (4.39 s)	0.220 Hz (4.55 s)
SSI with FSFI, fore-aft	0.205 Hz (4.88 s)	0.180 Hz (5.56 s)

Figure 13 shows the peak values of accelerations at the tower top, as well as the shear forces and bending moments at the base of the legs for the optimised jacket. These values are provided for the different SSI configurations and for each load case and load alignment considered. Each coloured bar represents the results obtained for the models that consider fixed-base condition (no SSI), SSI using the corresponding stiffnesses to the single foundations (SSI without FSFI), and FSFI (SSI with FSFI). On the other hand, Figure 14 displays the RMS values for shear forces and bending moments, thus enabling a comparison with the peak values and an assessment of the consistency of the observed trends.

The trends in accelerations and bending moments are similar to those observed in the original jacket, where the highest peak values occur when SSI is included, particularly when FSFI is considered. However, the trends in shear forces exhibit an increase towards the FSFI, particularly in E-2 and E-3, in contrast to the original OC4 jacket. In addition, in comparison to the original jacket, the RMS values present a correlation between the trends in both internal forces, although the differences in RMS shear forces values in the different SSI hypotheses are less pronounced.

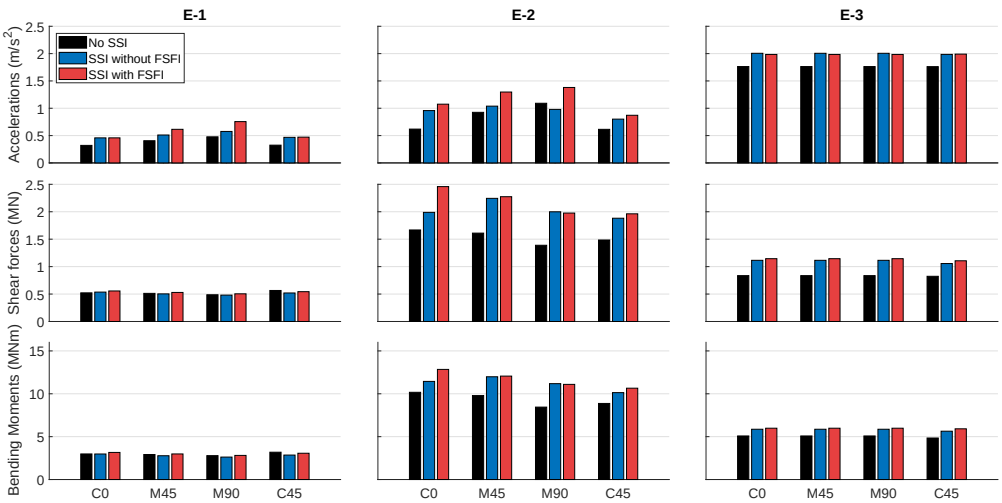

Figure 13. Peak response in terms of accelerations at the tower top, shear forces, and bending moments at the base of the legs for all load cases and SSI hypotheses, during power production. Optimised jacket.

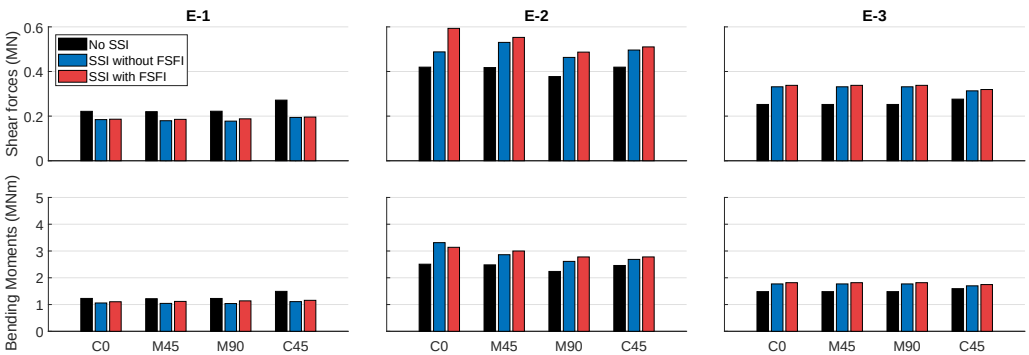

Figure 14. RMS response in terms of shear forces and bending moments at the base of the legs for all load cases and SSI hypotheses, during power production. Optimised jacket.

It is crucial to emphasise that the optimised jacket experiences higher peak accelerations, shear forces, and bending moments when soil–structure interaction (either considering FSFI or not) is considered, compared to the fixed-base scenario. This trend is consistent across all analysed cases. However, this behaviour is not observed in the shear forces of the reference jacket.

Finally, Figure 15 presents the peak and RMS response in terms of von Mises stresses at the different levels of the jacket substructure, for the E-2 case. The von Mises stresses are shown with coloured bars for the legs and grey bars for the bracing elements.

The results are largely similar to those obtained in the reference jacket. The highest peak stress areas are located at levels 1 and 4 of the leg. Additionally, the bracing elements demonstrate relatively uniform stresses across all levels, in contrast to the legs, where significant variations are observed. The maximum stresses occur when wind and waves loads are aligned at 45°. The difference in peak values is approximately 8% higher when comparing SSI with FSFI to SSI without FSFI. In contrast, for the OC4 jacket, this difference is notably larger, at approximately 21% when FSFI is considered. However, in the optimised

jacket, smaller differences in RMS values are observed when considering the different SSI hypotheses, in contrast to the reference jacket, where the FSFI notably increased the RMS values. Moreover, with regard to the RMS values, von Mises stresses across the different leg levels are more similar. It is noteworthy that the maximum RMS value is not observed at level 1, as in the original jacket. This highlights the significance of the different SSIs on each jacket individually, indicating that the influence of FSFI in each jacket must be thoroughly analysed.

It is important to emphasise that the optimised jacket was designed assuming fixed-base hypothesis [66]. However, when considering soil–structure interaction, the observed reduction in natural frequency and the increase in von Mises stresses indicate that the jacket structure becomes unsuitable for the loading conditions analysed in this study.

After comparing the influence of considering the bucket–soil–bucket interaction in different substructures, distinct behaviours are observed in both jackets. In terms of individual internal forces, the SSI exhibits variable behaviours depending on the jacket, highlighting the importance of analysing SSI in the performance of each substructure for the same wind turbine. This effect significantly depends on the natural frequencies of the system and the dynamic loads. Therefore, the relevance of studying the effects of SSI on the dynamic behaviour of each specific jacket becomes evident.

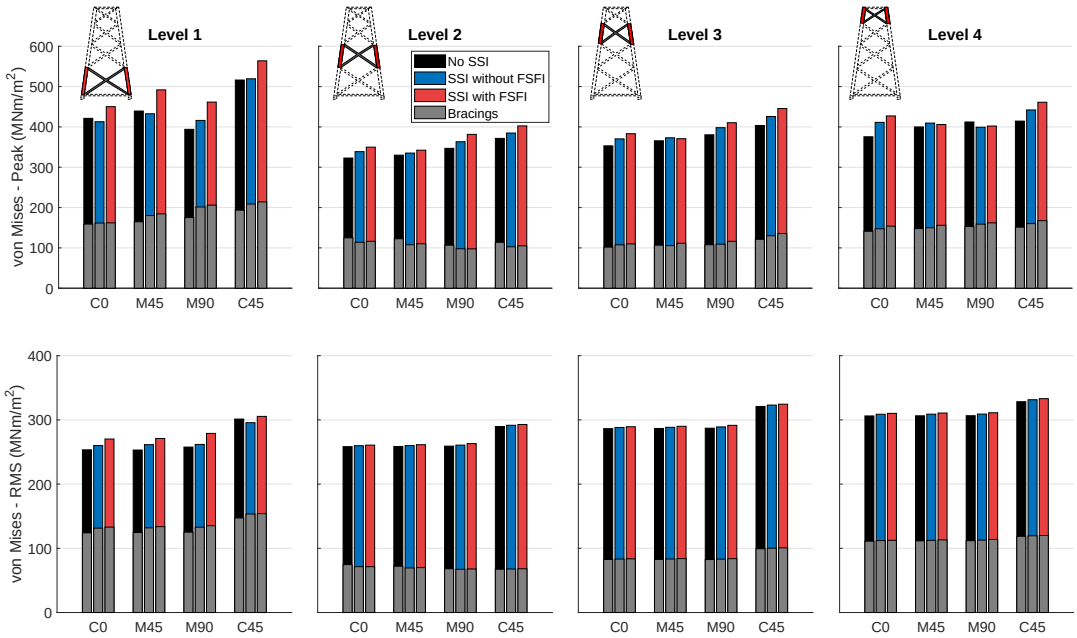

Figure 15. Peak and RMS von Mises stress responses in the optimised jacket for the different load cases and SSI hypotheses under power production. Coloured bars are used to represent stresses in leg members, and grey bars for stresses in bracing elements.

5. Discussion

Foundation–soil–foundation interaction (FSFI) has been shown to produce significant effects on the dynamic response of the system. First, the influence of soil–structure interaction (SSI) is more pronounced in the reference jacket, where a 35% reduction in natural frequency is noted. In contrast, in the optimised jacket, the reduction is significantly less pronounced as a consequence of the increased flexibility of the system. Nevertheless, in both cases, the incorporation of the FSFI leads to a decrease in natural frequency, which is consistent with previous studies, such as those by Salem et al. [52] and Bordón et al. [44].

Moreover, in the optimised jacket, whose natural frequency is already close to the 1P rotor frequency, the additional reduction caused by SSI leads to the natural frequency falling to values unsuitable for the wind turbine design. Consequently, it can be concluded that incorporating the SSI effect in the design and optimisation process of jackets is essential to ensure adequate structural performance and prevent resonance issues.

In regard to accelerations and displacements, the consideration of SSI and FSFI results in an increase in peak values. This increase can have significant implications for the nacelle components, potentially affecting the service life of the OWT. The increase in accelerations results in higher dynamic demands on the structure, which could accelerate fatigue processes in critical components, further highlighting the importance of incorporating these effects in the design and analysis of the OWT jacket.

SSI induces significant variations in the different internal forces analysed at the foundation. The authors can conclude that SSI and FSFI can have both positive and negative impacts on the analysis of internal forces in the jacket structure. Therefore, it is crucial to conduct a detailed SSI analysis for each jacket design, as the structural behaviour can vary significantly depending on the specific conditions.

Based on the results obtained by comparing different operating modes, the power production mode is consistently the most unfavourable condition for the internal forces in the substructure. However, in some of the analysed load cases, the obtained results showed smaller differences. Therefore, it is recommended that the dynamic response be analysed on a case-by-case basis.

Considering FSFI produces the most unfavourable results in terms of stresses, particularly when the stresses align at 45° relative to the jacket's orientation. This behaviour is not explicitly detailed in current standards, which is understandable in the case of monopiles due to their cylindrical symmetry. However, in jacket substructures, this effect causes a significant increase in stresses, highlighting the importance of considering this phenomenon in foundation design. The highest stresses consistently concentrate in the lower part of the jacket, specifically at level 1, particularly in the legs. This behaviour is observed across all load conditions and for both jackets analysed.

6. Conclusions

This study has investigated the influence of foundation–soil–foundation interaction on the dynamic behaviour of jacket substructures founded on buckets for offshore wind turbines. A parametric analysis was conducted, incorporating critical load cases identified for conservative foundation design, as outlined by Jalbi et al. [55] for jacket structures. The study considered four different load configurations, including collinear wind and wave loads, as well as misaligned cases at 45° and 90°, providing a comprehensive assessment of the varying loading directions. The dynamic response of the system was evaluated in terms of key structural parameters, such as, bending moments, shear forces, and stresses on the jacket substructure. In order to evaluate the influence of FSFI on different substructure configurations, simulations were performed considering the NREL 5MW OWT mounted on the jacket defined in the OC4 project, and a comparative analysis employed an optimised jacket. The dynamic response was analysed with an OpenFAST model that incorporated soil–structure interaction and accounted for the presence of multi-bucket foundations for a homogeneous soil profile.

It was found that foundation–soil–foundation interaction can play a role in increasing the magnitude of the structural response in terms not only of accelerations but, more importantly, in terms of shear forces, bending moments, and stresses in many different situations. In other words, ignoring the influence of the interaction between nearby foundations (as is usually assumed in the analysis of this systems) may contribute to underestimating the structural response of the jacket. One of the reasons that explains this influence of foundation–soil–foundation interaction over the structural response is the changes produced in the fundamental frequency of the structure: foundation–soil–foundation interaction modifies the stiffnesses of each individual foundation in the group (the well-known

group effect of the foundations) and, given that the modes and natural frequencies of the whole system depend on such stiffnesses, they are also modified. In turn, if modes and natural frequencies change, the structural response of every element is also affected.

Therefore, even though additional future work is still needed for the development of more elaborated models that include the aspects that have been disregarded in this first study, the authors recommend considering the effects of foundation–soil–foundation interaction in the analysis and design processes of jacket support structures for OWTs.

Author Contributions: Conceptualisation, C.R.-S. and L.A.P.; methodology, C.R.-S., L.A.P. and J.D.R.B.; software, C.R.-S.; validation, C.R.-S.; formal analysis, C.R.-S. and L.A.P.; investigation, C.R.-S., L.A.P. and J.D.R.B.; resources, L.A.P.; data curation, C.R.-S.; writing—original draft preparation, C.R.-S.; writing—review and editing, L.A.P. and J.D.R.B.; visualisation, C.R.-S.; supervision, L.A.P.; project administration, L.A.P.; funding acquisition, C.R.-S. and L.A.P. All authors have read and agreed to the published version of the manuscript.

Funding: This research was funded by the Agencia Estatal de Investigación and the Ministerio de Ciencia, Innovación y Universidades of Spain (MCIN/AEI/10.13039/501100011033) through Research Project PID2020-120102RB-I00 and predoctoral research fellowship TESIS2022010011 (C. Romero-Sanchez) from the Consejería de Universidades, Ciencia e Innovación y Cultura, and by the European Social Fund Plus (ESF+).

Institutional Review Board Statement: Not applicable.

Informed Consent Statement: Not applicable.

Data Availability Statement: The data that support the findings of this study are available from the corresponding author upon reasonable request.

Conflicts of Interest: The authors declare no conflicts of interest.

Abbreviations

The following abbreviations are used in this manuscript:

OWT	Offshore wind turbine
SSI	Soil–structure interaction
FSFI	Foundation–soil–foundation interaction
FEM	Finite Element Method
BEM	Boundary Element Method
D	Diameter of the bucket
L	Length of the bucket
ν	Poisson's ratio of the soil
μ	Shear modulus of the soil
K_0^{no-int}	Stiffness matrix without considering foundation–soil–foundation interaction
K_0^{int}	Stiffness matrix considering foundation–soil–foundation interaction
$\tilde{s}$	Dimensionless spacing (distance) between closest foundations (polygonal arrangement)
γ	Group effect stiffness correction factor
V_r	Rated wind speed
H_{jacket}	Height jacket
H_{top}	Height hub from mean sea level
W	Height water
s_{top}	Spacing jacket top
s	Spacing jacket bottom
DLCs	Design Load Cases
NTM	Normal Turbulence Model
ETM	Extreme Turbulence Model
EOG	Extreme Operating Gust
ESS	Extreme Sea States
EWH	Extreme Wave Height
C0	Wind and waves loads are collinear (0°)

M90	Wind and waves loads are misalignment by 90°
M45	Wind and waves loads are misalignment by 45°
C45	Wind and waves loads act at 45° relative to the structure
H_S	Significant wave height
T_S	Significant wave period
H_m	Maximum wave height
T_m	Maximum wave period

References

1. Council, G.W.E. *Global Offshore Wind Report 2024*; Technical Report; GWEC: Brussels, Belgium, 2024.
2. McCoy, A.; Musial, W.; Hammond, R.; Mulas Hernando, D.; Duffy, P.; Beiter, P.; Perez, P.; Baranowski, R.; Reber, G.; Spitsen, P. *Offshore Wind Market Report: 2024 Edition*; Technical Report; National Renewable Energy Laboratory (NREL): Golden, CO, USA, 2024.
3. Zania, V. Natural vibration frequency and damping of slender structures founded on monopiles. *Soil Dyn. Earthq. Eng.* **2014**, *59*, 8–20. [CrossRef]
4. Damgaard, M.; Zania, V.; Andersen, L.V.; Ibsen, L.B. Effects of soil–structure interaction on real time dynamic response of offshore wind turbines on monopiles. *Eng. Struct.* **2014**, *75*, 388–401. [CrossRef]
5. Álamo, G.; Aznárez, J.; Padrón, L.; Martínez-Castro, A.; Gallego, R.; Maeso, O. Dynamic soil-structure interaction in offshore wind turbines on monopiles in layered seabed based on real data. *Ocean Eng.* **2018**, *156*, 14–24. [CrossRef]
6. Medina, C.; Álamo, G.; Quevedo-Reina, R. Evolution of the seismic response of monopile-supported offshore wind turbines of increasing size from 5 to 15 MW including dynamic soil-structure interaction. *J. Mar. Sci. Eng.* **2021**, *9*, 1285. [CrossRef]
7. Li, W.; Li, X.; Zhao, X.; Yin, Q.; Zhu, M.; Yang, L. The Method of the Natural Frequency of the Offshore Wind Turbine System Considering Pile–Soil Interaction. *J. Mar. Sci. Eng.* **2024**, *12*, 1912. [CrossRef]
8. Abdullahi, A.; Wang, Y.; Bhattacharya, S. Comparative modal analysis of monopile and jacket supported offshore wind turbines including soil-structure interaction. *Int. J. Struct. Stab. Dyn.* **2020**, *20*, 2042016. [CrossRef]
9. Abhinav, K.; Saha, N. Coupled hydrodynamic and geotechnical analysis of jacket offshore wind turbine. *Soil Dyn. Earthq. Eng.* **2015**, *73*, 66–79. [CrossRef]
10. Quevedo-Reina, R.; Álamo, G.; Aznárez, J. Global Sensitivity Analysis of the Fundamental Frequency of Jacket-Supported Offshore Wind Turbines Using Artificial Neural Networks. *J. Mar. Sci. Eng.* **2024**, *12*, 2011. [CrossRef]
11. Arany, L.; Bhattacharya, S.; Macdonald, J.H.; Hogan, S.J. Closed form solution of Eigen frequency of monopile supported offshore wind turbines in deeper waters incorporating stiffness of substructure and SSI. *Soil Dyn. Earthq. Eng.* **2016**, *83*, 18–32. [CrossRef]
12. Jalbi, S.; Bhattacharya, S. Closed form solution for the first natural frequency of offshore wind turbine jackets supported on multiple foundations incorporating soil-structure interaction. *Soil Dyn. Earthq. Eng.* **2018**, *113*, 593–613. [CrossRef]
13. Kaynia, A.M.; Kausel, E. Dynamics of piles and pile groups in layered soil media. *Soil Dyn. Earthq. Eng.* **1991**, *10*, 386–401. [CrossRef]
14. Padrón, L.; Aznárez, J.; Maeso, O. BEM–FEM coupling model for the dynamic analysis of piles and pile groups. *Eng. Anal. Bound. Elem.* **2007**, *31*, 473–484. [CrossRef]
15. Carbonari, S.; Morici, M.; Dezi, F.; Gara, F.; Leoni, G. Soil-structure interaction effects in single bridge piers founded on inclined pile groups. *Soil Dyn. Earthq. Eng.* **2017**, *92*, 52–67. [CrossRef]
16. Latini, C.; Zania, V. Dynamic lateral response of suction caissons. *Soil Dyn. Earthq. Eng.* **2017**, *100*, 59–71. [CrossRef]
17. Bordón, J.; Aznárez, J.; Maeso, O. Dynamic model of open shell structures buried in poroelastic soils. *Comput. Mech.* **2017**, *60*, 269–288. [CrossRef]
18. Latini, C.; Zania, V. Vertical dynamic impedance of suction caissons. *Soils Found.* **2019**, *59*, 1113–1127. [CrossRef]
19. He, R.; Kaynia, A.M. Dynamic impedances and load carrying mechanism for skirted foundations. *Mar. Struct.* **2021**, *79*, 103023. [CrossRef]
20. Gazetas, G. Formulas and charts for impedances of surface and embedded foundations. *J. Geotech. Eng.* **1991**, *117*, 1363–1381. [CrossRef]
21. Doherty, J.; Deeks, A. Elastic response of circular footings embedded in a non-homogeneous half-space. *Géotechnique* **2003**, *53*, 703–714. [CrossRef]
22. *Offshore Standard DNV-OS-J101*; Design of Offshore Wind Turbine Structures. DNV: Bærum, Norway; DetNorske Veritas AS: Shenzhen, China, 2014.
23. Wong, H.; Luco, J. Dynamic interaction between rigid foundations in a layered half-space. *Soil Dyn. Earthq. Eng.* **1986**, *5*, 149–158. [CrossRef]
24. Dobry, R.; Gazetas, G. Simple method for dynamic stiffness and damping of floating pile groups. *Geotechnique* **1988**, *38*, 557–574. [CrossRef]
25. Zhong, M.; Meng, K. Dynamic Interaction Factor of Pipe Group Piles Considering the Scattering Effect of Passive Piles. *J. Mar. Sci. Eng.* **2023**, *11*, 1698. [CrossRef]
26. Reumers, P.; Lombaert, G.; Degrande, G. The effect of foundation–soil–foundation interaction on the response of continuous, multi-span railway bridges. *Eng. Struct.* **2024**, *299*, 117096. [CrossRef]

27. Zeolla, E.; de Silva, F.; Sica, S. Towards a practice-oriented procedure to account for static and dynamic interaction among three adjacent shallow foundations. *Comput. Geotech.* **2024**, *170*, 106242. [CrossRef]
28. Karabalis, D.L.; Mohammadi, M. 3-D dynamic foundation-soil-foundation interaction on layered soil. *Soil Dyn. Earthq. Eng.* **1998**, *17*, 139–152. [CrossRef]
29. Chen, L. Dynamic interaction between rigid foundations on multi-layered stratum. *J. Earthq. Eng.* **2016**, *20*, 505–534. [CrossRef]
30. Zeolla, E.; de Silva, F.; Sica, S. A simplified approach to account for through-soil interaction between two adjacent shallow foundations. *Bull. Earthq. Eng.* **2023**, *21*, 2503–2532. [CrossRef]
31. Aji, H.D.; Heiland, T.; Wuttke, F.; Stark, A.; Dineva, P. Dynamic impedance and compliance surfaces of twin adjacent surface foundations under synchronous and asynchronous loads. *Soil Dyn. Earthq. Eng.* **2024**, *182*, 108740. [CrossRef]
32. Alati, N.; Failla, G.; Arena, F. Seismic analysis of offshore wind turbines on bottom-fixed support structures. *Philos. Trans. R. Soc. A Math. Phys. Eng. Sci.* **2015**, *373*, 20140086. [CrossRef]
33. Abhinav, K.; Saha, N. Nonlinear dynamical behaviour of jacket supported offshore wind turbines in loose sand. *Mar. Struct.* **2018**, *57*, 133–151. [CrossRef]
34. Romero-Sánchez, C.; Padrón, L. Influence of wind and seismic ground motion directionality on the dynamic response of four-legged jacket-supported Offshore Wind Turbines. *Eng. Struct.* **2024**, *300*, 117191. [CrossRef]
35. Ju, S.H.; Huang, Y.C. Analyses of offshore wind turbine structures with soil-structure interaction under earthquakes. *Ocean Eng.* **2019**, *187*, 106190. [CrossRef]
36. James, M.; Haldar, S. Seismic vulnerability of jacket supported large offshore wind turbine considering multidirectional ground motions. *Structures* **2022**, *43*, 407–423. [CrossRef]
37. Bhattacharya, S.; Nikitas, N.; Garnsey, J.; Alexander, N.; Cox, J.; Lombardi, D.; Wood, D.M.; Nash, D.F. Observed dynamic soil–structure interaction in scale testing of offshore wind turbine foundations. *Soil Dyn. Earthq. Eng.* **2013**, *54*, 47–60. [CrossRef]
38. Jalbi, S.; Nikitas, G.; Bhattacharya, S.; Alexander, N. Dynamic design considerations for offshore wind turbine jackets supported on multiple foundations. *Mar. Struct.* **2019**, *67*, 102631. [CrossRef]
39. Plodpradit, P.; Kwon, O.; Dinh, V.N.; Murphy, J.; Kim, K.D. Suction bucket pile–soil–structure interactions of offshore wind turbine jacket foundations using coupled dynamic analysis. *J. Mar. Sci. Eng.* **2020**, *8*, 416. [CrossRef]
40. Antoniou, M.; Kourkoulis, R.; Gelagoti, F.; Anastasopoulos, I. Simplified method for performance-based seismic design of suction caissons supporting jacket offshore wind turbines. *Soil Dyn. Earthq. Eng.* **2022**, *155*, 107169. [CrossRef]
41. Cheng, Y.; Luo, Y.; Wang, J.; Dai, K.; Wang, W.; El Damatty, A. Fragility and vulnerability development of offshore wind turbines under aero-hydro loadings. *Eng. Struct.* **2023**, *293*, 116625. [CrossRef]
42. Zhang, B.; Liu, R.; Wang, L.; Wang, X.; Wang, L.; Li, W.; Hong, Y. Cyclic response and load transfer mechanism of suction bucket jackets supporting offshore wind turbines in soft clay. *Ocean Eng.* **2024**, *313*, 119135. [CrossRef]
43. Zhu, H.; Lian, J.; Guo, Y.; Wang, H. A Numerical Model for the Scour Effect on the Bearing Capacity of an Offshore Wind Turbine with a Five-Bucket Jacket Foundation. *J. Mar. Sci. Eng.* **2024**, *12*, 753. [CrossRef]
44. Bordón, J.D.R.; Aznárez, J.J.; Maeso, O.; Bhattacharya, S. Simple approach for including foundation–soil–foundation interaction in the static stiffnesses of multi-element shallow foundations. *Géotechnique* **2021**, *71*, 686–699. [CrossRef]
45. Wei, K.; Myers, A.T.; Arwade, S.R. Dynamic effects in the response of offshore wind turbines supported by jackets under wave loading. *Eng. Struct.* **2017**, *142*, 36–45. [CrossRef]
46. Liang, F.; Yuan, Z.; Liang, X.; Zhang, H. Seismic response of monopile-supported offshore wind turbines under combined wind, wave and hydrodynamic loads at scoured sites. *Comput. Geotech.* **2022**, *144*, 104640. [CrossRef]
47. Mroczek, M.M.; Arwade, S.R.; Lackner, M.A. Design optimization of offshore wind jacket piles by assessing support structure orientation relative to metocean conditions. *Wind Energy Sci. Discuss.* **2023**, *2023*, 807–817. . [CrossRef]
48. Sun, M.; Shan, Z.; Wang, W.; Xu, S.; Liu, X.; Zhang, H.; Guo, X. Numerical Investigation into the Stability of Offshore Wind Power Piles Subjected to Lateral Loads in Extreme Environments. *J. Mar. Sci. Eng.* **2024**, *12*, 915. [CrossRef]
49. Padrón, L.; Carbonari, S.; Dezi, F.; Morici, M.; Bordón, J.; Leoni, G. Seismic response of large offshore wind turbines on monopile foundations including dynamic soil–structure interaction. *Ocean Eng.* **2022**, *257*, 111653. [CrossRef]
50. Jonkman, J.; Butterfield, S.; Musial, W.; Scott, G. *Definition of a 5-MW Reference Wind Turbine for Offshore System Development*; Technical Report; National Renewable Energy Lab. (NREL): Golden, CO, USA, 2009.
51. Vorpahl, F.; Popko, W.; Kaufer, D. *Description of a Basic Model of the "UpWind reference Jacket" for Code Comparison in the OC4 Project Under IEA Wind Annex XXX*; Fraunhofer Institute for Wind Energy and Energy System Technology (IWES): Bremerhaven, Germany, 2011; Volume 450.
52. Salem, A.; Jalbi, S.; Bhattacharya, S. Vertical stiffness functions of rigid skirted caissons supporting offshore wind turbines. *J. Mar. Sci. Eng.* **2021**, *9*, 573. [CrossRef]
53. *Offshore Standard DNV-ST-0437*; Loads and Site Conditions for Wind Turbines. DNV: Bærum, Norway; DetNorske Veritas AS: Shenzhen, China, 2016.
54. *IEC 61400-1:2020*; Wind Energy Generation Systems—Part 1: Design Requirements. International Electrotechnical Commission: London, UK, 2020.
55. Jalbi, S.; Bhattacharya, S. Concept design of jacket foundations for offshore wind turbines in 10 steps. *Soil Dyn. Earthq. Eng.* **2020**, *139*, 106357. [CrossRef]

56. Romero-Sánchez, C.; Padrón, L.A. Seismic response of jacket-supported offshore wind turbines for different operational modes considering earthquake directionality. *Ocean Eng.* **2024**, *311*, 118798. [CrossRef]
57. Meng, J.; Dai, K.; Zhao, Z.; Mao, Z.; Camara, A.; Zhang, S.; Mei, Z. Study on the aerodynamic damping for the seismic analysis of wind turbines in operation. *Renew. Energy* **2020**, *159*, 1224–1242. [CrossRef]
58. Bordón, J.; Aznárez, J.; Padrón, L.; Maeso, O.; Bhattacharya, S. Closed-form stiffnesses of multi-bucket foundations for OWT including group effect correction factors. *Mar. Struct.* **2019**, *65*, 326–342. [CrossRef]
59. Wolf, J.P.; Deeks, A.J. *Foundation Vibration Analysis: A Strength of Materials Approach*; Elsevier: Amsterdam, The Netherlands, 2004.
60. National Renewable Energy Laboratory. OpenFAST Documentation. Release v3.5.2. 2024. Available online: https://openfast.readthedocs.io/en/main/ (accessed on 1 October 2024).
61. Moriarty, P.; Hansen, A. *AeroDyn Theory Manual*; Technical Report; National Renewable Energy Lab.: Golden, CO, USA, 2005.
62. Jonkman, B. *TurbSim User's Guide: Version 1.50*; Technical Report; National Renewable Energy Lab. (NREL): Golden, CO, USA, 2009.
63. Jonkman, J.M.; Robertson, A.; Hayman, G.J. *HydroDyn User's Guide and Theory Manual*; National Renewable Energy Laboratory: Golden, CO, USA, 2014.
64. Damiani, R.; Jonkman, J.; Hayman, G. *SubDyn User's Guide and Theory Manual*; Technical Report; National Renewable Energy Lab. (NREL): Golden, CO, USA, 2015.
65. Dnv, G. *Offshore Soil Mechanics and Geotechnical Engineering (DNVGL-RP-C212)*; DNV: Bærum, Norway, 2017.
66. Couceiro, I.; París, J.; Navarrina, F.; Guizán, R.; Colominas, I. Optimization of offshore steel jackets: Review and proposal of a new formulation for time-dependent constraints. *Arch. Comput. Methods Eng.* **2020**, *27*, 1049–1069. [CrossRef]

Disclaimer/Publisher's Note: The statements, opinions and data contained in all publications are solely those of the individual author(s) and contributor(s) and not of MDPI and/or the editor(s). MDPI and/or the editor(s) disclaim responsibility for any injury to people or property resulting from any ideas, methods, instructions or products referred to in the content.

2.4 Autorship documents

ULPGC Universidad de Las Palmas de Gran Canaria | Escuela de Doctorado

AUTORSHIP DOCUMENT FOR COMPENDIUM THESIS

The undersigned, as co-authors of the published paper entitled “Influence of wind and seismic ground motion directionality on the dynamic response of four-legged jacket-supported Offshore Wind Turbines”, published in Engineering Structures on February 1, 2024:

- We recognize as main author to Mr/Mrs Carlos Romero Sánchez, with ID number 54162509Q.
- We renounce to use this publication as main nucleus of other doctoral theses, without prejudice to the fact that said publications may be presented as complementary merits in the doctoral theses that the other authors of said publications may present.

Las Palmas de Gran Canaria, May 12 ,2025

Firmado por PADRON HERNANDEZ LUIS ALBERTO - ***5505** el día 12/05/2025 con un certificado emitido por AC FNMT Usuarios

Luis Alberto Padrón Hernández

ULPGC Universidad de Las Palmas de Gran Canaria | Escuela de Doctorado

AUTORSHIP DOCUMENT FOR COMPENDIUM THESIS

The undersigned, as co-authors of the published paper entitled “Seismic response of jacket-supported offshore wind turbines for different operational modes considering earthquake directionality”, published in Ocean Engineering on November 1, 2024:

- We recognize as main author to Mr/Mrs Carlos Romero Sánchez, with ID number 54162509Q.
- We renounce to use this publication as main nucleus of other doctoral theses, without prejudice to the fact that said publications may be presented as complementary merits in the doctoral theses that the other authors of said publications may present.

Las Palmas de Gran Canaria, May 12 ,2025

Firmado por PADRON HERNANDEZ LUIS ALBERTO - ***5505** el día 12/05/2025 con un certificado emitido por AC FNMT Usuarios

Luis Alberto Padrón Hernández

ULPGC Universidad de Las Palmas de Gran Canaria | Escuela de Doctorado

AUTORSHIP DOCUMENT FOR COMPENDIUM THESIS

The undersigned, as co-authors of the published paper entitled "Influence of Foundation-Soil-Foundation Interaction on the Dynamic Response of Offshore Wind Turbine Jackets Founded on Buckets", published in Journal of Marine Science and Engineering on November 19, 2024:

- We recognize as main author to Mr/Mrs Carlos Romero Sánchez, with ID number 54162509Q.
- We renounce to use this publication as main nucleus of other doctoral theses, without prejudice to the fact that said publications may be presented as complementary merits in the doctoral theses that the other authors of said publications may present.

Las Palmas de Gran Canaria, May 12 ,2025

Firmado por PADRON HERNANDEZ LUIS ALBERTO - ***5505** el día 12/05/2025 con un certificado emitido por AC FNMT Usuarios

Luis Alberto Padrón Hernández

Firmado por RODRIGUEZ BORDON JACOB DAVID - ***1349** el día

Jacob David Rodríguez Bordón

3. Summary, conclusions and future research directions

3.1 Summary and conclusions
3.2 Future research directions

3.1 Summary and conclusions

The present dissertation focuses on the dynamic and seismic structural analysis of jacket substructures for offshore wind turbines using advanced numerical modelling. The study integrates multiple subsystems and nonlinear phenomena while accounting for the effects of dynamic soil-structure interaction in multi-supported substructures. In addition, this research explores foundation-soil-foundation interaction phenomena in multi-supported structures and examines the influence of kinematic interaction on the seismic behaviour of the system.

The research presented combines advanced dynamic soil-structure interaction models, developed by the research group, with an aero-hydro-servo-elastic code for wind turbines, enabling detailed modelling of their dynamic response. This dissertation develops the formulation required to implement multi-support seismic input motions into the open-source software OpenFAST, with the aim of facilitating the use of this tool for the dynamic and seismic analysis of wind turbines. Lumped parameter models (LPMs) are employed as an effective approach to incorporate soil-structure interaction into the simulation framework. This methodology not only accounts for the static stiffness of the foundation but also approximates its impedance, dynamic stiffness and damping characteristics. The LPM approached employed in this work enables the simultaneous modelling and fitting of translational, rotational, and coupled horizontal-rocking complex-valued impedance functions, while vertical and torsional impedances are represented using a spring-damper model [57]. Furthermore, this approach facilitates the integration of key aspects of these frequency-domain impedance functions into the time-domain simulation of the complete system in OpenFAST. The impedance functions and kinematic interaction factors are computed using the numerical model previously developed by the research group, described by Álamo et al. [17] or by Bordón et al. [18], for the dynamic analysis of pile and bucket foundations in complex soil conditions.

In addition, the incorporation of foundation–soil–foundation interaction effects into an OpenFAST model of a jacket-supported offshore wind turbine requires a formulation compatible with the OpenFAST framework. To achieve this, bucket–soil–bucket interaction effects are incorporated by modifying the stiffness functions that characterize the response of individual foundations. These expressions, presented in closed-form by Bordón et al. [58], enable efficient implementation. Soil–structure interaction within the OpenFAST environment is modelled using a substructuring approach, where linear springs are attached to the base of the jacket legs.

After verification of the proposed models, in the present dissertation different problems involving jacket substructures on piles and suction buckets have been considered:

First, in order to explore the dynamic and seismic behaviour of the jacket substructure, an interesting factor to consider is the influence of wind and seismic ground motion directionality on the dynamic response of four-legged jacket-supported OWTs. It was observed that, due to aeroelastic damping (which is significantly higher in the fore–aft direction than in the side-to-side direction), the vibration amplitude is considerably more pronounced when seismic shaking occurs in the side-to-side direction,

compared to when it acts along the fore–aft direction. However, the situation differs when considering internal forces. In this case, maximum internal forces are typically observed when the ground motion is aligned with the diagonal direction of the jacket structure, rather than with the wind direction. Additionally, the direction of seismic shaking generally exerts a greater influence on peak internal forces than the wind direction. In any case, it is evident that load combinations assuming aligned wind and ground motion directions are often not the the worst-case scenario. On the other hand, the seismic response of the considered substructures varies with different earthquakes signals. Therefore, a sufficiently comprehensive set of seismic signals (ideally including data from offshore stations) and combinations of ground motion and wind directions must be considered during the detailed design phase of jacket substructures for offshore wind turbines in areas with a high seismic risk. The combinations that result in the maximum peak values vary within these ranges depending on the specific characteristics of different earthquakes.

Secondly, the study also focuses on the influence of operational modes on the seismic response of jacket substructures. Emergency shutdown is not necessarily beneficial in terms of reducing peak accelerations at the nacelle. In contrast, the lowest peak accelerations are observed during power production mode when the earthquake acts in the fore–aft direction. This is due to the higher aerodynamic damping, which helps reduce the magnitude of vibrations induced by the earthquake. However, emergency shutdown tends to produce the largest oscillations in displacement at the tower top. At locations of maximum stress, such as the top and bottom of the legs, the variations in average peak von Mises stress across different modes are generally small. Conversely, along the intermediate sections of the legs, where stresses are lower, the average peak von Mises stresses can vary significantly between operational modes. Maximum stresses typically occur during power production, except at the top of the legs, where higher stresses are observed during emergency shutdown in several cases.

Lastly, the dissertation studies the foundation–soil–foundation interaction effects on the dynamic response of offshore wind turbine supported by jackets. It was found that foundation–soil–foundation interaction can significantly increase the magnitude of the structural response, not only in terms of accelerations but, more notably, in terms of shear forces, bending moments, and stresses across a variety of scenarios. In other words, neglecting the influence of interactions between nearby foundations (a common assumption in the analysis of these systems) may lead to an underestimation of the jacket's structural response. One key reason for this impact of foundation–soil–foundation interaction on the structural response is the alteration of the fundamental frequency of the system. This interaction changes the stiffness of each individual foundation within the group (known as the group effect), which in turn modifies the modes and natural frequencies of the entire system. As the modes and frequencies are altered, the structural response of each element is also affected.

Additionally, the influence of kinematic interaction on the seismic response of jacket-supported offshore wind turbines is analysed. For monopile substructures, rotational motion significantly influences accelerations and shear forces, while the effect of the translational filtered signal is comparatively minor. Regarding bending moments, the

differences in responses with and without kinematic interaction are notably smaller than those observed for accelerations and shear forces. In contrast, for jacket substructures, the impact of rotational motion is less substantial. Accounting for kinematic interaction factors in these substructures results in a slight increase in accelerations and internal forces, but the effect remains much less significant compared to an OWT supported by a monopile.

A comprehensive analysis of each of these problems, along with more detailed conclusions, can be found in the respective publications.

3.2 Future research directions

This section outlines several potential avenues for future research, identified based on the insights and knowledge gained throughout the course of this study. The suggested directions are intended to address unanswered questions, expand upon the findings, and explore new perspectives that emerged during the research process. The proposed lines of research are expected to contribute significantly to the advancement of the field, building on the original work presented in this thesis. The following sections provide a detailed overview of the proposed research lines:

Use of the developed advanced models:

- This research work has focused on four-legged jackets. It would be beneficial to conduct comparative studies with other types of multi-supported substructures to ascertain whether the conclusions drawn in this study are consistent. This could include jackets with different numbers of supports, such as three or five legs, as well as other types of multi-supported substructures, such as tripods.

- The rapid advancement of wind energy in recent years has led to the development of novel wind turbines with greater capacities, requiring the construction of larger towers and rotor-nacelle assembly. As a result, analysing the seismic dynamic response of jacket substructures as support structures of these larger wind turbines may produce results that differ significantly from those observed for smaller models. Given the observed trend in monopile-supported OWTs, where SSI tends to have a beneficial effect with increasing turbine size [35], it is crucial to perform a detailed assessment of SSI in jacket substructures.

- The methodology developed may be applied to the design of jacket substructures to specific locations in the Canary Islands and Europe with high wind potential and moderate seabed depths. The objective is to conduct a comprehensive assessment of the potential influence of design factors, including structural typology, foundation type and the feasibility of fixed-bottom technologies, in these regions.

- The model proposed in this dissertation have been used to conduct different parametric analysed of the seismic analysis of multi-supported on pile groups

and subjected to vertically incident plane shear S waves. The application of this code, which allows to stablish different input motions at each support, can be employed for future studies where inclined seismic incidence is considered. In addition, different types of seismic waves (P,S and Rayleigh waves) could be analysed [59–61].

Enhancement of the models:

- The models developed in this thesis were verified using numerical models from the scientific literature. An interesting option is to perform comparative analyses with established experimental models, with the aim of refining the numerical model in accordance with the insights gained. In this way, the results obtained from the advanced model considering soil-structure interaction and foundation-soil-foundation interaction could be compared with shaking table tests [62, 63], or with experimental data from installed OWTs.
- A future avenue of research involves the development and implementation of non-linear pile-soil interaction models, based on the Beam-On-Nonlinear-Winkler-Foundation (BNWF) approach [64–66], into OpenFAST, to analyse pile foundations under time-dependent loads or earthquakes. Particular attention should be given to the influence of soil and structural non-linearity [44, 67–69], including potential plastic behaviour, on the overall system response. In this context, the use of macro-elements that efficiently reproduce the essential features of soil–foundation interaction represents a valuable approach [45, 70, 71].

A. Conference Papers

A Conference Papers

A.1 First conference paper: Romero-Sánchez and Padrón, CMN 2022, Implementation of Ground Input Motion and Dynamic Soil-Structure Interaction into Openfast for the Seismic Analysis of Offshore Wind Turbines.

A.2 Second conference paper: Romero-Sánchez and Padrón, COMPDYN 2023, An implementation of multi-support seismic input motion into OpenFast for the earthquake analysis of offshore wind turbines.

A.3 Third conference paper: Romero-Sánchez et al., EURODYN 2023, Comparative study of the influence of kinematic interaction on the seismic response of monopile and jacket supported offshore wind turbines.

A.1 First conference paper: Romero-Sánchez and Padrón, CMN 2022, Implementation of Ground Input Motion and Dynamic Soil-Structure Interaction into Openfast for the Seismic Analysis of Offshore Wind Turbines.

Table A.1. First conference paper data.

Title	Implementation of Ground Input Motion and Dynamic Soil-Structure Interaction into Openfast for the Seismic Analysis of Offshore Wind Turbines
Authors	C. Romero-Sánchez and L.A. Padrón
Conference	Congress on Numerical Methods in Engineering (CMN 2022)
ISBN	978-84-123222-9-3
Publisher	International Center for Numerical Methods in Engineering (CIMNE)
Date	September 2022

Congreso de Métodos Numéricos en Ingeniería
12-14 septiembre 2022, Las Palmas de Gran Canaria, España
© SEMNI, 2022

IMPLEMENTATION OF GROUND INPUT MOTION AND DYNAMIC SOIL-STRUCTURE INTERACTION INTO OPENFAST FOR THE SEISMIC ANALYSIS OF OFFSHORE WIND TURBINES

Carlos Romero-Sánchez* **and Luis A. Padrón**

Instituto Universitario de Sistemas Inteligentes y Aplicaciones Numéricas en Ingeniería
Universidad de Las Palmas de Gran Canaria
Las Palmas de Gran Canaria 35017, Spain
e-mail: {carlos.romero, luis.padron}@ulpgc.es, web: http://www.mmc.siani.es/

Keywords: Offshore wind turbines, Soil-structure interaction, Seismic response, Lumped parameter models, OpenFAST

Abstract. *The development of offshore wind energy is expected to contribute significantly to the decarbonization of the electrical energy production sector, and the number of offshore wind farms is growing fast due to the maturity of the technology, the reduction in costs, and the increase in size and power of the turbines. Floating offshore wind is developing fast, but offshore wind turbines (OWTs) founded to the sea floor are still the dominant technology, with different types of support structures (monopiles, jackets, tripods) depending on the sea depth and the conditions of the location. The dynamic properties of these support structures are a key factor in the design of the system from a civil engineering point of view, and the distinctive features of OWTs (including the nature of the loads and the variable geometry of the system due to the rotation of the blades and the continuous actions of the control system) suggest that specific tools, able to adequately model the different subsystems, should be used in structural and seismic analyses. For this reason, input ground motion and dynamic soil-structure interaction capabilities have been implemented in OpenFAST, an open-source nonlinear aero–hydro–servo–elastic code for the simulation of wind turbines, in which the environmental loads and the response of all the main elements are taken into account through specific models and modules. This paper presents the equations of motion and the specific procedure followed to implement input ground motion and soil-structure interaction into the SubDyn module, and presents validation results to illustrate the applicability of the approach.*

1 INTRODUCTION

Geopolitical instabilites and military tensions with Russia, added to the current Climate Emergency situation, show once again that Europe needs to move fast towards energy independence based on renewable energies with the lowest possible environmental impact. Among the renewable energy sources of these characteristics available in Europe, and in which Europe can be independent to a large extent, we can mention offshore wind energy, whose potential is much greater than of onshore energy. Most of the offshore wind turbines installed in Europe are located in places where the depth of the sea allows founding them directely to the seabed. Floating wind turbines is growing in the last years, however, in Europe monopiles remain the preferred choice of developers, 80.5% new installation in 2020 and 19% on jackets [1].

With the expansion in the number of wind farms comes the need of placing new offshore wind turbines in locations with worse geotechnical properties, greater depths and increasing seismic risk. Therefore, there exists the need for numerical tools to study the seismic response of offshore wind turbines, regardless of their structural typology, and including the phenomena of soil-structure interaction and kinematic interaction between foundations and incident seismic waves. There are many models with different levels of simplification to do this for offshore wind turbines, but it is ideal to have an advanced tool that can take into account the different subsystems that composed a wind turbine.

In this regard, an interesting option is OpenFAST [2], which is a multi-physics, multi-fidelity tool for simulating the coupled dynamic response of wind turbines. It is open-source, is programmed in Fortran 95, and it might be considered not as a single program, but as a framework that couples computational modules for aerodynamics, hydrodynamics for offshore structures, control and electrical system (servo) dynamics, and structural dynamics to enable coupled nonlinear aero-hydro-servo-elastic simulation in the time domain. The main modules regarding the dynamic response of the system are: BeamDyn for modelling the dynamic behaviour of the blades; ServoDyn for modelling the generator and the control system; ElastoDyn for modelling the dynamic response of the tower in the fore-aft and side-to-side directions, and based on a modal approach that takes into account only the first two vibration modes in each direction; and SubDyn for modelling the dynamic response of the substructure, from the Transition Piece (TP) at the base of the structure to the base. In this work, the proposed modifications will be implemented in this last module, SubDyn. The different modules interact in a loosely coupled time-integration scheme, where a glue-code transfers data among modules at each time step. This glue code is the FAST driver, that gathers all the information and drives the time–domain solution forward step–by– step using a predictor–corrector scheme. Each module inputs and outputs relevant information. For more information, OpenFAST documentation [2].

Thus, this paper presents the implementation of seismic input motions and dynamic soil–structure interaction into OpenFAST. The first item includes not only horizontal ground input motions, but translational, vertical and rotational foundation input motions, while the second aspect is introduced through a simplified lumped parameter model that is

previously fitted to represent the dynamic response of the foundation. The use of lumped parameter models is considered here as a tool to introduce dynamic soil-structure interaction into the model because, contrary to a static stiffness matrix, this approach allows to take into account, not only the static stiffness of the foundation, but an approximation to its impedance, i.e., the dynamic stiffness and damping functions. This damping, arising not only from material damping but most importantly from radiation damping, can be relevant in the dynamic response of the structure. These capabilities have been implemented in OpenFAST, version 2.2.0, and the code can be downloaded here: https://github.com/CarlosRomeroSanchez/openfast_2.2.0_seismic .
This paper presents, firstly, a general overview of the original formulation implemented in the SubDyn module. Then, the proposed formulation is presented and verified by comparison against a different simplified model for some specific verification cases. Finally, results of a specific illustration example are presented.

2 GENERAL OVERVIEW OF THE FINITE ELEMENTS METHOD FORMULATION IMPLEMENTED IN SUBDYN.

This section presents a general overview of SubDyn [3]. The module integrates its equations through its own solver. The main steps are: discretization of the substructuring following the strategies of classical linear beam Finite Elements motion equations, application of Craig-Bampton modal reduction and rearrangement of the equations into State-Space type formulation for time-domain resolution and coupling with the rest of modules.

2.1 Dynamic System of Equations

The structure is discretized with the following simplifying assumptions: Two-noded Euler-Bernoulli or Timoshenko three-dimensional beams with 12 degrees of freedom, linear response and rigid joints, leading to a classical equation of motion of the type:

$$\mathbf{M}\ddot{u}(t) + \mathbf{C}\dot{u}(t) + \mathbf{K}u(t) = F(t) \tag{1}$$

$$\begin{bmatrix} M_{RR} & M_{RL} \\ M_{LR} & M_{LL} \end{bmatrix} \begin{pmatrix} \ddot{u}_R \\ \ddot{u}_L \end{pmatrix} + \begin{bmatrix} C_{RR} & C_{RL} \\ C_{LR} & C_{LL} \end{bmatrix} \begin{pmatrix} \dot{u}_R \\ \dot{u}_L \end{pmatrix} + \begin{bmatrix} K_{RR} & K_{RL} \\ K_{LR} & K_{LL} \end{bmatrix} \begin{pmatrix} u_R \\ u_L \end{pmatrix} = \begin{pmatrix} F_R \\ F_L \end{pmatrix} \tag{2}$$

where M, C and K are the global mass, damping and stiffness matrices, u and F are the displacements and external forces along all of the DOFs of the assembled system. The subindex R identifies the boundary nodes (at the base and at the Transition Piece) and L identifies the rest of nodes (interior nodes).

2.2 Craig-Bampton modal reduction

The Craig–Bampton method reduces the number of the internal generalized degrees of freedom of the substructure, using a subset q_m ($m \leq L$). Equation (3) relates physical

DOFs and generalized DOFs (q_L):

$$\left\{ \begin{array}{c} U_R \\ U_L \end{array} \right\} = \left[\begin{array}{cc} I & 0 \\ \Phi_R & \Phi_L \end{array} \right] \left\{ \begin{array}{c} U_R \\ q_L \end{array} \right\} \tag{3}$$

where I is the identity matrix; Φ_R (matrix) represents the physical displacements of the interior nodes for static, rigid body motion at the boundary and Φ_L (matrix) represents the internal eigenmodes. The Craig-Bampton transformation is therefore represented by:

$$\left\{ \begin{array}{c} U_R \\ U_L \end{array} \right\} = \left[\begin{array}{cc} I & 0 \\ \Phi_R & \Phi_m \end{array} \right] \left\{ \begin{array}{c} U_R \\ q_m \end{array} \right\} \tag{4}$$

where Φ_m is the matrix that represents the truncated set of Φ_L. Premultiplying both sides by equation (2) yields:

$$\left[\begin{array}{cc} M_{BB} & M_{Bm} \\ M_{mB} & I \end{array} \right] \left(\begin{array}{c} \ddot{u}_R \\ \ddot{q}_m \end{array} \right) + \left[\begin{array}{cc} C_{BB} & C_{Bm} \\ C_{mB} & 2\zeta\Omega_m \end{array} \right] \left(\begin{array}{c} \dot{u}_R \\ \dot{q}_m \end{array} \right) + \left[\begin{array}{cc} K_{BB} & 0 \\ 0 & \Omega_m^2 \end{array} \right] \left(\begin{array}{c} u_R \\ q_m \end{array} \right) = \left(\begin{array}{c} F_B \\ F_m \end{array} \right) \tag{5}$$

where:

$$M_{BB} = M_{RR} + M_{RL}\Phi_R + \Phi_R^T M_{LR} + \Phi_R^T M_{LL}\Phi_R \tag{6}$$
$$C_{BB} = C_{RR} + C_{RL}\Phi_R + \Phi_R^T C_{LR} + \Phi_R^T C_{LL}\Phi_R \tag{7}$$
$$K_{BB} = K_{RR} + K_{RL}\Phi_R \tag{8}$$
$$M_{mB} = \Phi_m^T M_{LR} + \Phi_m^T M_{LL}\Phi_R \tag{9}$$
$$C_{mB} = \Phi_m^T C_{LR} + \Phi_m^T C_{LL}\Phi_R \tag{10}$$
$$M_{Bm} = M_{mB}^T, C_{Bm} = C_{mB}^T \tag{11}$$
$$F_B = F_R + \Phi_R^T F_L \tag{12}$$
$$F_M = \Phi_M^T F_L \tag{13}$$

After modal decomposition, this superposition is made not with all modes, but with only a few (m modes), as usual in this kind of strategies, leading to a significant decrease in the number of degrees of freedom of the system. Introducing this idea into the FEM equations, and concentrating the motions at the boundary in the Transition Piece of the OWT (joint between tower and substructure) the equations are written as:

$$\left[\begin{array}{cc} \tilde{M}_{BB} & \tilde{M}_{Bm} \\ \tilde{M}_{mB} & I \end{array} \right] \left(\begin{array}{c} \ddot{u}_{tp} \\ \ddot{q}_m \end{array} \right) + \left[\begin{array}{cc} \tilde{C}_{BB} & \tilde{C}_{Bm} \\ \tilde{C}_{mB} & 2\zeta\Omega_m \end{array} \right] \left(\begin{array}{c} \dot{u}_{tp} \\ \dot{q}_m \end{array} \right) + \left[\begin{array}{cc} \tilde{K}_{BB} & 0 \\ 0 & \Omega_m^2 \end{array} \right] \left(\begin{array}{c} u_{tp} \\ q_m \end{array} \right) = \left(\begin{array}{c} \tilde{F}_{tp} \\ \tilde{F}_m \end{array} \right) \tag{14}$$

where the overhead bar here and below denotes matrices/vectors after the fixed-bottom boundary conditions are applied. u_{tp} is the 6 DOFs of the rigid transition piece.

2.3 State-space formulation

To arrange variables in sets of inputs and outputs that can communicate with the rest of modules, the equations are cast in state-space formulation, defining $x = x(t) = (q_m \quad \dot{q}_m)^T$ as the states; $u = (U_{TP} \quad \dot{U}_{TP} \quad \ddot{U}_{TP} \quad F_{L,e} \quad F_{R,e})^T$ as the inputs from other modules; $Y_1 = Y_1(t) = -F_{TP}$ as outputs to tower (ElastoDyn); $Y_2 = Y_2(t)$ as outputs to HydroDyn (motion of the substructure).
Then, equation 14 can be cast into state equation form as:

$$\dot{x} = Ax + Bu + F_x \tag{15}$$

$$-Y_1 = C_1 x + D_1 u + F_{y1} \tag{16}$$

$$Y_2 = C_2 x + D_2 u + F_{y2} \tag{17}$$

where $A, B, F_x, C_1, C_2, D_1, D_2, F_{y1}$ and F_{y1} are arrays and matrices of constant coefficients that are computed only, at initialization.

3 IMPLEMENTATION OF UNIFORM BASE INPUT MOTION AND SOIL-STRUCTURE INTERACTION MODEL INTO SUBDYN MODULE

3.1 Generic equation of motion

Equation (1) assumes fixed-base, taking into account prescribed displacement in the base, the main equations of motion describing the dynamic response of the substructure can be written as:

$$\mathbf{M}\ddot{u}^t(t) + \mathbf{C}\dot{u}(t) + \mathbf{K}u(t) = F(t) \tag{18}$$

where now u and u^t represent relative and total displacements. If kinematic input motion at time t, taking into account the presence of the foundation and its interaction with the incident seismic field, is denoted by vector $u_b(t)$ ($u_b = U, V, \theta$), the relationship between displacements can be written as:

$$u(t) = u^t(t) - \Lambda u_b(t) \tag{19}$$

where Λ is a matrix composed by Λ_U, Λ_V and Λ_θ, which the influence vectors (Chopra [4]) representing the displacement of the different degrees of freedom as a consequence of the static application of unitary lateral, vertical or rotational ground displacements, respectively. Writing the equation of motion in absolute terms yield:

$$\mathbf{M}\ddot{u}^t(t) + \mathbf{C}\dot{u}^t(t) + \mathbf{K}u^t(t) = F(t) + \mathbf{C}\Lambda\dot{u}_b(t) + \mathbf{K}\Lambda u_b(t) \tag{20}$$

After the assembly, the system of equation can be written as:

$$\begin{aligned} \begin{bmatrix} M_{RR} & M_{RL} \\ M_{LR} & M_{LL} \end{bmatrix} \begin{pmatrix} \ddot{u}_R \\ \ddot{u}_L \end{pmatrix}^t + \begin{bmatrix} C_{RR} & C_{RL} \\ C_{LR} & C_{LL} \end{bmatrix} \begin{pmatrix} \dot{u}_R \\ \dot{u}_L \end{pmatrix}^t + \begin{bmatrix} K_{RR} & K_{RL} \\ K_{LR} & K_{LL} \end{bmatrix} \begin{pmatrix} u_R \\ u_L \end{pmatrix}^t = \\ \begin{pmatrix} F_R \\ F_L \end{pmatrix} + \begin{bmatrix} C_{RR} & C_{RL} \\ C_{LR} & C_{LL} \end{bmatrix} \begin{pmatrix} \Lambda_R \\ \Lambda_L \end{pmatrix} \dot{u}_b + \begin{bmatrix} K_{RR} & K_{RL} \\ K_{LR} & K_{LL} \end{bmatrix} \begin{pmatrix} \Lambda_R \\ \Lambda_L \end{pmatrix} u_b \end{aligned} \tag{21}$$

where $F_R = F_{R,e} + F_{R,g}$, with $F_{R,e}$ being external loads from other modules, the hydrodynamic forces over the boundary nodes and the forces transfered to and from ElastoDyn through the Transition Piece; and g stands for the gravity loads.
The interior degrees of freedom are hence transformed from physical DOFs to modal DOFs, and pre-multiplying by Craig-Bampton transformation (equation 4) both sides of equation of motion, can be rewritten as:

$$\begin{bmatrix} M_{BB} & M_{Bm} \\ M_{mB} & I \end{bmatrix} \begin{pmatrix} \ddot{u_R} \\ \ddot{q_m} \end{pmatrix}^t + \begin{bmatrix} C_{BB_f} & C_{Bm_f} \\ C_{mB_f} & C_{mm_f} + 2\zeta\Omega_m \end{bmatrix} \begin{pmatrix} \dot{u_R} \\ \dot{q_m} \end{pmatrix}^t + \begin{bmatrix} K_{BB} & 0 \\ 0 & \Omega_m^2 \end{bmatrix} \begin{pmatrix} u_R \\ q_m \end{pmatrix}^t = \begin{pmatrix} F_R + \Phi_R^T F_L \\ \Phi_m^T F_L \end{pmatrix} + \begin{bmatrix} C_{BB_f} & C_{Bm_f} \\ C_{mB_f} & C_{mm_f} + 2\zeta\Omega_m \end{bmatrix} \begin{pmatrix} \Lambda_R \\ \Lambda_m \end{pmatrix} \dot{u_b} + \begin{bmatrix} K_{BB} & 0 \\ 0 & \Omega_m^2 \end{bmatrix} \begin{pmatrix} \Lambda_R \\ \Lambda_m \end{pmatrix} u_b \tag{22}$$

where the damping matrix is composed of the structural damping ($2\zeta\Omega_m$) and damping terms related to the LPM foundation model (C_f). On the other hand, Λ_m is obtained as the truncation of Λ_L as:

$$\Lambda_L = \Phi_R \Lambda_R + \Phi_m \Lambda_M \tag{23}$$

$$\Lambda_m = \bar{\Lambda}_L \tag{24}$$

3.2 Equation of motion with lateral, vertical and rotational foundation input motion

The vector of displacements at the boundary nodes contains the displacement at the interface node with the tower (u_I) and the displacements at base nodes, which would move following the ground motion according to the relevant portion Λ of the influence vector:

$$u_R = \begin{pmatrix} \Lambda_U U_b + \Lambda_\theta \theta_b + \Lambda_V V_b \\ u_I \end{pmatrix} \tag{25}$$

where U_b is the lateral kinematic input motion, V_b is the vertical kinematic input motion and θ_b is the rotational kinematic input motion. Accordingly, the matrices of related to the boundary nodes can be decompose as:

$$M_{BB} = \begin{bmatrix} M_{bb} & M_{bI} \\ M_{Ib} & \bar{M}_{BB} \end{bmatrix} \quad ; \quad M_{Bm} = \begin{bmatrix} M_{bm} \\ \bar{M}_{Bm} \end{bmatrix} \quad ; \quad M_{mB} = \begin{bmatrix} M_{mb} \\ \bar{M}_{mB} \end{bmatrix} \tag{26}$$

where b is base nodes and I is interface nodes. The overhead bar here and below denotes matrices/vectors after the fixed-bottom boundary condition are applied.

$$\begin{bmatrix} \bar{M}_{BB} & \bar{M}_{Bm} \\ \bar{M}_{mB} & I \end{bmatrix} \begin{pmatrix} \ddot{u}_{tp} \\ \ddot{q}_m \end{pmatrix}^t + \begin{bmatrix} \bar{C}_{BB_f} & \bar{C}_{Bm_f} \\ \bar{C}_{mB_f} & C_{mm_f} + 2\zeta\Omega_m \end{bmatrix} \begin{pmatrix} \dot{u}_{tp} \\ \dot{q}_m \end{pmatrix}^t + \begin{bmatrix} \bar{K}_{BB} & 0 \\ 0 & \Omega_m^2 \end{bmatrix} \begin{pmatrix} u_{tp} \\ q_m \end{pmatrix}^t = \begin{pmatrix} \bar{F}_R + \Phi_R^T F_L \\ \Phi_m^T F_L \end{pmatrix} + \begin{bmatrix} \bar{C}_{BB_f} & \bar{C}_{Bm_f} \\ \bar{C}_{mB_f} & C_{MM} + 2\zeta\Omega_m \end{bmatrix} \begin{pmatrix} \Lambda_I \\ \Lambda_m \end{pmatrix} \dot{u}_b + \begin{bmatrix} \bar{K}_{BB} & 0 \\ 0 & \Omega_m^2 \end{bmatrix} \begin{pmatrix} \Lambda_I \\ \Lambda_m \end{pmatrix} u_b - \begin{bmatrix} M_{Ib} \\ M_{mb} \end{bmatrix} \Lambda_b \ddot{u}_b \quad (27)$$

The interfaces nodes and the Transition Piece (that is assumed as a rigid body) are considered as rigidly connected, so that the following relationships hold:

$$u_I = T_I u_{tp} \quad (28)$$

$$F_{tp} = T_I^T F_R \quad (29)$$

where T_I is a simple transformation matrix depending on the differences between the locations between both points. Taking these two relations into account, eq. (27) can be written as:

$$\begin{bmatrix} \tilde{M}_{BB} & \tilde{M}_{Bm} \\ \tilde{M}_{mB} & I \end{bmatrix} \begin{pmatrix} \ddot{u}_{tp} \\ \ddot{q}_m \end{pmatrix}^t + \begin{bmatrix} \tilde{C}_{BB_f} & \tilde{C}_{Bm_f} \\ \tilde{C}_{mB} & C_{mm} + 2\zeta\Omega_m \end{bmatrix} \begin{pmatrix} \dot{u}_{tp} \\ \dot{q}_m \end{pmatrix}^t + \begin{bmatrix} \tilde{K}_{BB} & 0 \\ 0 & \Omega_m^2 \end{bmatrix} \begin{pmatrix} u_{tp} \\ q_m \end{pmatrix}^t = \begin{pmatrix} \tilde{F}_{tp} \\ \tilde{F}_m \end{pmatrix} + \begin{bmatrix} F_{IsisK-U} \\ F_{MsisK-U} \end{bmatrix} U_b(t) + \begin{bmatrix} F_{IsisC-U} \\ F_{MsisC-U} \end{bmatrix} \dot{U}_b(t) - \begin{bmatrix} F_{IsisM-U} \\ F_{MsisM-U} \end{bmatrix} \ddot{U}_b(t) + \begin{bmatrix} F_{IsisK-V} \\ F_{MsisK-V} \end{bmatrix} V_b(t) + \begin{bmatrix} F_{IsisC-V} \\ F_{MsisC-V} \end{bmatrix} \dot{V}_b(t) - \begin{bmatrix} F_{IsisM-V} \\ F_{MsisM-V} \end{bmatrix} \ddot{V}_b(t) + \begin{bmatrix} F_{IsisK-\theta} \\ F_{MsisK-\theta} \end{bmatrix} \theta_b(t) + \begin{bmatrix} F_{IsisC-\theta} \\ F_{MsisC-\theta} \end{bmatrix} \dot{\theta}_b(t) - \begin{bmatrix} F_{IsisM-\theta} \\ F_{MsisM-\theta} \end{bmatrix} \ddot{\theta}_b(t) \quad (30)$$

where:

$$\tilde{M}_{BB} = T_I^T \bar{M}_{BB} T_I \quad (31)$$

$$\tilde{C}_{BB_f} = T_I^T \bar{C}_{BB_f} T_I \quad (32)$$

$$\tilde{K}_{BB} = T_I^T \bar{K}_{BB} T_I \quad (33)$$

$$\tilde{M}_{Bm} = T_I^T \bar{M}_{Bm} \quad (34)$$

$$\tilde{C}_{Bm_f} = T_I^T \bar{C}_{Bm_f} \quad (35)$$

$$\tilde{F}_{tp} = F_{tp} + T_I^T \bar{F}_{R,e} + T_I^T \bar{F}_{R,g} + T_I^T \bar{\Phi}_R^T (F_{L,e} + F_{L,g}) \quad (36)$$

$$\tilde{F}_m = \Phi_m^T (F_{L,e} + F_{L,g}) \quad (37)$$

$$F_{IsisK-U} = T_I^T(\bar{K}_{BB}\Lambda_{U_I}) \tag{38}$$
$$F_{MsisK-U} = \Omega_m^2\Lambda_{U_m} \tag{39}$$
$$F_{IsisC-U} = T_I^T(\bar{C}_{BB_f}\Lambda_{U_I} + \bar{C}_{Bm_f}\Lambda_{U_m}) \tag{40}$$
$$F_{MsisC-U} = \bar{C}_{mB_f}\Lambda_{U_I} + (C_{mm_f} + 2\zeta\Omega_m)\Lambda_{U_m} \tag{41}$$
$$F_{IsisM-U} = T_I^T\bar{M}_{Ib}\Lambda_{U_b} \tag{42}$$
$$F_{MsisM-U} = M_{Mb}\Lambda_{U_b} \tag{43}$$
$$F_{IsisK-\theta} = T_I^T(\bar{K}_{BB}\Lambda_{\theta_I}) \tag{44}$$
$$F_{MsisK-\theta} = \Omega_m^2\Lambda_{\theta_m} \tag{45}$$
$$F_{IsisC-\theta} = T_I^T(\bar{C}_{BB_f}\Lambda_{\theta_I} + \bar{C}_{Bm_f}\Lambda_{\theta_m} \tag{46}$$
$$F_{MsisC-\theta} = \bar{C}_{mB_f}\Lambda_{\theta_I} + (C_{mm_f} + 2\zeta\Omega_m)\Lambda_{\theta_m} \tag{47}$$
$$F_{IsisM-\theta} = T_I^T\bar{M}_{Ib}\Lambda_{\theta_b} \tag{48}$$
$$F_{MsisM-\theta} = M_{Mb}\Lambda_{\theta_b} \tag{49}$$
$$F_{IsisK-V} = T_I^T(\bar{K}_{BB}\Lambda_{V_I}) \tag{50}$$
$$F_{MsisK-V} = \Omega_m^2\Lambda_{V_m} \tag{51}$$
$$F_{IsisC-V} = T_I^T(\bar{C}_{BB_f}\Lambda_{V_I} + \bar{C}_{Bm_f}\Lambda_{V_m} \tag{52}$$
$$F_{MsisC-V} = \bar{C}_{mB_f}\Lambda_{V_I} + (C_{mm_f} + 2\zeta\Omega_m)\Lambda_{V_m} \tag{53}$$
$$F_{IsisM-V} = T_I^T\bar{M}_{Ib}\Lambda_{V_b} \tag{54}$$
$$F_{MsisM-V} = M_{Mb}\Lambda_{V_b} \tag{55}$$

3.3 Simplified Lumped Model Parameter Model into SubDyn

The introduction of an LPM can be simply understood as adding one (or several) additional elements at the base of the substructure. At this point, the simplified Lumped Parameter Model proposed by Carbonari et al. [5], depicted in figure 1, is adopted for the lateral vibrations, while the spring-damper model depicted in figure 2 is adopted for vertical and torsional vibrations (assuming that their influence on the response of the system is, in any case, smaller). These assumptions lead to the following stiffness, damping and mass matrices:

$$\mathbf{K} = \begin{bmatrix} \mathbf{K}_{ii} & \mathbf{K}_{ij} \\ (\text{sym}) & \mathbf{K}_{jj} \end{bmatrix}; \quad \mathbf{C} = \begin{bmatrix} \mathbf{C}_{ii} & \mathbf{C}_{ij} \\ (\text{sym}) & \mathbf{C}_{jj} \end{bmatrix}; \quad \mathbf{M} = \begin{bmatrix} \mathbf{0} & \mathbf{0} \\ (\text{sym}) & \mathbf{M}_{jj} \end{bmatrix} \tag{56}$$

where node i is the ground, node j is the base of the substructure, and the submatrices are defined as follows:

$$u_b^T = \begin{bmatrix} u_{xb} & u_{yb} & u_{zb} & \theta_{xb} & \theta_{yb} & \theta_{zb} \end{bmatrix} \tag{57}$$

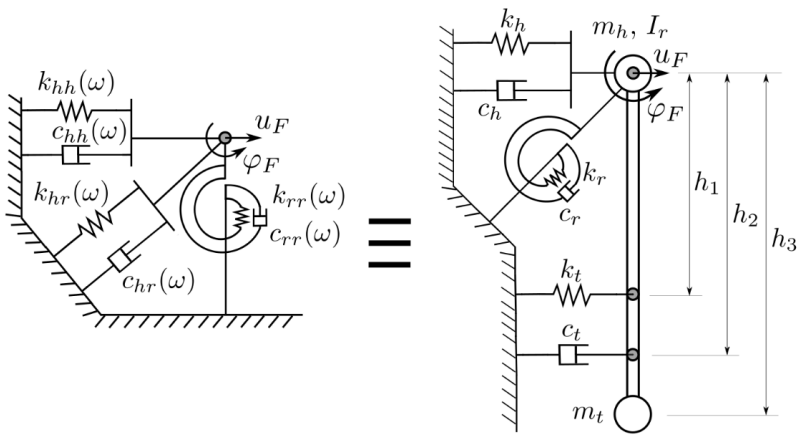

Figure 1. Scheme of the simplified LPM, adopted for lateral vibrations [6]

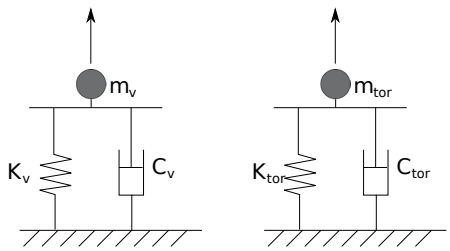

Figure 2. Scheme of the mass-spring-damper model, adopted for vertical and torsional vibrations [6]

$$\mathbf{K}_{jj} = \begin{bmatrix} k_h + k_t & 0 & 0 & 0 & -k_t h_1 & 0 \\ & k_h + k_t & 0 & k_t h_1 & 0 & 0 \\ & & k_z & 0 & 0 & 0 \\ & & & k_r + k_t h_1^2 & 0 & 0 \\ & & & & k_r + k_t h_1^2 & 0 \\ & & & & & k_{\text{tor}} \end{bmatrix} \tag{58}$$

$$\mathbf{K}_{ji} = \mathbf{K}_{ij}^T = \begin{bmatrix} -(k_h + k_t) & 0 & 0 & 0 & k_t h_1 & 0 \\ 0 & -(k_h + k_t) & 0 & -k_t h_1 & 0 & 0 \\ 0 & 0 & -k_z & 0 & 0 & 0 \\ 0 & k_t h_1 & 0 & -(k_r + k_t h_1^2) & 0 & 0 \\ -k_t h_1 & 0 & 0 & 0 & -(k_r + k_t h_1^2) & 0 \\ 0 & 0 & 0 & 0 & 0 & -k_{\text{tor}} \end{bmatrix} \tag{59}$$

$$\mathbf{C}_{jj} = \begin{bmatrix} c_h + c_t & 0 & 0 & 0 & -c_t h_2 & 0 \\ & c_h + c_t & 0 & c_t h_2 & 0 & 0 \\ & & c_z & 0 & 0 & 0 \\ & & & c_r + c_t h_2^2 & 0 & 0 \\ & & & & c_r + c_t h_2^2 & 0 \\ & & & & & c_{\text{tor}} \end{bmatrix} \tag{60}$$

$$\mathbf{C}_{ji} = \mathbf{C}_{ij}^T = \begin{bmatrix} -(c_h + c_t) & 0 & 0 & 0 & c_t h_2 & 0 \\ 0 & -(c_h + c_t) & 0 & -c_t h_2 & 0 & 0 \\ 0 & 0 & -c_z & 0 & 0 & 0 \\ 0 & c_t h_2 & 0 & -(c_r + c_t h_2^2) & 0 & 0 \\ -c_t h_2 & 0 & 0 & 0 & -(c_r + c_t h_2^2) & 0 \\ 0 & 0 & 0 & 0 & 0 & -c_{\text{tor}} \end{bmatrix} \tag{61}$$

$$\mathbf{M}_{jj} = \begin{bmatrix} m_h + m_t & 0 & 0 & 0 & -m_t h_3 & 0 \\ & m_h + m_t & 0 & m_t h_3 & 0 & 0 \\ & & m_z & 0 & 0 & 0 \\ & & & I_r + m_t h_3^2 & 0 & 0 \\ & & & & I_r + m_t h_3^2 & 0 \\ & & & & & I_{\text{tor}} \end{bmatrix} \tag{62}$$

where the SLPM coefficients are calculated using least squares to be optimaly adapted to the impedance functions defining the dynamic response of the wind turbine foundation.

3.4 State-space formulation

These equations must be cast in a form useful for implementation into the general framework of OpenFAST and SubDyn, taking into account which are the input variables to SubDyn and the output variables from SubDyn to other modules. The equations are written in state-space form. The states are defined as:

$$x = \begin{pmatrix} q_m^t & \dot{q}_m^t \end{pmatrix}^T \tag{63}$$

and the input vector are defined as:

$$u = \begin{pmatrix} U_{tp}^t & \dot{U}_{tp}^t & \ddot{U}_{tp}^t & F_{L,e} & F_{R,e} \end{pmatrix}^T \tag{64}$$

3.4.1 State equation

Equation (30) is cast into standard linear system state equation of the form:

$$\dot{x} = X = \mathbf{A}x + \mathbf{B}u + F_x \tag{65}$$

To do, the second row of equation (30) needs to be written down and solved for $\ddot{U}_L$. After doing so, the matrices of the state equation can be found to be:

$$\mathbf{A} = \begin{bmatrix} 0 & I \\ -\Omega_m^2 & -C_{mm_f} - 2\zeta\Omega_m \end{bmatrix} \tag{66}$$

$$\mathbf{B} = \begin{bmatrix} 0 & 0 & 0 & 0 & 0 \\ 0 & -\tilde{C}_{mB_f} & -\tilde{M}_{mB} & \Phi_m^T & 0 \end{bmatrix} \tag{67}$$

$$Fx = \begin{bmatrix} 0 \\ \Phi_m^T F_{Lg} + \sum_i F_{MsisK-i} u_b + \sum_i F_{MsisC-i} \dot{u}_b - \sum_i F_{MsisM-i} \ddot{u}_b \end{bmatrix} \tag{68}$$

where I is the identity matrix and $i = U, V, \theta$

3.4.2 Output equation to ElastoDyn

The first output equation computes the interaction forces between tower and substructure at the Transition Piece.

$$y_1 = Y_1 = -F_{tp} \tag{69}$$

Writting the first row of (30) and solving for F_{tp}, the output equation can be written as:

$$-Y_1 = \mathbf{C}_1 x + \mathbf{D}_1 \bar{u} + F_{y_1} \tag{70}$$

where

$$\mathbf{C}_1 = \begin{bmatrix} -\tilde{M}_{Bm}\Omega_m^2 & -\tilde{M}_{Bm}(C_{mm_f} + 2\zeta\Omega_m) + \tilde{C}_B m_f \end{bmatrix} \tag{71}$$

$$\mathbf{D}_1 = \begin{bmatrix} \tilde{K}_{BB} & -\tilde{C}_{mB_f}\tilde{M}_{Bm} + \tilde{C}_{BB_f} & -\tilde{M}_{mB}\tilde{M}_{Bm} + \tilde{M}_{BB} & \tilde{M}_{Bm}\Phi_m^T - T_I^T \Phi_R^T & -T_I^T \end{bmatrix} \tag{72}$$

$$F_{y_1} = -T_I^T(\bar{F}_{Ig} + \bar{\Phi}_R^T F_{Lg}) - \sum_i F_{IsisK-i} u_b - \sum_i F_{IsisC-i} \dot{u}_b + \sum_i F_{IsisM-i} \ddot{u}_b + \tilde{M}_{Bm}\left[\sum_i F_{MsisK-i} u_b + \sum_i F_{MsisC-i} \dot{u}_b - \sum_i F_{MsisM-i} \ddot{u}_b + \Phi_m^T F_{Lg}\right]; i = U, V, \theta \tag{73}$$

3.4.3 Output equation to HydroDyn

The second output equation gathers all the motions needed by the module HydroDyn to compute hydrodynamic loads on the substructure.

$$y_2 = Y_2 = \{ \; u_I^t \quad u_L^t \quad \dot{u}_I^t \quad \dot{u}_L^t \quad \ddot{u}_I^t \quad \ddot{u}_L^t \; \}^T \tag{74}$$

$$Y_2 = \mathbf{C}_2 x + \mathbf{D}_2 u + F_{y_2} \tag{75}$$

where

$$\mathbf{C}_2 = \begin{bmatrix} 0 & 0 \\ \Phi_m & 0 \\ 0 & 0 \\ 0 & \Phi_m \\ 0 & 0 \\ -\Phi_m \Omega_m^2 & -\Phi_m (C_{mm_f} + 2\zeta\Omega_m) \end{bmatrix} \tag{76}$$

$$\mathbf{D}_2 = \begin{bmatrix} T_I & 0 & 0 & 0 & 0 \\ \bar{\Phi}_R T_I & 0 & 0 & 0 & 0 \\ 0 & T_I & 0 & 0 & 0 \\ 0 & \bar{\Phi}_R T_I & 0 & 0 & 0 \\ 0 & 0 & T_I & 0 & 0 \\ 0 & -\Phi_m \tilde{C}_{mB_f} & \tilde{\Phi}_R T_I - \Phi_m \tilde{M}_{mB} & \Phi_m \Phi_m^T & 0 \end{bmatrix} \tag{77}$$

$$F_{y_2} = \begin{bmatrix} 0 \\ 0 \\ 0 \\ 0 \\ 0 \\ \Phi_m \Phi_m^T F_{Lg} + \Phi_m (\sum_i F_{MsisK-i} u_b + \sum_i F_{MsisC-i} \dot{u}_b - \sum_i F_{MsisM-i} \ddot{u}_b) \end{bmatrix} \tag{78}$$

where $i = U, \theta, V$.

4 VERIFICATION RESULTS

The correct implementation into OpenFAST of the input ground motion and the simplified Lumped Parameter Model at the base of the substructure has been initially verified by comparison against results obtained from a simplified model written in matlab for this purpose. Firstly, this model is first briefly described. Afterwards, the cases designed for verification are presented and the results of the comparison are shown.

4.1 Reference simple model for comparison

The model used for comparison is depicted in figure 3. It can be understood as an inverted pendulum on a beam comprised of two different parts: the inferior part corresponding to the substructure with constant properties along height; and the upper part corresponding to the tower, with varying properties along height. On top, the rotor-nacelle-assembly (RNA) is modeled as a punctual rigid concentrated inertia. The model can be run as fixed based or as compliant base.
Again, the equation of motion can be written as:

$$\mathbf{M}\, \ddot{u}^t(t) + \mathbf{C}\, \dot{u}(t) + \mathbf{K}\, u(t) = \mathbf{0} \tag{79}$$

where $\mathbf{M}$, $\mathbf{C}$ and $\mathbf{K}$ are the mass, damping and stiffness matrices. The beam elements implemented are identical to those already implemented in SubDyn. Vectors u and u^t represent relative and total (or absolute) displacements at the different DOFs in the structure. If the input ground displacement at time t is denoted by $u_b(t)$, and eq. (19) is taken into account, the equation of motion in relative terms, yields:

$$\mathbf{M}\,\ddot{u}(t) + \mathbf{C}\,\dot{u}(t) + \mathbf{K}\,u(t) = -\mathbf{M}\Lambda\,\ddot{u}_b(t) \tag{80}$$

Assuming steady–state harmonic response, motions can be written as:

$$u(t) = U(\omega)\mathrm{e}^{\mathrm{i}\omega t} \tag{81}$$

where ω is the circular frecuency of the excitation. Thus, the time-harmonic equation of motion employed can be written as:

$$\left(\mathbf{K} + \mathrm{i}\omega\mathbf{C} - \omega^2\mathbf{M}\right) U(\omega) = -\mathbf{M}\Lambda\,\ddot{U}_b(\omega) = \omega^2\mathbf{M}\Lambda\,U_b(\omega) \tag{82}$$

As usual, time domain response will be therefore obtained through Frecuency Domain Analysis [4] making use of the Fast Fourier Transform. This reference simplified model was implemented in an independent matlab© code.

4.2 Reference Configuration

The reference configuration adopted for this study is the widely used 5MW NREL reference turbine. More precisely, the base configuration is the one defined for the OC3 (Offshore Code Comparison Collaboration) for the offshore 5MW NREL reference turbine on a monopile. Specific data can be found in Jonkman and Musial [7]. The main data for tower and substructure can be found in tables 1 and 2.

4.3 Verification cases

Table 3 lists the main characteristics of the input motions used for the four simplified verification cases presented herein together with the base configuration (fixed or compliant) in each case. ξ_t denotes the structural tower damping ratio. On the other hand, table 4 presents the parameters obtained for the SLPM from fitting the impedance functions corresponding to the foundation of this turbine [7]. The impedance functions were obtained from detailed boundary elements model [8].

4.4 Verification results

This section presents the validation results described in the previous section. Figure 4 present the comparisons between the results obtained using the modified version of OpenFAST and those of the reference inverted pendulum matlab code. Motions at the top of the tower, and at the platform are represented. It is shown that the agreement is very good in terms of displacements. It is worth highlighting, however, the major difference between both codes, being the OpenFAST model much more elaborated than

Parameter	Value
Tower-top height above mean sea level (MSL)	87.6 m
Tower base height above mean sea level	10.0 m
Water depth (from mean sea level)	20.0 m
Tower lenght	77.6 m
Water depth (from mean sea level)	20.0 m
Diameter at the base of the tower	6.0 m
Diameter at the top of the tower	3.87 m
Thickness at the base of the tower	0.027
Thickness at the top of the tower	0.019
RNA mass	349389.842 kg
RNA center of mass above tower top	1.96699 m
Second moment of inertia around RNA's center of mass	$I_{xx} = 4.37 \cdot 10^7$ kg $\cdot$ m
	$I_{yy} = 2.35 \cdot 10^7$ kg $\cdot$ m
	$I_{zz} = 2.54 \cdot 10^7$ kg $\cdot$ m

Table 1. Tower and turbine main properties, 5MW.

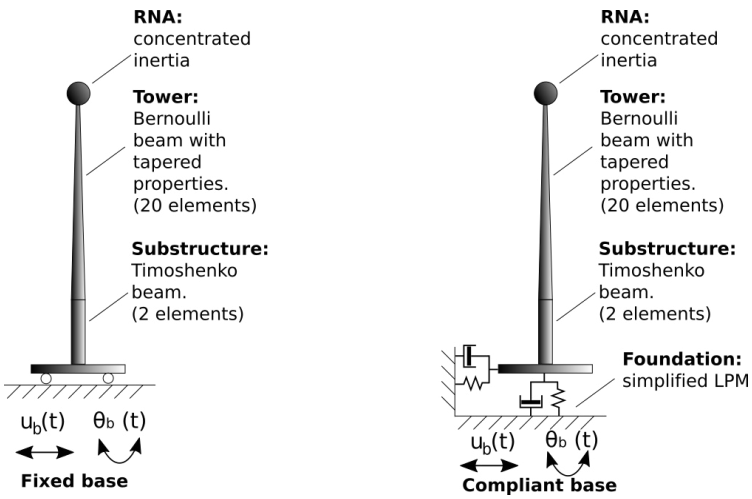

Figure 3. Depiction of the reference simple model used for comparison

Parameter	Value
Height	30.0 m
Diameter	6.0 m
Thickness	0.60 m

Table 2. Monopile main propeties

N	Motion	Base configuration	ξ_t	Input base motion
1	Lateral	Fixed base	5%	Quarter of sine ($f = 0.1$ Hz, $A = 0.1$ m)
2	Rotational	Fixed base	2%	Quarter of sine ($f = 0.1$ Hz, $A = 0.05$ m)
3	Lateral	Fixed base	2%	Chi-Chi earthquake
4	Lateral	Compliant base	2%	Chi-Chi earthquake

Table 3. Verification cases

$K_{\mathbf{SLPM}}$	**Value**	$C_{\mathbf{SLPM}}$	**Value**	$M_{\mathbf{SLPM}}$	**Value**
k_h	5.478e+4	c_h	1.212e+7	m_h	55.92
k_r	1.078e+11	c_r	3.633e+8	I_r	1.0
k_t	2.274e+9	c_t	4.966e+7	m_t	5.047e+05
k_z	4.787e+9	c_z	2.117e+8	m_z	1.0
k_{tor}	7.13e+10	c_{tor}	4.414e+8	I_{tor}	8.60e+6
h_1	-4.794	h_2	-4.417	h_3	0.08194

Table 4. SLPM parameters

the reference model, and being the first one solved in time domain and the second one in frequency domain. As expected, response on a softer foundation (previously verified against the matlab reference model) provides a longer period. It also allows to see that the great influence that the properties of the foundation exert on the system global response. Table 5 shows the fundamental frequencies as a function of the assumed base condition.

Base condition	**Fundamental frequency**
Fixed base, fore-aft:	0.2797 Hz (T=3.58 s)
Compliant base, fore-aft:	0.2597 Hz (T=3.85 s)

Table 5. Fundamental frequencies obtained for Fixed Base and Compliant base conditions

5 ILUSTRATION EXAMPLE

After having verified the implementation of the kinematic input motions for a simplified inverted pendulum configuration, this section illustrates the use of the code for the analysis of the seismic response of the offshore wind turbine while the turbine is operating and is subjected to wind, waves and currents. The NREL 5 MW reference OWT described above is considered here too. The simplified Lumped Parameter Model is used to represent the flexibility of the soil-foundation system (see Figure 5), as stated above. At the same time, the system is assumed to be subjected to vertically-incident shear waves. The Chi-Chi earthquake is considered as free-field ground-surface seismic action. The simulation is allowed to run for 220 seconds before the earthquake shaking arrive, in order to allow the dissipation of the transient response generated at the beginning of the simulation. No emergency shutdown is considered. The time-harmonic kinematic interaction factors corresponding to the monopile foundation were computed through the

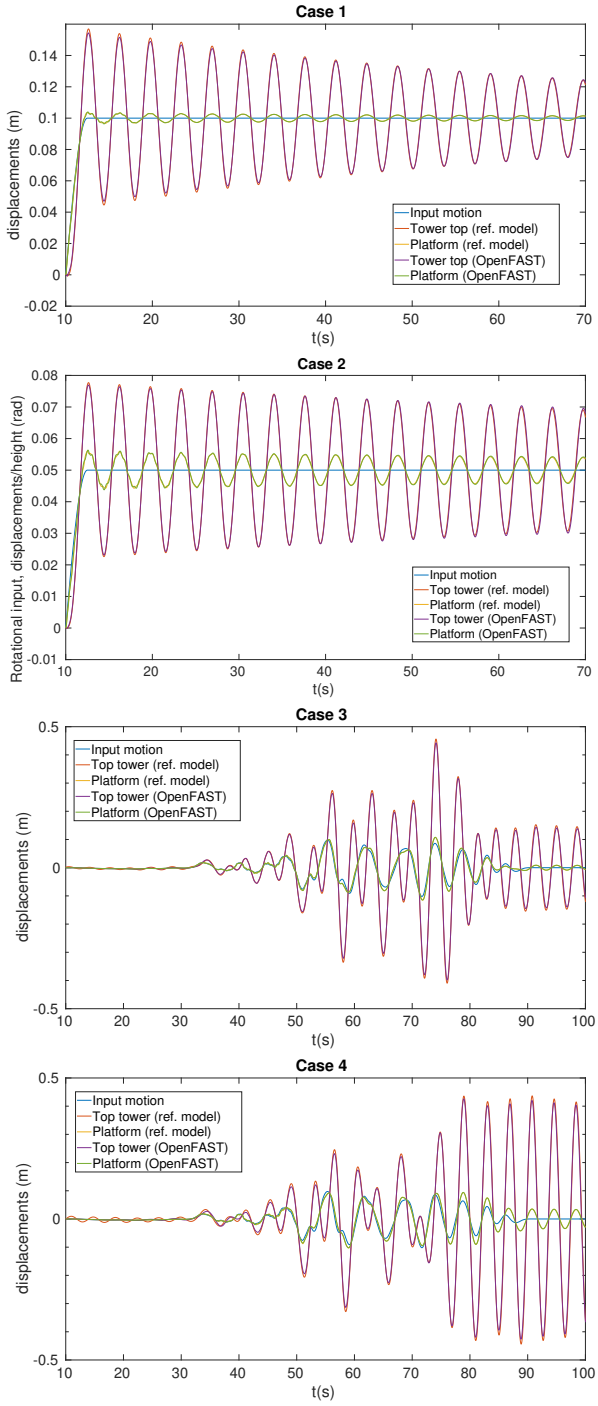

Figure 4. Results corresponding to verification cases

same boundary element model employed to compute the impedance functions [8]. These kinematic interaction factors allow to compute the translational and rotational kinematic input motions (see Figure 6) that are then defined at the base of the SLPM.
Figure 7 presents the computed seismic response in terms of tower top displacements, tower top accelerations and mudline shear forces and bending moments in the monopile. Each plot presents the response of the OWT computed under four different loading situations: a) only environmental loads (wind, waves and currents); b) taking into account both translational and rotational foundation input motions; c) taking into account only translational foundation input motion (with zero rotational input motion); and d) considering the original seismic input motion as translational input motion, i.e., without taking into account the filtering produced by the pipe pile foundation.

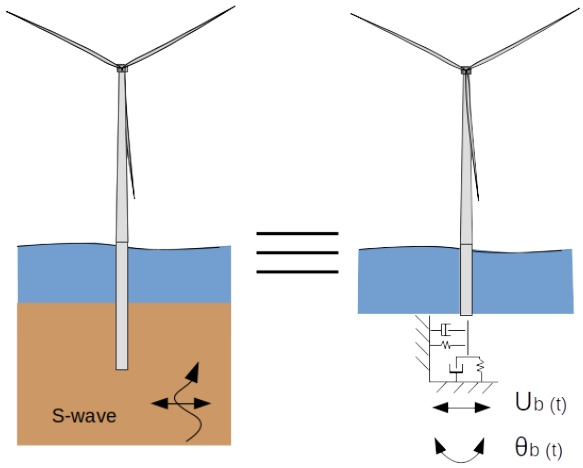

Figure 5. Ilustration example model

As expected, the seismic action increases the response of the structure in terms of displacements and accelerations at the tower top. Accelerations, in particular, increase by a factor of 3 due to the arrival of the earthquake. Bending moments and shear forces at mudline, on the contrary, are less affected by the earthquake, being the environmental loads the ones that contribute more importantly to the resulting internal efforts. The rotational component of the FIM produces an increase in the seismic response, as observed from the comparison of the responses computed taking or not into account the rotational input motion (red and green curves). However, this increase is not very significant when compared to the oscillations of the response of the system under the rest of loads. Finally, the difference between considering the original earthquake signal or the filtered earthquake signal is negligible.

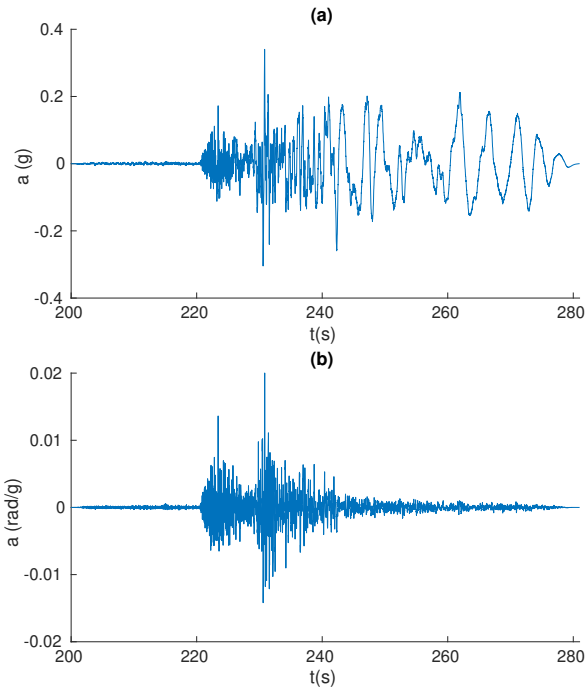

Figure 6. Lateral FIM (a) and Rotational FIM (b). Obtained from KIF of monopile foundation and Chi-Chi Earthquake

6 CONCLUSIONS

The paper develops the formulation needed for the implementation of seismic input motions and new dynamic soil-structure interaction capabilities into the open-source software OpenFAST, with the aim of facilitating the use of this tool for the seismic analysis of wind turbines.

Not only horizontal, but also vertical and rotational foundation input motions are considered. In the ilustration example, horizontal and rotational foundation input motions are computed taking the monopile kinematic interaction factors into account, and the relevance of this filtering is also discussed.

On the other hand, the use of lumped parameter models is considered here as a tool to introduce soil-structure interaction into the model because this approach allows to take into account, not only the static stiffness of the foundation, but an approximation to its impedance, i.e., the dynamic stiffness and damping functions.

These capabilities have been implemented in OpenFAST, version 2.2.0, and the code can be downloaded here: https://github.com/CarlosRomeroSanchez/openfast_2.2.0_seismic . The authors are now working on the generalization of the formulation to non-uniform input motions, and its implementation in the latest version of OpenFAST.

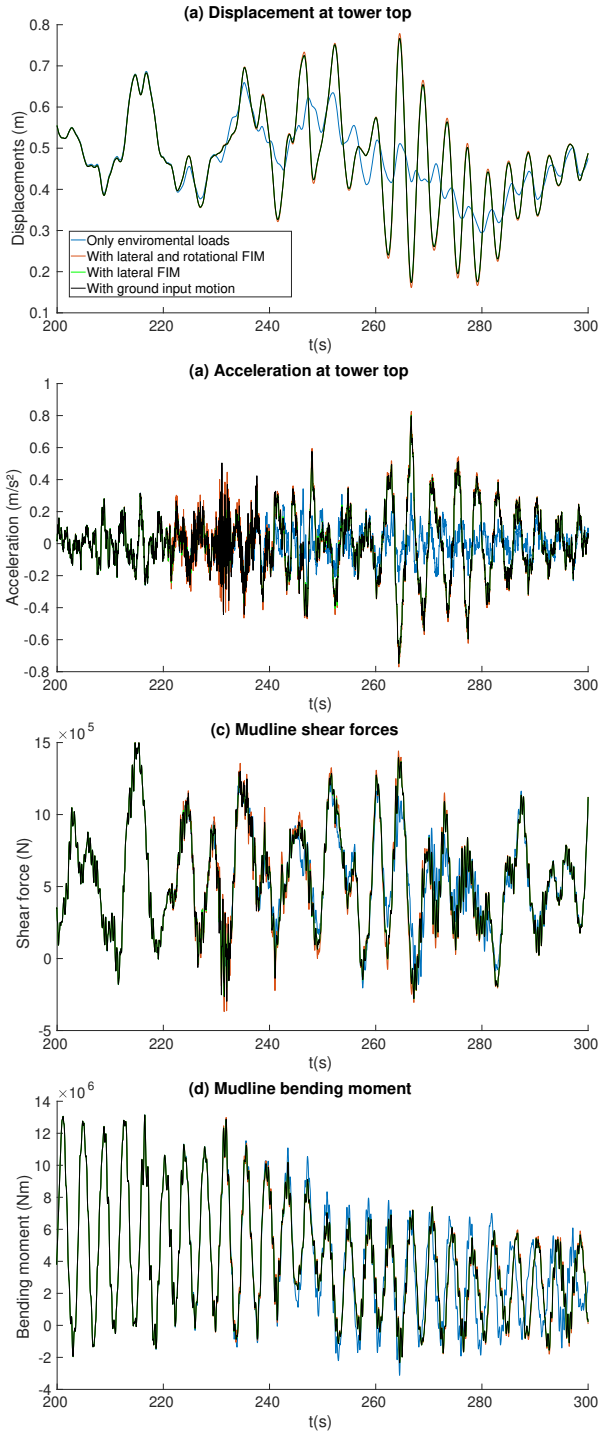

Figure 7. Results corresponding to ilustration example

AKNOWLEDGEMENTS

This research was funded by Consejería de Economía, Conocimiento y Empleo (Agencia Canaria de la Investigación, Innovación y Sociedad de la Información) of the Gobierno de Canarias and FEDER through research project ProID2020010025.

REFERENCES

[1] EWEA, Offshore Wind in Europe - Key trends and statistics 2020, *Wind Europe*, (2021).

[2] OpenFAST Documentation, Release v3.1.0, National Renewable Energy Laboratory, (2022). https://openfast.readthedocs.io/en/main/. Code published at https://github.com/OpenFAST/openfast.

[3] Damiani R., Jonkman J., Hayman G., *SubDyn user's guide and theory manual*, techreport NREL/TP-5000-63062, National Renewable Energy Laboratory, (2015).

[4] Chopra A.K., *Dynamics of Structures.Theory and applications to earthquake engineering*. Pearson, 7th ed. edition, (2017).

[5] Carbonari S., Morici M., Dezi F., Leoni G., *A lumped parameter model for time-domain inertial soil-structure interaction analysis of structures on pile foundations* , Earthquake Engineering & Structural Dynamics, Vol. 47, 2147-2171.(2018)

[6] González F., Padrón L. A., Carbonari S., Morici M., Aznárez J. J., Dezi F., Leoni G., *Seismic response of bridge piers on pile groups for different soil damping models and lumped parameter representations of the foundation.* Earthquake Engineering & Structural Dynamics, Vol. 48, 306–327 (2019).

[7] Jonkman J., Musial W., *Offshore Code Comparison Collaboration (OC3) for IEA Task 23 Offshore Wind Technology and Deployment*, techreport NREL/TP-5000-48191, National Renewable Energy Laboratory, (2010).

[8] Bordón J. D. R., Aznárez J. J., Maeso O., *Dynamic model of open shell structures buried in poroelastic soils*, Computational Mechanics, Vol. 60, 269–288 (2017).

A.2 Second conference paper: Romero-Sánchez and Padrón, COMPDYN 2023, An implementation of multi-support seismic input motion into OpenFast for the earthquake analysis of offshore wind turbines.

Table A.2. Second conference paper data.

Title	An implementation of multi-support seismic input motion into OpenFast for the earthquake analysis of offshore wind turbines
Authors	C. Romero-Sánchez and L.A. Padrón
Conference	9th International Conference on Computational Methods in Structural Dynamics and Earthquake Engineering (COMPDYN 2023)
Journal	COMPDYN Proceedings
DOI	10.7712/120123.10396.20431
ISSN	2623-3347
Publisher	ECCOMAS Proceedia
Date	June 2023

Available online at www.eccomasproceedia.org
Eccomas Proceedia COMPDYN (2023) 172-185

ECCOMAS Proceedia

COMPDYN 2023
9th ECCOMAS Thematic Conference on
Computational Methods in Structural Dynamics and Earthquake Engineering
M. Papadrakakis, M. Fragiadakis (eds.)
Athens, Greece, 12-14 June 2023

AN IMPLEMENTATION OF MULTI-SUPPORT SEISMIC INPUT MOTION INTO OPENFAST FOR THE EARTHQUAKE ANALYSIS OF OFFSHORE WIND TURBINES.

Carlos Romero-Sánchez[1] **and Luis A. Padrón**[1]

[1]Instituto Universitario en Sistemas Inteligentes y Aplicaciones Numéricas en Ingeniería
Universidad de Las Palmas de Gran Canaria
Las Palmas de Gran Canaria 35017, Spain
e-mail: {carlos.romero,luis.padron}@ulpgc.es

Abstract. *Nowadays offshore wind energy plays a key role in the development of renewable energies in Europe. Most of offshore wind turbines installed are fixed to the seabed, with monopiles being the most commonly used substructures in this field. However, the use of multi-support substructures, such as jackets and tripods has increased considerably in recent years due to the greater depth of new wind farms locations. Dynamic behaviour and seismic risk are two factors of special importance in the design of these structures. Due to this problem, there is a need to study the seismic response of offshore wind turbines on this type of substructure. In this area, one of the most widely-used open-source advanced tool available in the literature is OpenFAST, which is a multi-physics and multi-fidelity software for the simulation of the coupled dynamic response of wind turbines in the time domain. This paper presents a formulation for the implementation of multi-support seismic input motion into OpenFAST, specifically into the SubDyn module. On the other hand, validation results for a reference offshore wind turbines on a jacket substructure are shown, conducting a number of cases with different seismic signals (translational and rotational motion) to demonstrate the correct implementation. The new modified code allows to analyse the accelerations and internal forces of offshore wind turbines on multisupport substructures, taking into account seismic input motion (including input rotation at each individual support) and soil-structure interaction.*

Keywords: OpenFAST, Offshore wind turbine, Jacket, Seismic response, Soil-structure interaction

ISSN:2623-3347 © 2023 The Authors. Published by Eccomas Proceedia.
Peer-review under responsibility of the organizing committee of COMPDYN 2023.
doi: 10.7712/120123.10396.20431

1 INTRODUCTION

In recent years, offshore wind energy plays a key role in the development of renewable energies in Europe. Most of the offshore wind turbines are currently installed in locations where the depth of the sea allows them to be founded directly to the seabed, with monopiles being the most common substructures used in this field. However, the use of multi-support substructures, such as jackets and tripods, has increased considerably due to the greater depth of new wind farms locations.

Two factors of special importance in the design of these structures are the dynamic behaviour and the seismic risk. Nowadays, the growth in the number of wind farm installations is due to the need of placing new offshore wind turbines in locations with worse geotechnical properties and increased seismic risk. That is why for the correct design of offshore wind turbine substructures is essential to take into account the seismic response of offshore wind turbines, regardless of their structural typology.

One of the most widely-used open-source advanced tools available in the literature is OpenFAST [1], which is a multi-physics and multi-fidelity software for the simulation of the coupled dynamic response of wind turbines in the time domain. OpenFAST is programmed in Fortran 95, and it might be considered not as a single program, but as a framework that couples computational modules. Aerodynamic loads on blades and tower are computed in AeroDyn, while HydroDyn determines the hydrodynamics loads (waves, currents...) for offshore structures. In addition, the ServoDyn module is used for the simulation of control and electrical subsystems of the wind turbine. ElastoDyn is the module where the structural dynamic responses of rotor, nacelle and tower is calculated and SubDyn is applied for modelling the dynamic response of the substructure, from the Transition Piece (TP) at the base of the tower to the base. This framework allows coupled nonlinear aero-hydro-servo-elastic simulation in the time domain. OpenFAST documentation can be found in [1].

Romero-Sánchez and Padrón [2] developed a formulation for the implementation of uniform ground input base motion and soil-structure interaction into SubDyn [3]. This paper presents an implementation of multi-support seismic input motions and dynamic soil-structure interaction into OpenFAST. The implemented multi-support seismic input motion includes translational, vertical and rotational foundation input motions at each support, while soil-structure interaction is introduced through a simplified lumped parameter model that is previously fitted to represent the dynamic response of the foundation. In this case, the use of lumped parameter models is considered as a tool to introduce dynamic soil-structure interaction into the model because, contrary to a static stiffness matrix, this approach allows to take into account the static stiffness of the foundation and an approximation to its impedance (the dynamic stiffness and damping functions). These capabilities have been implemented in OpenFAST, version 3.0.0, and the code can be downloaded at: https://github.com/mmc-siani-es/openfast_3.0.0_multisupport.

In addition, verification results are shown for a reference offshore wind turbine on a jacket substructure, conducting a number of cases with different seismic signals (translational and rotational motion). The new modified code allows to analyse the accelerations and internal forces of offshore wind turbines on multisupport substructures, taking into account seismic input motion (including input rotation at each individual support) and soil-structure interaction.

2 IMPLEMENTATION OF MULTI-SUPPORT SEISMIC INPUT MOTION AND SOIL-STRUCTURE INTERACTION MODEL INTO SUBDYN MODULE

2.1 General overview of SubDyn module

The module integrates its equations through its own solver. SubDyn [3] can be defined in three different main steps. Discretization of the substructuring following the strategies of classical linear beam Finite Elements motion equations. The existance of a substructure introduces a number of new degrees of freedom that can be very large for complex substructures (such as jackets), but more importantly, the model of a substructure with high natural frequencies leads to the necessity of smaller time steps in the general time integration framework. For this reason, the module implements Craig-Bampton modal reduction. Finally, the equations are rearranged into State-Space type formulation for time-domain resolution and coupling with the rest of modules, specifically with the HydroDyn and ElastoDyn modules.

2.2 Generic equation of motion

Uniform base input motion is commonly adopted for the analysis of multi-degree of freedom systems subjected to earthquake excitations (see for instance Chopra [4]). This assumption leads to very easy-to-handle equations where an influence vector (Λ) is used, representing the motions of the different degrees of freedom as a consequence of the static aplication of a unit rigid support displacement or rotation. That was the strategy implemented in [2] for the study of monopile substructures. However, in the case of multi-support structures subjected to differential seismic excitations for each support, a more generic approach is needed. For this reason, in this section the formulation of the equations of motion to allow different prescribed motions at each support is generalised following the approach presented, for instance, in Clough and Penzien [5].

The original equation in the SubDyn module assumes a fixed base. The equation of motion describing the dynamic response of the substructure in partitioned matrix form can be written as:

$$\begin{bmatrix} \mathbf{M} & \mathbf{M}_g \end{bmatrix} \begin{pmatrix} \ddot{u}(t) \\ \ddot{u}_g(t) \end{pmatrix} + \begin{bmatrix} \mathbf{C} & \mathbf{C}_g \end{bmatrix} \begin{pmatrix} \dot{u}(t) \\ \dot{u}_g(t) \end{pmatrix} + \begin{bmatrix} \mathbf{K} & \mathbf{K}_g \end{bmatrix} \begin{pmatrix} u(t) \\ u_g(t) \end{pmatrix} = F(t) \quad (1)$$

where the motion vectors have been partitioned to separate the response quantities from the input. The motions vectors contains two parts: $u(t)$ includes the degrees of freedom of the structure and $u_g(t)$ contains the components of the foundation input motions at each support. The dots represent differentiation with respect to time. The global mass, damping and stiffness matrices have been partitioned to correspond. The coupling matrices that express forces in the response of degrees of freedom due to motions of the supports are denoted with the subindex g. $F(t)$ represents the external forces acting at each degree of freedom of the structure. An expression for the effective seismic loading is obtained by separating the support motion effects from the response quantities and transferring these input terms to right hand side [5]:

$$\mathbf{M}\ddot{u}(t) + \mathbf{C}\dot{u}(t) + \mathbf{K}u(t) = F(t) - \mathbf{M}_g\ddot{u}_g(t) - \mathbf{C}_g\dot{u}_g(t) - \mathbf{K}_g u_g(t) \quad (2)$$

The beam elements in the substructure are modelled as Euler-Bernoulli or Timoshenko three-dimensional beams, and discretized using two-nodes 12-dofs finite elements defined by the stiffnes and mass matrices. The damping matrix, on the contrary, is not assembled from the element contribution. This matrix can be specified in three different ways: no damping, Rayleigh

damping or user defined matrix. After the assembly in SubDyn, as described in equation (1), the system of equation can be written as:

$$\begin{bmatrix} M_{RR} & M_{RL} \\ M_{LR} & M_{LL} \end{bmatrix} \begin{pmatrix} \ddot{u}_R \\ \ddot{u}_L \end{pmatrix} + \begin{bmatrix} C_{RR} & C_{RL} \\ C_{LR} & C_{LL} \end{bmatrix} \begin{pmatrix} \dot{u}_R \\ \dot{u}_L \end{pmatrix} + \begin{bmatrix} K_{RR} & K_{RL} \\ K_{LR} & K_{LL} \end{bmatrix} \begin{pmatrix} u_R \\ u_L \end{pmatrix} = \begin{pmatrix} F_R \\ F_L \end{pmatrix} \tag{3}$$

where the subindex R identifies the boundary nodes (at the base and at the Transition Piece) and L identifies the rest of nodes (interior nodes). The applied forces include external forces, the hydrodynamic forces over the boundary nodes and the forces transfered to and from ElastoDyn through the Transition Piece. The Craig-Bampton transformation is therefore represented by:

$$\begin{Bmatrix} U_R \\ U_L \end{Bmatrix} = \begin{bmatrix} I & 0 \\ \Phi_R & \Phi_m \end{bmatrix} \begin{Bmatrix} U_R \\ q_m \end{Bmatrix} \tag{4}$$

Pre-multiplying by the Craig-Bampton transformation (eq. (4)), both sides of eq. (3), the interior degrees of freedom are hence transformed from physical DOFs to modal DOFs.

$$\begin{aligned} &\begin{bmatrix} M_{BB} & M_{Bm} \\ M_{mB} & I \end{bmatrix} \begin{pmatrix} \ddot{u}_R \\ \ddot{q}_m \end{pmatrix} + \begin{bmatrix} C_{BB} & C_{Bm} \\ C_{mB} & C_{mm} \end{bmatrix} \begin{pmatrix} \dot{u}_R \\ \dot{q}_m \end{pmatrix} \\ &\qquad + \begin{bmatrix} K_{BB} & 0 \\ 0 & K_{mm} \end{bmatrix} \begin{pmatrix} u_R \\ q_m \end{pmatrix} = \begin{pmatrix} F_B \\ F_m \end{pmatrix} \end{aligned} \tag{5}$$

where:

$$M_{BB} = M_{RR} + M_{RL}\Phi_R + \Phi_R^T M_{LR} + \Phi_R^T M_{LL}\Phi_R \tag{6}$$
$$C_{BB} = C_{RR} + C_{RL}\Phi_R + \Phi_R^T C_{LR} + \Phi_R^T C_{LL}\Phi_R \tag{7}$$
$$K_{BB} = K_{RR} + K_{RL}\Phi_R \tag{8}$$
$$M_{mB} = \Phi_m^T M_{LR} + \Phi_m^T M_{LL}\Phi_R \tag{9}$$
$$C_{mB} = \Phi_m^T C_{LR} + \Phi_m^T C_{LL}\Phi_R \tag{10}$$
$$M_{Bm} = M_{mB}^T, C_{Bm} = C_{mB}^T \tag{11}$$
$$F_B = F_R + \Phi_R^T F_L \tag{12}$$
$$F_M = \Phi_M^T F_L \tag{13}$$

Once the general equation of motion after Craig-Bampton reduction is obtained, the matrices are partitioned as described in equation 2. The vector of displacements at the boundary nodes contains the displacements at the interface node with the tower (u_I) and the displacements at base nodes, which would move following the ground motion vector (u_g):

$$U_R = \begin{pmatrix} u_g \\ u_I \end{pmatrix} \tag{14}$$

Accordingly, the mass matrices after Craig-Bampton modal reduction can be decomposed as:

$$M_{BB} = \begin{bmatrix} M_{bb} & M_{bI} \\ M_{Ib} & \bar{M}_{BB} \end{bmatrix} \quad ; \quad M_{Bm} = \begin{bmatrix} M_{bm} \\ \bar{M}_{Bm} \end{bmatrix} \quad ; \quad M_{mB} = \begin{bmatrix} M_{mb} \\ \bar{M}_{mB} \end{bmatrix} \tag{15}$$

On the one hand, subindex *b* and subindex *I* represent base and interface nodes, respectively. On the other hand, the overhead bar here and below denotes matrices/vectors after the fixed-bottom boundary condition are applied. The same process is applied to the damping (C) and the stiffness (K) matrices. Finally, the new motion equation can be writting as:

$$\begin{bmatrix} \tilde{M}_{BB} & \tilde{M}_{Bm} \\ \tilde{M}_{mB} & I \end{bmatrix} \begin{pmatrix} \ddot{u}_I \\ \ddot{q}_m \end{pmatrix}^t + \begin{bmatrix} \tilde{C}_{BB} & \tilde{C}_{Bm} \\ \tilde{C}_{mB} & C_{mm} \end{bmatrix} \begin{pmatrix} \dot{u}_I \\ \dot{q}_m \end{pmatrix}^t + \begin{bmatrix} \tilde{K}_{BB} & 0 \\ 0 & K_{mm} \end{bmatrix} \begin{pmatrix} u_I \\ q_m \end{pmatrix}^t = \begin{pmatrix} (F_I + F_{Ig}) + \Phi_R^T(F_L + F_{Lg}) \\ \Phi_m^T(F_L + F_{Lg}) \end{pmatrix} - \begin{bmatrix} M_{Ib} \\ M_{mb} \end{bmatrix} \ddot{u}_g - \begin{bmatrix} C_{Ib} \\ C_{mb} \end{bmatrix} \dot{u}_g - \begin{bmatrix} K_{Ib} \\ K_{mb} \end{bmatrix} u_g \quad (16)$$

The interface nodes and the Transition Piece (that is assumed as a rigid body) are considered as rigidly connected.

$$u_I = T_I u_{tp} \quad (17)$$

$$F_{tp} = T_I^T F_I \quad (18)$$

Where T_I is a simple transformation matrix depending on the differences between the locations between both points. Including these two relation into eq. (16), one can write

$$\begin{bmatrix} \tilde{M}_{BB} & \tilde{M}_{Bm} \\ \tilde{M}_{mB} & I \end{bmatrix} \begin{pmatrix} \ddot{u}_I \\ \ddot{q}_m \end{pmatrix}^t + \begin{bmatrix} \tilde{C}_{BB} & \tilde{C}_{Bm} \\ \tilde{C}_{mB} & C_{mm} \end{bmatrix} \begin{pmatrix} \dot{u}_I \\ \dot{q}_m \end{pmatrix}^t + \begin{bmatrix} \tilde{K}_{BB} & 0 \\ 0 & K_{mm} \end{bmatrix} \begin{pmatrix} u_I \\ q_m \end{pmatrix}^t = \begin{pmatrix} \tilde{F}_{tp} \\ \tilde{F}_m \end{pmatrix} - \begin{bmatrix} F_{IsisM} \\ F_{MsisM} \end{bmatrix} \ddot{u}_g(t) - \begin{bmatrix} F_{IsisC} \\ F_{MsisC} \end{bmatrix} \dot{u}_g(t) - \begin{bmatrix} F_{IsisK} \\ F_{MsisK} \end{bmatrix} u_g(t) \quad (19)$$

These terms can be defined as:

$$\tilde{M}_{BB} = T_I^T \bar{M}_{BB} T_I \quad (20)$$

$$\tilde{C}_{BB} = T_I^T \bar{C}_{BB} T_I \quad (21)$$

$$\tilde{K}_{BB} = T_I^T \bar{K}_{BB} T_I \quad (22)$$

$$\tilde{M}_{Bm} = T_I^T \bar{M}_{BM} \quad (23)$$

$$\tilde{C}_{Bm} = T_I^T \bar{C}_{BM} \quad (24)$$

$$C_{mm} = \Phi_m^T C_{LL} \Phi_m \quad (25)$$

$$K_{mm} = \Omega_m^2 \quad (26)$$

$$\tilde{F}_{tp} = F_{tp} + T_I^T \bar{F}_{R,e} + T_I^T \bar{F}_{R,g} + T_I^T \bar{\Phi}_R^T (F_{L,e} + F_{L,g}) \quad (27)$$

$$\tilde{F}_m = \Phi_m^T (F_{L,e} + F_{L,g}) \quad (28)$$

$$F_{IsisK} = T_I^T (\bar{K}_{Ib}) \quad (29)$$

$$F_{MsisK} = K_{mb} \quad (30)$$

$$F_{IsisC} = T_I^T (C_{Ib}) \quad (31)$$

$$F_{MsisC} = C_{mb} \quad (32)$$

$$F_{IsisM} = T_I^T (M_{Ib}) \quad (33)$$

$$F_{MsisM} = M_{mb} \quad (34)$$

where $F_R = F_{R,e} + F_{R,g}$, with $F_{R,e}$ being the external loads from other modules, the hydrodynamic forces over the boundary nodes and the forces transfered to and from ElastoDyn through the Transition Piece; and $F_{R,g}$ consists of the SubDyn gravitational loads.

For the cases studied in this paper, the same input signal has been implemented on all supports due to the proximity of the foundations and to the nature of the vertically-incident plane waves assumed in this study. No different Kinematic Input Factors (KIFs) are expected on each pile if the seismic incidence is vertical. In any case, each pile head rotates independently, as the base is not considered as rigid body. Figure 1 shows the same input motion in each support.

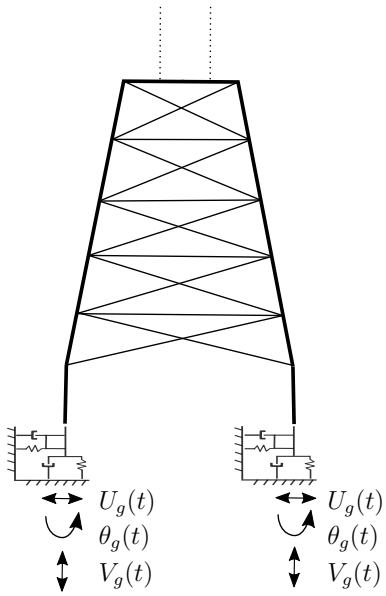

Figure 1: Ground input motion at different supports.

2.3 Simplified Lumped Parameter Model into SubDyn

The introduction of an LPM can be simply understood as adding one (or several) additional elements at the base of the substructure. At this point, the simplified Lumped Parameter Model proposed by Carbonari et al. [6], is adopted for the lateral vibrations, while the spring-damper model is adopted for vertical and torsional vibrations. More information related to the introduction of this model into SubDyn can be found at [2]. SLPM coefficients are calculated using least squares to be optimally adapted to the impedance functions defining the dynamic response of the wind turbine foundation.

2.4 State-space formulation

Variables are arranged in sets of inputs and outputs that can communicate with the rest of modules (HydroDyn and ElastoDyn). The equations are written in state-space form. The states are defined as:

$$x = \begin{pmatrix} q_m & \dot{q}_m \end{pmatrix}^T \tag{35}$$

The input vector are defined as:

$$u = \begin{pmatrix} U_{tp} & \dot{U}_{tp} & \ddot{U}_{tp} & F_{L,e} & F_{R,e} \end{pmatrix}^T \tag{36}$$

2.4.1 State equation

Equation (19) is cast into standard linear system state equation of the form:

$$\dot{x} = X = \mathbf{A}x + \mathbf{B}u + F_x \tag{37}$$

To do, the second row of equation (19) needs to be written down and solved for $\ddot{U}_L$. After doing so, the matrices of the state equation can be found to be:

$$\mathbf{A} = \begin{bmatrix} 0 & I \\ -\tilde{K}_{mm} & -C_{mm_f} - \tilde{C}_{mm} \end{bmatrix} \tag{38}$$

$$\mathbf{B} = \begin{bmatrix} 0 & 0 & 0 & 0 & 0 \\ 0 & -\tilde{C}_{mB_f} & -\tilde{M}_{mB} & \Phi_m^T & 0 \end{bmatrix} \tag{39}$$

$$Fx = \begin{bmatrix} 0 \\ \Phi_m^T F_{L,g} + F_{MsisK} u_g + F_{MsisC} \dot{u}_g - F_{MsisM} \ddot{u}_g \end{bmatrix} \tag{40}$$

where the damping matrix is composed of the structural damping (C) and damping terms related to the LPM foundation model (C_f).

2.4.2 Output equation to ElastoDyn

The first output equation computes the interaction forces between tower and substructure at the Transition Piece.

$$y_1 = Y_1 = -F_{tp} \tag{41}$$

Writting the first row of (19) and solving for F_{tp}, the output equation can be written as:

$$-Y_1 = \mathbf{C}_1 x + \mathbf{D}_1 \bar{u} + F_{y_1} \tag{42}$$

where

$$\mathbf{C}_1 = \begin{bmatrix} -\tilde{M}_{Bm}\Omega_m^2 & -\tilde{M}_{Bm}(C_{mm_f} + \tilde{C}_{mm}) + \tilde{C}_B m \end{bmatrix} \tag{43}$$

$$\mathbf{D}_1 = \begin{bmatrix} \tilde{K}_{BB} & -\tilde{C}_{mB_f}\tilde{M}_{Bm} + \tilde{C}_{BB_f} & -\tilde{M}_{mB}\tilde{M}_{Bm} + \tilde{M}_{BB} & \tilde{M}_{Bm}\Phi_m^T - T_I^T \Phi_R^T & -T_I^T \end{bmatrix} \tag{44}$$

$$F_{y_1} = -T_I^T(\bar{F}_{Ig} + \bar{\Phi}_R^T F_{Lg}) - F_{IsisK} u_b - F_{IsisC}\dot{u}_b + F_{IsisM}\ddot{u}_b + \tilde{M}_{Bm}\left[F_{MsisK} u_b + F_{MsisC}\dot{u}_b - F_{MsisM}\ddot{u}_b + \Phi_m^T F_{Lg}\right] \tag{45}$$

2.4.3 Output equation to HydroDyn

The second output equation collects all the motions needed by the HydroDyn module to compute hydrodynamic loads.

$$y_2 = Y_2 = \{ \; U_I \quad U_L \quad \dot{U}_I \quad \dot{U}_L \quad \ddot{U}_I \quad \ddot{U}_L \; \}^T \tag{46}$$

$$Y_2 = \mathbf{C}_2 x + \mathbf{D}_2 u + F_{y_2} \tag{47}$$

where

$$\mathbf{C}_2 = \begin{bmatrix} 0 & 0 \\ \Phi_m & 0 \\ 0 & 0 \\ 0 & \Phi_m \\ 0 & 0 \\ -\Phi_m \tilde{K}_{mm} & -\Phi_m (C_{mm_f} + \tilde{C}_{mm}) \end{bmatrix} \tag{48}$$

$$\mathbf{D}_2 = \begin{bmatrix} T_I & 0 & 0 & 0 & 0 \\ \bar{\Phi}_R T_I & 0 & 0 & 0 & 0 \\ 0 & T_I & 0 & 0 & 0 \\ 0 & \bar{\Phi}_R T_I & 0 & 0 & 0 \\ 0 & 0 & T_I & 0 & 0 \\ 0 & -\Phi_m \tilde{C}_{mB_f} & \tilde{\Phi}_R T_I - \Phi_m \tilde{M}_{mB} & \Phi_m \Phi_m^T & 0 \end{bmatrix} \tag{49}$$

$$F_{y_2} = \begin{bmatrix} 0 \\ 0 \\ 0 \\ 0 \\ 0 \\ \Phi_m \Phi_m^T F_{Lg} + \Phi_m (F_{MsisK} u_b + F_{MsisC} \dot{u}_b - F_{MsisM} \ddot{u}_b) \end{bmatrix} \tag{50}$$

3 VERIFICATION RESULTS

The implementation into OpenFAST of the multi-support input ground motion and the Simplified Lumped Parameter Model at the base of the substructure has been initially verified by comparison against results obtained from a simplified model written in matlab for this purpose. To begin with, the verification model is first described. Subsequently, the cases designed for verification are presented. Lastly, the results obtained from the comparison are evaluated.

3.1 Reference simple model for comparison

The model used for the comparison is a 3D Finite Element Model (FEM) with Timoshenko beam elements, consisting of two different structures: the inferior part corresponding to the jacket and the upper part corresponding to the tower, with varying properties along height. On top, the rotor-nacelle-assembly (RNA) is modeled as a punctual rigid concentrated inertia.

Again, the equation of motion can be written as:

$$\mathbf{M}\,\ddot{u}(t) + \mathbf{C}\,\dot{u}(t) + \mathbf{K}\,u(t) = -\mathbf{M_b}\ddot{u}_b(t) - \mathbf{C_b}\dot{u}_b(t) - \mathbf{K_b}u_b(t) \tag{51}$$

where the global mass, damping and stiffness matrices is partitioned into two terms. $\mathbf{M_b}$, $\mathbf{C_b}$ and $\mathbf{K_b}$ are the coupling matrices that express forces in the response degrees of freedom due to

motions of the supports and $\mathbf{M}$, $\mathbf{C}$ and $\mathbf{K}$ are the remaining terms of global matrices. The input ground displacement at time t is denoted by $u_b(t)$, and transfering the inputs terms to the right hand. The beam elements implemented are identical to those already implemented in SubDyn

Assuming steady–state harmonic response:

$$u(t) = U(\omega)\mathrm{e}^{\mathrm{i}\omega t} \tag{52}$$

where ω is the circular frecuency of the excitation. The time-harmonic equation of motion employed can be written as:

$$\left(\mathbf{K} + \mathrm{i}\omega\mathbf{C} - \omega^2\mathbf{M}\right) U(\omega) = \left(-\mathbf{K_b} - \mathrm{i}\omega\mathbf{C_b} + \omega^2\mathbf{M_b}\right) U_b(\omega) \tag{53}$$

This reference simplified model was implemented in an independent matlab© code. As usual, time domain response will be therefore obtained through Frecuency Domain Analysis [4] making use of the Fast Fourier Transform.

3.2 Reference configuration and verification cases

The reference configuration adopted for this study is the widely used 5MW NREL (National Renewable Energy Laboratory) reference turbine. More precisely, the base configuration is the one defined for the OC4 (Offshore Code Comparison Collaboration) for the offshore 5MW NREL reference turbine on a jacket. Specific data can be found in Popko et al. [7].

Table 1 lists the main characteristics of the foundation input motions (FIM) used for the three simplified verification cases presented. The model allows the soil-structure interaction (SSI) to be considered. ξ_t denotes the structural tower damping ratio and Rayleigh damping is used at jacket substructure ($\alpha = \beta = 2\%$). Additionally, Table 2 presents the parameters obtained for the SLPM from fitting the impedance functions corresponding to the foundation of this turbine [8]. The units of the SLPM parameters are those of the International System, as desribed in [6]. The impedance functions and the time-harmonic kinematic interaction factors corresponding to the pile foundation were obtained from a finite elements - boundary elements model [9]. These kinematic interaction factors allow to compute the translational and rotational foundation input motions

N	FIM	SSI	ξ_t	Input base motion
1	Lateral	×	5%	Quarter of sine ($f = 0.1$ Hz, $A = 0.1$ m)
2	Rotational	×	2%	Quarter of sine ($f = 0.1$ Hz, $A = 0.05$ rad)
3	Lateral & Rotational	✓	2%	Chi-Chi earthquake

Table 1: Verification cases.

3.3 Verification results

This section provides the validation results of the different cases described in Table 1. Figure 2 presents the comparisons between the results obtained using the modified version of OpenFAST and those of the reference simplified model (matlab code). Motions at the top of the tower, and at the platform are represented. It is shown that the agreement is very good in terms of displacements and rotations. It is important to keep in mind the major difference between both codes, being the OpenFAST model much more elaborated than the reference model, and being the first one solved in time domain and the second one in frequency domain.

K_{SLPM}	Value	C_{SLPM}	Value	M_{SLPM}	Value
k_h	1.295e+6	c_h	4.187e+6	m_h	1.0
k_r	8.952e+9	c_r	1.226e+7	I_r	32.79
k_t	9.071e+8	c_t	1.061e+7	m_t	1.757e+5
k_z	2.679e+9	c_z	7.081e+7	m_z	1.0
k_{tor}	7.131e+10	c_{tor}	4.414e+8	I_{tor}	8.602e+6
h_1	-2.488	h_2	-2.974	h_3	-0.592

Table 2: SLPM parameters.

Table 3 shows the fundamental frequencies as a function of the assumed base condition. As expected, the consideration of soil-structure interaction provides a longer period. This phenomenon also allows to see the relevant influence that the properties of the foundation exert on the system global response.

SSI	Fundamental frequency
×	0.316 Hz (T=3.16 s)
✓	0.301 Hz (T=3.32 s)

Table 3: Fundamental frequencies in the fore-aft direction obtained for different base conditions

4 ILUSTRATION EXAMPLE

After having verified the implementation of the kinematic input motions for a simplified model configuration, this section illustrates the use of the code for the analysis of the seismic response of the offshore wind turbine while the turbine is operating and is subjected to enviromental conditions. The NREL 5 MW reference OWT [7] described above is considered in the ilustration example. The simplified Lumped Parameter Model is used to represent the flexibility of the soil-foundation system (see Figure 3). The system is assumed to be subjected to vertically-incident shear waves. The Imperial Valley earthquake (PEER Ground Motion Database [10], RSN: 192) is considered as free-field ground-surface seismic action. The simulation is allowed to run for 200 seconds before the earthquake shaking arrive, in order to allow the dissipation of the transient response generated at the beginning of the simulation. The wind turbine remains in power production mode when the earthquake occurs. The time-harmonic kinematic interaction factors corresponding to the pile foundation were computed through the same boundary element model employed to compute the impedance functions [9]. These kinematic interaction factors allow to compute the translational and rotational foundation input motions (see Figure 4) that are then defined at the base of the SLPM.

Figure 5 presents the computed seismic response in terms of tower top accelerations and axial forces and bending moments in the jacket, specifically at the jacket node where the highest values of axial forces and bending moments occur. Each plot presents the response of the OWT computed under three different loading situations: a) only environmental loads (wind, waves and currents); b) taking into account both translational and rotational foundation input motions; and c) considering the original seismic input motion as translational input motion.

The seismic action increases the response of the structure in terms of accelerations at the tower top, by a factor of 4. In particular, considering the maximum internal forces without earthquake loads, in operational mode, the values increase by a factor of 2-3 in axial forces and 4-5 in bending moments, in the studied nodes.

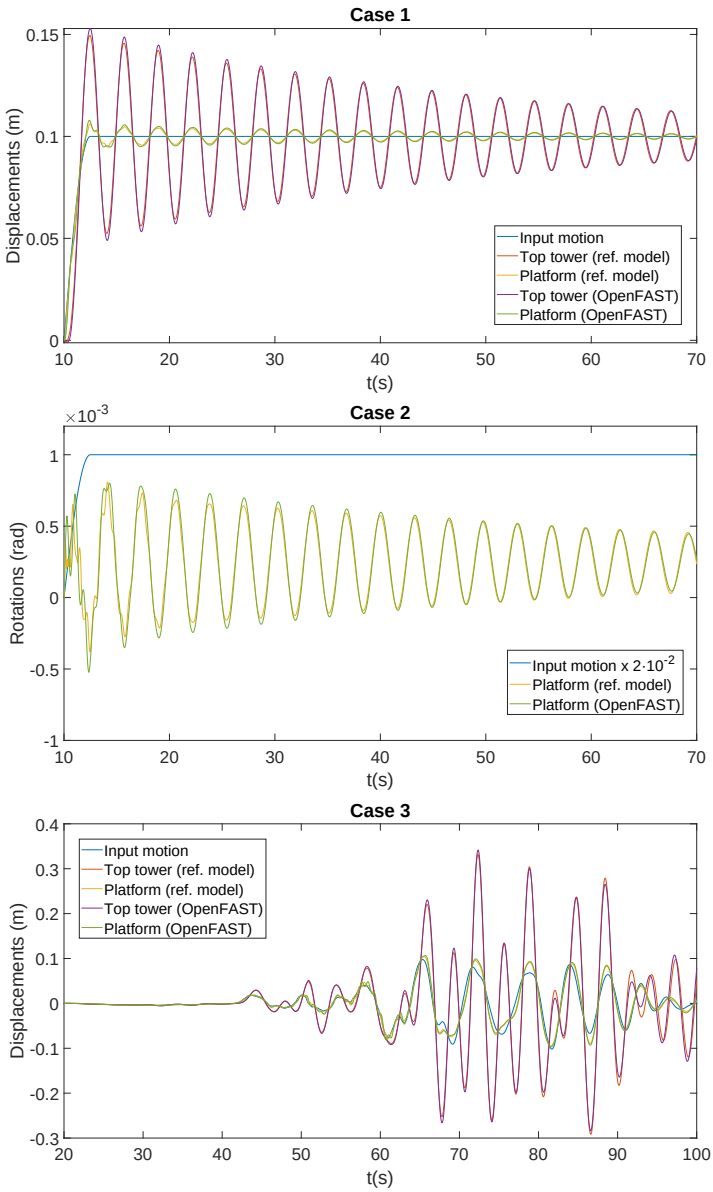

Figure 2: Results corresponding to verification cases.

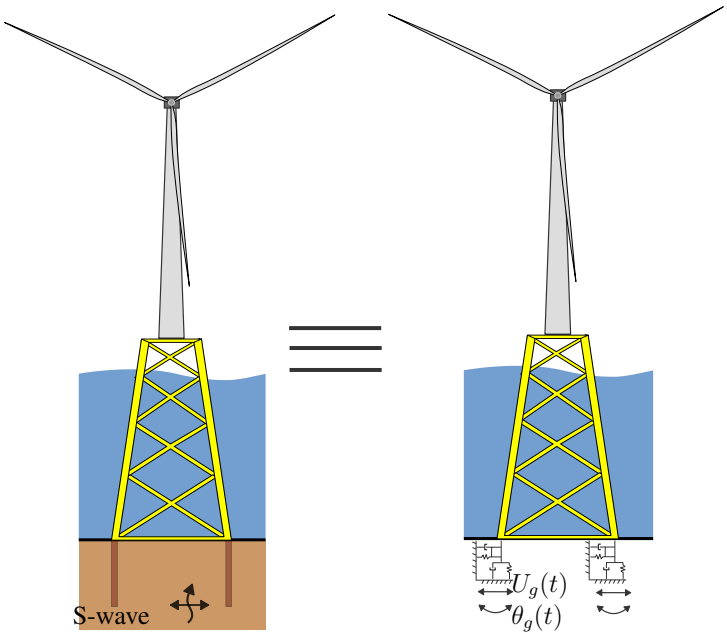

Figure 3: Ilustration Example Jacket.

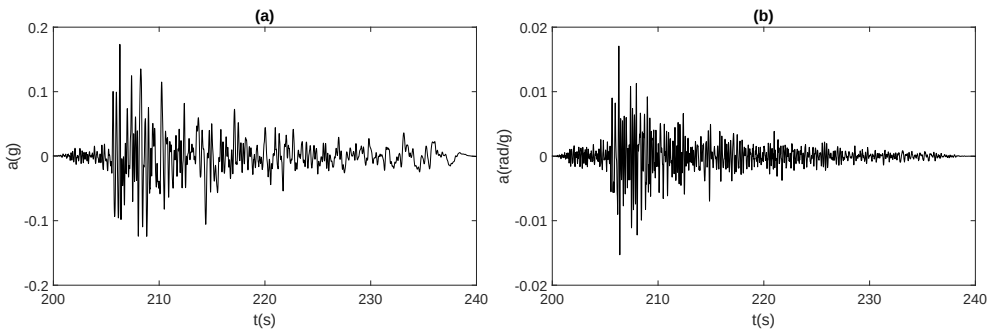

Figure 4: Lateral FIM (a) and Rotational FIM (b). Imperial Valley earthquake.

Finally, in this specific ilustration example, the difference between considering the original earthquake signal or the filtered earthquake signal is negligible in axial forces, and it is not very relevant in terms of accelerations and bending moments.

5 CONCLUSIONS

The paper develops the formulation needed for an implementation of multi-support seismic input motions into the open-source software OpenFAST, with the aim of facilitating the use of

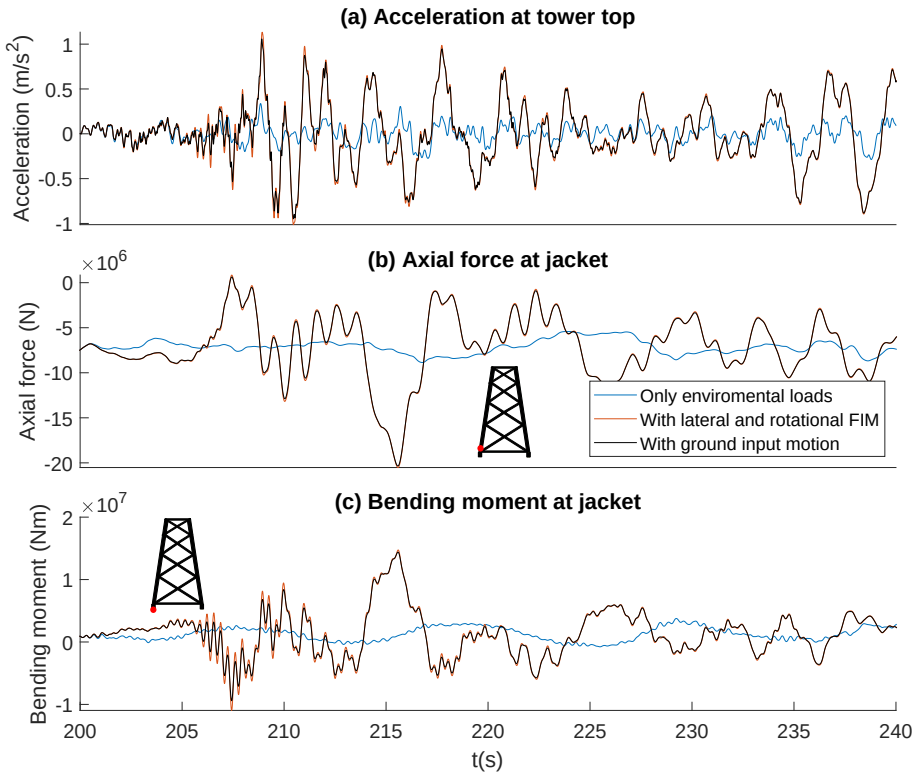

Figure 5: Results corresponding to ilustration example.

this tool for the seismic analysis of wind turbines. This code allows not only horizontal, but also vertical and rotational foundation input motions to be considered, on a single-support substructure (monopile) and with multiple supports (tripods and jackets). In the ilustration example, a wind turbine on a jacket with piles has been studied. Horizontal and rotational foundation input motions are computed taking the pile kinematic interaction factors into account.

The use of lumped parameter models is considered here as a tool to introduce soil-structure interaction into the model because this approach allows to take into account, not only the static stiffness of the foundation, but an approximation to its impedance, i.e., the dynamic stiffness and damping functions.

These capabilities have been implemented in OpenFAST, version 3.0.0, and the code can be downloaded at: https://github.com/mmc-siani-es/openfast_3.0.0_multisupport. The application of this code, which allows to stablish different input motion in each support, can be relevant for future studies where inclined seismic incidence is considered.

AKNOWLEDGEMENTS

This research was funded by Consejería de Economía, Conocimiento y Empleo (Agencia Canaria de la Investigación, Innovación y Sociedad de la Información) of the Gobierno de Canarias and FEDER through research project ProID2020010025 and by the Ministerio de

Ciencia, Innovación y Universidades and the Agencia Estatal de Investigación of Spain, and FEDER, through research project PID2020-120102RB-I00. In addition, C. Romero-Sánchez is a recipient of the research fellowship (TESIS2022010011), from the Program of predoctoral fellowships from the Consejería de Economía, Conocimiento y Empleo (Agencia Canaria de la Investigación, Innovación y Sociedad de la Información) of the Gobierno de Canarias and Fondo Social Europeo. The authors are grateful for this support.

REFERENCES

[1] OpenFAST Documentation, Release v3.4.0, National Renewable Energy Laboratory. https://openfast.readthedocs.io/en/main/. Code published at https://github.com/OpenFAST/openfast , 2023.

[2] C. Romero-Sánchez and L.A. Padrón, Implementation of Ground Input Motion and Dynamic Soil-Structure Interaction into Openfast for the Seismic Analysis of Offshore Wind Turbines, *Congress on Numerical Methods in Engineering (CMN 2022)*,337-356., Las Palmas de Gran Canaria, Spain, September 12-14, 2022.

[3] R. Damiani , J. Jonkman and G. Hayman, SubDyn user's guide and theory manual, *techreport NREL/TP-5000-63062, National Renewable Energy Laboratory*, 2015.

[4] A.K. Chopra, *Dynamics of Structures. Theory and applications to earthquake engineering, 7th edition*. Pearson, , 2017.

[5] R.W. Clough and J. Penzien, *Dynamics of Structures, 3th edition*. Computers & Structures, Inc., 1995.

[6] S. Carbonari, M. Morici M., F. Dezi and G. Leoni, A lumped parameter model for time-domain inertial soil-structure interaction analysis of structures on pile foundations , *Earthquake Engineering & Structural Dynamics*, **47**, 2147-2171, 2018.

[7] W. Popko, F. Vorpahl, A. Zuga, M. Kohlmeier, J. Jonkman, A. Robertson, T.J. Larsen, A. Yde, K. Sætertrø, Knut M. Okstad, J. Nichols, T.A. Nygaard, Z. Gao, D. Manolas, K. Kim, Q. Yu, W. Shi, H. Park, A. Vásquez-Rojas, J. Dubois, D. Kaufer, P. Thomassen, M.J. de Ruiter, J.M. Peeringa, H. Zhiwen and H. von Waaden, Offshore Code Comparison Collaboration Continuation (OC4), Phase I-Results of Coupled Simulations of an Offshore Wind Turbine with Jacket Support Structure, *Journal of Ocean and Wind Energy*, **1**, 1-11, 2014.

[8] N. Alati, G. Failla G. and F. Arena, Seismic analysis of offshore wind turbines on bottom-fixed support structures, *Philosophical Transactions, Royal Society*, A **373**, 20140086, 2015.

[9] J.D.R Bordón, J.J. Aznárez and O. Maeso, Dynamic model of open shell structures buried in poroelastic soils, *Computational Mechanics*, **60**, 269–288, 2017.

[10] Pacific Earthquake Engineering Research Center (PEER), NGA-West2 Ground Motion Database. http://ngawest2.berkeley.edu/ , 2023.

A.3 Third conference paper: Romero-Sánchez et al., EURODYN 2023, Comparative study of the influence of kinematic interaction on the seismic response of monopile and jacket supported offshore wind turbines.

Table A.3. Third conference paper data.

Title	Comparative study of the influence of kinematic interaction on the seismic response of monopile and jacket supported offshore wind turbines
Authors	C. Romero-Sánchez, L.A. Padrón, G.M. Álamo, C. Medina, J.J. Aznárez and O. Maeso
Conference	XII International Conference on Structural Dynamics, (EURODYN 2023)
Journal	Journal of Physics: Conference Series
DOI	10.1088/1742-6596/2647/11/112002
ISSN	1742-6596
Date	July 2023

XII International Conference on Structural Dynamics IOP Publishing
Journal of Physics: Conference Series **2647** (2024) 112002 doi:10.1088/1742-6596/2647/11/112002

Comparative study of the influence of kinematic interaction on the seismic response of monopile and jacket supported offshore wind turbines

Carlos Romero-Sánchez, Luis A. Padrón, Guillermo M. Álamo, Cristina Medina, Juan J. Aznárez and Orlando Maeso

Instituto Universitario de Sistemas Inteligentes y Aplicaciones Numéricas en Ingeniería, Universidad de Las Palmas de Gran Canaria, Las Palmas de Gran Canaria 35017, Spain

E-mail: {carlos.romero, luis.padron, guillermo.alamo, cristina.medina, juanjose.aznarez, orlando.maeso}@ulpgc.es

Abstract. In the last few years, offshore wind energy has been increasing significantly, being the energetic potential of this technology much higher than that of other renewables energies. Most of Offshore Wind Turbines (OWTs) installed in Europe are founded to the sea floor but, due to the increase in offshore wind turbine installations and the visual impact problem, new locations are being considered with greater depths and increasing seismic risk. In this field, jackets substructures are one of the most attractive options. Despite the low natural frequencies that characterise these systems, the effect of the kinematic interaction can be highly relevant in OWTs on monopiles. For this reason, the need arises to analyse the importance of the influence of kinematic interaction on the seismic responses of multi-supported substructures, such as jackets with deep foundations. This paper presents a comparison of the kinematic interaction effects on the seismic response of two types of substructures for OWTs. OpenFAST is used to analyse the dynamic behaviour of OWTs founded either on monopiles or through jacket substructures on deep foundations, taking soil-structure interaction into account. The comparative study shows that the influence of kinematic interaction in both cases is notably different. As expected, in the case of the monopile, the rotational motion has a strong effect on the accelerations and the internal forces in the structure, although the impact of the translational filtered signal is small. However, in the jacket, the influence of the rotational motion is less pronounced.

1. Introduction

Nowadays offshore wind energy has been increasing significantly, being the energetic potential of this technology much higher than that of other renewables energies. Most of Offshore Wind Turbines (OWTs) installed in Europe are founded to the sea floor but, due to the increase in offshore wind turbine installations and the visual impact problem, new locations are being considered with greater depths and increasing seismic risk. In this field, jackets substructures are one of the most attractive options. Despite the low natural frequencies that characterise these systems, the effect of the kinematic interaction (rotational and horizontal) can be highly relevant in OWTs on monopiles, as pointed out by Kaynia [1]. For this reason, the need arises to analyse the importance of the influence of kinematic interaction on the seismic responses of multi-supported substructures, such as jackets with deep foundations.

Content from this work may be used under the terms of the Creative Commons Attribution 4.0 licence. Any further distribution of this work must maintain attribution to the author(s) and the title of the work, journal citation and DOI.
Published under licence by IOP Publishing Ltd

XII International Conference on Structural Dynamics IOP Publishing
Journal of Physics: Conference Series **2647** (2024) 112002 doi:10.1088/1742-6596/2647/11/112002

This paper presents a comparison of the kinematic interaction effects on the seismic response of two types of substructures for OWTs. OpenFAST [2] is used to analyse the dynamic behaviour of OWTs founded either on monopiles or through jacket substructures on deep foundations, taking soil-structure interaction into account.

2. Problem definition

2.1. Reference wind turbines and substructures

The reference wind turbine is the NREL 5 MW three-bladed turbine [3]. Two different substructures are considered in this study to compare the influence of kinematic interaction. The monopile described in the OC3 project [5] and the jacket used in the OC4 project [6] are selected for this study. Table 1 and Figure 1 show the main properties of each substructure.

In addition, steel material properties are considered for the substructures: Young's modulus, 210 GPa, shear modulus, 80.8 GPa, mass density, 8500 kg/m^3 in the monopile, 7850 kg/m^3 in the jacket and damping ratio, 2%. The fundamental frecuencies in the fore-aft direction for parked conditions are 0.300 Hz for the OWT on jacket substructure and 0.259 Hz for the OWT on monopile substructure.

Table 1. Key parameters of the considered substructures.

	Monopile	Jacket
Tower top (H_{top}) [m]	87.6	88.15
Tower base [m]	10	20.15
Water depth (W)[m]	20	50
Substructure height (H_{sub}) [m]	30	70.15
Pile diameter [m]	6.0	2.082
Pile thickness [mm]	60	60
Pile depth [m]	36.0	34.0

2.2. Soil profile

In this study, monopile and piles are assumed to be embedded in a three-layer sandy soil deposit, as described in [5] and in Table 2.

Table 2. Properties of the soil deposit.

	Stratified Soil
Soil profile	layered, sand
Poisson's ratio, ν_s [-]	0.35
Density, ρ_s [kg/m^3]	2000
Shear wave velocity, v_s [m/s]	145.9 ($0 < z < 5$ m)
	175.9 ($5 < z < 9$ m)
	209.0 ($9 < z < \infty$ m)
Damping, $\zeta_s[-]$	0.05

XII International Conference on Structural Dynamics IOP Publishing
Journal of Physics: Conference Series **2647** (2024) 112002 doi:10.1088/1742-6596/2647/11/112002

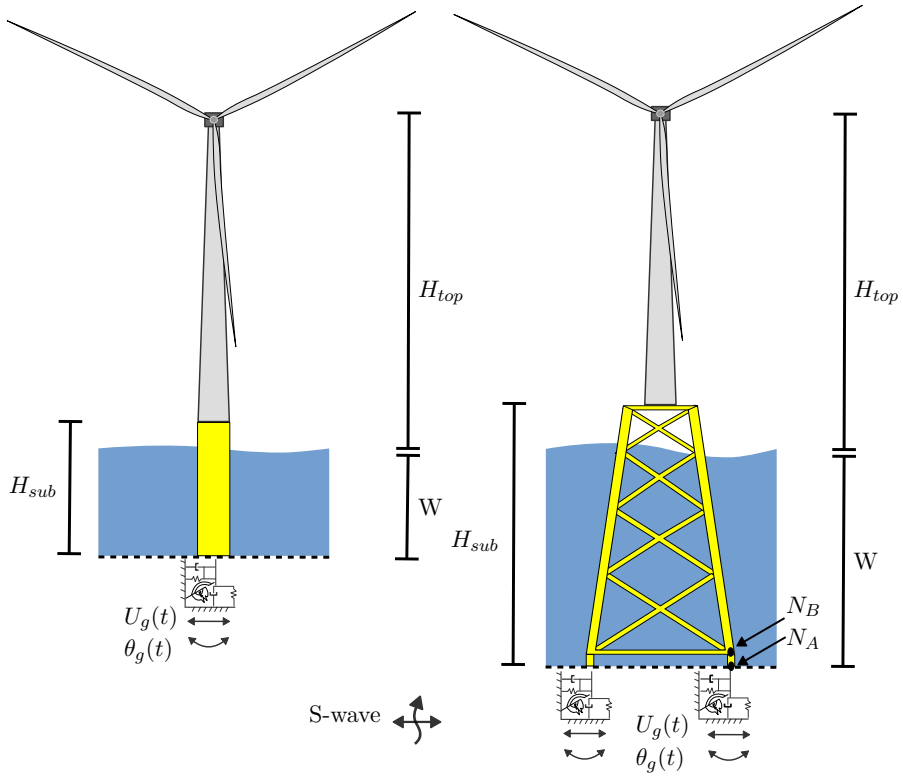

Figure 1. Offshore wind turbine on monopile and jacket support.

2.3. Seismic signals

Different accelerograms have been considered to compare the influence of kinematic interaction on the seismic response of the two proposed systems. In particular, two different acceleration signals extracted from PEER Ground Motion Database [7] are selected. The choice has been made on the basis of stations located over soils with average shear wave velocities in a range close to that of the proposed soil deposit ($V_{s,30}$ = 190-200 m/s). Table 3 shows the selected accelerograms.

Table 3. Main information about the accelerograms [7].

RSN	Dir.(^{o})	Event name	Year	Situation name	$V_{s,30}$(m/s)	a_g(g)
192	180	Imperial Valley-06	1979	Westmorland Fire Station	194	0.11
777	180	Loma Prieta	1989	Hollister City Hall	199	0.22

XII International Conference on Structural Dynamics IOP Publishing
Journal of Physics: Conference Series **2647** (2024) 112002 doi:10.1088/1742-6596/2647/11/112002

Figure 2 presents the pseudo-spectral accelerations (PSA) and the accelerograms. This study assumes that these seismic signals, defined at free-field ground surface, are generated by vertically–incident far-field S-waves that produce the seismic shaking in a particular direction. Specifically in this paper, the shaking direction is considered to be aligned with the environmental loads in the fore-aft direction.

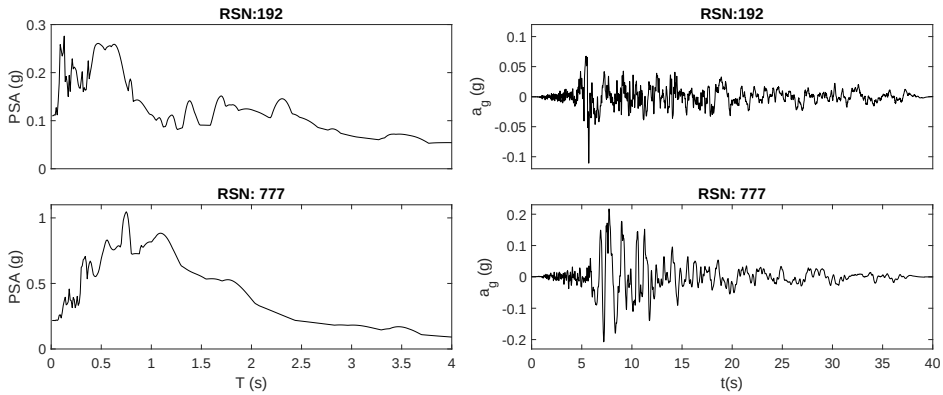

Figure 2. Pseudo-spectral accelerations (PSA) and ground acceleration (a_g) of the seismic signal used.

3. Methodology

Firstly, the numerical model is described in section 3.1. The dynamic response of the offshore wind turbines is modeled using OpenFAST [2], including the impedance of the soil-foundation subsystem and the ground input motion. Section 3.2 describes the model used to compute the impedance and the kinematics factors.

3.1. OpenFAST

The numerical tool used in this paper is based on OpenFAST [2], which is a multi-physics and multi-fidelity tool for simulating the coupled dynamic response of wind turbines, in time domain. It is open-source, programmed in Fortran 95, it is managed by National Renewable Energy Lab and it might be considered not as a single program, but as a framework that couples computational modules. The different modules interact in a loosely coupled time-integration scheme, where a glue-code transfers data among modules at each time step.

The SubDyn module [4] was modified in order to be able to take into account dynamic soil–structure interaction and ground input motion. The module integrates its equations through its own solver. The equation of motion of the substructure is written as:

$$\mathbf{M}\,\ddot{\mathbf{u}}(t) + \mathbf{C}\,\dot{\mathbf{u}}(t) + \mathbf{K}\,\mathbf{u}(t) = \mathbf{F}(t) - \mathbf{M_g}\,\ddot{\mathbf{u}}_\mathbf{g}(t) - \mathbf{C_g}\,\dot{\mathbf{u}}_\mathbf{g}(t) - \mathbf{K_g}\,\mathbf{u_g}(t) \tag{1}$$

where the motion vectors have been partitioned to separate the response quantities from the input. The motions vectors contain two parts: $u(t)$ includes the degrees of freedom of the structure and $u_g(t)$ contains the components of the foundation input motions at each support. The dots represent differentiation with respect to time. The global mass, damping and stiffness matrices have been partitioned accordingly. The expression for the effective seismic loading is

XII International Conference on Structural Dynamics IOP Publishing
Journal of Physics: Conference Series **2647** (2024) 112002 doi:10.1088/1742-6596/2647/11/112002

obtained by separating the support motion effects from the response quantities and transferring these input terms to right hand side [8]. For more information, the implementation is described in Romero-Sánchez and Padrón [9].

3.2. Computation of impedances and kinematic interaction factors

The soil-foundation system response is modelled through impedance functions and kinematic interaction factors computed with a continuum model [10] for the dynamic analysis of pile foundations. Thus, linear-elastic behavior is assumed for the whole soil-foundation-structure system. OpenFAST is a nonlinear aero-hydro-servo code for the simulation of wind turbines in the time domain. In order to be able to introduce the soil-foundation impedance functions in the OpenFAST model, Lumped Parameter Models [11] are fitted and implemented. More information related to the introduction of this model into SubDyn can be found in [12]. The resulting LPM is introduced in the finite elements model of the substructure as an additional element at mudline level. The LPM configuration allows to model and fit simultaneously the traslational, rotational and horizontal-rocking coupled impedance functions, while the spring-damper model is adopted for vertical and torsional vibrations.

The lateral I_u and rotational I_θ kinematic interaction factors quantify the filtering effect due to the presence of the pile in the soil in terms of the ratio between the pile head displacement or rotation with respect to the free-field motion. To obtain these parameters, a single pile (without superstructure) subjected to an incident S-wave is considered. Once the kinematic interaction factors are obtained, in the frequency domain, the seismic signal is filtered.

4. Results

In order to understand the influence of kinematic interaction on the seismic response of monopile and jacket supported offshore wind turbines, the response of the turbines is simulated as operating in power production. The environmental loads are described in the reference projects [5, 6]. The arrival time of the earthquake ocurrs at t=200 s, and each case is simulated during 300 s. The results are analysed since the arrival of the earthquake until the end of the simulation. The time duration of the earthquakes is described in Figure 3. In all cases, all the forces (wind, waves and seismic loading) are aligned in the fore-aft direction.

Three different cases are considered, as described in the results: a) taking into account both translational and rotational foundation input motions (With KI); b) taking into account only translational foundation input motions (Only I_u); and c) considering the original seismic input motion as translational input motion (Without KI).

4.1. Tower top accelerations

Figure 3 shows the time histories of the tower top acceleration for the 5MW OWT founded on soil profile and subjected to the environmental conditions and the seismic input signals considered in this study. The figure presents the acceleration of the top tower (a_{top}) versus time (t). Each line in the figure represents the acceleration of the tower top in the three different cases considered in the study, also the accelerogram is shown.

In both systems, in this specific case, when only lateral kinematic interaction factor is considered, no significant increases are observed in the acceleration of the top tower. The relevant role of the rotational kinematic interaction factors is appreciated in the monopiled system. In the OWT on the jacket substructure, rotational KIF is noticiable, but not very relevant in terms of accelerations. On the other hand, the rotational kinematic interaction factor is clearly more relevant in the RSN:192 earthquake compared to the RSN:777.

XII International Conference on Structural Dynamics IOP Publishing
Journal of Physics: Conference Series **2647** (2024) 112002 doi:10.1088/1742-6596/2647/11/112002

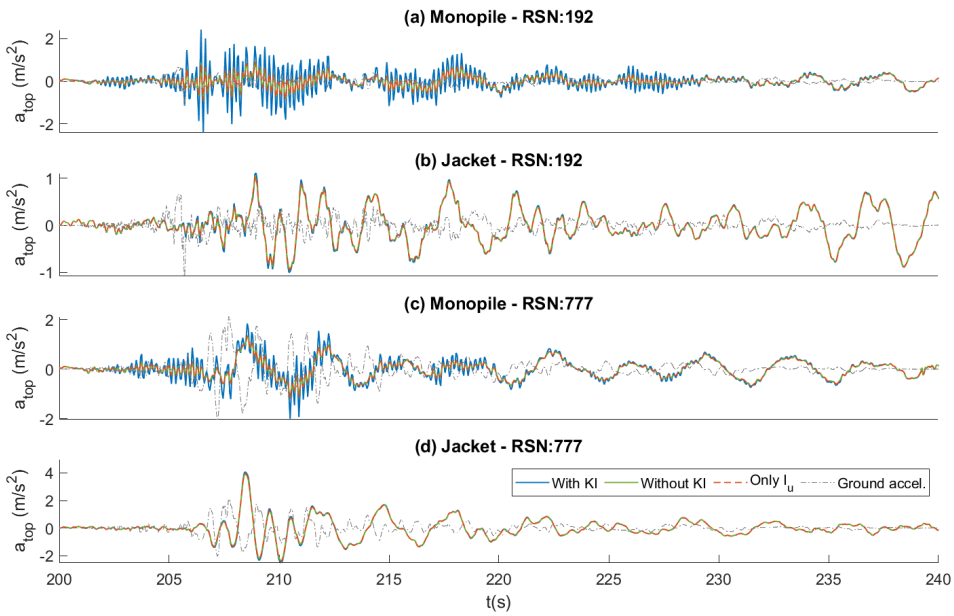

Figure 3. Time histories of the tower top acceleration for the two substructures, monopile and jacket, subjected to the two seismic signals and environmental conditions.

4.2. Internal forces in the substructures

The bending moments obtained in the substructure of the two systems considered in this study reach their maximum value at the mudline level, for both the monopile and the jacket. Furthermore, shear forces are also analised. In the case of the monopile substructure the node studied is at the mudline level and in the jacket, the internal forces in two different nodes are obtained. N_A and N_B, at the mudline level and the node immediately above it, respectively. These nodes are marked in Figure 1.

Figures 4 and 5 present the response of the systems in terms of shear forces and bending moments, respectively. In both figures, the time history presented for the jacket is at the point N_A.

An important role of the rotational kinematic interaction factors is appreciated in the monopile substructure in terms of shear forces. In the OWT on jacket substructure, the influence of the rotational KIF is appreciable in the peak values of shear forces, although considerably less than in the monopile. When considering only lateral KIF, the influence on the seismic response is not very relevant, the behaviour is similar to that obtained for accelerations.

In the case of bending moments, the increase produced in the peak value when comparing the response between taking into account, or disregarding, kinematic interaction, is lower than the values obtained for the accelerations and shear forces. In spite of this, a greater influence of KIFs in terms of internal forces is observed in the monopile compared to the jacket.

XII International Conference on Structural Dynamics IOP Publishing
Journal of Physics: Conference Series **2647** (2024) 112002 doi:10.1088/1742-6596/2647/11/112002

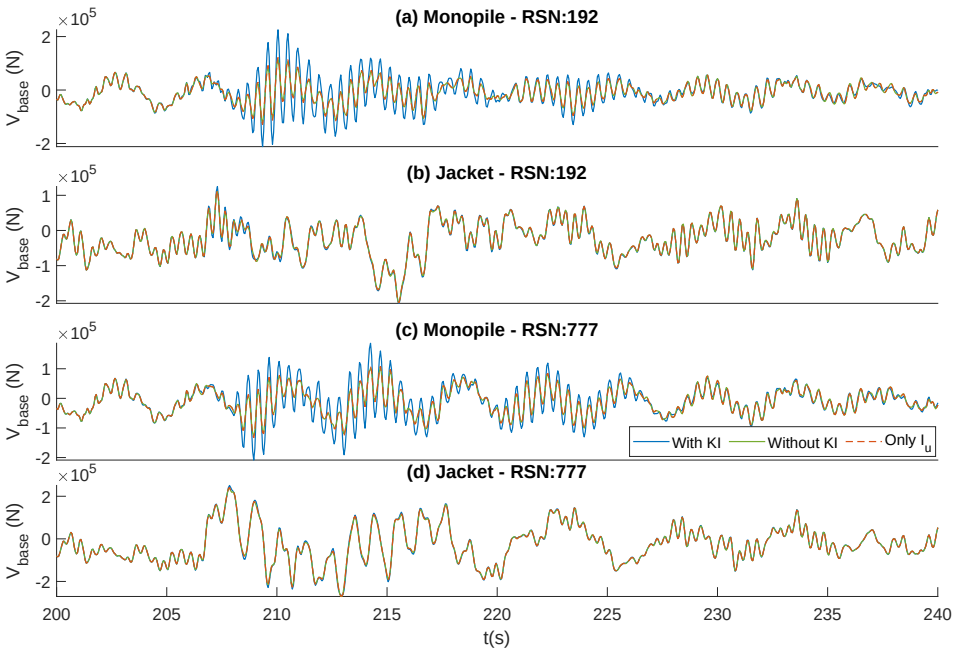

Figure 4. Time histories of the shear forces at mudline level for the two substructures, monopile and jacket, subjected to the two seismic signal and environmental conditions.

4.3. Discussion

Table 4 and 5 present the peak values of the accelerations at the tower top, and the peak values of shear forces and bending moments at selected sections, respectively, when both traslational and rotational kinematic interaction factors are considered. In the case of the monopile, the internal forces at mudline level are obtained while nodes N_A and N_B are considered for the jacket substructure. The differences between the responses computed taking into account (R_{KI}), or disregarding (R_{NOKI}), kinematic interaction, are also presented in both tables for accelerations (Δa_{KI}), shear forces (ΔV_{KI}) and bending moments (ΔM_{KI}). The equation (2) is used to compute these porcentages, where R represents the peak values.

Table 4. Peak accelerations at tower top obtained in the cases considered with the kinematic interaction.

Case	a_{top} [m/s^2]	Δa_{KI} [%]
M - RSN: 192	2.43	176.67
M - RSN: 777	2.01	52.46
J - RSN: 192	1.12	5.70
J - RSN: 777	4.09	3.91

XII International Conference on Structural Dynamics IOP Publishing
Journal of Physics: Conference Series **2647** (2024) 112002 doi:10.1088/1742-6596/2647/11/112002

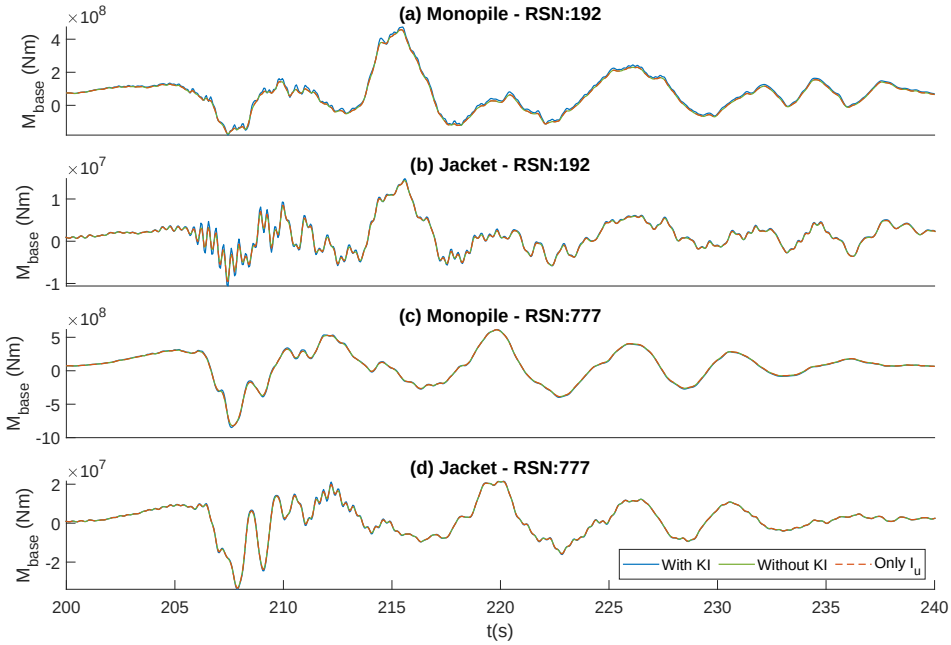

Figure 5. Time histores of the bending moments at mudline level for the two substructures, monopile and jacket, subjected to the two seismic signal and environmental conditions.

Table 5. Peaks shear forces and bending moments obtained in the cases considered with the kinematic interaction.

Case	V_{max}[MN]	M_{max}[MNm]	ΔV_{KI} [%]	ΔM_{KI} [%]
M - RSN: 192	0.225	473.93	81.32	6.22
M - RSN: 777	0.209	849.44	63.2	4.48
J - RSN: 192 (N_A)	0.303	14.82	3.88	2.46
J - RSN: 777 (N_A)	0.206	34.37	2.39	2.65
J - RSN: 192 (N_B)	0.299	13.64	6.81	2.39
J - RSN: 777 (N_B)	0.202	31.60	2.59	2.19

$$\Delta R_{KI} = \frac{R_{KI} - R_{NOKI}}{R_{KI}} \times 100 \tag{2}$$

When taking kinematic interaction factors into account, significantly higher values are obtained in terms of accelerations and shear forces, in the case of the monopile. In addition, the increase in peak values of the bending moment is higher than in the jacket. This indicates that the influence of kinematic factors in the case of an OWT on a monopile is very relevant.

XII International Conference on Structural Dynamics IOP Publishing
Journal of Physics: Conference Series **2647** (2024) 112002 doi:10.1088/1742-6596/2647/11/112002

On the other hand, the influence of KIFs in the peak values obtained in the jacket is much lower than those obtained in the monopile, being less than 10% in the accelerations and the internal forces considered.

5. Conclusions

The comparison of the influence of kinematic interaction on the seismic response of the two systems studied presents a notable difference. Results are presented in terms of peak response values of the tower top accelerations, shear forces and bending moments at the mudline level. In addition, another node of the legs is analysed in the jacket substructure. Each seismic signal is filtered to obtain three different scenarios: taking both traslational and rotational kinematic interaction factors into account; taking only the traslational kinematic interaction factor into account; or disregarding kinematic interaction completely. Environmental loads under normal operation conditions are considered to be aligned with the seismic excitation.

As expected, in the case of the monopile, the rotational motion has a strong effect on the accelerations and the shear forces, although the impact of the translational filtered signal is small. In the case of bending moments, the differences between the responses computed taking into account, or disregarding, kinematic interaction is significantly lower than for accelerations and shear forces.

However, in the jacket, the influence of the rotational motion is less pronounced. Considering the kinematic interaction factors in this type of substructure produces a light increase in the accelerations and the internal forces considered, but with a considerably smaller importance than in an OWT on a monopile.

Acknowledgments

This research was funded by Consejería de Economía, Conocimiento y Empleo (Agencia Canaria de la Investigación, Innovación y Sociedad de la Información) of the Gobierno de Canarias and FEDER through research project ProID2020010025 and by the Ministerio de Ciencia, Innovación y Universidades and the Agencia Estatal de Investigación of Spain, and FEDER, through research project PID2020-120102RB-I00. In addition, C. Romero-Sánchez is a recipient of the research fellowship (TESIS2022010011), from the Program of predoctoral fellowships from the Consejería de Economía, Conocimiento y Empleo (Agencia Canaria de la Investigación, Innovación y Sociedad de la Información) of the Gobierno de Canarias and Fondo Social Europeo. The authors are grateful for this support.

References

[1] Kaynia AM 2020 Effect of kinematic interaction on seismic response of offshore wind turbines on monopiles *Earthquake Engineering & Structural Dynamics* **50** 777-790.

[2] OpenFAST Documentation, National Renewable Energy Laboratory (version 3.4.0, February 12, 2023). Updates and new releases of OpenFAST can be found on `https://github.com/OpenFAST/openfast` and `https://openfast.readthedocs.io/en/main/`.

[3] Jonkman J, Butterfield S, Musial W and Scott G 2009 Definition of a 5-MW Reference Wind Turbine for Offshore System Development *Technical Report NREL/TP-500-38060 National Renewable Energy Laboratory.*

[4] Damiani R, Jonkman J, and Hayman G 2015 SubDyn user's guide and theory manual *Technical Report NREL/TP-5000-63062 National Renewable Energy Laboratory.*

[5] Jonkman J and Musial W 2010 Offshore Code Comparison Collaboration (OC3) for IEA Task 23 Offshore Wind Technology and Deployment *Technical Report NREL/TP-5000-48191 National Renewable Energy Laboratory.*

[6] Popko W et al. 2014 Offshore Code Comparison Collaboration Continuation (OC4), Phase I-Results of Coupled Simulations of an Offshore Wind Turbine with Jacket Support Structure *Journal of Ocean and Wind Energy* **1** 1-11.

[7] Pacific Earthquake Engineering Research Center (PEER, February 20, 2023). NGA-West2 Ground Motion Database can be found on `http://ngawest2.berkeley.edu/`.

XII International Conference on Structural Dynamics IOP Publishing
Journal of Physics: Conference Series **2647** (2024) 112002 doi:10.1088/1742-6596/2647/11/112002

[8] Clough RM and Penzien J 1995 Dynamics of Structures *3th edition Computers & Structures, Inc.*
[9] Romero-Sánchez C and Padrón LA 2023 An implementation of multi-support input motion into openfast for the earthquake analysis of offshore wind turbines. *9th International Conference on Computational Methods in Structural Dynamics and Earthquake Engineering* (Athens: COMPDYN 2023).
[10] Álamo GM, Bordón JDR and Aznárez JJ 2021 On the application of the beam model for linear dynamic analysis of pile and suction caisson foundations for offshore wind turbines *Comp. Geotech* **134** 104107.
[11] Carbonari S, Morici M, Dezi F and Leoni G 2018 A lumped parameter model for time-domain inertial soil-structure interaction analysis of structures on pile foundations *Earthquake Engineering* & *Structural Dynamics* **47** 2147-2171.
[12] Romero-Sánchez C and Padrón LA 2022 Implementation of Ground Input Motion and Dynamic Soil-Structure Interaction into Openfast for the Seismic Analysis of Offshore Wind Turbines *Congress on Numerical Methods in Engineering* (Las Palmas de Gran Canaria: CMN 2022) 337-356.

B. Resumen en castellano

B Resumen en castellano
B.1 Introducción
B.2 Objetivos
B.3 Publicaciones derivadas de la tesis doctoral
B.4 Justificación
B.5 Conclusiones

Título de la Tesis Doctoral: Avances en el análisis dinámico y sísmico de estructuras tipo jacket para el soporte de aerogeneradores marinos

B.1 Introducción

La comunidad internacional se inclina, cada vez con más claridad, hacia el desarrollo y utilización de tecnologías que permitan el aprovechamiento de energías de origen renovable con el fin de limitar las emisiones de gases de efecto invernadero. La reducción de emisiones de CO2 es una de las líneas prioritarias del Pacto Verde promovido por el Consejo de Europa y que recoge el compromiso de sus miembros de alcanzar la neutralidad climática en 2050. A corto plazo, los miembros del Consejo se han comprometido a adaptar sus legislaciones y sistemas productivos para alcanzar una reducción del 55% de emisiones en 2030. En el paquete de medidas se incluye como propuesta el aumento de la cuota de participación de las fuentes de energía renovables (mínimo 40%) en la combinación energética global de la Unión Europea.

La energía eólica y, en particular, la eólica marina, es una de las alternativas de futuro más prometedoras para contribuir a este objetivo, con una expansión muy notable en los últimos años, y con proyecciones de potencia instalada global que alcanzan los 380 GW para 2030 [1]. En este ámbito, y aunque en los últimos años se han producido avances en el desarrollo de dispositivos flotantes, la mayoría de los aerogeneradores marinos que se instalan en la actualidad están cimentados directamente en el lecho marino. A medida que se instalan aerogeneradores de mayor potencia en profundidades cada vez mayores, la estructura de soporte está sometida a requerimientos más exigentes. De este modo, la expansión de esta tecnología se encamina al desarrollo de diseños cada vez más complejos que permitan cimentar a profundidades mayores y a mayores distancias de la costa.

El análisis de la respuesta dinámica estructural de aerogeneradores terrestres y marinos es un tema de estudio relativamente reciente que, dependiendo del objetivo perseguido, ha sido abordado utilizando modelos y metodologías de muy diversa índole [2–4]). La interacción dinámica suelo-estructura es uno de los aspectos que los modelos integrados deben incorporar, ya que son muchos los estudios han puesto de manifiesto no solo que dicha interacción modifica el comportamiento dinámico de dispositivos reales [5, 7] sino incluso que los efectos de interacción suelo-estructura pueden ser perjudiciales para el conjunto y, por tanto, la utilización de modelos en base rígida puede dar lugar a diseños inseguros [9–11].

Incluso cuando incluyen la interacción suelo-estructura, muchos de los modelos de análisis dinámico disponibles en la bibliografía se basan en modelos sencillos de subestructuración que consideran resortes y amortiguadores puntuales en la base de la torre [12, 13] cuyos valores se estiman en muchos casos a partir de expresiones o aproximaciones simplificadas. Sin embargo, se obtienen modelos más precisos si se acude a formulaciones más evolucionadas de medio continuo para calcularlos [14–19].

Por otro lado, es importante destacar que la mayor parte de los estudios publicados sobre la respuesta dinámica y sísmica de aerogeneradores marinos se centran en el estudio de aerogeneradores monopilotados, mientras que las estructuras tipo jacket han recibido menos atención. Los trabajos de Jalbi et al. [20–22], Couceiro et al. [23] y Abdullahi et al. [24] representan esfuerzos relevantes en los últimos años en avanzar en la comprensión de la respuesta y el diseño de este tipo de estructuras.

Desde el punto de vista de las cargas a considerar en el diseño de la estructura de estos dispositivos, las principales guías y estándares de aplicación [25, 26] se centran fundamentalmente en las cargas generadas por el viento, las olas, las corrientes y el hielo; todo ello en condiciones de operación, arranque, transporte, etc. Las cargas de origen sísmico, por otra parte, han recibido menos atención, en parte por la percepción de tratarse de estructuras intrínsecamente seguras ante terremotos [4] por su elevado periodo fundamental de vibración en relación con las frecuencias características de la mayor parte de los terremotos [27]. Por el contrario, un número significativo de autores han destacado la relevancia de las acciones sísmicas en los sistemas estructurales de los aerogeneradores marinos (ver, entre otros, [8, 28, 29]). En línea con esta motivación, es relevante destacar los resultados presentados por Alati et al. [30]. Para un caso particular, los autores concluyen que la combinación de viento, olas y cargas sísmicas es más desfavorable que las combinaciones de cargas prescritas por el estándar de referencia para el diseño de estas estructuras. Cheng et al. [31] exploraron cómo la respuesta dinámica del jacket se ve influenciada por las direcciones variables del viento y las olas, destacando el impacto significativo de la parada de emergencia y las condiciones de estacionamiento en las evaluaciones de fragilidad para los estados de daños graves en la torre y la subestructura. Ju y Huang [29] examinaron el aerogenerador offshore de 5 MW de NREL sobre un jacket, destacando que la combinación de cargas sísmicas y ambientales durante la producción de energía suele regir el diseño estructural de las subestructuras jacket. Además, James y Haldar se centraron en el comportamiento de las tensiones obtenidas en los elementos tubulares del jacket, incorporando el movimiento multidireccional del terreno. Sus conclusiones subrayaron la importancia de tener en cuenta los efectos de los modos superiores y las fuerzas sísmicas multidireccionales al analizar el comportamiento estructural del sistema, identificando los segmentos superior e inferior de las patas del jacket como especialmente vulnerables.

Varios de los estudios mencionados se centran principalmente en las propiedades estructurales de los aerogeneradores utilizando modelos simplificados en el dominio de la frecuecia. Las propiedades dinámicas de estas estructuras de soporte desempeñan un papel crucial en el diseño del sistema. Las características distintivas de los aerogeneradores marinos, incluida la naturaleza específica de las cargas, la geometría variable del sistema debido a la rotación de las palas y la influencia continua del sistema de control, sugieren que en los análisis estructurales y de respuesta dinámica se utilicen herramientas específicas, capaces de modelar adecuadamente los distintos subsistemas. Los análisis en el dominio del tiempo, que incorporan simulaciones aero-hidro-servo-elásticas no lineales, son esenciales para captar con precisión el comportamiento dinámico del sistema en los diferentes modos de operación [29, 33–35].

B.2 Objetivos

La tesis propuesta pretende avanzar en la comprensión de la respuesta estructural dinámica y sísmica de aerogeneradores marinos soportados por estructuras tipo jacket con apoyos múltiples sobre pilotes o cajones de succión. La investigación tiene como objetivo contribuir al avance de esta tecnología, particularmente para aplicaciones en aguas profundas y ubicaciones con riesgo sísmico.

Los objetivos de este trabajo son fundamentalmente dos:

1. Avanzar en el desarrollo de metodologías, modelos y herramientas para el análisis dinámico y sísmico de estructuras soporte tipo jacket para aerogeneradores offshore cimentados en el fondo marino, incluyendo modelos avanzados de interacción dinámica suelo-cimentación-estructura, y teniendo en cuenta las características del suelo de cimentación.

2. Profundizar en dos aspectos poco estudiados y que pueden determinar los diseños obtenidos en zonas con riesgo sísmico relevante:

    - El estudio de los fenómenos de interacción dinámica cimentación-suelo-cimentación que tienen lugar en las estructuras portantes multiapoyadas.
    - El análisis de la influencia de la interacción cinemática en la respuesta sísmica del conjunto.

B.3 Publicaciones derivadas de la tesis doctoral

Las tres primeras contribuciones en revistas JCR que se enumeran a continuación constituyen la tesis por compendio.

- C. Romero-Sánchez and L.A. Padrón. Influence of wind and seismic ground motion directionality on the dynamic response of four-legged jacket-supported Offshore Wind Turbines. Engineering Structures, 300, 117191, 2024.

- C. Romero-Sánchez and L.A. Padrón. Seismic response of jacket-supported offshore wind turbines for different operational modes considering earthquake directionality. Ocean Engineering, 311 Part 1, 118798, 2024.

- C. Romero-Sánchez, J.D.R. Bordón and L.A. Padrón. Influence of Foundation–Soil–Foundation Interaction on the Dynamic Response of OffshoreWind Turbine Jackets Founded on Buckets. Journal of Marine Science and Engineering, 12, 2089, 2024.

- A. J. Romero-Monzón, C. Romero-Sánchez, G. M. Álamo and L. A. Padrón. Can a simple static-equivalent model be used to predict major trends in the dynamic structural response of monopile offshore wind turbines?. Applied Sciences, 15(3):1633, 2025.

- A. M. Kaynia, D. M. Pedersen, H. Askheim and C. Romero-Sánchez. Implementation of seismic soil-structure interaction in openfast and application to an offshore wind turbine on jacket structure. Marine Structures, 103:103832, 2025.

Contribuciones en congresos

Se han realizado cuatro contribuciones a congresos, publicando 3 artículos en actas de congresos que se detallan en el apéndice A.

- C. Romero-Sánchez and L.A. Padrón. Implementation of Ground Input Motion and Dynamic Soil-Structure Interaction into Openfast for the Seismic Analysis of Offshore Wind Turbines. Congress on Numerical Methods in Engineering, CMN 2022.

- C. Romero-Sánchez and L.A. Padrón. An implementation of multi-support seismic input motion into OpenFast for the earthquake analysis of offshore wind turbines. 9th International Conference on Computational Methods in Structural Dynamics and Earthquake Engineering, COMPDYN 2023.

- C. Romero-Sánchez, L.A. Padrón, G.M. Álamo, C. Medina, J.J. Aznárez and O. Maeso, Comparative study of the influence of kinematic interaction on the seismic response of monopile and jacket supported offshore wind turbines. J. Phys.: Conf. Ser. 2647, 112002, 2024. XII International Conference on Structural Dynamics, EURODYN 2023.

- C. Romero-Sánchez and L.A. Padrón, Dynamic structural response of four-legged jacket-supported offshore wind turbine considering the effect of wind and seismic ground motion directionality. 3rd Conference on Structural Dynamics, DinEst 2024.

B.4 Justificación

La estructura portante de los aerogeneradores marinos se encuentra sometida a solicitaciones variables en el tiempo y es necesario, por tanto, plantear su diseño y análisis desde una perspectiva vinculada a la dinámica estructural. Al mismo tiempo, el diseño y dimensionamiento de las estructuras tipo jacket es un problema complejo teniendo en cuenta el elevado número de parámetros que determinan la respuesta y las abundantes limitaciones y requerimientos que debe verificar la estructura. Por otro lado, los fenómenos de interacción dinámica con el fondo marino pueden ser significativos dependiendo de las propiedades de ambos y del tipo de cimentación empleado. También debe tenerse en cuenta el carácter no acotado de dicho lecho marino. Por tanto, para el estudio de este problema se requiere, en general, de modelos de análisis que representen

todos los elementos implicados (estructura, cimentación y fondo marino), sus interacciones mutuas y la especial consideración del último como un medio semi-infinito y de naturaleza heterogénea en el caso general.

Inicialmente, se acoplaron modelos avanzados de interacción dinámica suelo-cimentación-estructura desarrollados por el grupo de investigación con un código hidro-aero-servo-estructural del aerogenerador capaz de modelar en detalle su respuesta dinámica. En concreto, el código empleado es OpenFAST [36], un código abierto con este propósito impulsado por el National Renewable Energy Laboratory. Se trata de un código en desarrollo y con amplia aceptación entre la comunidad técnica y científica pero que no cuenta aún con modelos avanzados para representar la interaccion dinámica con el suelo y la cimentación. Dada la naturaleza no-lineal de la respuesta de algunos subsistemas del aerogenerador (que constituye además un sistema no invariante), la resolución de las ecuaciones que representan el estado del sistema se realiza en el dominio del tiempo, mediante un esquema paso a paso. Por contra, los modelos avanzados desarrollados por el grupo han sido formulados en el dominio de la frecuencia [17, 18, 56], lo que permite explotar las ventajas que ellos representa en el análisis dinámico de sistemas. Por esta razón, se exploraró e implementó las estrategias numéricas necesarias y metodológicas para poder acoplar ambos esquemas.

Por otro lado, la verificación de los modelos obtenidos mediante comparacion con resultados presentes en la literatura científica son presentados en diferentes publicaciones [52, 53]. Una vez implementado y validado el nuevo modelo, se ha realizado una serie de estudios relacionados con el comportamiento dinámico de estructuras jackets:

- La influencia de la dirección de las cargas de viento y sacudida sísmica en la respuesta dinámica de un jacket es analizada en la primera publicación [47]. La influencia de la direccionalidad del viento y del movimiento del suelo en la respuesta dinámica y sísmica de los aerogeneradores marinos soportadas por subestructuras tipo jacekt, y la identificación de la combinación más exigente, sigue siendo una cuestión abierta en la literatura científica. El artículo discute los rangos específicos del ángulo de desalineación entre las direcciones del viento y del movimiento sísmico dentro de los cuales se espera encontrar las fuerzas internas máximas.

- El estudio del impacto de los modos de operación del aerogenerador en la respuesta sísmica de jacket es presentado en la segunda publicación [48]. El objetivo de este estudio es analizar cómo responden a las acciones sísmicas los aerogeneradors marinos soportadas por jacket que funcionan en tres modos operativos diferentes (producción de energía, parada de emergencia y modo estacionado) cuando están sometidas a diferentes direcciones de viento entrante y direcciones de sacudida del movimiento del suelo .

- Finalmente, la tercera publicación investiga el impacto de la interacción cimentación-suelo-cimentación, es decir, los efectos de la interacción a través del suelo entre dos o más cimentaciones, en una subestructura jacket cimentada con cajones de

succión. Se realizó un análisis paramétrico centrado en los casos críticos de carga para un diseño conservador de la cimentación [49].

Adicionalmente, la influencia de la interacción cinemática en la respuesta dinámica y sísmica en subestructuras jackets ha sido evaluada [54]. Particularmente, en este trabajo se presenta una comparación de los efectos de la interacción cinemática en la respuesta sísmica de dos tipos de subestructuras para aerogeneradores, monopilotes y jackets sobre pilotes.

B.5 Conclusiones

La presente tesis se centra en el análisis estructural dinámico y sísmico de subestructuras tipo jacket para aerogeneradores marinos mediante modelado numérico avanzado. El estudio integra múltiples subsistemas y fenómenos no lineales, considerando los efectos de la interacción dinámica suelo-estructura en subestructuras con múltiples apoyos. Además, esta investigación analiza los fenómenos de interacción cimentación-suelo-cimentación en estructuras con múltiples apoyos y examina la influencia de la interacción cinemática en el comportamiento sísmico de la estructura.

La investigación presentada combina modelos avanzados de interacción dinámica suelo-cimentación-estructura desarrollados por el grupo solicitante con un código aero-hidro-servo-estructural del aerogenerador capaz de modelar en detalle su respuesta dinámica. Tras la verificación de los modelos propuestos, se han considerado diversos problemas que involucran subestructuras tipo jacket sobre pilotes y cajones de succión. Todos estos estudios han sido presentados en las distintas publicaciones descritas en el documento de tesis doctoral en acceso abierto. En cada una de las publicaciones se detalla la metodología utilizada y los distintos problemas estudiados.

En primer lugar, para explorar el comportamiento dinámico y sísmico de la subestructura tipo jacket, un factor relevante a considerar es la influencia de la direccionalidad del viento y del movimiento sísmico del suelo en la respuesta dinámica de aerogeneradores marinos soportados por jackets. Cabe destacar que las fuerzas internas máximas suelen encontrarse cuando la sacudida sísmica está alineada con la dirección de la diagonal de la base del jacket y no alineada con la dirección del viento. Además, la dirección de las sacudidas sísmicas tiende a influir más en las fuerzas internas máximas que la dirección del viento. En cualquier caso, las combinaciones de carga que asumen direcciones de viento y movimiento del suelo alineadas a menudo no son el peor escenario posible. En el estudio se proporciona rangos con un margen relativamente estrecho dentro del cual se puede encontrar la combinación del peor escenario posible, aunque no se puede especificar una combinación concreta para todos los casos. Esto se debe en parte a que las combinaciones para las que se encuentran los valores máximos de pico varían, dentro de estos márgenes, con los distintos terremotos. Por consiguiente, durante las fases de diseño detallado de las subestructuras de cubierta de los aerogeneradores marinos situados en zonas con un nivel de riesgo sísmico suficientemente elevado, debe tenerse en cuenta un conjunto suficientemente amplio de

señales sísmicas (que, idealmente, incluya también estaciones offshore) y de diferentes combinaciones de direcciones sacudidas sísmicas y del viento.

En segundo lugar, tras analizar la influencia de los distintos modos de funcionamiento de un aerogenerador ante la llegada de un sismo sobre una subestructura jacket (producción de energía normal, con parada de emergencia o modo estacionado), se han estraído una serie de conclusiones. La parada de emergencia no es necesariamente beneficiosa para reducir las aceleraciones máximas en la góndola. Por otra parte, las aceleraciones máximas más bajas se obtienen para el modo de producción de energía normal cuando el sísmo actúa a lo largo de la dirección proa-popa. Esto se debe a la mayor amortiguación aerodinámica, que tiene un efecto beneficioso al reducir la magnitud de las vibraciones inducidas por el sísmo. Debido a la geometría de la estructura jacket de cuatro apoyos, las tensiones de von Mises máximas suelen encontrarse cuando las sacudidas del terreno actúan a lo largo de una de las diagonales de la estructura y no alineadas con la dirección del viento en los tres modos operativos. Además, las tensiones máximas aparecen casi siempre en el caso de la producción de energía, con la excepción de la parte superior de las patas, donde en varios casos aparecen tensiones mayores durante la parada de emergencia.

Por último, los efectos de la interacción cimentación-suelo-cimentación en el comportamiento dinámico de subestructuras tipo jacket cimentadas sobre cajones de succión para aerogeneradores marinos son analizados. Se observó que la interacción cimentación-suelo-cimentación puede desempeñar un papel en el aumento de la magnitud de la respuesta estructural en términos no sólo de aceleraciones sino, lo que es más importante, en términos de esfuerzos cortantes, momentos flectores y tensiones en muchas situaciones diferentes. En otras palabras, ignorar la influencia de la interacción entre cimentaciones cercanas (como se suele suponer en el análisis de estos sistemas) puede contribuir a subestimar la respuesta estructural del jacket. Una de las razones que explican esta influencia sobre la respuesta estructural son los cambios producidos en la frecuencia fundamental de la estructura: la interacción cimentación-suelo-cimentación modifica las rigideces de cada cimentación individual del grupo (el conocido efecto de grupo) y, dado que los modos y frecuencias naturales de todo el sistema dependen de dichas rigideces, también se modifican. A su vez, si los modos y las frecuencias naturales cambian, la respuesta estructural de cada elemento también se ve afectada.

Adicionalmente, la influencia de la interacción cinemática en la respuesta sísmica de los sistemas monopilotados o con subestructura jacket ha sido analizada, presentando diferencias notables. En el caso del monopilote, el movimiento rotacional tiene un fuerte efecto sobre las aceleraciones y los esfuerzos cortantes, aunque el impacto de la señal filtrada traslacional es pequeño. En el caso de los momentos flectores, las diferencias entre las respuestas calculadas teniendo en cuenta, o despreciando, la interacción cinemática son significativamente menores que para las aceleraciones y los esfuerzos cortantes. Sin embargo, en el jacket, la influencia del movimiento de rotación es menos pronunciada. La consideración de los factores de interacción cinemática en este tipo de subestructura produce un ligero aumento de las aceleraciones y las fuerzas internas consideradas, pero con una importancia considerablemente menor que en un

aerogenerador sobre un monopilote.

Un análisis exhaustivo de cada uno de estos problemas, junto con conclusiones más detalladas, puede encontrarse en las respectivas publicaciones que conforman la tesis.

REFERENCES

[1] G. W. E. Council. Global offshore wind report 2024. Technical report, GWEC: Brussels, Belgium, 2024.

[2] V. Zania. Natural vibration frequency and damping of slender structures founded on monopiles. Soil Dynamics and Earthquake Engineering, 59:8–20, 2014.

[3] M. Asareh, W. Schonberg and J. Volz. Effects of seismic and aerodynamic load interaction on structural dynamic response of multi-megawatt utility scale horizontal axis wind turbines. Renewable energy, 86:49–58, 2016.

[4] E. I. Katsanos, S. Thöns and C. T. Georgakis. Wind turbines and seismic hazard: a state-of-the-art review. Wind Energy, 19(11):2113–2133, 2016.

[5] D. Lombardi, S. Bhattacharya and D. Wood. Dynamic soil–structure interaction of monopile supported wind turbines in cohesive soil. Soil dynamics and earthquake engineering, 49:165–180, 2013.

[6] R. Kjørlaug and A. Kaynia. Vertical earthquake response of megawatt-sized wind turbine with soil-structure interaction effects. Earthquake Engineering and Structural Dynamics, 44(13):2341–2358, 2015.

[7] G. M. Álamo, J. J. Aznárez, L. A. Padrón, A. E. Martínez-Castro, R. Gallego and O. Maeso. Dynamic soil-structure interaction in offshore wind turbines on monopiles in layered seabed based on real data. Ocean Engineering, 156:14–24, 2018.

[8] A. M. Kaynia. Seismic considerations in design of offshore wind turbines. Soil Dynamics and Earthquake Engineering, 124:399–407, 2019.

[9] M. Vatanchian and A. Shooshtari. Investigation of soil–structure interaction effects on seismic response of a 5 MW wind turbine. International Journal of Civil Engineering, 16:1–17, 2018.

[10] T. Huo, L. Tong and Y. Zhang. Dynamic response analysis of wind turbine tubular towers under long-period ground motions with the consideration of soil-structure interaction. Advanced Steel Construction, 14(2):227–250, 2018.

[11] J.-T. Seong and D.-S. Kim. Seismic evaluation of offshore wind turbine by geotechnical centrifuge test. Wind Energy, 22(8):1034–1042, 2019.

[12] L. Arany, S. Bhattacharya, S. Adhikari, S. Hogan and J. H. G. Macdonald. An analytical model to predict the natural frequency of offshore wind turbines on three-spring flexible foundations using two different beam models. Soil Dynamics and Earthquake Engineering, 74:40–45, 2015.

[13] L. Arany, S. Bhattacharya, J. H. Macdonald and S. J. Hogan. Closed form solution of eigen frequency of monopile supported offshore wind turbines in deeper waters incorporating stiffness of substructure and SSI. Soil Dynamics and Earthquake Engineering, 83:18–32, 2016.

[14] A. M. Kaynia and E. Kausel. Dynamics of piles and pile groups in layered soil media. Soil Dynamics and Earthquake Engineering, 10(8):386–401, 1991.

[15] L. A. Padrón, J. J. Aznárez and O. Maeso. BEM–FEM coupling model for the dynamic analysis of piles and pile groups. Engineering Analysis with Boundary Elements, 31(6):473–484, 2007.

[16] M. Liingaard, L. Andersen and L. B. Ibsen. Impedance of flexible suction caissons. Earthquake Engineering & Structural Dynamics, 36(14):2249–2271, 2007.

[17] G. M. Álamo, A. E. Martínez-Castro, L. A. Padrón, J. J. Aznárez, R. Gallego and O. Maeso. Efficient numerical model for the computation of impedance functions of inclined pile groups in layered soils. Engineering Structures, 126:379–390, 2016.

[18] J. D. R. Bordón, J. J. Aznárez and O. Maeso. Dynamic model of open shell structures buried in poroelastic soils. Computational Mechanics, 60(2):269–288, 2017.

[19] M. Saitoh. On the modeling of frequency-and intensity-dependent impedance functions at the head of horizontally loaded single piles. Soils and Foundations, 62(2):101107, 2022.

[20] S. Jalbi and S. Bhattacharya. Closed form solution for the first natural frequency of offshore wind turbine jackets supported on multiple foundations incorporating soil-structure interaction. Soil Dynamics and Earthquake Engineering, 113:593–613, 2018.

[21] S. Jalbi, G. Nikitas, S. Bhattacharya and N. Alexander. Dynamic design considerations for offshore wind turbine jackets supported on multiple foundations. Marine Structures, 67:102631, 2019.

[22] S. Jalbi and S. Bhattacharya. Concept design of jacket foundations for offshore wind turbines in 10 steps. Soil Dynamics and Earthquake Engineering, 139:106357, 2020.

[23] I. Couceiro, J. París, F. Navarrina, R. Guizán and I. Colominas. Optimization of offshore steel jackets: Review and proposal of a new formulation for time-dependent constraints. Archives of Computational Methods in Engineering, 27:1049–1069, 2020.

[24] A. Abdullahi, Y. Wang and S. Bhattacharya. Comparative modal analysis of monopile and jacket supported offshore wind turbines including soil-structure interaction. International Journal of Structural Stability and Dynamics, 20(10):2042016, 2020.

[25] DNV-OS-J101. Design of Offshore Wind Turbine Structures. Offshore Standard. DetNorske Veritas AS, 2014.

[26] IEC 61400-3-1:2019. Wind energy generation systems - Part 3-1: Design requirements for fixed offshore wind turbines. International Electrotechnical Commission, 2019.

[27] S. Bhattacharya and K. Goda. Use of offshore wind farms to increase seismic resilience of nuclear power plants. Soil Dynamics and Earthquake Engineering, 80:65–68, 2016.

[28] F. Gelagoti, R. Kourkoulis, I. Georgiou and S. Karamanos. Soil–structure interaction effects in offshore wind support structures under seismic loading. Journal of Offshore Mechanics and Arctic Engineering, 141(6), 2019.

[29] S.-H. Ju and Y.-C. Huang. Analyses of offshore wind turbine structures with soil-structure interaction under earthquakes. Ocean Engineering, 187:106190, 2019.

[30] N. Alati, G. Failla and F. Arena. Seismic analysis of offshore wind turbines on bottom-fixed support structures. Philosophical Transactions of the Royal Society A: Mathematical, Physical and Engineering Sciences, 373(2035):20140086, 2015.

[31] Y. Cheng, Y. Luo, J. Wang, K. Dai, W. Wang and A. El Damatty. Fragility and vulnerability development of offshore wind turbines under aero-hydro loadings. Engineering Structures, 293:116625, 2023.

[32] M. James and S. Haldar. Seismic vulnerability of jacket supported large offshore wind turbine considering multidirectional ground motions. Structures, 43:407–423, 2022.

[33] K. Wei, A. T. Myers and S. R. Arwade. Dynamic effects in the response of offshore wind turbines supported by jackets under wave loading. Engineering Structures, 142:36–45, 2017.

[34] K. Abhinav and N. Saha. Nonlinear dynamical behaviour of jacket supported offshore wind turbines in loose sand. Marine Structures, 57:133–151, 2018.

[35] L. A. Padrón, S. Carbonari, F. Dezi, M. Morici, J. D. R. Bordón and G. Leoni. Seismic response of large offshore wind turbines on monopile foundations including dynamic soil–structure interaction. Ocean Engineering, 257:111653, 2022.

[36] National Renewable Energy Laboratory. OpenFAST Documentation. Release v3.5.2, 2024. https://openfast.readthedocs.io/en/main/. Code published at https://github.com/OpenFAST/openfast.

[37] J. Jonkman and W. Musial. Offshore code comparison collaboration (OC3) for IEA Wind Task 23 offshore wind technology and deployment, 2010.

[38] W. Popko, F. Vorpahl, A. Zuga, M. Kohlmeier, J. Jonkman, A. Robertson, T. J. Larsen, A. Yde, K. Sætertrø, K. M. Okstad et al. Offshore code comparison collaboration continuation (OC4), phase 1-results of coupled simulations of an

offshore wind turbine with jacket support structure. In ISOPE International Ocean and Polar Engineering Conference, ISOPE–I. ISOPE, 2012.

[39] R. Bergua, A. Robertson, J. Jonkman, A. Platt, A. Page, J. Qvist, E. Amet, Z. Cai, H. Han, A. Beardsell et al. OC6 phase II: Integration and verification of a new soil–structure interaction model for offshore wind design. Wind Energy, 25(5):793–810, 2022.

[40] L. Carmo, R. Bergua, L. Wang and A. Robertson. Validation of local structural loads computed by OpenFAST against measurements from the focal experimental campaign. In International Conference on Offshore Mechanics and Arctic Engineering, volume 87851, V007T09A048. American Society of Mechanical Engineers, 2024.

[41] R. Damiani, J. Jonkman and G. Hayman. SubDyn user's guide and theory manual. Technical report, National Renewable Energy Lab.(NREL), Golden, CO (United States), 2015.

[42] I. B. Løken and A. M. Kaynia. Effect of foundation type and modelling on dynamic response and fatigue of offshore wind turbines. Wind Energy, 22(12):1667–1683, 2019.

[43] R. Bergua, A. Robertson, J. Jonkman and A. Platt. Specification document for OC6 phase II: Verification of an advanced soil-structure interaction model for offshore wind turbines. Technical report, National Renewable Energy Lab.(NREL), Golden, CO (United States), 2021.

[44] V. Krathe and A. Kaynia. Implementation of a non-linear foundation model for soil-structure interaction analysis of offshore wind turbines in FAST. Wind Energy, 20(4):695–712, 2016.

[45] A. M. Page, G. Grimstad, G. R. Eiksund and H. P. Jostad. A macro-element pile foundation model for integrated analyses of monopile-based offshore wind turbines. Ocean Engineering, 167:23–35, 2018.

[46] L. Wang and T. Ishihara. A new FounDyn module in OpenFAST to consider foundation dynamics of monopile supported wind turbines using a site-specific soil reaction framework. Ocean Engineering, 266:112692, 2022.

[47] C. Romero-Sánchez and L. A. Padrón. Influence of wind and seismic ground motion directionality on the dynamic response of four-legged jacket-supported offshore wind turbines. Engineering Structures, 300:117191, 2024.

[48] C. Romero-Sánchez and L. A. Padrón. Seismic response of jacket-supported offshore wind turbines for different operational modes considering earthquake directionality. Ocean Engineering, 311:118798, 2024.

[49] C. Romero-Sánchez, J. D. R. Bordón and L. A. Padrón. Influence of foundation–soil–foundation interaction on the dynamic response of offshore wind turbine jackets founded on buckets. Journal of Marine Science and Engineering, 12(11):2089, 2024.

[50] A. J. Romero-Monzón, C. Romero-Sánchez, G. M. Álamo and L. A. Padrón. Can a simple static-equivalent model be used to predict major trends in the dynamic structural response of monopile offshore wind turbines?. Applied Sciences, 15(3):1633, 2025.

[51] A. M. Kaynia, D. M. Pedersen, H. Askheim and C. Romero-Sánchez. Implementation of seismic soil-structure interaction in OpenFAST and application to an offshore wind turbine on jacket structure. Marine Structures, 103:103832, 2025.

[52] C. Romero-Sánchez and L. A. Padrón. Implementation of ground input motion and dynamic soil-structure interaction into OpenFAST for the seismic analysis of offshore wind turbines. Congress on Numerical Methods in Engineering, 2022.

[53] C. Romero-Sánchez and L. A. Padrón. An implementation of multi-support input motion into OpenFAST for the earthquake analysis of offshore wind turbines. COMPDYN Proceedings, 2023.

[54] C. Romero-Sánchez, L. A. Padrón, G. M. Álamo, C. Medina, J. J. Aznárez and O. Maeso. Comparative study of the influence of kinematic interaction on the seismic response of monopile and jacket supported offshore wind turbines. In Journal of Physics: Conference Series, volume 2647, 112002. IOP Publishing, 2024.

[55] C. Romero-Sánchez and L. A. Padrón. Dynamic structural response of four-legged jacket-supported offshore wind turbine considering the effect of wind and seismic ground motion directionality. 3rd Conference on Structural Dynamics (DinEst 2024), 2024.

[56] G. M. Álamo, J. D. R. Bordón and J. J. Aznárez. On the application of the beam model for linear dynamic analysis of pile and suction caisson foundations for offshore wind turbines. Computers and Geotechnics, 134:104107, 2021.

[57] S. Carbonari, M. Morici, F. Dezi and G. Leoni. A lumped parameter model for time-domain inertial soil-structure interaction analysis of structures on pile foundations. Earthquake Engineering & Structural Dynamics, 47(11):2147–2171, 2018.

[58] J. D. R. Bordón, J. J. Aznárez, O. Maeso and S. Bhattacharya. Simple approach for including foundation–soil–foundation interaction in the static stiffnesses of multi-element shallow foundations. Géotechnique, 71(8):686–699, 2021.

[59] J. D. Achenbach. Wave propagation in elastic solids. North-Holland, Amsterdam, 1973.

[60] A. C. Eringen and E. S. Suhubi. Elastodynamics, vol. 2 - Linear theory. Academic press, NY, 1975.

[61] A. M. Kaynia and M. Novak. Response of pile foundations to Rayleigh waves and obliquely incident body waves. Earthquake Engineering & Structural Dynamics, 21(4):303–318, 1992.

[62] S. Liu, H. Li, J. Zhang, S. Yang and T. Zhang. Shaking table test and numerical simulation of jacket offshore platform considering soil-water-structure interaction. Ocean Engineering, 313:119542, 2024.

[63] B. Ma, A. Zhou and K. Lin. Influence of seismic direction on dynamic responses of wind turbine in operation: An experimental study by combining wind tunnel and shaking table tests. Earthquake Engineering & Structural Dynamics, 2025.

[64] S. Bisoi and S. Haldar. Design of monopile supported offshore wind turbine in clay considering dynamic soil–structure-interaction. Soil Dynamics and Earthquake Engineering, 73:103–117, 2015.

[65] A. A. Markou and A. M. Kaynia. Nonlinear soil-pile interaction for offshore wind turbines. Wind Energy, 21(7):558–574, 2018.

[66] Y. Sun, C. Xu, X. Du, M. H. El Naggar, X. Zhang and J. Jia. Nonlinear lateral response of offshore large-diameter monopile in sand. Ocean Engineering, 216:108013, 2020.

[67] Y. Hochi, Y. Murono, M. Saitoh and C. S. Goit. Earthquake motion filtering effect by pile foundations considering nonlinearity of soil and piles. Soil Dynamics and Earthquake Engineering, 125:105748, 2019.

[68] X. Cheng, T. Wang, J. Zhang, P. Wang, W. Tu and W. Li. Dynamic response analysis of monopile offshore wind turbines to seismic and environmental loading considering the stiffness degradation of clay. Computers and Geotechnics, 155:105210, 2023.

[69] E. Rodríguez-Galván, G. M. Álamo, J. J. Aznárez and O. Maeso. Non-linear behaviour of soil–pile interaction phenomena and its effect on the seismic response of owt pile foundations. validity range of a linear approach through non-degraded soil properties. Computers and Geotechnics, 168:106188, 2024.

[70] W. D. Iwan. On a class of models for the yielding behavior of continuous and composite systems. Journal of Applied Mechanics, 34(3):612–617, 09 1967.

[71] K. S. Skau, H. P. Jostad, G. Eiksund and H. Sturm. Modelling of soil-structure-interaction for flexible caissons for offshore wind turbines. Ocean Engineering, 171:273–285, 2019.

INSTITUTO UNIVERSITARIO
SIANI
INGENIERIA COMPUTACIONAL

Edificio Central del Parque Tecnológico
Campus Universitario de Tafira
35017 Las Palmas de Gran Canaria
e-mail: info@siani.es · www.siani.es

UNIVERSIDAD DE LAS PALMAS
DE GRAN CANARIA